MIT-2344-8
MITNE-76

MASSACHUSETTS INSTITUTE OF TECHNOLOGY
DEPARTMENT OF NUCLEAR ENGINEERING
Cambridge, Massachusetts 02139

THE MEASUREMENT OF REACTOR PARAMETERS IN SLIGHTLY ENRICHED URANIUM, HEAVY WATER MODERATED MINIATURE LATTICES

by
E. Sefchovich, I. Kaplan, T. J. Thompson

October, 1966

Contract AT (30-1) 2344
U.S. Atomic Energy Commission

MASSACHUSETTS INSTITUTE OF TECHNOLOGY
DEPARTMENT OF NUCLEAR ENGINEERING
Cambridge 39, Massachusetts

THE MEASUREMENT OF REACTOR PARAMETERS IN SLIGHTLY ENRICHED URANIUM, HEAVY WATER MODERATED MINIATURE LATTICES

by

E. Sefchovich, I. Kaplan, T. J. Thompson
October, 1966

MIT-2344-8
MITNE-76

AEC Research and Development Report
UC-34 Physics
(TID-4500, 47th Edition)
Contract AT(30-1)2344
U.S. Atomic Energy Commission

DISTRIBUTION

MIT-2344-8 MITNE-76

AEC Research and Development Report

UC-34 Physics

(TID-4500, 47^{th} Edition)

1. USAEC, New York Operations Office (D. Richtmann)
2. USAEC, Division of Reactor Development (P. Hemmig)
3-5. USAEC, Division of Reactor Development (I. Zartman)
6. USAEC, Division of Reactor Development (S. Strauch)
7. USAEC, Division of Reactor Development (H. Honeck)
8. USAEC, New York Patents Office (H. Potter)
9. USAEC, New York Operations Office (H. Fish)
10. USAEC, New York Operations Office, Research and Development Division
11. USAEC, Maritime Reactors Branch
12. USAEC, Civilian Reactors Branch
13. USAEC, Army Reactors Branch
14. USAEC, Naval Reactor Branch
15. Advisory Committee on Reactor Physics (E. R. Cohen)
16. ACRP (G. Dessauer)
17. ACRP (D. de Bloisblanc)
18. ACRP (M. Edlund)
19. ACRP (R. Ehrlich)
20. ACRP (I. Kaplan)
21. ACRP (J. Chernick)
22. ACRP (F. C. Maienschein)
23. ACRP (R. Avery)
24. ACRP (P. F. Zweifel)
25. ACRP (P. Gast)
26. ACRP (G. Hansen)
27. ACRP (S. Krasik)
28. ACRP (L. W. Nordheim)
29. ACRP (T. M. Snyder)
30. ACRP (J. J. Taylor)

31-33. O.T.I.E., Oak Ridge, for Standard Distribution

34-150. Internal Distribution

ABSTRACT

Reactor physics parameters were measured in six heavy water lattices which were miniature versions of lattices investigated extensively in the exponential assembly at M.I.T. The lattices consisted of 0.25-inch-diameter rods in two U^{235} concentrations, 1.143% and 1.027%, and three spacings, 1.25, 1.75 and 2.50 inches. The following quantities were measured in each lattice: the ratio of epicadmium to subcadmium capture rates in U^{238} (ρ_{28}); the ratio of epicadmium to subcadmium fission rates in U^{235} (δ_{25}); the ratio of the total capture rate in U^{238} to the total fission rate in U^{235} (C^*); the U^{238}-to-U^{235} fission ratio (δ_{28}); the intracellular distribution of the activity of bare and cadmium covered gold foils; and the axial and radial activity distributions of bare and cadmium covered gold foils. Corrections derived from theory had to be applied to account for the presence of source neutrons and boundary effects. The age-diffusion model developed by Peak was improved and corrections were obtained to extrapolate the miniature lattice data to exponential, critical and infinite assemblies. To test the validity of the extrapolation methods, the results obtained by extrapolating the miniature lattice data to exponential assemblies were compared with the results of measurements made in the exponential assembly at M.I.T. The extrapolated and measured results agreed generally within the experimental error.

It is shown that to extrapolate the values of ρ_{28}, δ_{25} and C^* measured in the miniature lattice to larger assemblies, it is only necessary to describe theoretically the measured spatial distribution of the cadmium ratio of gold.

The experimental determination of the material buckling in miniature lattices was investigated. It is apparent that the inclusion of transport effects may be necessary, first, to define the material buckling and, second, to obtain its value.

The correction factors for ρ_{28}, δ_{25} and C^* were shown to depend on k_∞ so that k_∞ cannot be determined directly from measurements in the miniature lattice. An iterative procedure was developed to determine k_∞ which converges rapidly and, for the lattices investigated, led to results that were in agreement with the values of k_∞ obtained from measurements in the exponential assembly at M.I.T.

ACKNOWLEDGEMENTS

The success of this work and the M.I.T. Heavy Water Lattice Project, as a whole, has been due to the support of the U.S. Atomic Energy Commission and to the contribution of a number of individuals, Overall direction of the Lattice Project, while this research was done, was shared by Professors Irving Kaplan, Theos J. Thompson and Michael Driscoll. The author wishes to thank Dr. David Lanning for encouragement to undertake this research and Professors Thompson and Kaplan for guidance at all stages of this work. Discussions with Professor Driscoll and Messrs. E. Pilat and H. Bliss were fruitful. Professor F. Clikeman was of great assistance in the maintenance of the counting equipment. Thanks are due to Miss Barbara Kelley for the procurement of foil material. Messrs. Joseph Barch, Norman Berube, and Albert Supple have been of great assistance in the experimental work.

The staffs of the M.I.T. Reactor, of the Machine Shop, of the Electronic Shop, and of the Radiation Protection Office have provided assistance and advice during the experimental work. Messrs. Francis Woodworth, John Wasik and Thomas Green gave much assistance in the fabrication of experimental equipment. Mrs. Mary Bosco has ably prepared the final manuscript.

The patience, encouragement and support of the author's wife were instrumental to the completion of this work; his wife also assisted in typing the early versions of this report.

All computer calculations were done at the M.I.T. Computation Center.

TABLE OF CONTENTS

LIST OF FIGURES

LIST OF TABLES

CHAPTER 1

INTRODUCTION

1.1 THE M.I.T. HEAVY WATER LATTICE PROJECT

The Nuclear Engineering Department at M.I.T. is engaged in a research program, the Heavy Water Lattice Project, under the sponsorship of the United States Atomic Energy Commission. The purpose of this project is to carry out experimental and theoretical studies of the physics of subcritical assemblies of slightly enriched uranium rods in heavy water. Several reports have been published (H1, H2, H3, H4, H5), describing results obtained in this project.

One of the most important purposes of the project is the investigation of new techniques for obtaining reactor physics parameters.

The present work is concerned with the feasibility of using miniature lattices to measure reactor physics parameters.

1.2 PARAMETERS OF INTEREST

Reactor physics is, to a large extent, the study of critical assemblies because these assemblies have great practical importance. The most important information is the critical size of an assembly — that is, the size that an assembly must have in order that the production of neutrons be balanced exactly by the losses of neutrons by absorption and leakage. Criticality is expressed by the fact that the effective multiplication factor is unity.

In the design of reactors, it is convenient to simplify the problem by assuming that there is no leakage of neutrons. The multiplication factor for an infinite medium, k_∞, is then calculated by the familiar four-factor formula. The leakage of neutrons is introduced through the material buckling, B_m^2, which is related to the critical dimensions of the assembly.

Another parameter of interest is the initial conversion factor, C. It is an important factor in establishing the fuel cycle cost by determining the core life of a reactor. The parameter C is defined as the ratio of the number of Pu^{239} atoms created in the assembly to the number of atoms of U^{235} consumed.

The Heavy Water Lattice Project has been concerned with the determination of the parameters which enter into the four-factor formula of k_∞, of C, and of B_m^2.

1.3 POSSIBLE APPROACHES TO EXPERIMENTAL REACTOR PHYSICS

A number of different definitions of k_∞ are in use. In this work, k_∞ is taken to be equal to the ratio of the total number of neutrons produced to the total number of neutrons absorbed in an infinite medium. For a predominantly thermal reactor, k_∞ can be expressed as:

$$k_\infty = \eta \epsilon p f \ . \tag{1.1}$$

In Eq. (1.1), it is important that the four factors be defined consistently, with each process in the neutron cycle taken into account once and only once. The following definitions form a consistent set. The factor η is the average number of fast neutrons produced by fission in U^{235} for one thermal neutron absorbed in the fuel. The fast fission factor ϵ is defined as the total number of fast neutrons produced by fissions in both U^{235} and U^{238}, due to incident neutrons of all energies for each neutron produced by fission in U^{235}. The factor p is the probability that a neutron will escape absorption while slowing down to thermal energies. The thermal utilization, f, is the probability that a neutron, once thermal, is absorbed in the fuel.

The factors that appear in Eq. (1.1) cannot be measured directly. Quantities related to them can, however, be determined. The details are given in Section 3.1. It is important to realize that the factors in Eq. (1.1) must be determined for an infinite assembly. The parameters related to them cannot, of course, be measured in an infinite assembly and corrections for leakage must be applied.

Critical assemblies have the advantages that when lattice parameters are measured in them, corrections for neutron leakage are smaller than those needed for subcritical assemblies, and the energy spectrum resembles closely the spectrum of neutrons in the operating reactor of interest. The use of critical lattices, however, has several disadvantages. First, they require elaborate safety provisions to prevent the assembly from becoming supercritical. Second, they require a larger investment in materials than do subcritical assemblies. Third, if it is desired to investigate a large number of different assemblies, their use becomes cumbersome.

When the study of a large area of interest is undertaken, as in the case of the Heavy Water Lattice Project at M.I.T. which has been concerned with lattices of metallic uranium rods moderated by heavy water, it is more convenient to use subcritical assemblies. The safety provisions required are not as extensive and the amount of material involved is smaller than in a critical facility. Exponential experiments have some inherent disadvantages. The higher leakage rate, as compared with that in a critical assembly, may necessitate corrections in some of the measurements. Source effects, which are totally absent in a critical experiment, may be troublesome in an exponential experiment. Nevertheless, exponential assemblies remain useful tools for the testing of reactor theory and for reactor design.

When subcritical assemblies are used for the measurement of lattice parameters, experimenters prefer the use of assemblies which are not far from critical. Over a large portion of such an assembly, the neutron spectrum resembles closely that in a critical lattice. Moreover, the measurements can be made far enough from the source and boundaries so that corrections for neutron leakage and source neutrons are not too large. The values of the parameters that are measured are, therefore, close to their value in a critical assembly.

Exponential assemblies moderated by heavy water involve a large financial investment because of the cost of the heavy water. To keep contamination of the D_2O at a low level, it is desirable to avoid frequent experimental changes. Yet, there is need for a more flexible facility, one which does not involve too much heavy water. The miniature lattice is such a facility. The amount of material is small and experiments can be made with relative ease in the miniature lattice facility. Miniature lattices have also an economic advantage over exponential or critical facilities. But, before miniature lattices can be used extensively, it is necessary to find out whether meaningful results can be obtained. Because of the small dimensions of the assembly, the effect of source and boundaries is not negligible. The interpretation of measurements made in these lattices must, therefore, account properly for these effects.

1.4 PREVIOUS WORK WITH MINIATURE LATTICES

Small subcritical assemblies have been used in the past. Wikdahl and Akerhielm (W5), in Sweden, used miniature lattices to measure disadvantage factors in single rods and clusters of UO_2 rods in D_2O. Relatively small assemblies were used by Kouts and coworkers (K2) at the Brookhaven National Laboratory to measure quantities related to k_∞ in lattices of slightly enriched U-metal rods in H_2O. In both cases, the results were encouraging.

Peak (P2) at M. I. T. made measurements of lattice parameters in miniature lattices of slightly enriched U-metal rods moderated by three different mixtures of D_2O and H_2O; three moderator-to-fuel volume ratios were investigated for a total of nine lattices. The measurements included the average cadmium ratio of U^{238} in the fuel, the ratio of the fission rate in U^{238} to the fission rate in U^{235}, and the subcadmium disadvantage factor. A theoretical model based on age-diffusion theory was developed to extrapolate these results to those that would be observed in a critical or infinite assembly. The corrections developed for the average cadmium ratio of U^{238} in the fuel were applied to the measurements made in the nine lattices investigated. In six of these assemblies, measurements were made at two different positions in the lattice and the application of the corrections led to values that agreed to within 2%. A similar consistency was observed in the results obtained for the U^{238}-to-U^{235} fission ratio. The consistency observed was sufficiently encouraging so that further work in miniature lattices was considered desirable.

1.5 PURPOSE OF THIS WORK

The work of Peak (P2), which was exploratory in nature, was limited in that similar measurements have not been made in exponential or critical assemblies of the same composition and arrangement. Comparison of the results obtained in miniature lattices with the results of measurements made in such facilities was, therefore, not possible.

Since the time of Peak's work, the Heavy Water Lattice Project at M. I. T. has made measurements of lattice parameters in a considerable number of exponential assemblies of metallic uranium rods in heavy water (H1, H2, H3, H4, H5). Thus, by selecting properly the miniature lattices to be investigated, the validity of measurements made in them can be tested.

The purpose of this thesis is to study the feasibility of miniature lattices for the measurement of lattice parameters. In order to study the validity of these measurements, six lattices which have been investigated extensively in the exponential facility at the M. I. T. reactor were chosen. It was then possible to compare measurements made in miniature lattices with those performed in facilities where they can be better substantiated.

Measurements were made of the following quantities which can be related to one of the four factors in k_∞ or to the initial conversion factor. (For reasons which will be discussed in Chapter 5, the material buckling cannot be determined accurately in the miniature lattice.) The quantities measured are:

1. The ratio ρ_{28} of the epicadmium to subcadmium capture rates in U^{238} averaged over the fuel,

2. The ratio δ_{25} of epicadmium to subcadmium fission rates in U^{235} averaged over the fuel,

3. The ratio δ_{28} of fissions in U^{238} (fast) to the total number of fissions in U^{235},

4. The ratio C^* of the total capture rate in U^{238} to the total fission rate in U^{235},

5. The intracellular subcadmium and epicadmium activity distributions of gold,

6. The axial and radial activity distributions of both bare and cadmium-covered gold foils. This measurement also gave the spatial distribution of the cadmium ratio of gold.

Because of the small size of the assembly, source and boundary effects are important. Measurements made in it must, therefore, be corrected for these effects. In this report, a method for making these corrections, based on age-diffusion theory, will be developed. The method is an extension of that of Peak (P2). Use will also be made of the work done by Woodruff (W4), in the high energy range, to obtain the correction factor for δ_{28}.

The correction factors obtained allow the extrapolation of the results obtained in the miniature lattice to those that would be obtained in an exponential assembly. This procedure will allow a direct comparison between the results of this work and those obtained in the exponential facility at M. I. T. Corrections which permit the extrapolation to critical or infinite assemblies will also be developed.

Because of the importance of the neutron source in the interpretation of the results obtained in the miniature lattice, the properties of the neutron source were studied. It was found necessary, as a result of these studies, to modify the azimuthal and radial distribution of the source neutrons.

1.6 ORGANIZATION OF THIS REPORT

Chapter 2 is a description of the experimental facilities and techniques used in these measurements. The theoretical methods and the correction factors derived from them are discussed in Chapter 3. Chapter 4 gives the experimental results as well as a comparison of the corrected results with those obtained in the exponential facility at M. I. T. Chapter 5 is a discussion of the results and the quantities required to obtain the corrections. The conclusions reached and recommendations for future work are given in Chapter 6.

Appendix A gives the computer codes programmed specifically for this work as well as their FORTRAN II listing. The bibliography is given in Appendix B. Appendix C is a discussion of the neutron source and the modifications made on it. It also describes the harmonic analysis made of the radial distribution of the source. Appendix D describes age measurements made in connection with this work. The procedures for reducing the data for ρ_{28}, δ_{25} and C^* are given in Appendix E.

CHAPTER 2

EXPERIMENTAL TECHNIQUES AND FACILITIES USED

2.1 INTRODUCTION

The experimental facilities and the techniques used in the measurement of lattice parameters in miniature lattices will be described in this chapter.

2.2 EXPERIMENTAL FACILITIES

2.2.1 Description of the Medical Therapy Facility

The source of neutrons for the irradiations carried out is the M.I.T. Reactor. The reactor utilizes MTR-type fuel elements highly enriched in U^{235}. It is moderated and cooled by heavy water. The nominal power of the reactor during the course of these experiments was 5 MW.

The Medical Therapy Facility is a surgical operating room under the reactor. An intense beam of thermal neutrons with a negligible amount of fast neutrons and gamma rays (R2) may be admitted to the facility through a hole in the ceiling of the room. A cut-away view of the facility and its relative position with respect to the rest of the M.I.T. Reactor is shown in Fig. 2.1.

A conically-shaped aluminum tank with the narrow end facing downward is positioned 4 inches below the reactor tank and slightly off-center from the vertical centerline. The tank is about 38 inches deep. To shut off the beam, the tank is filled with demineralized water; in addition, a 1/4-inch-thick boral shutter and a 9-1/8-inch-thick lead shutter can be made to slide in under the beam port. As an extra safety provision, an auxiliary masonite slab can be slid under the beam if necessary. At 5 MW, the flux varies from about 5×10^{10} n/cm^2-sec at the center, to about 10^9 n/cm^2-sec near the edge of the beam port.

The water and the lead and boral shutters are operated from the main control panel, just outside the room. A viewing window filled

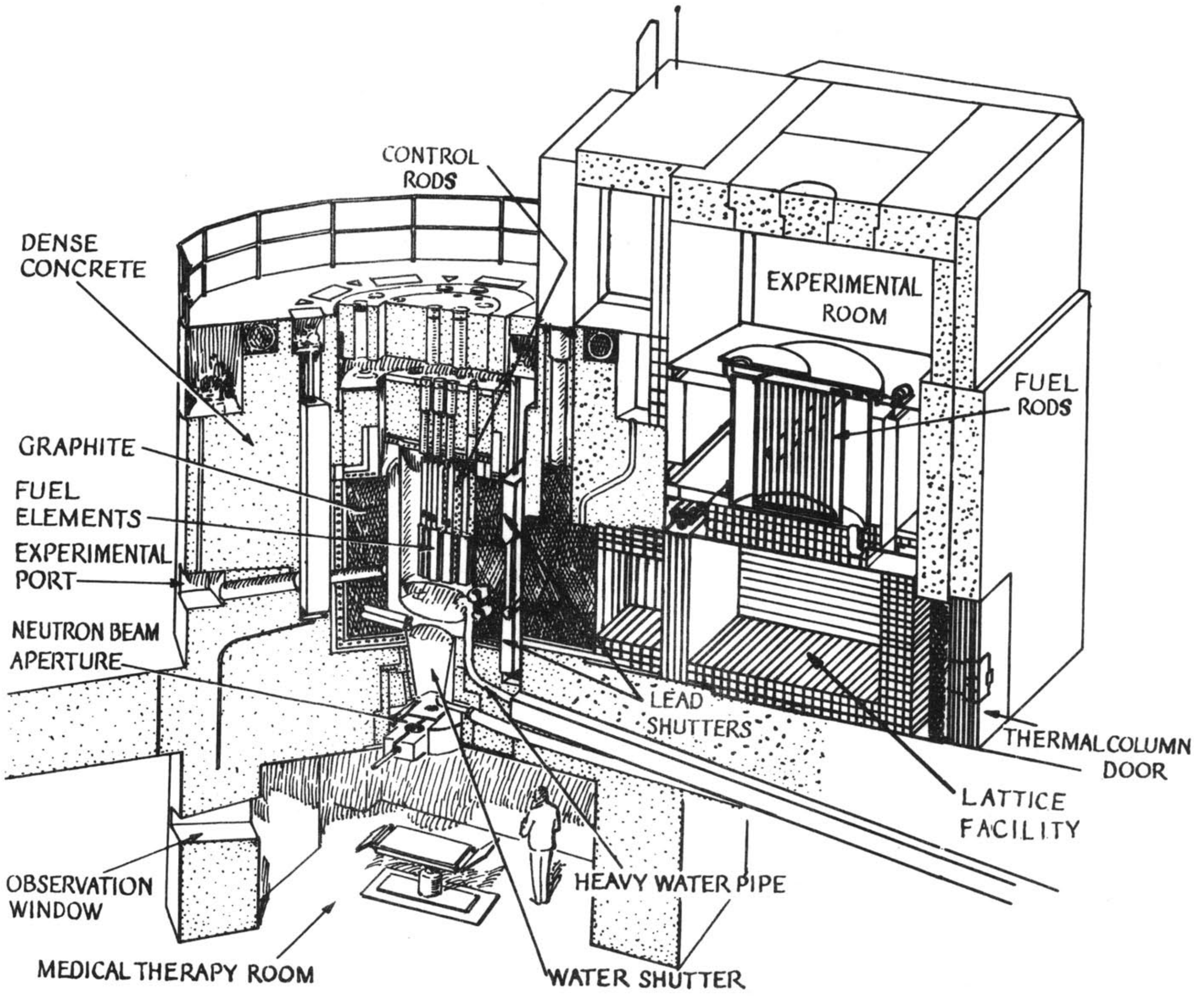

FIG. 2.1 CUT-AWAY VIEW OF THE MIT RESEARCH REACTOR

with mineral oil, for the observation of the room from the control area, is provided. In the course of this work, it was found necessary to add a 2-inch-thick sliding lead slab outside the window to keep the dose, for irradiations at 5 MW, within the permissible limits. Directly under the beam hole, space is provided for placing special source collimators. In this work, it was found necessary to add a collimator to modify the spatial distribution of the neutrons entering the miniature lattice facility. The details of this work are given in Appendix C. The facility is also provided with a hydraulic hoist directly beneath the downward-directed neutron beam port, which permits the lifting of experimental arrangements to the beam hole for irradiation.

2.2.2 Description of the Miniature Lattice Facility

The tank for the miniature lattice was fabricated at M. I. T. by J. Bratten (B3) and modified by Peak (P2) for miniature lattice experiments. It is a thin-walled aluminum tank in the shape of a right cylinder, 21 inches high and 20 inches in diameter, with a removable base plate of 1/2-inch-thick aluminum. The tank wall and top are made of 1/16-inch-thick aluminum sheet. The tank is equipped with a wheeled stand, as well as valves and pipes to allow filling or draining from a 3/4-inch-diameter line. Figure 2.2 is a sketch of the assembly.

The grid plate arrangement that holds the lattices consists of two 3/8-inch-thick aluminum plates kept apart by 5/16-inch-diameter aluminum rods. The distance between plates is 15.75 inches. The center of the top plates has a hexagonal hole in the center through which an experimental cluster, consisting of at least the centermost rod and the first ring of rods around it, is inserted in the assembly. A picture of one of the lattices is shown in Fig. 2.3. During an experiment, the assembly is positioned under the neutron beam port in the Medical Therapy Facility. Fast and slow neutron shields are placed around it and the entire assembly, with the shielding, is lifted on the hoist to a position 16 inches below the beam port. The shielding was added for two purposes: first, to prevent the irradiation of the room; and second, to approximate as closely as possible, a bare assembly. With this latter purpose in mind, the walls of the environment surrounding the lattice tank were lined with cadmium to prevent the

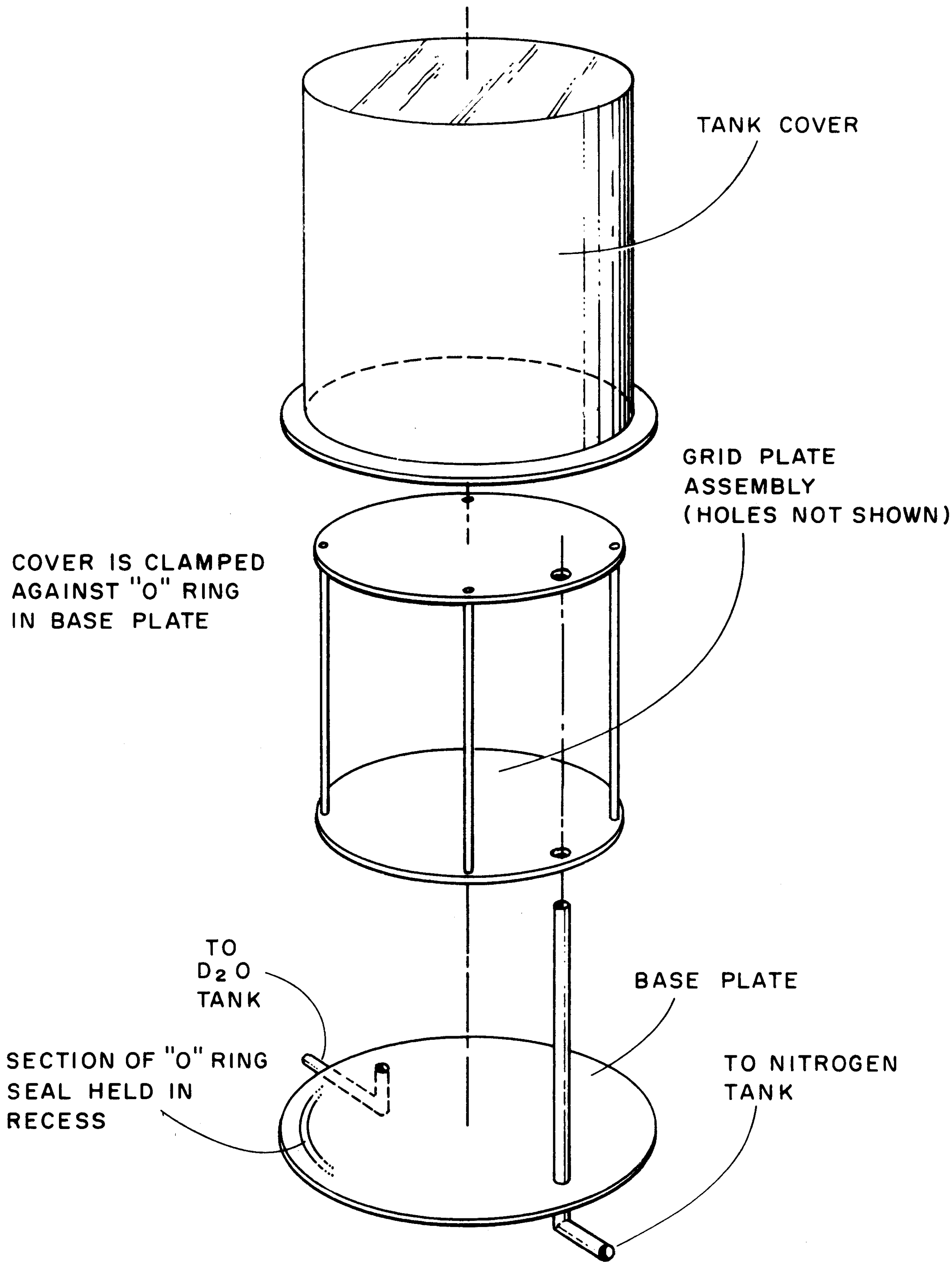

FIG. 2.2 SCHEMATIC DIAGRAM OF THE M.I.T.
SMALL EXPONENTIAL ASSEMBLY

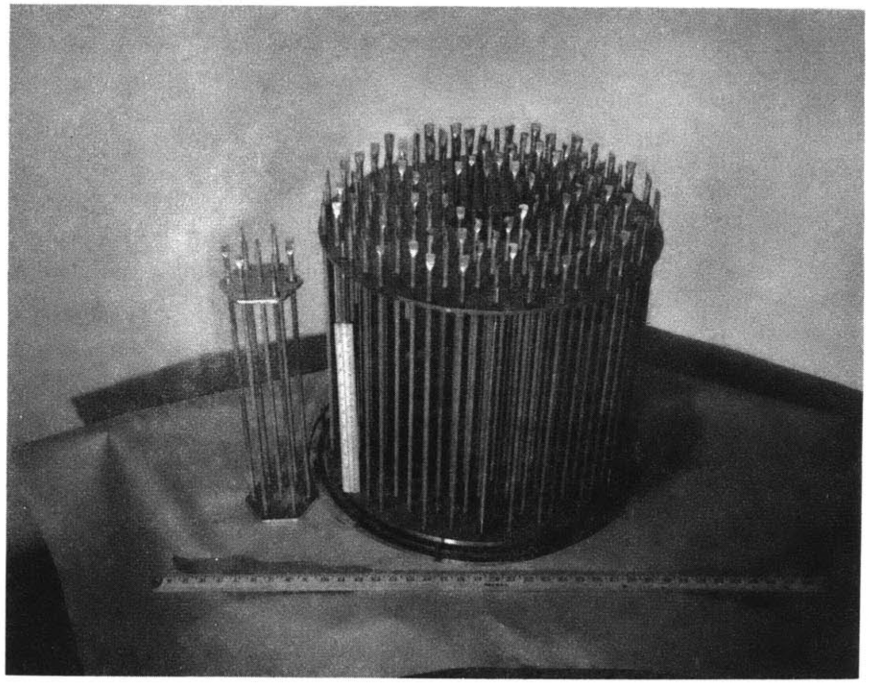

FIG. 2.3. VIEW OF TYPICAL MINIATURE LATTICE AND EXPERIMENTAL CLUSTER.

reflection of thermal neutrons and force the thermal neutron flux inside the lattice to vanish at the extrapolated boundary. As cadmium has little effect on epithermal neutrons, a 1/4-inch layer of borated plastic was added, followed by 3 inches of paraffin, a layer of cadmium and 3 inches more of paraffin. The plastic and paraffin layers proved effective in slowing down the epithermal and fast neutrons leaving the assembly. The boron contained in the plastic and the outer layer of cadmium were useful in absorbing the neutrons reaching thermal energies. A diagram showing the experimental setup during irradiation is shown in Fig. 2.4.

An irradiation time of two hours was found to be convenient. It gave an adequate activity for the experimental purposes envisioned, and the dose rate to the experimenter was within tolerable limits during the time interval when the foils were removed after irradiation. Typical dose rates at contact with the top of the tank varied from about 2 r/hr two hours after the irradiation was completed, to about 100 mr/hr after twelve hours.

2.3 EXPERIMENTAL PROGRAM

To investigate the feasibility of miniature lattices for the measurement of reactor parameters, steady-state measurements were made in six miniature lattices. These lattices were miniature versions of six lattices studied extensively in the exponential assembly at M. I. T. Results obtained in the miniature lattices can then be directly compared with measurements in lattices where their validity is better substantiated. The description of these lattices is given in Table 2.1.

Measurements were made of the axial and radial activity distributions of both bare and cadmium-covered gold foils. These activity distributions gave the spatial distribution of the cadmium ratio of gold. Intracellular activity distributions of both bare and cadmium-covered gold foils were measured as well as the parameters ρ_{28}, δ_{25}, δ_{28} and C^*.

The experimental methods used were, in general, those developed by workers at the Heavy Water Lattice Project (B2, P1, H6, W3, D1, S1), with some modifications made to apply them to miniature lattices. A description of the methods used follows.

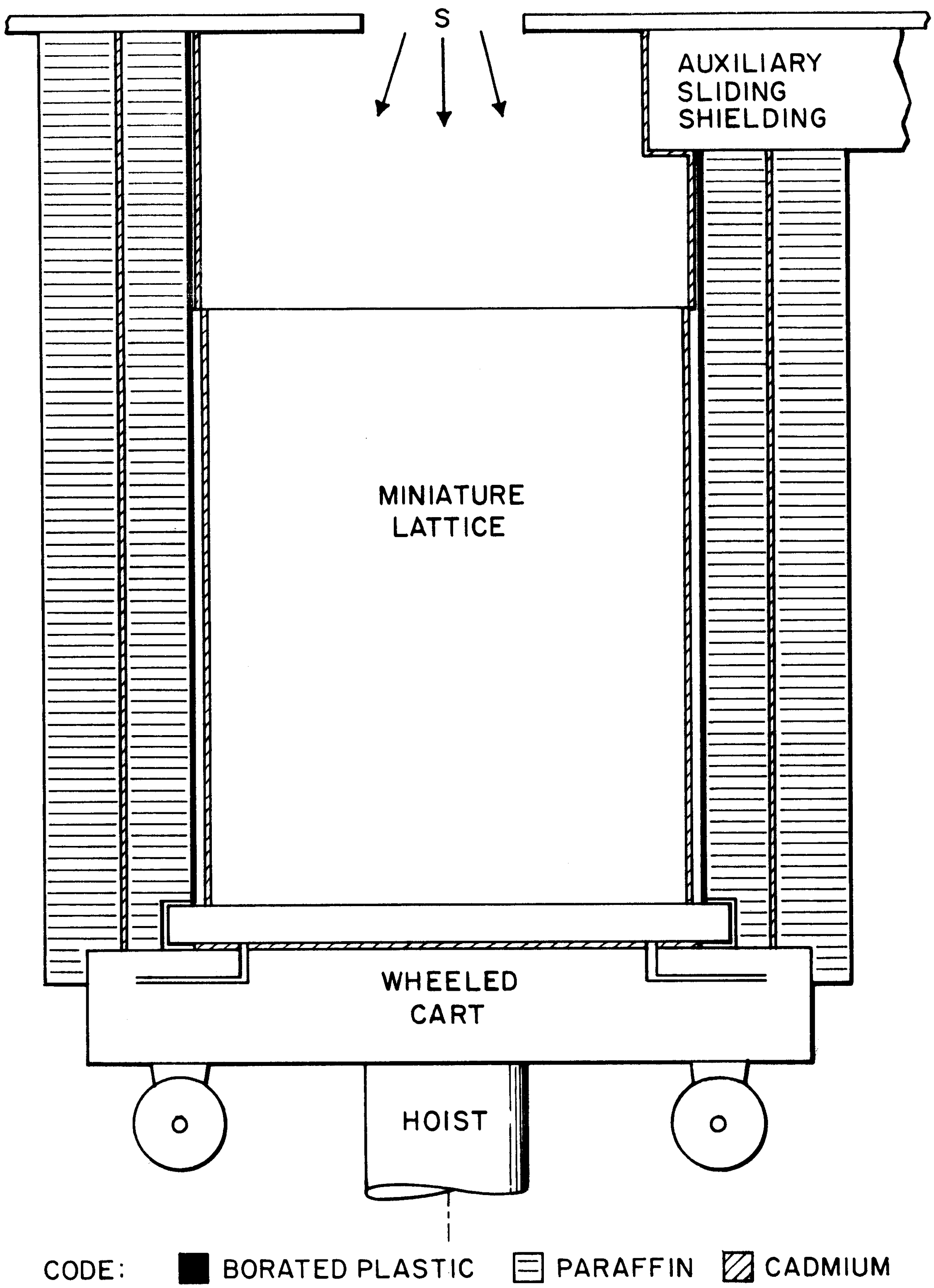

FIG. 2.4 EXPERIMENTAL SETUP DURING IRRADIATION.

Table 2.1

Lattices Investigated[1]

U^{235} Concentration of Fuel (Percent)	Rod-to-Rod Distance (Inches)	Denomination of Lattice
1.143	1.25	ML2
1.143	1.75	ML7
1.143	2.50	ML3
1.027[2]	1.25	ML4
1.027	1.75	ML6
1.027	2.50	ML5

(1) All lattices moderated by 99.75 mole percent D_2O. Fuel rods are 0.25 inch in diameter in aluminum tubes of 0.318-inch O. D.

(2) There are indications (H5) that the enrichment of these fuel rods is actually 1.016%. This small difference has a negligible effect on the final results of this work.

2.4 AXIAL AND RADIAL GOLD ACTIVITY TRAVERSES

The method used to obtain the axial and radial activity distribution of gold is that used by Palmedo (P1) and Harrington (H6) except for minor modifications made necessary by the small size of the miniature lattice facility.

The gold foils used were 0.005 inch thick and 1/8 inch in diameter. Two axial foil holders made of 3/16-inch-thick, 1/2-inch-wide aluminum bar were used for the measurement. Bare and cadmium-covered foils were placed alternately, one inch apart, on recesses made on the holder. The cadmium-covered foils were placed inside cadmium pillboxes built according to the design of Simms (S1). A sketch showing the pillbox is shown in Fig. 2.5. Bare foils and cadmium pillboxes were attached to the foil holders with 0.001-inch-thick Mylar tape. Care was taken to place equal amounts of tape on each foil and pillbox. For the irradiation, the foil holders were attached with Mylar tape to two fuel elements symmetric about the centermost rod in the experimental cluster. A portion of this arrangement is

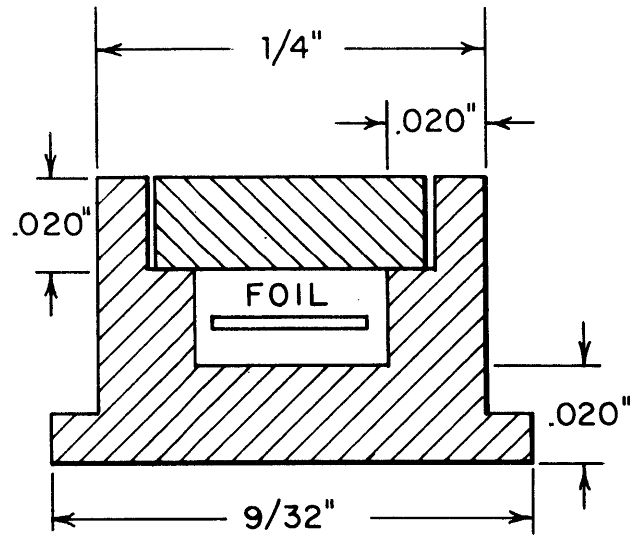

FIG. 2.5 CADMIUM PILLBOX USED FOR EPICADMIUM AXIAL AND RADIAL GOLD TRAVERSES

shown in Fig. 2.6. Brown (B2) has shown that the separation of one inch between foils is enough to damp out the effect of the cadmium on the neighboring bare foil.

The radial foil holders were similar to the axial holders except that the milled recesses were made on the narrow side of the aluminum bar. The foil recesses were made so that the alternately placed bare and cadmium-covered foils were exactly halfway between rods. In other words, the separation between foils was equal to the lattice spacing.

Two radial foil holders were used for each experiment: one 6.75 inches from the top of the lattice, and the other 9.75 inches, each placed along a diameter of the lattice. The lattices with the widest rod-to-rod separation, 2.50 inches, had only four rings of fuel elements so that the radial activity measurement had only four data points. To increase the number of radial data points, one foil holder was added at each height placed along the chord closest to the diameter of the assembly.

2.5 INTRACELLULAR GOLD ACTIVITY DISTRIBUTION

Intracellular activity distributions of both bare and cadmium-covered gold foils were made in all the lattices studied. The techniques used were a modified version of those given in Refs. (B2) and (S1).

The foils used were 1/16 inch in diameter and 0.005 inch thick. As intracellular measurements are made inside the fuel and in the moderator, the foil holders used were different in the two cases. The difference stems from the fact that the foil holders must have nuclear properties that are as close as possible to those of the surrounding medium to minimize their effect on the measurement.

2.5.1 Foil Holders

The foils irradiated, bare or cadmium-covered, in the fuel rod were placed in 0.012-inch holes milled on both sides of a fuel button, 0.060 inch thick and 1/4 inch in diameter, as shown in Fig. 2.7a. The foils were held in the uranium button with Mylar tape, trimmed to the 1/4-inch diameter of the button. The tape also prevented the contamination by fission products from the uranium rods.

The fuel button with the foils for the measurement of the activity

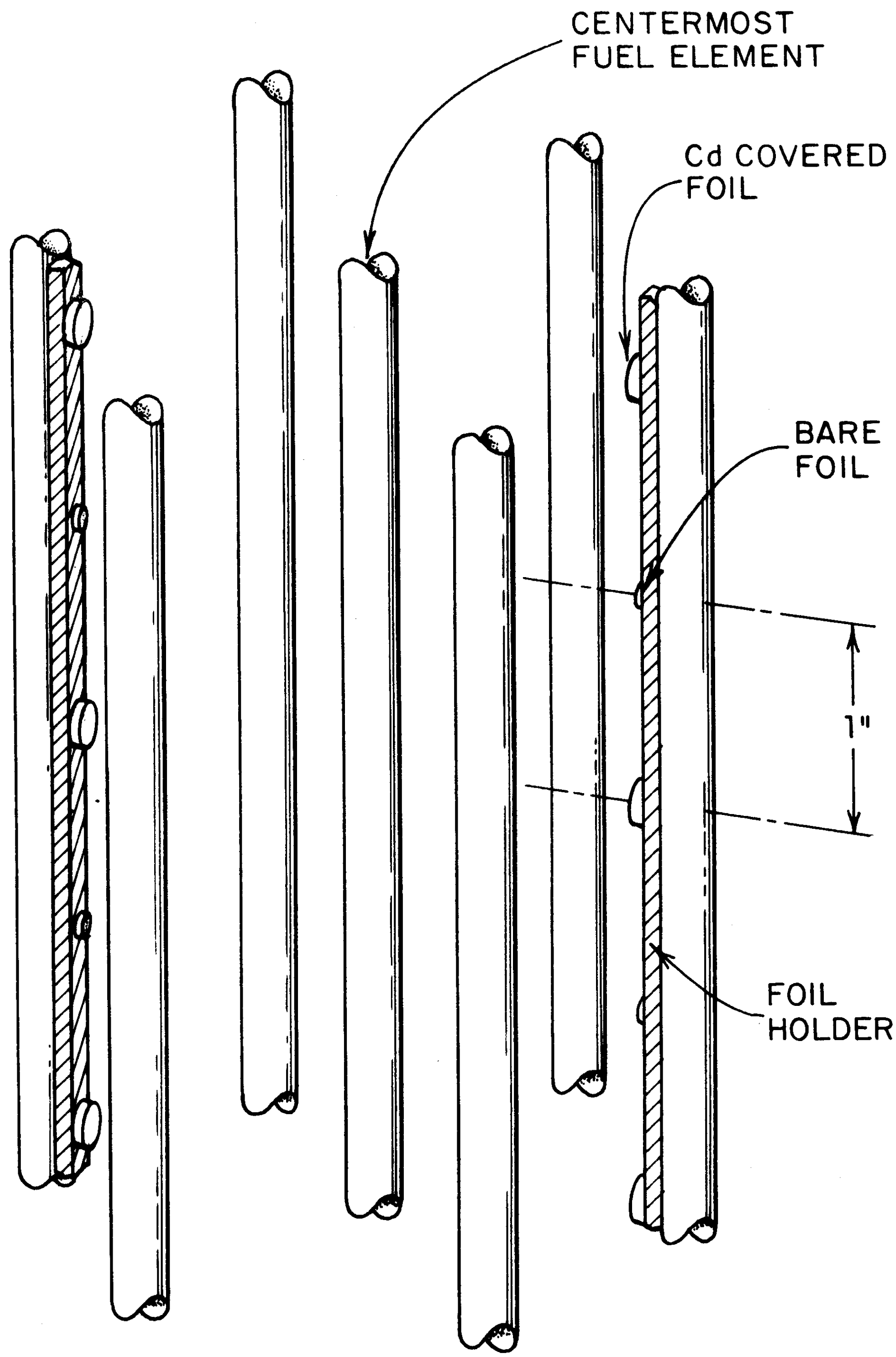

FIG. 2.6 ARRANGEMENT FOR AXIAL Au TRAVERSES IN EXPERIMENTAL CLUSTER

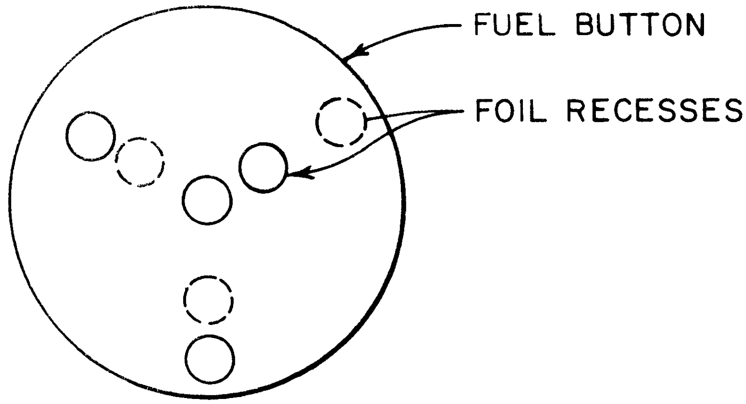

FIG. 2.7a FOIL HOLDER FOR INTRACELLULAR Au DISTRIBUTION MEASUREMENT WITHIN THE FUEL

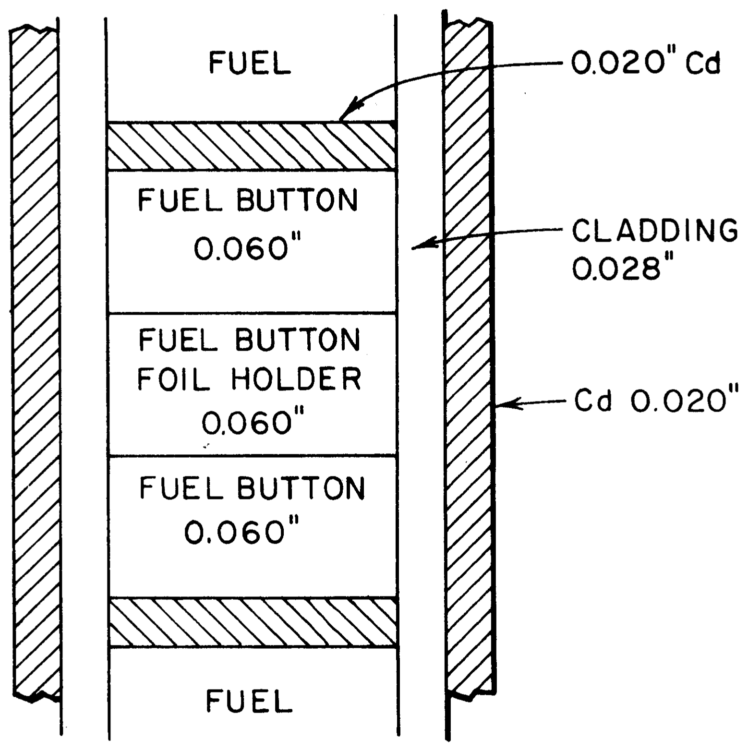

FIG. 2.7b FOIL PACKET FOR INTRACELLULAR ACTIVITY DISTRIBUTION MEASUREMENT, WITH CADMIUM-COVERED GOLD FOILS WITHIN THE FUEL.

distribution of the cadmium-covered foils was placed in a packet as shown in Fig. 2.7b. The fuel buttons next to the foil holder were necessary to insure that there was no streaming of epithermal neutrons.

A schematic diagram of a foil holder used in the moderator is shown in Fig. 2.8. The bare foils were placed in 1/16-inch holes milled in a 0.016-inch-thick aluminum sheet and held in place by Mylar tape. The foil holder was held fast to the three rods by wrapping the tabs around the rods, and was kept from sliding by Mylar tape. Cadmium-covered foils were placed in pillboxes similar to that shown in Fig. 2.5, but of smaller size. The boxes were embedded in 1/8-inch-diameter holes milled in a foil holder similar to that shown in Fig. 2.8.

The effect of the Mylar tape on the observed distribution of the activity of gold has been found to be negligible (B2).

2.5.2 Experimental Arrangement

The foil holders in the fuel were placed within the centermost rod in the experimental cluster. The separation between the fuel button with cadmium-covered foils and that with the bare gold foils was 3.5 inches. The foil holders in the moderator were placed symmetrically about the centermost rod. The foil holder with the cadmium-covered gold foils was positioned two inches below the fuel button holding the cadmium-covered gold foils in the fuel. The foil holder with the bare foils was placed at the same height as the bare foils in the fuel. The experimental arrangement during irradiation is shown in Fig. 2.9.

The axial activity distributions of bare and cadmium-covered gold foils were used to correct all measurements for the difference in axial position of the foil holders in the intracellular measurement, as discussed in Section 4.2.2.

2.6 COUNTING PROCEDURE FOR GOLD ACTIVITY

Two counting systems were used. One had a 1/2-inch sodium iodide crystal, the other a 1.75-inch crystal. The electronic equipment was the same in the two systems. For convenience, Nuclear-Chicago automatic sample changers were used in conjunction with both systems. A schematic diagram of the counting equipment is shown in Fig. 2.10.

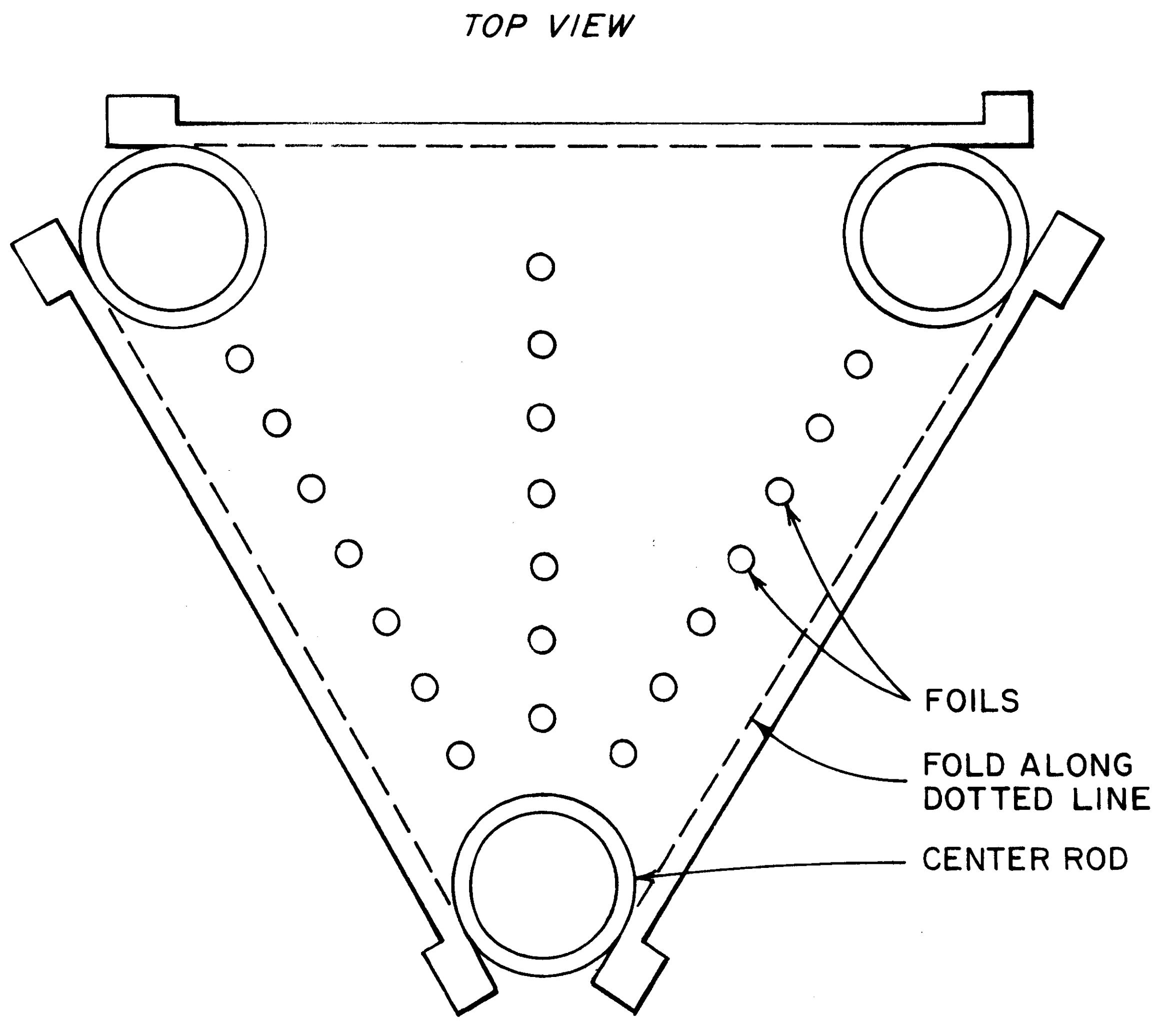

FIG. 2.8 MODERATOR FOIL HOLDER FOR INTRACELLULAR TRAVERSES WITH GOLD FOILS

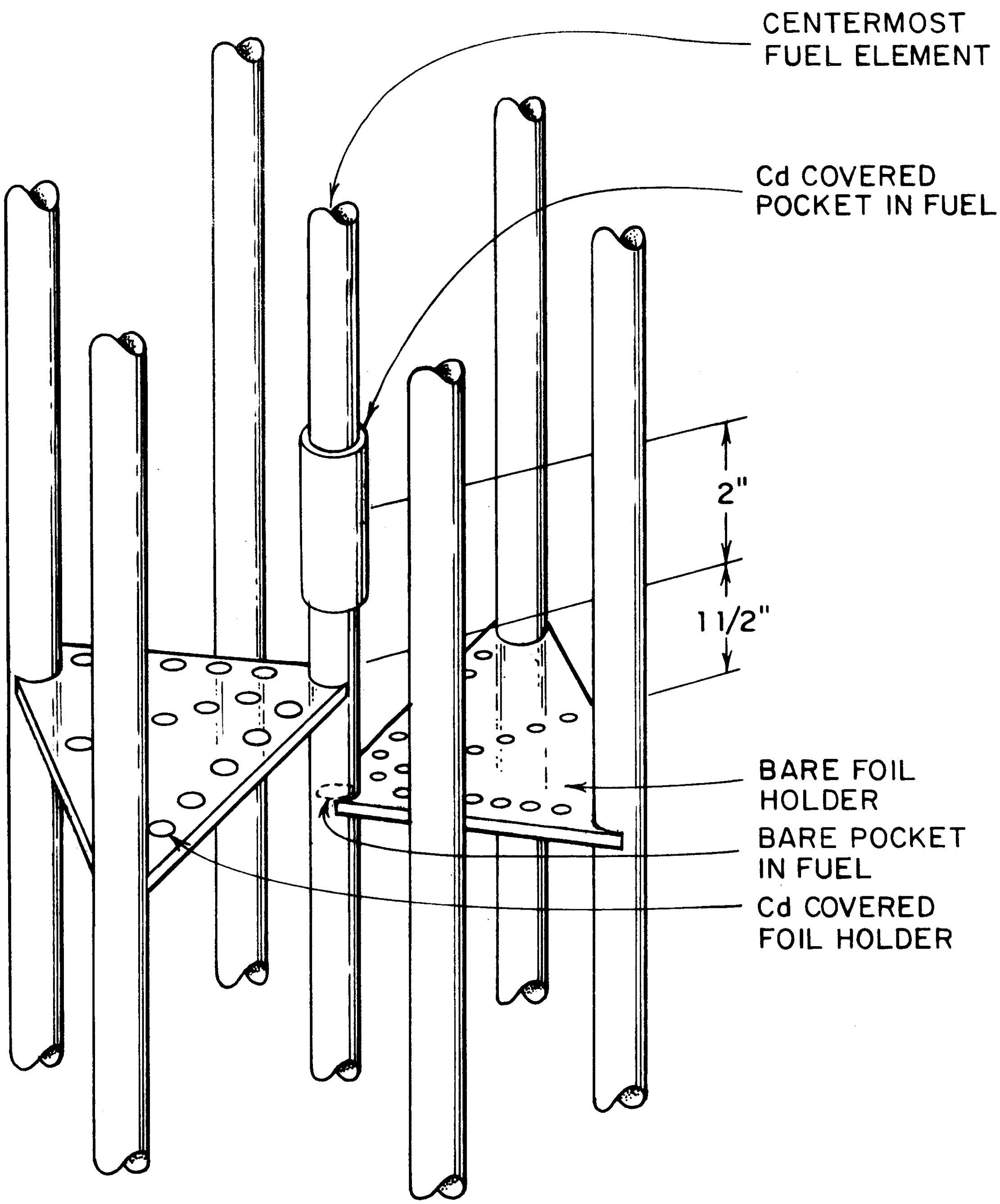

FIG. 2.9 FOIL ARRANGEMENT IN EXPERIMENTAL CLUSTER. INTRACELLULAR MEASUREMENTS WITH GOLD FOILS.

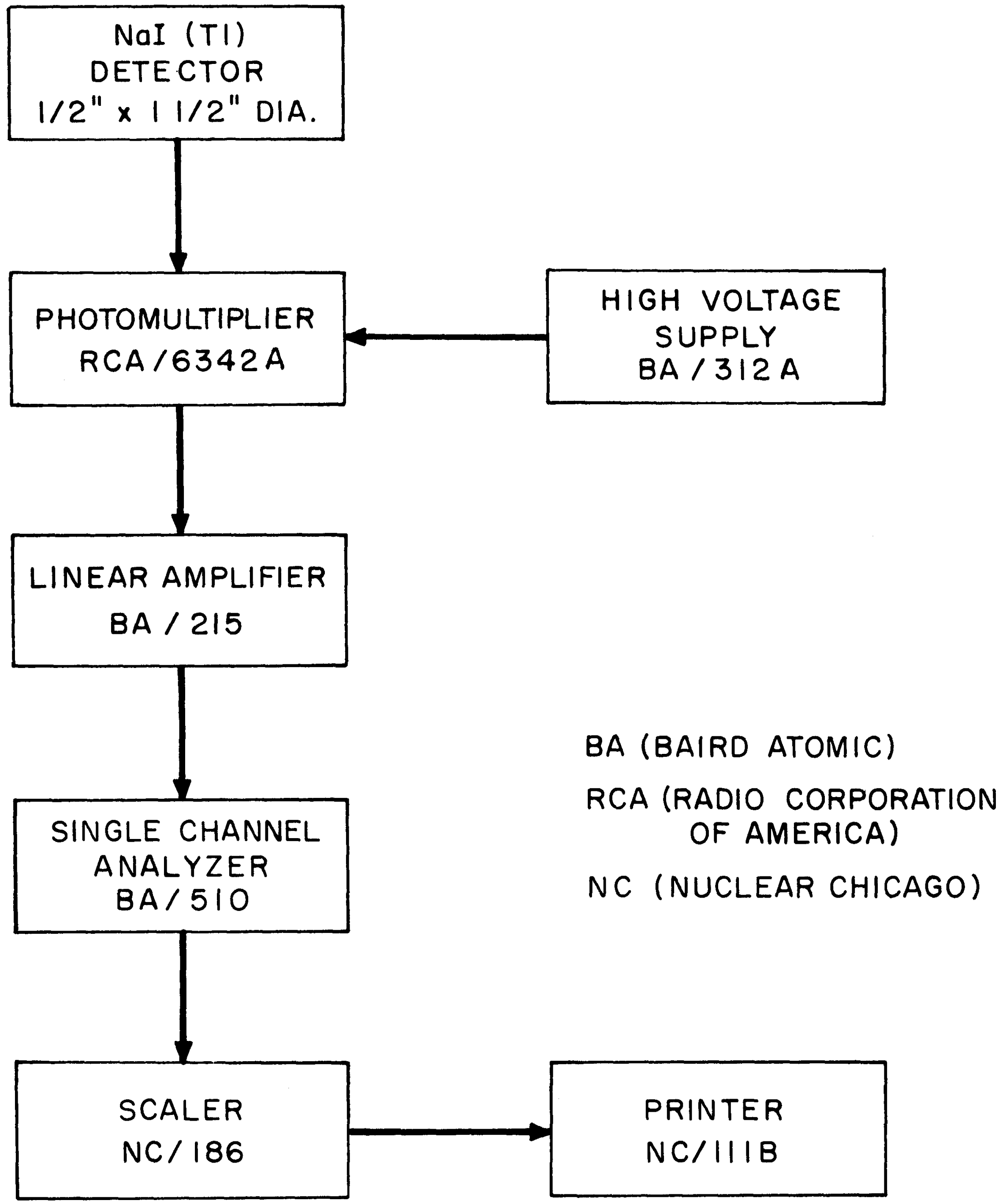

FIG. 2.10 BLOCK DIAGRAM OF GAMMA-COUNTING SYSTEM

The counting technique was the same for both 1/8-inch and 1/16-inch gold foils. Neutron activation of gold yields Au^{198}, with a half-life of 2.7 days. The main gamma radiation is a 411-kev gamma ray. The foils were integral-counted by setting the baseline at about 320 kev, the lowest point in the gamma spectrum of Au^{198}, just below the 411-kev photopeak. The window was opened so that all gamma rays above 320 kev were counted. Since the foils in the stack affect the background of the foil being counted, it was found convenient to count bare and cadmium-covered foils separately. The counting setup was calibrated for each run and monitor foils were used to correct for any drift in the system between runs, if necessary. For each run, at least four passes through the counter were made. In this manner, it was assured that any counter drift was spread evenly over all the foils within a run. Moreover, several passes provide a half-life check on the foils. The deviations from the half-life of 2.7 days were found to be negligible. The total number of counts for each foil was always such that the statistical uncertainty due to counting was kept below 0.5%.

2.7 EXPERIMENTAL DETERMINATION OF ρ_{28}, δ_{28}, δ_{25} AND C^*

The four parameters ρ_{28}, δ_{28}, δ_{25} and C^* were measured in all the lattices studied. Their relation to the factors in k_∞ is given in Section 3.1. In this section, these parameters are defined and the experimental techniques used in their measurement, which were developed by D'Ardenne (D1), are discussed.

2.7.1 The Parameter ρ_{28}

The parameter ρ_{28} is related to the cadmium ratio for the average capture rate in U^{238} in the fuel:

$$\rho_{28} = \frac{1}{R_{28} - 1}$$

$$\rho_{28} = \frac{\text{average epicadmium } U^{238} \text{ capture rate in the fuel}}{\text{average subcadmium } U^{238} \text{ capture rate in the fuel}} . \tag{2.1}$$

The value of R_{28} was obtained by irradiating two identical uranium foils, depleted in U^{235} content to 18 ppm. They were placed in equivalent positions (position of equal height and radius) inside fuel rods in the experimental cluster of the miniature lattice; one foil was surrounded by cadmium. The Np^{239} activity of each foil was measured; the cadmium ratio R_{28} was obtained from the ratio:

$$R_{28} = \frac{D_b^{39}}{D_c^{39}}, \tag{2.2}$$

where D refers to depleted uranium foils, the superscript 39 means that the measured activity was the activity of Np^{239}, and the subscripts b and c refer to bare and cadmium-covered detector foils, respectively.

2.7.2 <u>The Parameter δ_{28}</u>

The fast fission ratio δ_{28} is defined by the relation:

$$\delta_{28} = \frac{\text{average total } U^{238} \text{ fission rate in the fuel}}{\text{average total } U^{235} \text{ fission rate in the fuel}}, \tag{2.3}$$

which may be written as (W3):

$$\delta_{28} = P(t)\,\frac{EC \cdot a \cdot \gamma(t) - S}{1 - a \cdot \gamma(t)}, \tag{2.4}$$

where the terms are defined as follows:

P(t) is the ratio of the measured fission product activity per U^{235} fission to the measured fission product activity per U^{238} fission;

$\gamma(t)$ is the ratio of the measured fission product activity of a foil depleted in U^{235} to the fission product activity of a foil of natural uranium, with both foils irradiated in the same neutron flux;

a is given by:

$$a = \left(\frac{W_N}{W_D}\right)\left(\frac{N_N}{N_D}\right)^{28}, \tag{2.5}$$

where the W's represent foil weights and the N's number of atoms per cm^3; the subscripts D and N denote depleted uranium foil and natural uranium foil, respectively;

EC is the ratio $\left(\frac{N_N}{N_F}\right)^{25}\left(\frac{N_F}{N_N}\right)^{28}$, an enrichment correction, where the subscript F refers to the fuel material;

S is the ratio, $\left(\frac{N_D}{N_F}\right)^{25}\left(\frac{N_F}{N_D}\right)^{28}$.

Equation (2.4) is derived in detail from the definition, Eq. (2.3), in Refs. (W3) and (B1).

To determine δ_{28}, both P(t) and $\gamma(t)$ in Eq. (2.4) must be measured. Two independent measurements are needed in all the methods used so far. First, a reference value of the fast fission factor, δ^*_{28}, is obtained in a particular lattice configuration by using the La^{140} counting technique discussed in Refs. (D1) and (W3). The quantity, $\gamma(t)$, is measured in the same lattice, and P(t) is determined by using Eq. (2.4) with the measured values of $\gamma(t)$ and δ^*_{28}. Once P(t) is determined, it will remain the same for all lattices with the same fuel rods, provided the counting setup remains unchanged. Hence, further determinations of δ_{28} require only the measurement of $\gamma(t)$, which is then used in Eq. (2.4).

Extensive measurements of P(t) in 1/4-inch rods have been made in the exponential facility at M.I.T. (B1, H5, D1). Since the counting arrangement in this work was the same as that used during the determinations of δ_{28} in the exponential assemblies, the value of P(t) was assumed to be the same. The value of P(t) was found to be independent of time and given by:

$$P(t) = 1.14 \pm 0.02 . \tag{2.6}$$

The quantity $\gamma(t)$ was measured by irradiating two uranium foils, one depleted in U^{235} and the other a natural uranium foil. The foils were inserted at the same position inside a fuel rod in the center cluster of the miniature lattice. The gross fission product activity of each foil was measured, and $\gamma(t)$ was calculated from the relation:

$$\gamma(t) = \frac{D_b^{FP}}{N_b^{FP}} , \tag{2.7}$$

where N refers to a natural uranium foil, the superscript FP indicates that the gross fission product activity was the measured activity, and the subscript b means that bare foils were irradiated.

2.7.3 The Parameter δ_{25}

The parameter δ_{25} is defined by the relation:

$$\delta_{25} = \frac{\text{average epicadmium } U^{235} \text{ fission rate in the fuel}}{\text{average subcadmium } U^{235} \text{ fission rate in the fuel}}, \tag{2.8}$$

or

$$\delta_{25} = \frac{A_{EC}^{25}}{A_{SC}^{25}}. \tag{2.9}$$

It is shown in Refs. (B1) and (H3) that δ_{25} is obtained from the measured fission product activities as:

$$\delta_{25} = \frac{\left[N_C^{FP} - \left(\frac{1-\epsilon_N}{1-\epsilon_D}\right)D_C^{FP}\right]}{\left[N_b^{FP} - \left(\frac{1-\epsilon_N}{1-\epsilon_D}\right)D_b^{FP}\right] - \left[N_C^{FP} - \left(\frac{1-\epsilon_N}{1-\epsilon_D}\right)D_C^{FP}\right]}, \tag{2.10}$$

where ϵ_N and ϵ_D are the atom fractions of U^{235} in the natural and depleted uranium detector foils, respectively. All activities in Eq. (2.10) are to be determined at the same time after simultaneous irradiation.

The value of δ_{25} was determined by irradiating two sets of foils in equivalent positions inside fuel rods in the experimental cluster; one set of foils was surrounded by cadmium. Each set consisted of a natural uranium foil and a depleted uranium foil. After the relative fission product activity of each foil was measured, δ_{25} was calculated from Eq. (2.10).

2.7.4 The Parameter C^*

The parameter C^* is defined by the relation:

$$C^* = \frac{\text{average total } U^{238} \text{ capture rate in the fuel}}{\text{average total } U^{235} \text{ fission rate in the fuel}} \tag{2.11}$$

It is shown in Ref. (D1) that C^* is given by:

$$C^* = C^*_M R_N / R_F, \tag{2.12}$$

where

$$R_N = \frac{A_b^{39}}{A_M^{39}} \tag{2.13}$$

is the ratio of the measured Np^{239} activity in a bare, depleted uranium foil irradiated in the lattice to that measured in a depleted foil irradiated in a Maxwellian flux (subscript M); R_F is given by:

$$R_F = \frac{A_b^{25}}{A_M^{25}}, \tag{2.14}$$

and represents the ratio of the measured U^{235} fission product activity in a bare foil irradiated in the lattice to the similar quantity measured in a Maxwellian flux; C^*_M denotes the value of C^* calculated for a Maxwellian flux and is given by:

$$C^*_M = \left(\frac{\Sigma_a^{28}}{\Sigma_f^{25}}\right)_M . \tag{2.15}$$

The quantities A_b^{39} and A_b^{25} were measured by irradiating a natural uranium foil and a depleted uranium foil back-to-back inside a fuel rod in the experimental cluster of the miniature lattice; A_M^{39} and A_M^{25} were determined by simultaneous irradiation of a natural uranium foil and a depleted uranium foil placed back-to-back in a small aluminum tube positioned on the center of the top of the miniature lattice tank. This position, which is 5 inches above the lattice, itself, faces directly the neutron source, the spectrum of which is very nearly Maxwellian (A2).

The Np^{239} activity of the depleted uranium foils and the gross fission product activity of both natural and depleted uranium foils were measured. The two ratios, R_N and R_F, were then obtained from the relations:

$$R_N = \frac{D_b^{39}}{D_M^{39}}, \tag{2.16}$$

and

$$R_F = \frac{N_b^{FP} - \left(\frac{1-\epsilon_N}{1-\epsilon_D}\right) D_b^{FP}}{N_M^{FP} - \left(\frac{1-\epsilon_N}{1-\epsilon_D}\right) D_M^{FP}}. \tag{2.17}$$

The value of C^* can also be obtained from the measured values of ρ_{28} and δ_{25}, by means of the relation (W2):

$$C^* = \frac{1+\rho_{28}}{1+\delta_{25}} \left(\frac{\Sigma_a^{28}}{\Sigma_f^{25}}\right)_{SC}, \tag{2.18}$$

where $\left(\Sigma_a^{28}/\Sigma_f^{25}\right)_{SC}$ is the ratio of U^{238} capture rate in the fuel to the fission rate of U^{235} in the fuel below the cadmium cutoff energy of about 0.4 ev.

2.7.5 Experimental Arrangement for the Measurement of ρ_{28}, δ_{25}, δ_{28} and C^*

The four parameters described in this section were measured by irradiating simultaneously three sets of uranium detector foils. Each set consisted of a natural uranium foil and a depleted uranium foil. Two of the sets were irradiated in the experimental cluster of the miniature lattice, and the other set was irradiated at the center of the top of the miniature lattice tank. One of the sets in the experimental cluster was surrounded by 0.020-inch-thick cadmium.

The foils used were 1/4 inch in diameter and 0.005 inch-thick. The depleted uranium had a measured atom concentration of eighteen U^{235} atoms per million U^{238} atoms (W2). Both the natural and depleted uranium, obtained from the Oak Ridge National Laboratory, were of high purity and no observable activities due to impurities were produced during irradiation. The foils used in these experiments were the same that were employed in the corresponding determinations made in the exponential facility. The foils were weighed with an accuracy of about 0.02% on a high precision balance.

Fuel slugs of different lengths, varying from 0.020 inch to 10 inches were available. Thus, by appropriate combination of slugs, detector foils could be located inside an experimental rod at any desired height.

A foil packet was made up for each set of foils placed in the lattice. Each detector foil was sandwiched between two uranium "catcher" foils, identical in size and composition to the detector foil. The catcher foils prevent the contamination of the detector foil by fission products produced in uranium of a different U^{235} concentration. The three depleted uranium foils and the three natural uranium foils were placed back-to-back between two 0.060-inch-thick fuel buttons.

The foil assemblies were placed between two fuel slugs in a fuel element. In the case of the cadmium-covered detector foil assembly, a 0.020-inch-thick cadmium sleeve was positioned outside the 0.028-inch-thick aluminum cladding of the fuel element. The midpoint of the cadmium sleeve was positioned so as to coincide with the midpoint of the foil packet. A schematic diagram of the foil arrangement is shown in Fig. 2.11.

The bare detector foils and the cadmium-covered foils were irradiated at heights between 8 and 10 inches from the source end of the lattice, and in two diametrically opposite fuel rods adjacent to the central fuel rod in the experimental cluster. Bare gold foils were placed in each fuel rod about 3-1/2 inches below the foil packets so that the flux at the uranium detector foil locations could be monitored and normalized if necessary. The gold monitor foils were 0.250 inch in diameter and 0.005 inch thick. Figure 2.12 shows the fuel rod arrangements and detector foil locations.

The set of foils irradiated on top of the miniature lattice tank had each detector foil sandwiched between two foils identical in size and composition to the detector foil. The three depleted uranium foils and

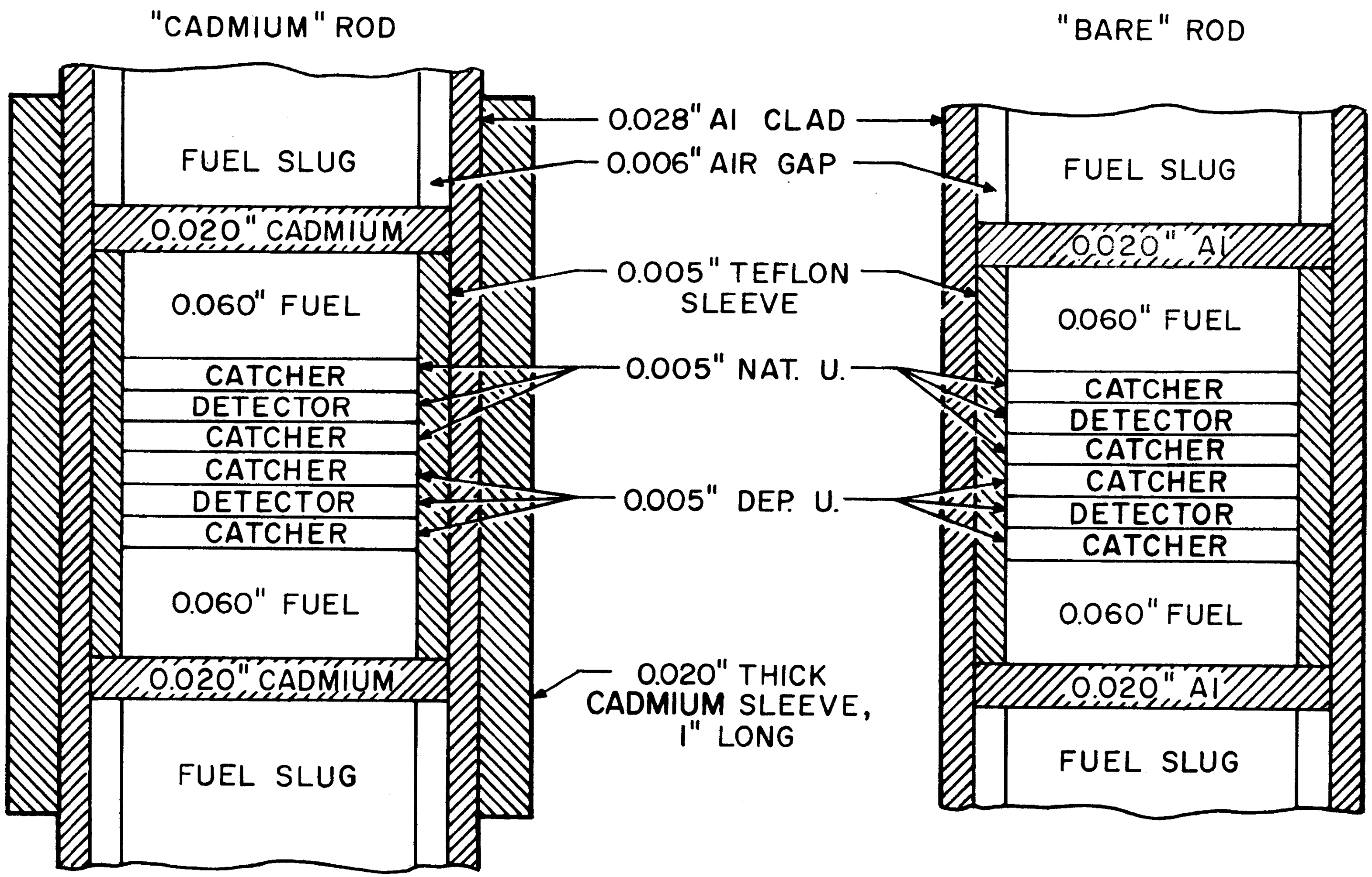

URANIUM FOIL ARRANGEMENTS IN THE FUEL RODS FOR ρ_{28}, δ_{28}, δ_{25} AND C* MEASUREMENTS

FIG. 2.11

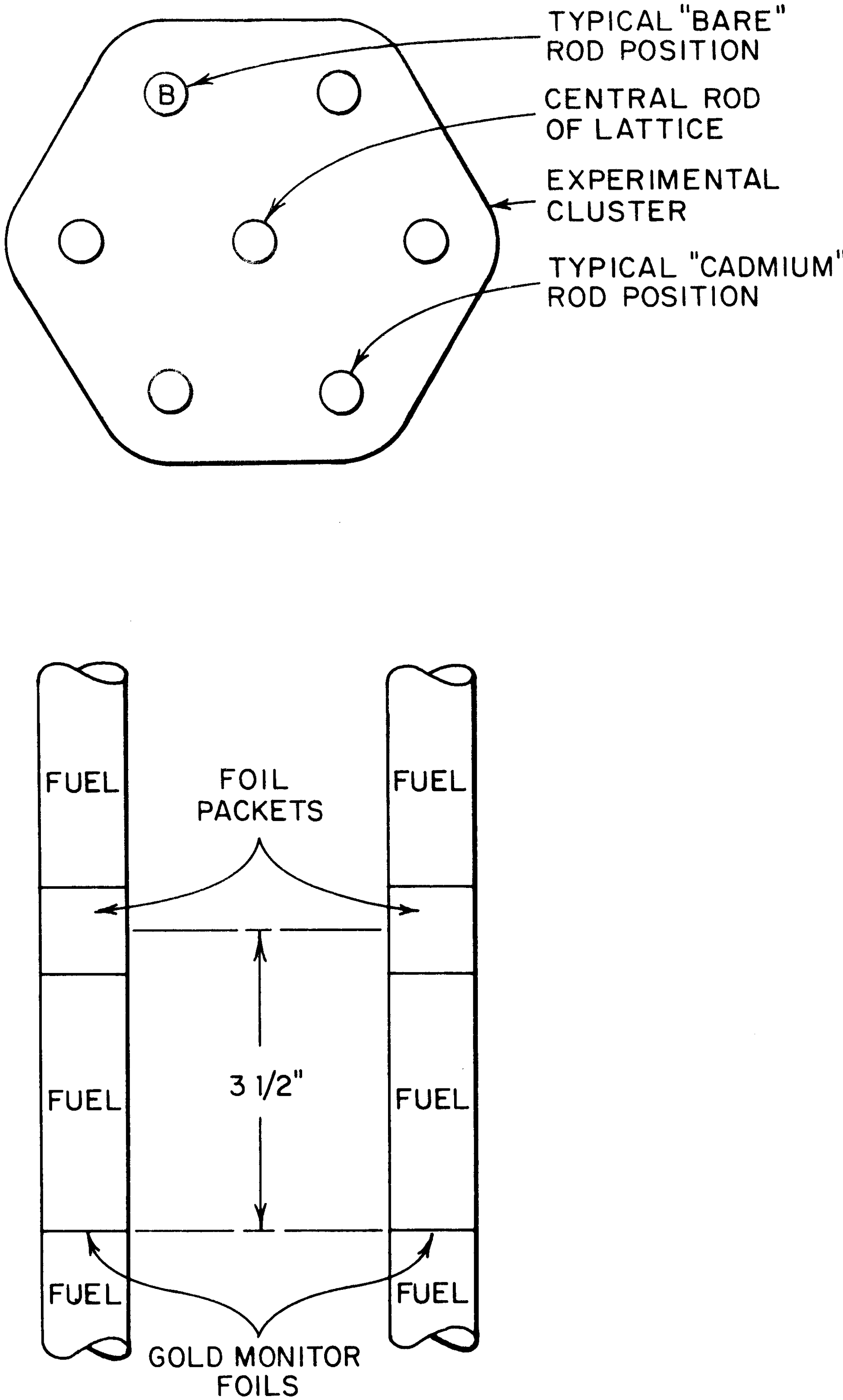

FIG. 2.12 FUEL ROD ARRANGEMENT AND FOIL PACKET LOCATIONS FOR THE MEASUREMENT OF ρ_{28}, δ_{28}, δ_{25}, AND C*

the three natural uranium foils were placed back-to-back inside a 2-inch-long, 1/4-inch-diameter aluminum sleeve. Two 1/4-inch-diameter aluminum rods were inserted from both ends to keep the foil set tight and centered. The packet was held in place on the tank by Mylar tape. The foil arrangement is shown in Fig. 2.13.

2.7.6 Counting Techniques for Np^{239} and Fission Product Activities

The depleted uranium detector foils were counted for gamma activity from both fission products and Np^{239}. Natural foils were gamma-counted for fission product activity only.

The fission product counting equipment consisted of a Baird Atomic Model 815 BL scintillation detector, a Baird Atomic Model 215 linear amplifier, and a Baird Atomic Model 960 timer. The scintillation detector contained a 1-3/4-inch-thick, 2-inch-diameter NaI(T1) crystal, an RCA 6342A photomultiplier and a preamplifier. A schematic diagram is shown in Fig. 2.14. The foils were counted for fission activity by the integral gamma-ray counting technique with a baseline corresponding to 0.72 Mev. Before being counted, the foils were allowed to cool for about four hours to let the 23-minute U^{239} activity formed decay almost completely to Np^{239}. In its decay process, U^{239} emits a 1.2-Mev beta ray. The cooling period prevents the possible inclusion in the fission product counting of the 1.2-Mev beta-ray bremsstrahlung radiation. The foils were counted between about 4 and 10 hours after irradiation. After 10 hours, the activity of the depleted foils was too low to give statistically meaningful data. The 667-kev and 840-kev photopeaks of Cs^{137} and Mn^{54}, respectively, were used to calibrate the setup. The foils were counted for six consecutive passes.

Counting of the Np^{239} activity in the depleted uranium foils was begun between 4 and 18 hours after the counting of the fission product activity was completed. The counting system consisted of an integral-counting probe unit containing a 1/2-inch-thick, 1-1/2-inch-diameter NaI(T1) crystal and an RCA 6342A photomultiplier; a preamplifier built by Mr. Gwinn, a Sturrup, Inc. Model 4201 high voltage supply and a Radiation Instrument Development Laboratory (RIDL) single-channel spectrometer. The spectrometer consisted of a RIDL Model 30-19

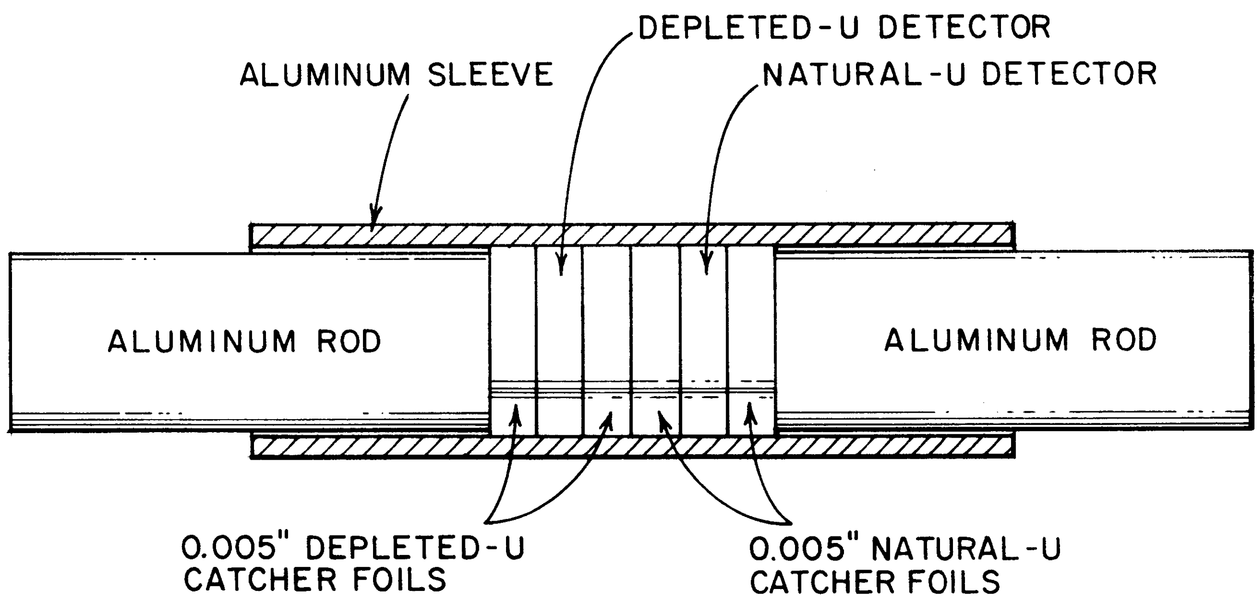

FIG. 2.13 FOIL ARRANGEMENT FOR IRRADIATION OF URANIUM FOILS IN MAXWELLIAN FLUX

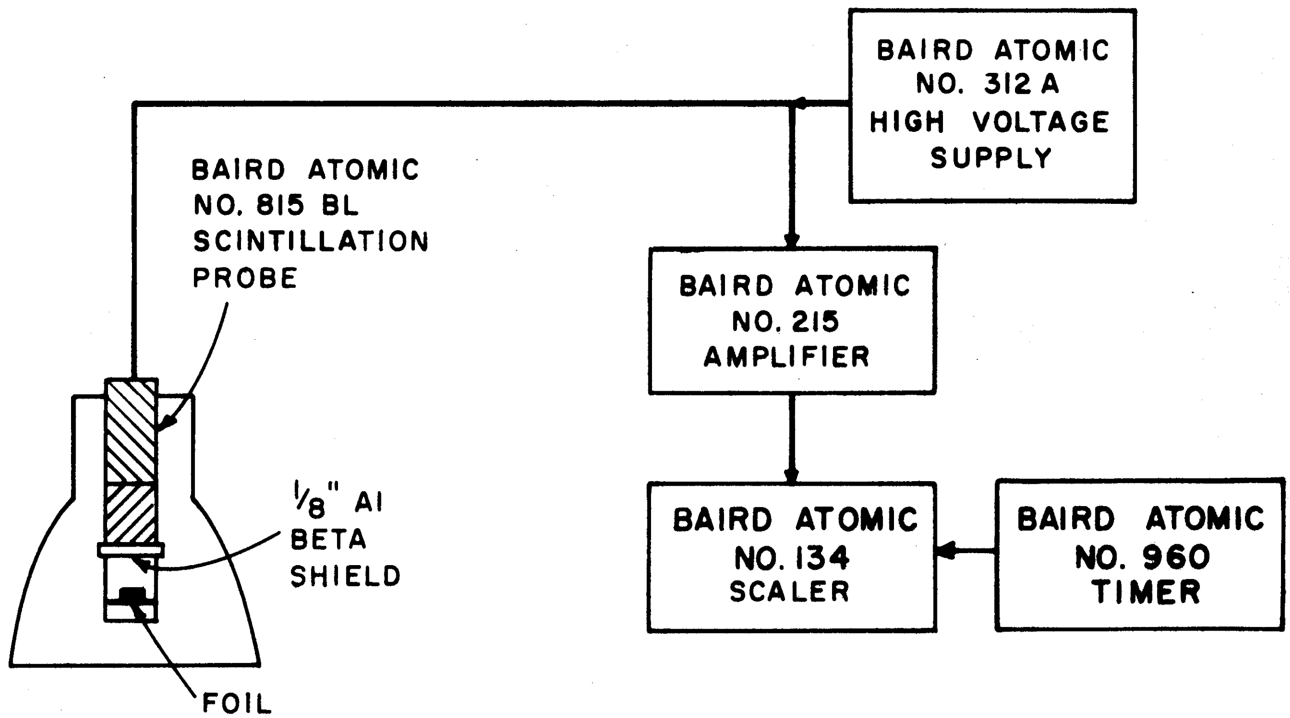

COUNTING SYSTEM USED TO MEASURE THE GROSS FISSION PRODUCT ACTIVITY OF THE NATURAL AND DEPLETED URANIUM FOILS

FIG. 2.14

amplifier, a RIDL Model 33-10 single-channel analyzer and a RIDL Model 49-25 combination scaler-timer, all mounted in a RIDL Model 29-1 chassis. A diagram of the setup is shown in Fig. 2.15. A differential gamma-ray counting method was utilized. The 103-kev peak in the gamma- and X-ray spectrum of Np^{239} was straddled with a window width corresponding to 38 kev. The lower limit of the analyzer window was set at an equivalent energy of 84 kev; the upper limit, at 123 kev. The 84-kev gamma ray of Tm^{170} was used to set the lower limit of the window, and the 123-kev gamma ray of Co^{57}, to set the upper limit. The calibration was made every time the system was used. Between six and nine passes were made with each foil.

The gold monitor foils were counted in the fission product counting system. The foils were integral-counted with the baseline set at the minimum before the 411-kev photopeak of Au^{198} (about 320 kev).

2.8 EXPERIMENTAL PROCEDURE

2.8.1 Macroscopic and Microscopic Gold Activity Traverses

The same experimental procedure was followed for the measurement of the axial and radial traverses and the intracellular distribution of gold.

Before irradiation, all foil holders were cleaned with acetone, then loaded in the miniature lattice and the lattice tank lid tightly bolted to the base plate. The assembly was then purged with nitrogen gas for about 20 minutes, so that an inert atmosphere was present in the tank during irradiation. The tank was then slowly filled with heavy water and all the valves tightened. While the experimental setup was being prepared for irradiation, care was taken to insure that the centerlines of both lattice and neutron source were as closely aligned as possible, since this is of particular importance in miniature lattice experimentation. The alignment obtained was good to within one-eighth of an inch. The lattice was then irradiated for two hours.

To minimize the dose rate to the experimenter, it was found convenient to let the lattice cool until the morning after irradiation. The assembly was then removed, drained and dismantled; the foils were removed from the lattice and placed on special aluminum trays for counting on either of the automatic systems described in Section 2.6.

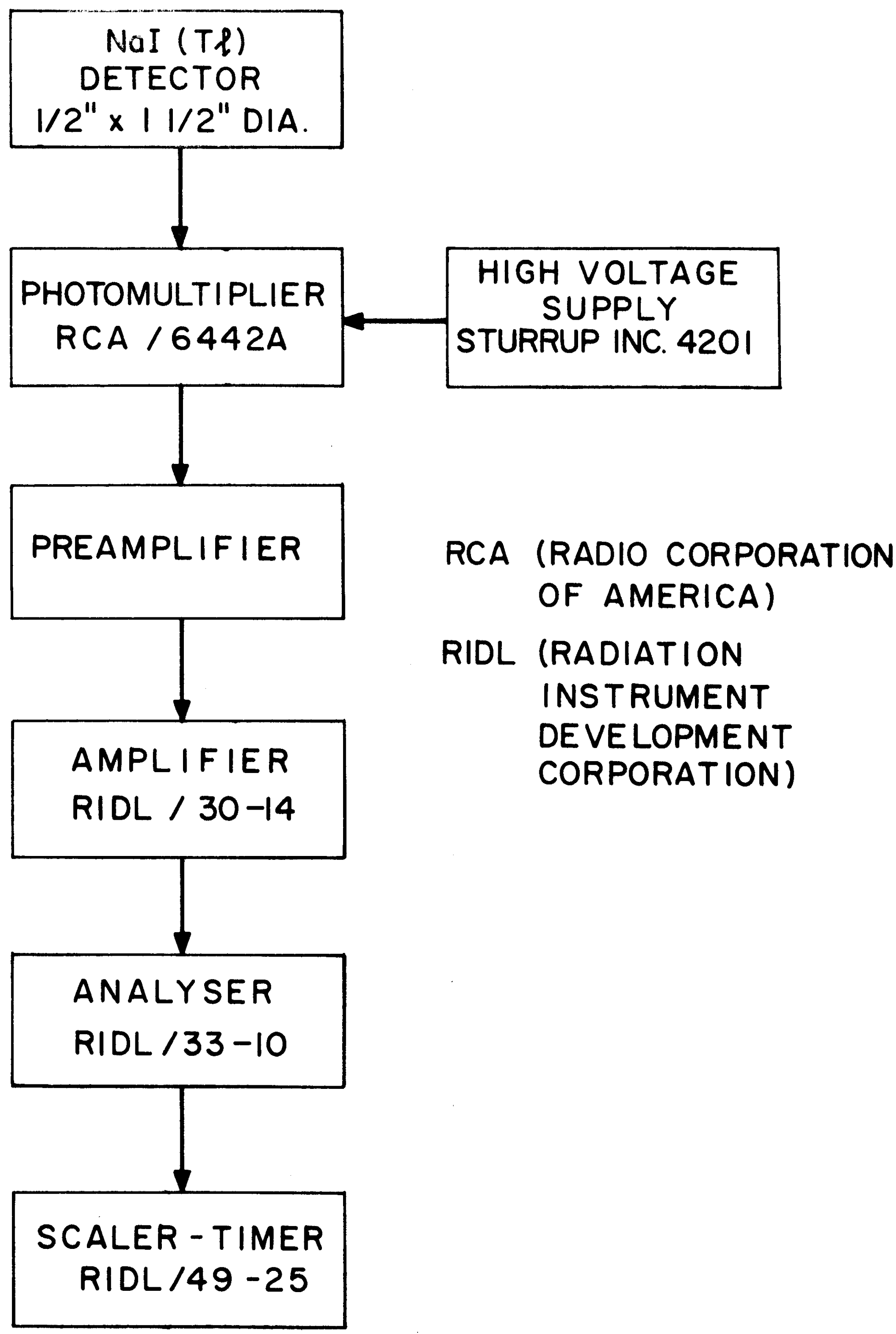

FIG. 2.15 COUNTING SYSTEM USED TO MEASURE THE Np^{239} ACTIVITY OF THE DEPLETED URANIUM FOILS

2.8.2 Experimental Procedure for the Measurement of ρ_{28}, δ_{28}, δ_{25} and C^*

The uranium detector foils to be irradiated were chosen so as to have minimum weight differences among themselves. The foils were cleaned with acetone and mounted on aluminum planchets. The two counting systems, the Np^{239} counting system and the fission product counting system, were calibrated as described in Section 2.7.6. The natural uranium foils were background-counted in the fission product activity counting system; the depleted uranium foils were background-counted in both the fission product activity and the Np^{239} counting systems to determine the natural and residual activities of the foils. In addition, a natural uranium foil and a depleted uranium foil, both with irradiation histories similar to those of the detector foils, were also background-counted. These additional foils were not irradiated and were counted with the detector foils each time they were counted after irradiation. This procedure allowed monitoring of the background of the detector foils from the time their background was counted to the time they were counted after irradiation.

The foils were loaded in the lattices as described in Section 2.7.5. The irradiation then proceeded as in the case of the macroscopic and microscopic gold activity traverses. After a two-hour irradiation, the lattices were allowed to cool for about two hours. As the dose rate levels at this time were high, the removing, draining and dismantling of the assembly had to be done quickly. After the experimental fuel rods were removed, the detector and monitor foils were unloaded inside a glove box and cleaned with acetone. Each foil was then remounted on the aluminum trays used to background-count them before irradiation.

The fission product counting system was then calibrated and all the uranium foils were counted for fission product activity from about four to ten hours after irradiation. The room background and control foils were counted in each of the six passes made through the counter.

The depleted uranium detector foils were Np^{239}-counted as described in Section 2.7.6 once or twice a day for several days after irradiation. The foils of each experiment were counted at least six times. The control background foil and room background were counted each time the detector foils were counted.

After all the detector foils had been counted, the monitor gold foils were counted as described in Section 2.7.6.

CHAPTER 3
THEORETICAL METHODS

3.1 INTRODUCTION

The theoretical methods used in this work are discussed in this chapter. The four factors in k_∞ will be defined, and the role played by the measurable parameters defined in Section 2.7 will be pointed out. The relation between C^* and the initial conversion ratio, C, will also be discussed.

The measurable parameters defined in Section 2.7 are often measured in an assembly different from that in which their values are desired. The problem of extrapolating the data from the assembly in which they are obtained to that in which they are desired will be discussed as well as the effects that must be considered.

A method, based on age-diffusion theory, will be developed which allows the extrapolation of the values of the parameters ρ_{28}, δ_{25} and C^* measured in the miniature lattice to those appropriate to an exponential, a critical and an infinite assembly. A model, based on the work of Woodruff (W4), is also discussed. This model permits the extrapolation of the value of δ_{28} measured in the miniature lattice to that in an exponential assembly and in an infinite lattice. The procedure which allows the correction of the measured intracellular subcadmium activity distribution of gold to that which would be obtained in an infinite assembly is also discussed.

The corrections derived in this chapter will be applied to the data obtained in the miniature lattice and the results compared with analogous measurements made in the exponential facility at M.I.T. This comparison will be made in Chapter 4.

3.1.1 Relation of Measurable Parameters to k_∞ or C

The multiplication factor in an infinitely large assembly, k_∞, is defined as follows:

$$k_\infty = \frac{\text{total number of neutrons produced by fission}}{\text{total number of neutrons absorbed}} .$$

The usual procedure is to express k_∞ as:

$$k_\infty = \eta \epsilon p f , \tag{3.1}$$

where the four factors must be determined for an infinite assembly. In defining the four factors in Eq. (3.1), it is important that all processes occurring in the assembly be accounted for. From the point of view of the experimentalist, it is convenient to separate the processes occurring in subcadmium reactions from those that take place in the epicadmium and high energy ranges. Accordingly, we define:

$$\eta = \frac{\text{number of neutrons produced by all fissions in } U^{235}}{\text{number of subcadmium neutrons absorbed in the fuel}} ,$$

which may be expressed as:

$$\eta = \eta_{SC} \xi , \tag{3.2}$$

where

$$\eta_{SC} = \frac{\text{number of neutrons produced by subcadmium fissions in } U^{235}}{\text{number of subcadmium neutrons absorbed in the fuel}} ,$$

and is given by:

$$\eta_{SC} = \nu_{25}^{SC} \left(\frac{\Sigma_f^{25}}{\Sigma_a^{25} + \Sigma_a^{28}} \right)_{SC} . \tag{3.3}$$

The subscript SC indicates that the quantities must be averaged over the energy spectrum below the cadmium cutoff energy; η_{SC} cannot be measured directly and is, in general, a calculated quantity. The factor ξ corrects η_{SC} for epicadmium fission in U^{235}. It is defined as:

$$\xi = \frac{\text{net number of neutrons produced by all fission in } U^{235}}{\text{number of neutrons produced by subcadmium fission in } U^{235}} ,$$

and is given by:

$$\xi = 1 + \delta_{25}^{\infty} \frac{\nu_{25}^{EC} - 1 - \alpha_{25}^{EC}}{\nu_{25}^{SC}} , \tag{3.4}$$

where ν_{25}^{EC} is the number of neutrons produced per epicadmium fission in U^{235}, and

$$\alpha_{25}^{EC} = \left(\frac{\sigma_c^{25}}{\sigma_f^{25}}\right)_{EC} . \tag{3.5}$$

The subscript ∞ on the measurable parameter δ_{25}, defined in Eq. (2.8), denotes the value of δ_{25} that would be measured in an infinite assembly.

The fast fission factor, ϵ, is defined as the ratio:

$$\epsilon = \frac{\text{net number of neutrons produced by all fissions}}{\text{number of neutrons produced by fissions in } U^{235}} ,$$

and is given by:

$$\epsilon = 1 + \delta_{28}^{\infty} \frac{\nu_{28} - 1 - \alpha_{28}}{\nu_{25}} , \tag{3.6}$$

where ν_{28} is the number of neutrons produced by fission in U^{238}, and

$$\alpha_{28} = \left(\frac{\sigma_c^{28}}{\sigma_f^{28}}\right) .$$

Again, δ_{28}^{∞} denotes the value of the measurable parameter δ_{28}, defined in Eq. (2.3), that would be measured in an infinite assembly. The value of ν_{25} in Eq. (3.6) must be properly averaged over the subcadmium and epicadmium energy ranges. Since ν_{25}^{EC} is very nearly equal to ν_{25}^{SC}, we may set:

$$\nu_{25} \simeq \nu_{25}^{SC} .$$

The thermal utilization factor, f, is defined by the relation:

$$f = \frac{\text{number of subcadmium neutrons absorbed in the fuel}}{\text{total number of subcadmium neutrons absorbed in the assembly}} ,$$

and is given by:

$$f = \frac{\Sigma_a^F V_F \phi_F^{\infty}}{\Sigma_a^F V_F \phi_F^{\infty} + \Sigma_a^C V_C \phi_C^{\infty} + \Sigma_a^M V_M \phi_M^{\infty}} . \tag{3.7}$$

In Eq. (3.7), the subscripts F, C and M stand for fuel, cladding and moderator, respectively; Σ_a is the absorption cross section averaged over the subcadmium energy range, V is the volume, and $\phi^{\infty}_{( )}$ is the average subcadmium flux in the region designated by the subscript that would exist in an infinite assembly.

To close the neutron cycle, p, the resonance escape probability or, more accurately, the epicadmium absorption escape probability, must be defined as follows:

$$p = \frac{\text{number of subcadmium neutrons absorbed in the assembly}}{\text{total number of neutrons absorbed in the assembly}} ,$$

or

$$p = 1 - \frac{\text{number of epicadmium neutrons absorbed}}{\text{total number of neutrons absorbed}} ,$$

which can be expressed as (P3):

$$p = 1 - \frac{G\rho^{C}_{28}}{\eta\epsilon\mathcal{L}_r} , \tag{3.8}$$

where

$$G = \left(\frac{\Sigma^{28}_a}{\Sigma^{28}_a + \Sigma^{25}_a} \right)_{SC} ,$$

and $\mathcal{L}_r$ is the nonleakage probability for neutrons slowing down from fission energies to the effective resonance energy of U^{238} (e. g., $\mathcal{L}_r = e^{-B^2\tau_{28}}$). In Eq. (3.8), ρ^{C}_{28} represents the value of the parameter ρ_{28}, defined in Eq. (2.1), that would be measured in a critical assembly; η is given by Eq. (3.2) and ϵ by Eq. (3.6).

The formula for p, Eq. (3.8), differs from that derived by Kouts and Sher (K2) in that it includes 1/v epicadmium absorptions in U^{238}. Furthermore, Eq. (3.8) is obtained by starting the neutron cycle with one subcadmium neutron absorbed in the fuel, rather than one neutron born from fission in U^{235}. The value of p given by Eq. (3.8) is, consequently, slightly smaller than that obtained from the formula of Kouts and Sher. Their formulation, however, gives a smaller value of f, since the total absorptions in the cell must include 1/v epicadmium absorptions in U^{238}. The product, pf, however, is the same in the two formulations.

The formulation given here seems to be more convenient from the point of view of the experimentalist for two reasons. First, it does not require that the gold cadmium ratio in the fuel be measured to permit the subtraction of the 1/v captures from ρ_{28}, which is at best an inaccurate procedure. Second, Eq. (3.8) requires the knowledge of fewer quantities to obtain p from ρ_{28}^{C} than the formulation of Kouts and Sher, thus reducing the possibility of errors.

The definitions given in this section form a consistent and precise set. The only assumption that has been made is the hypothesis that epicadmium absorption is negligible in the moderator and cladding. In the lattices under consideration here, this assumption is valid.

The initial conversion factor, C, cannot be measured directly. It can be obtained, however, from the experimentally measurable quantity, C^*, defined in Eq. (2.11). They are related by the formula:

$$C = \frac{C^*}{(\overline{1+\alpha_{25}})}, \tag{3.9}$$

where

$$(\overline{1+\alpha_{25}}) = \left(\frac{\overline{\Sigma_a^{25}}}{\Sigma_f^{25}}\right). \tag{3.10}$$

The average of the ratio in Eq. (3.10) must be made over the whole energy range. The lattices under study in this work were all well thermalized so that the ratio in Eq. (3.10) is very nearly the average over the subcadmium energy range.

The value of C of interest is that in the assembly to be built, namely, the value in a critical lattice.

3.1.2 Need For Correction Factors

From the previous discussion, it is evident that one is especially interested in the values of ρ_{28} and C^* that would be measured in a critical assembly. The values of δ_{25}, δ_{28} and the intracellular subcadmium activity distribution which are of interest are those that would be measured in an infinite assembly. An infinite lattice can, of course, not be built and it is not always desirable or possible to perform measurements in a critical facility. Experimentation is then carried out in subcritical assemblies. Results obtained from subcritical lattices must, however, be corrected for source and boundary effects to obtain the desired parameters.

When the lattice parameters are determined in a large exponential facility, the values of interest are those obtained in the equilibrium region. This region is located far from source and boundaries so that their effect is greatly reduced. As a consequence, the neutron spectrum is nearly independent of position and resembles closely that in a critical assembly.

A miniature lattice differs from an exponential assembly of similar composition, in that its dimensions are such that boundary and source effects become important. Because of its small size, an equilibrium region is, in general, not achieved. Parameters obtained in a miniature lattice must, therefore, be properly corrected for these effects.

In conclusion, a feasibility study of miniature lattices must include, besides experimental determinations of the parameters of interest, a method which permits the extrapolation of the values obtained to values that would be appropriate to an exponential, a critical or an infinite assembly.

3.2 SUBCRITICAL ASSEMBLIES

The problem of subcritical assemblies is discussed in this section. The theoretical model that will be developed is applicable to both exponential and miniature lattices.

3.2.1 Discussion of Problem

To determine the thermal neutron flux and slowing-down density in the miniature lattice, source and boundary effects must be taken into account.

Source effects are generally of three kinds. First, the neutrons coming from the source (often a well-thermalized source) have a spectrum which is different from the spectrum of those neutrons that are born in the lattice. After a few collisions in the lattice, the spectrum of the source neutrons will approach the spectrum of the neutrons born in the assembly. Hence, a complex transition of the neutron spectrum occurs near the source. Second, the anisotropy of the source results in the presence of harmonics. Third, the source may be axially asymmetric; i. e., it may have an azimuthal dependence.

Boundaries contribute several difficulties to the problem: first, they introduce spatial harmonics; second, because of the small size of the assembly, the leakage of neutrons during the slowing-down process is greater than the leakage from the similar exponential lattice, resulting in a harder spectrum; third, the extrapolated dimensions of the assembly are particularly important, so that the boundaries of the neutron distribution must be defined with precision. Considerable improvement in defining the boundaries was obtained by designing the shielding that surrounds the assembly as described in Section 2.2. The first layer of cadmium is effective in defining the boundary for thermal neutrons; the subsequent layers helped considerably in defining the boundary for epithermal neutrons, although to a lesser extent.

The theory given in this section is aimed at taking into account the effects discussed above.

3.2.2 Assumptions

In the present development, the validity of age-diffusion theory is assumed. The hypotheses involved will be examined in some detail.

The lattices of interest in this investigation are widely spaced (in the tightest lattice, $V_M/V_F \simeq 25$), so that most of the volume is occupied by moderator. Consequently, $\Sigma_a/\Sigma_T \ll 1$ and diffusion theory is applicable. Near the source, transport effects are important. In this work, however, the theory will be used largely to describe the spatial distribution of cadmium ratios; the experimental results that will be reported in Chapter 4 indicate that for this purpose transport effects may be neglected. It will appear, however, from the discussion in Section 5.4, that transport effects are important to predict separately the axial distribution of the activity of bare and cadmium-covered gold foils.

The use of age theory to treat the slowing-down process in D_2O-moderated assemblies has been investigated in Ref. (L1). The expression for the fast nonleakage probability derived from age theory, $e^{-\tau B^2}$, is compared with a more precise expression calculated with the Greuling-Goertzel approximation, which does not involve the assumption of continuous slowing down basic to age theory. The comparison was made for assemblies moderated by deuterium. Although no single value of τ was found to give agreement between the age theory expression and those of the Greuling-Goertzel treatment for all values of B_m^2, for practical reactors ($B_m^2 \leq 0.01$ cm^{-2}), the range of values was found to be small (101.6 cm^2 to 107.2 cm^2 for the age from 2 Mev to the In resonance at 1.4 ev).

An experimental justification for the use of age theory to describe the slowing-down process in heavy water comes from the numerous age determinations that have been made in pure moderator (e. g., Ref. (W6)). Age measurements, like those described in Appendix D for the age of fission neutrons to the resonance of gold at 4.906 ev, indicate that the slowing-down kernel obtained from age theory describes the slowing-down density in pure moderator reasonably well.

On the basis of these arguments, it seemed justifiable to assume that age-diffusion theory should give an adequate representation of the flux and the slowing-down density in the assemblies of interest in this work. The ultimate test must, of course, be the ability of age-diffusion theory to do so, as shown by the experimental results.

To account for the difference in spectrum between source neutrons and lattice-born neutrons, it will be assumed that the thermal flux has two components. The flux of thermal neutrons provided by the source is denoted by ϕ_s; ϕ_ℓ represents the flux of thermal neutrons born in the lattice; Σ_a^s, D^s and L_s are, respectively, the thermal absorption cross section, the diffusion coefficient and the thermal diffusion length averaged over the energy spectrum of the source neutrons; Σ_a^ℓ, D^ℓ and L_ℓ denote the corresponding nuclear constants for the spectrum characteristic of the lattice.

In a cylinder, ϕ_s satisfies the equation:

$$D^s \nabla^2 \phi_s(r, z) - \Sigma_a^s \phi_s(r, z) = 0, \tag{3.11}$$

since source neutrons can only escape from the assembly or be absorbed in it. The boundary conditions are:

$$\phi_s(r,H) = \phi_s(R,z) = 0 \ ; \ -D^s\left[\frac{\partial\phi_s(r,z)}{\partial z}\right]_{z=0} = S(r), \tag{3.12}$$

where R and H are the extrapolated radius and height of the lattice, respectively, and S(r) represents the neutron source as a function of radius.

The thermal flux due to neutrons born in the lattice, ϕ_ℓ, satisfies the equation:

$$D^\ell\nabla^2\phi_\ell(r,z) - \Sigma_a^\ell\phi_\ell(r,z) + pq(r,z,\tau_t) = 0, \tag{3.13}$$

where $q(r,z,\tau_t)$ is the slowing-down density at τ_t, the age to thermal energies (~5 kT) and p is the resonance escape probability. The slowing-down density, $q(r,z,\tau)$, is assumed to satisfy the age equation:

$$\nabla^2 q(r,z,\tau) = \frac{\partial}{\partial\tau} q(r,z,\tau), \tag{3.14}$$

without absorption; the effect of absorption is included in p.

The only boundary conditions that can be specified for q and ϕ_ℓ are:

$$q(r,H,\tau) = q(R,z,\tau) = \phi_\ell(r,H) = \phi_\ell(R,z) = 0. \tag{3.15}$$

An initial condition can also be specified for $q(r,z,\tau)$:

$$q(r,z,\tau{=}0) = \frac{k_\infty}{p}\left[\Sigma_a^s\phi_s(r,z)+\Sigma_a^\ell\phi_\ell(r,z)\right]. \tag{3.16}$$

In other words, the neutrons that begin the slowing-down process come from fissions induced by source neutrons and by lattice-born neutrons.

The determination of the boundary condition for ϕ_ℓ and q at the source end presents a more complex problem. Because of neutron leakage due to the proximity of the source boundary during slowing down, $q(r,z,\tau)$ as a function of z and τ behaves as indicated in Fig. 3.1; that is, q goes to zero at different values of the extrapolation distance, depending on the value of τ. In other words, the neutrons that begin the slowing-down process will follow closely the thermal flux distribution, as implied by the initial condition, Eq. (3.16). As they proceed to slow down, the neutrons near the source end will escape more readily from the assembly than those neutrons that are further inside the assembly;

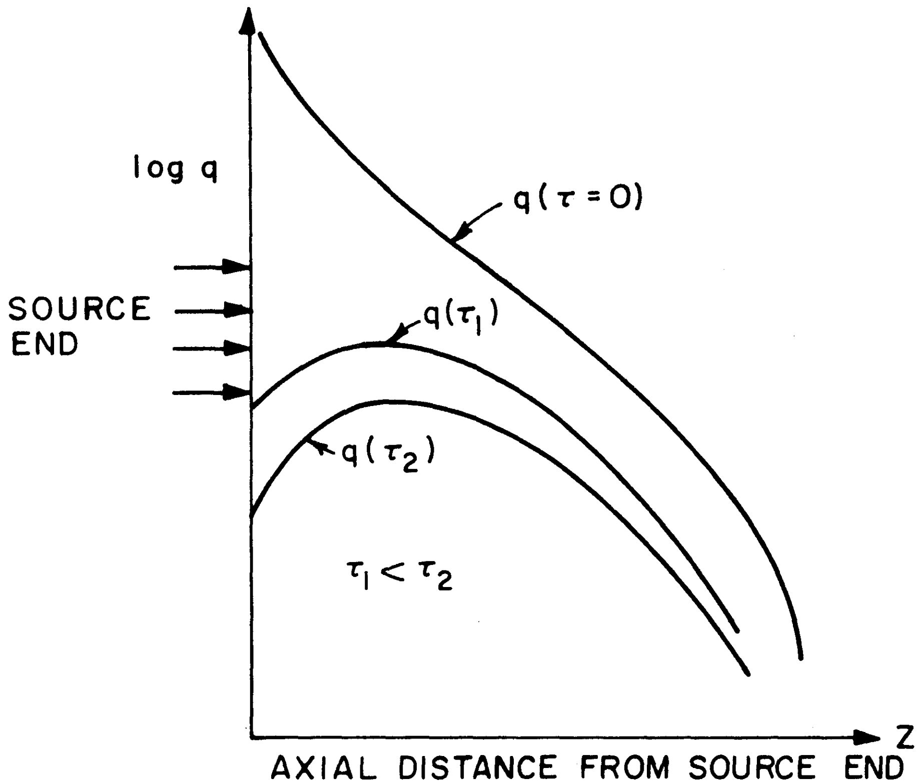

FIG. 3.1 BEHAVIOUR OF q AS A FUNCTION OF Z AND τ IN A SUBCRITICAL ASSEMBLY

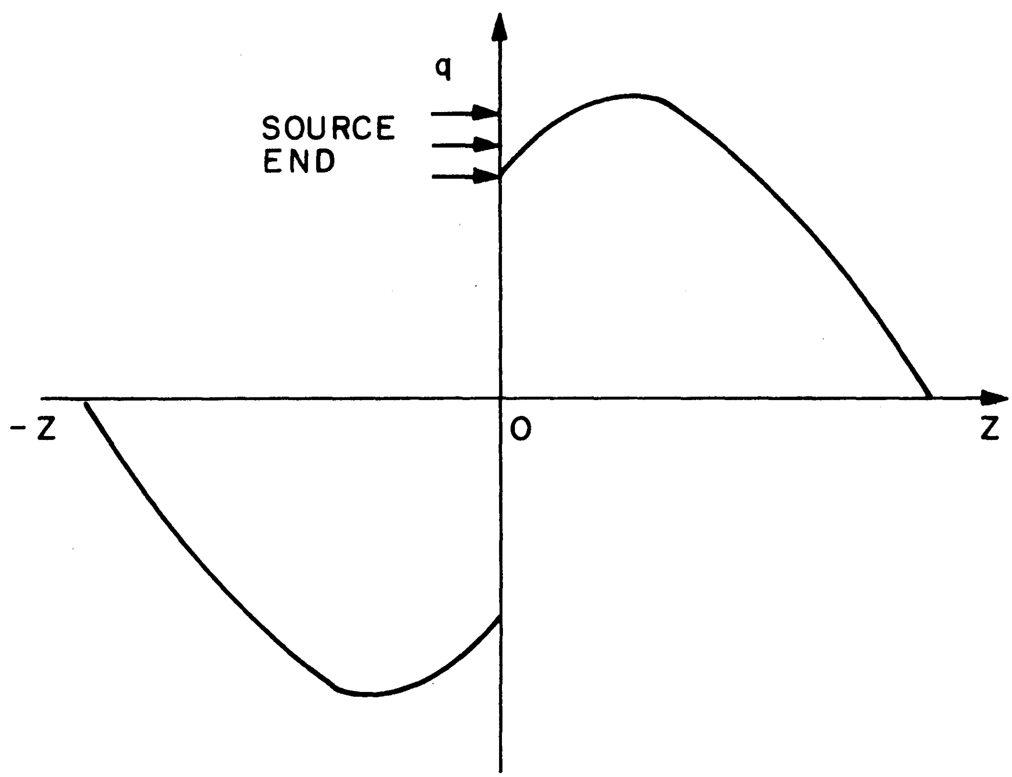

FIG. 3.2 ASSUMPTION OF PERIODICITY OF $q(Z, \tau)$

the depletion of neutrons near the source end will continue to increase with increasing values of τ. Hence, near the source end, one is faced with a problem in which the energy and space dependence are not separable. The attempt to use a variable extrapolation length would lead to a complicated mathematical problem.

It is known, however, that if the assembly were bare and critical, the thermal flux and the slowing-down density would have the same spatial dependence, vanishing at approximately the same extrapolation distance. In a cylindrical assembly, this spatial variation is given by:

$$J_o(\alpha r) \sin(\pi z/H), \tag{3.17}$$

where $\alpha = 2.405/R$. It seems reasonable, therefore, to approximate the solution of the nonseparable problem in subcritical assemblies by expansion of ϕ_ℓ and q in the characteristic functions of a bare, and critical, cylindrical assembly. Since the characteristic function in the z-direction is a sine, the distributions must be antisymmetric about the origin. In view of the behavior of q near zero, and the antisymmetry of the characteristic functions, it seems reasonable to assume that ϕ_ℓ and q go through zero at the source end in a discontinuous manner, as shown in Fig. 3.2, and that they are both cyclic with period 2H. Under this assumption, ϕ_ℓ and q satisfy Dirichlet's conditions (S3) and may, therefore, be expanded in cylindrical harmonics. The formalism in the next section then suggests itself for the solution of this problem.

3.2.3 Derivation of Theoretical Model

To expand the thermal flux and the slowing-down density in cylindrical harmonics, the following theorems (S3) will be used.

1. If f(r) satisfies Dirichlet's conditions in the interval (0,R) and if its finite Hankel transform in that range is defined to be:

$$\bar{f}_i = \int_0^R r f(r) J_o(\alpha_i r)\, dr, \tag{3.18}$$

where α_i is a root of the trancendental equation, $J_o(\alpha_i R) = 0$, then at any point of (0,R) at which the function f(r) is continuous:

$$f(r) = \frac{2}{R^2} \sum_{i=1}^{\infty} \bar{f}_i \frac{J_o(\alpha_i r)}{[J_1(\alpha_i R)]^2} . \tag{3.19}$$

2. If f(z) satisfies Dirichlet's conditions in the interval (0, H) and if in that range its finite sine transform is defined to be:

$$\bar{f}(n) = \int_0^H f(z) \sin \frac{n\pi z}{H} \, dz , \tag{3.20}$$

then, at each point of (0, H) at which f(z) is continuous:

$$f(z) = \frac{2}{H} \sum_{i=1}^{\infty} \bar{f}(n) \sin \frac{n\pi z}{H} . \tag{3.21}$$

If the first theorem is applied to the Laplacian operator in circular cylindrical coordinates, with no azimuthal dependence,

$$\nabla^2 f = \frac{1}{r} \frac{\partial}{\partial r} r \frac{\partial f}{\partial r} + \frac{\partial^2 f}{\partial z^2} ,$$

we have:

$$\int_0^R r[\nabla^2 f] J_o(\alpha_i r) \, dr = -\alpha_i^2 \bar{f}(\alpha_i, z) + \frac{\partial^2 \bar{f}(\alpha_i, z)}{\partial z^2} , \tag{3.22}$$

where the assumption has been made that f(R, z) = 0.

If the second theorem is applied to the second derivative, with f(0) = f(H) = 0, then:

$$\int_0^H \frac{\partial^2 f(z)}{\partial z^2} \sin \frac{n\pi z}{H} \, dz = -\left(\frac{n\pi}{H}\right)^2 \bar{f}(n). \tag{3.23}$$

Proceeding with the solution to the problem of subcritical assemblies, the assumption is made that the neutron source consists only of thermal neutrons. It is given by:

$$S(r) = Sf(r),$$

and according to the discussion in Appendix C, it will be assumed that the first theorem above may be applied to it. Thus, f(r) may be expressed as:

$$f(r) = \frac{2}{R^2} \sum_{i=1}^{\infty} \bar{f}_i \frac{J_o(\alpha_i r)}{[J_1(\alpha_i R)]^2} , \tag{3.24}$$

where

$$\bar{f}_i = \int_0^R rf(r)\, J_o(\alpha_i r)\, dr , \tag{3.25}$$

and R is the extrapolated radius of the assembly.

Taking the Hankel transform of Eq. (3.11), we get:

$$D^S \left[-\alpha_i^2 + \frac{\partial^2}{\partial z^2} \right] \bar{\phi}_s(\alpha_i, z) - \Sigma_a^S \bar{\phi}_s(\alpha_i, z) = 0, \tag{3.26}$$

where $\bar{\phi}_s(\alpha_i, z)$ is the Hankel transform of $\phi_s(r, z)$, or

$$\frac{\partial^2}{\partial z^2} \bar{\phi}_s(\alpha_i, z) - \beta_i^2 \bar{\phi}_s(\alpha_i, z) = 0, \tag{3.27}$$

where

$$\beta_i^2 = \frac{\Sigma_a^S}{D^S} + \alpha_i^2 = \frac{1}{L_s^2} + \alpha_i^2 . \tag{3.28}$$

Equation (3.28) can be solved with the transformed boundary conditions:

$$\bar{\phi}_s(\alpha_i, H) = 0 \; ; \quad S\bar{f}_i = -D^S \left[\frac{\partial \bar{\phi}_s(\alpha_i, z)}{\partial z} \right]_{z=0} . \tag{3.29}$$

The solution is:

$$\bar{\phi}_s(\alpha_i, z) = S \frac{\bar{f}_i}{D^S \beta_i} \frac{\sinh \beta_i (H-z)}{\cosh \beta_i H} . \tag{3.30}$$

Inversion of Eq. (3.30) yields the result:

$$\phi_s(r,z) = \frac{2S}{R^2 D^S} \sum_{i=1}^{\infty} \frac{\bar{f}_i}{\beta_i} \frac{\sinh \beta_i (H-z)}{\cosh \beta_i H} \frac{J_o(\alpha_i r)}{[J_1(\alpha_i R)]^2} . \tag{3.31}$$

To solve Eqs. (3.13) and (3.14) in accordance with the discussion in the previous section, Eqs. (3.22) and (3.23) will be applied to them. The resulting relations are:

$$-\left(\alpha_i^2+\left(\frac{n\pi}{H}\right)^2+\frac{\Sigma_a^\ell}{D^\ell}\right)\bar{\bar{\phi}}_\ell(\alpha_i,n)+\frac{p}{D^\ell}\,\bar{\bar{q}}(\alpha_i,n,\tau_t)=0\ , \tag{3.32}$$

and

$$-\left(\alpha_i^2+\left(\frac{n\pi}{H}\right)^2\right)\bar{\bar{q}}(\alpha_i,n,\tau)=\frac{\partial}{\partial\tau}\,\bar{\bar{q}}(\alpha_i,n,\tau)\ . \tag{3.33}$$

The solution to Eq. (3.33) can be written immediately with the aid of the initial condition, Eq. (3.16); thus,

$$\bar{\bar{q}}(\alpha_i,n,\tau)=\frac{k_\infty}{p}\left[\Sigma_a^s\bar{\bar{\phi}}_s(\alpha_i,n)+\Sigma_a^\ell\bar{\bar{\phi}}_\ell(\alpha_i,n)\right]\exp(-B_{in}^2\tau), \tag{3.34}$$

where

$$B_{in}^2=\alpha_i^2+\left(\frac{n\pi}{H}\right)^2 \tag{3.35}$$

is the geometric buckling for the i, nth mode. Substituting from Eq. (3.34) in Eq. (3.32), we get:

$$\Sigma_a^\ell\bar{\bar{\phi}}_\ell(\alpha_i,n)=\frac{k_{in}}{1-k_{in}}\,\Sigma_a^s\bar{\bar{\phi}}_s(\alpha_i,n)\ , \tag{3.36}$$

where

$$k_{in}=\frac{k_\infty e^{-B_{in}^2\tau_t}}{1+L_\ell^2B_{in}^2} \tag{3.37}$$

is the effective multiplication factor for the i, nth mode and

$$L_\ell^2=\frac{D^\ell}{\Sigma_a^\ell}\ . \tag{3.38}$$

To calculate $\bar{\bar{\phi}}_s(\alpha_i,n)$, the following result is needed:

$$\int_0^H\sinh\beta_i(H-z)\sin\frac{n\pi z}{H}\,dz=\frac{n\pi H}{(n\pi)^2+(\beta_iH)^2}\sinh\beta_iH,$$

which, when applied to Eq. (3.30), yields:

$$\bar{\bar{\phi}}_s(\alpha_i,n)=S\,\frac{\bar{f}_i}{D^s\beta_i}\,\frac{n\pi H}{(n\pi)^2+(\beta_iH)^2}\tanh\beta_iH\ . \tag{3.39}$$

Substitution of Eq. (3.39) into Eq. (3.36) yields the result:

$$\bar{\bar{\phi}}_{\ell}(\alpha_i, n) = S \frac{\Sigma_a^s}{\Sigma_a^{\ell}} \frac{\bar{f}_i}{D^s \beta_i} \frac{k_{in}}{1 - k_{in}} \frac{n\pi H}{(n\pi)^2 + (\beta_i H)^2} \tanh \beta_i H, \tag{3.40}$$

which, when inverted twice according to the two theorems stated above, gives the flux of thermal neutrons born in the assembly. The resulting expression is:

$$\phi_{\ell}(r, z) = \frac{4S}{R^2 D^s} \frac{\Sigma_a^s}{\Sigma_a^{\ell}} \sum_{i=1}^{\infty} \sum_{n=1}^{\infty} \frac{\bar{f}_i}{\beta_i} \frac{k_{in}}{1 - k_{in}} \frac{n\pi}{(n\pi)^2 + (\beta_i H)^2} \times$$

$$\times \tanh \beta_i H \sin \frac{n\pi z}{H} \frac{J_o(\alpha_i r)}{[J_1(\alpha_i R)]^2} . \tag{3.41}$$

Similarly, Eqs. (3.34) and (3.36) yield:

$$\bar{\bar{q}}(\alpha_i, n, \tau) = \frac{k_{\infty}}{p} \Sigma_a^s \frac{1}{1 - k_{in}} \bar{\bar{\phi}}_s(\alpha_i, n) \exp\left(-B_{in}^2 \tau\right) . \tag{3.42}$$

Substituting from Eq. (3.39) into Eq. (3.42) and inverting twice, the following expression for the slowing-down density is obtained:

$$q(r, z, \tau) = \frac{4S}{R^2 D^s} \frac{k_{\infty} \Sigma_a^s}{p} \sum_{i=1}^{\infty} \sum_{n=1}^{\infty} \frac{\bar{f}_i}{\beta_i} \frac{1}{1 - k_{in}} \exp\left(-B_{in}^2 \tau\right) \times$$

$$\times \frac{n\pi \tanh \beta_i H}{(n\pi)^2 + (\beta_i H)^2} \sin \frac{n\pi z}{H} \frac{J_o(\alpha_i r)}{[J_1(\alpha_i R)]^2} . \tag{3.43}$$

The total flux is, by definition, given by:

$$\phi_t(r, z) = \phi_s(r, z) + \phi_{\ell}(r, z). \tag{3.44}$$

A considerable simplification is obtained if

$$S(r) = S J_o(\alpha_1 r), \tag{3.45}$$

or

$$f(r) = J_o(\alpha_1 r); \tag{3.46}$$

in this case:

$$\bar{f}_i = \int_0^R r\, J_o(\alpha_1 r)\, J_o(\alpha_i r)\, dr = \frac{R^2}{2} [J_1(\alpha_1 R)]^2 \, \delta_{i1}, \tag{3.47}$$

where $\alpha_1 = 2.405/R$ and δ_{i1} is the Kronecker delta function. Thus, all summations over i reduce to the first term only.

In the course of this research, work was done to improve the radial and azimuthal dependence of the source neutrons. As a result of this work, the source neutrons have a nearly $J_o(\alpha_1 r)$ dependence although there are significant contributions from the higher order terms. The coefficients, $\bar{f}_i$, were determined experimentally, and the expressions derived for the thermal flux and slowing-down density were used in their general form. The details of the procedure used to determine the values of the $\bar{f}_i$ are given in Appendix C.

The numerical calculations were made with the assistance of the MINIFLUX computer program. This program is described and the listing in FORTRAN II language given in Appendix A.

3.3 CRITICAL AND INFINITE ASSEMBLIES

The case of critical and infinite assemblies is considerably simpler than that of subcritical assemblies. Since there are no external sources, all neutrons are born and slow down within the assembly; thus, the superscripts "s" and "ℓ" used to denote properties of source- and lattice-born neutrons, respectively, may be dropped. The subscripts "c" and "∞" will be used to represent quantities that correspond to critical and infinite assemblies, respectively.

Consider critical lattices first. The thermal flux ϕ_c and the slowing-down density q_c satisfy Eqs. (3.13) and (3.14), respectively. The boundary conditions are:

$$\begin{aligned} q_c(r, 0, \tau) = q_c(r, H, \tau) = q_c(R, z, \tau) = 0, \\ \phi_c(r, 0) = \phi_c(r, H) = \phi_c(R, z) = 0\ . \end{aligned} \tag{3.48}$$

The initial condition, Eq. (3.16), becomes:

$$q_c(r, z, \tau{=}0) = \frac{k_\infty}{p} \Sigma_a \phi_c(r, z). \tag{3.49}$$

Furthermore, only the fundamental mode is present (W1) so that the geometric buckling, B_g^2, equals the material buckling, B_m^2. The resulting relations for ϕ_c and q_c are, therefore:

$$\phi_c(r, z) = \phi_o J_o(\alpha r) \sin \frac{\pi z}{H} , \tag{3.50}$$

and

$$q_c(r, z, \tau) = \phi_o \frac{k_\infty \Sigma_a}{p} J_o(\alpha r) \sin \frac{\pi z}{H} e^{-B_m^2 \tau} , \tag{3.51}$$

where ϕ_o is a constant of integration which represents the thermal flux at the center of the assembly.

The expressions for the thermal flux and slowing-down density in an infinite assembly can be derived directly from Eqs. (3.50) and (3.51). There is neither leakage nor spatial variation in either ϕ_∞ or q_∞; the effect of energy dependence is included in the resonance escape probability. The solutions are:

$$\phi_\infty = \phi_o , \tag{3.52}$$

and

$$q_\infty = \frac{k_\infty \Sigma_a}{p} \phi_o . \tag{3.53}$$

3.4 TEST OF THEORY

It is next necessary to determine whether or not the model just developed leads to correct results in the lattices under investigation. As will be discussed in Section 3.5, the model will be used to correct the values of the parameters ρ_{28}, δ_{25} and C^*, all of which are related to cadmium ratios. The extrapolations to infinite assemblies of δ_{28} and of the intracellular distribution of the subcadmium activation of gold measured in the miniature lattice were found to require different treatment which is described in Sections 3.5.4 and 3.5.5. It is, therefore, necessary that the model just derived be able to predict the values of cadmium ratios.

3.4.1 Cadmium Ratio of Gold

Gold has several characteristics which make it a suitable detector for flux monitoring. In the thermal energy region, its neutron absorption cross section varies as 1/v. In the epithermal energy range, there is a prominent resonance at 4.906 ev. Gold is, therefore, convenient for the measurement of the slowing-down density. It is also easily handled, and its half-life of 2.7 days is a convenient one.

The axial and radial distributions of the activity of bare and cadmium-covered gold foils were measured with two purposes in mind. First, the distributions made it possible to relate measurements made at different positions within an assembly; second, they provided a means of testing the model derived in Section 3.2, through the spatial distribution of the cadmium ratio of gold.

The thermal flux is assumed to have a Maxwellian energy distribution M(E) which is assumed to join with the epithermal 1/E flux at 0.12 ev (~5 kT). A cadmium cutoff energy of 0.4 ev was assumed, which corresponds to a cadmium thickness of about 0.020 inches.

Let A_b and A_c be the saturated activity per unit nuclide of the bare and cadmium-covered gold foils, respectively. The subcadmium saturated activity, A_b-A_c, will have two contributions: between zero and 5 kT, the 1/v contribution averaged over the Maxwellian spectrum; and between 5 kT and 0.4 ev, the 1/v contribution averaged over the 1/E flux. The epicadmium saturated activity, A_c, will have a contribution due to resonance absorption and one due to absorption corresponding to the 1/v portion of the cross section. We may, therefore, write:

$$A_b(r,z) - A_c(r,z) = \int_0^{5\,kT} \sigma_{1/v} M(E)\, dE\, \phi_t(r,z) + \chi(r,z) \int_{5\,kT}^{0.4\,ev} \sigma_{1/v} \frac{dE}{E}, \quad (3.54)$$

where $\sigma_{1/v}$ represents the 1/v cross section of gold and $\chi(r, z)$ denotes the magnitude of the 1/E portion of the energy spectrum. The function $\chi(r, z)$ may be derived from the fact that the epithermal flux must join the thermal flux at about 5 kT. In the lattices investigated, the epithermal flux may be closely approximated by the expression:

$$\phi(r, z, E) = \frac{q(r, z, \tau)}{\xi \Sigma_s E}\, ; \quad (3.55)$$

thus,

$$\chi(r, z) = \frac{q(r, z, \tau)}{\xi \Sigma_s} , \tag{3.56}$$

where $\xi\Sigma_s$ is the slowing-down power of the assembly and the slowing-down density includes the effect of absorption during the slowing-down process. As mentioned above, there is the requirement that the epithermal flux join the thermal flux at about 5 kT; thus, the value of τ to be used in Eqs. (3.55) and (3.56) is that corresponding to 5 kT; i.e., τ_t. Equation (3.56) should, therefore, read:

$$\chi(r, z) = \frac{q(r, z, \tau_t)}{\xi \Sigma_s} .$$

In Section 3.2.3, $q(r, z, \tau)$ was obtained as the solution of the age equation without absorption; p must be determined separately to account for epicadmium absorption. It will be shown in Section 5.2.8 that epicadmium absorption in U^{238} may be assumed to occur at an effective age, τ_{28}. Moreover, it will be shown in Section 5.2.5 that the definition of p, Eq. (3.8), includes the leakage of neutrons while slowing down from τ_{28} to τ_t through the parameter ρ_{28}^c. The total leakage during the slowing-down process is, therefore, included in $\chi(r, z)$ if the latter is defined as:

$$\chi(r, z) = \frac{pq(r, z, \tau_{28})}{\xi \Sigma_s} , \tag{3.57}$$

where the slowing-down density is calculated by means of Eq. (3.43).

Hence, $A_b - A_c$ may be written as:

$$A_b(r,z) - A_c(r,z) = \phi_t(r,z) \int_0^{5\,kT} \sigma_{1/v} M(E)dE + \frac{pq(r,z,\tau_{28})}{\xi\Sigma_s} \int_{5\,kT}^{0.4\,ev} \sigma_{1/v} \frac{dE}{E} . \tag{3.58}$$

Taking 5 kT $\simeq$ 0.12 ev and carrying out the integration, we get:

$$A_b(r,z) - A_c(r,z) = 0.886\, \sigma_o \phi_t(r,z) + 0.414\, \sigma_o \frac{pq(r,z,\tau_{28})}{\xi\Sigma_s} , \tag{3.59}$$

where σ_o is the 2200 m/sec absorption cross section of gold. Similarly, $A_c(r, z)$ is given by:

$$A_c(r,z) = \frac{pq(r,z,\tau_{28})}{\xi\Sigma_s}\left\{\int_{0.4}^{\infty} \sigma_{res}(E)\,\frac{dE}{E} + \int_{0.4}^{\infty} \sigma_{1/v}\,\frac{dE}{E}\right\}, \tag{3.60}$$

where σ_{res} is the resonance cross section of gold. The integration gives:

$$\int_{0.4}^{\infty} \sigma_{res}(E)\,\frac{dE}{E} + \int_{0.4}^{\infty} \sigma_{1/v}\,\frac{dE}{E} = ERI_{Au} + 0.5\,\sigma_o, \tag{3.61}$$

so that

$$A_c(r,z) = \left[\frac{ERI_{Au}}{\sigma_o} + 0.5\right]\sigma_o\,\frac{pq(r,z,\tau_{28})}{\xi\Sigma_s}, \tag{3.62}$$

or

$$A_c(r,z) = S_{Au}\,\sigma_o\,\frac{pq(r,z,\tau_{28})}{\xi\Sigma_s}, \tag{3.63}$$

where

$$S_{Au} = \frac{ERI_{Au}}{\sigma_o} + 0.5 . \tag{3.64}$$

The ratio of subcadmium to epicadmium activity of gold, $R_{Au}(r,z) - 1$, where R_{Au} is the cadmium ratio of gold, is given by:

$$R_{Au}(r,z) - 1 = \frac{A_b(r,z) - A_c(r,z)}{A_c(r,z)}$$

$$= \frac{0.886 + 0.414\,\psi(r,z)}{S_{Au}\psi(r,z)}, \tag{3.65}$$

where

$$\psi(r,z) = \frac{pq(r,z,\tau_{28})}{\xi\Sigma_s\phi_t(r,z)} . \tag{3.66}$$

Equation (3.65) was used to test the theory in all the lattices investigated. The determination of the value of S_{Au} to be used in Eq. (3.65) will be discussed in Section 5.2.

3.5 CORRECTION PROCEDURE FOR LATTICE PARAMETERS

The correction factors which will permit the extrapolation of the parameters measured in the miniature lattice, will now be obtained. The indices ML, EX, C and ∞ will denote the value of a quantity in a miniature, an exponential, a bare critical and an infinite assembly, respectively.

The corrections for those parameters that require the use of the model derived above, will be derived first. The corrections for δ_{28} and the intracellular subcadmium activity distribution of gold will follow.

3.5.1 The Value of ρ_{28} or $R_{28} - 1$

This parameter was defined in Section 2.7.1 as the ratio of the average epicadmium to subcadmium capture rates in U^{238}. Since the measurement is made inside the fuel, a Maxwellian energy distribution cannot be assumed. Instead, σ_a^{28} is defined as the average thermal absorption cross section of U^{238} as obtained with the THERMOS (H10) code, which takes into account the hardening of the neutron energy spectrum.

By an analysis similar to that used in Section 3.4 for the activity of gold, the saturated Np^{239} activity per U^{238} nucleus of the bare depleted uranium foil is given by:

$$A_b^{28}(r,z) = \sigma_a^{28}\phi_t(r,z) + \left[ERI_{28} + 0.5\,\sigma_a^{28}\right]\frac{pq(r,z,\tau_{28})}{\xi\Sigma_s}\,. \tag{3.67}$$

Similarly, the saturated Np^{239} activity per U^{238} nucleus of the cadmium-covered uranium foil is given by:

$$A_c^{28}(r,z) = \left(ERI_{28} + 0.5\,\sigma_a^{28}\right)\frac{pq(r,z,\tau_{28})}{\xi\Sigma_s}\,. \tag{3.68}$$

Thus, the saturated Np^{239} activity per U^{238} nucleus due to the capture of subcadmium neutrons is:

$$A_b^{28}(r,z) - A_c^{28}(r,z) = \sigma_a^{28}\phi_t(r,z)\,. \tag{3.69}$$

From Eqs. +3.68) and (3.69), the ratio of epicadmium to subcadmium Np^{239} activity of U^{238} is given by:

$$\rho_{28}(r, z) = \frac{1}{R_{28}(r, z) - 1} = S_{28}\psi(r, z), \tag{3.70}$$

where $R_{28}(r, z)$ is the average cadmium ratio of U^{238},

$$S_{28} = \frac{ERI_{28}}{\sigma_a^{28}} + 0.5 ,$$

and the function $\psi(r, z)$ is defined by Eq. (3.66).

To relate the value of ρ_{28} measured in the miniature lattice to that measured in the equilibrium region of an exponential assembly, Eq. (3.70) is written for both assemblies and the ratio is taken; the resulting relation is:

$$\rho_{28}^{EX} = \frac{S_{28}^{EX}}{S_{28}^{ML}} \frac{\psi_{EX}(r^E, z^E)}{\psi_{ML}(r, z)} \rho_{28}^{ML}(r, z) , \tag{3.71}$$

where (r^E, z^E) denotes a position in the equilibrium region of the exponential assembly. The value of (r^E, z^E) is, evidently, immaterial since the equilibrium region is defined to be that in which ψ is, to a first approximation, constant.

To obtain the extrapolation factors to critical and infinite assemblies, it is sufficent to change the index EX in Eq. (3.71) to C and ∞, respectively.

The value of the quantity S_{28} will depend on the dimensions of the assembly considered. A discussion of this important quantity is given in Section 5.2.

3.5.2 Value of δ_{25}

The quantity δ_{25} was defined in Section 2.7.3 in a similar fashion as ρ_{28} but for fissions in U^{235}. As in the case of ρ_{28}, δ_{25} is measured inside the fuel and σ_f^{25} must be obtained with the THERMOS code (H10). Because of the similarity in the definitions of ρ_{28} and δ_{25}, the extrapolation factor can be written immediately as:

$$\delta_{25}^{EX} = \frac{S_{25}^{EX}}{S_{25}^{ML}} \frac{\psi_{EX}(r^E, z^E)}{\psi_{ML}(r, z)} \delta_{25}^{ML}(r, z), \tag{3.72}$$

where

$$S_{25} = \frac{ERI_{25}}{\sigma_f^{25}} + 0.5, \tag{3.73}$$

in which ERI_{25} is the effective resonance integral for fissions in U^{235}. The values of S_{25} will be discussed in Section 5.2.

Again, if the indices C or ∞ are written in Eq. (3.72) instead of EX, the correction factors to a bare critical and an infinite assembly are obtained, respectively.

3.5.3 The Ratio C^*

It was shown in Section 2.7.4 that the parameter C^* can be obtained in two independent ways. The definition,

$$C^* = \frac{1 + \rho_{28}}{1 + \delta_{25}} \left(\frac{\Sigma_a^{28}}{\Sigma_f^{25}} \right)_{SC},$$

can be corrected immediately with the aid of Eqs. (3.71) and (3.72). Thus,

$$C^*_{EX} = \frac{1 + \rho_{28}^{EX}}{1 + \rho_{28}^{ML}(r, z)} \; \frac{1 + \delta_{25}^{ML}(r, z)}{1 + \delta_{25}^{EX}} \; C^*_{ML}(r, z). \tag{3.74}$$

To correct the parameter C^* defined by means of:

$$C^* = C^*_M \, R_N/R_F,$$

the expression is rewritten as:

$$C^* = C^*_M \frac{A_b^{28}}{A_M^{28}} \frac{A_M^{25}}{A_b^{25}}, \tag{3.75}$$

where Eqs. (2.13) and (2.14) have been substituted for R_N and R_F, respectively. The values of the quantities A_M^{28} and A_M^{25}, defined in Section 2.7.4, are the same independent of the type of assembly being used for the measurement. The same may be said of C^*_M; only A_b^{28} and A_b^{25} need to be corrected. The following expressions for A_b^{28} and A_b^{25} hold:

$$A_b^{28}(r,z) = \epsilon^{28} N^{28} \sigma_a^{28} \left[\phi_t(r,z) + S_{28} \frac{pq(r,z,\tau_{28})}{\xi \Sigma_s} \right] , \tag{3.76}$$

and

$$A_b^{25}(r,z) = \epsilon^{25} N^{25} \sigma_a^{25} \left[\phi_t(r,z) + S_{25} \frac{pq(r,z,\tau_{28})}{\xi \Sigma_s} \right] , \tag{3.77}$$

where ϵ^{28} is efficiency of the counting apparatus for Np^{239} activity and ϵ^{25} is the efficiency of the counting system for fission product activity; N^{28} denotes the number of atoms of U^{238} per cm^3 and N^{25} is the analogous quantity for U^{235}. Thus,

$$\frac{A_b^{28}(r,z)}{A_b^{25}(r,z)} = \frac{\epsilon^{28} N^{28} \sigma_a^{28}}{\epsilon^{25} N^{25} \sigma_f^{25}} \; \frac{\phi_t(r,z) + S_{28} \dfrac{pq(r,z,\tau_{28})}{\xi \Sigma_s}}{\phi_t(r,z) + S_{25} \dfrac{pq(r,z,\tau_{28})}{\xi \Sigma_s}} . \tag{3.78}$$

On using Eq. (3.66) and writing Eq. (3.78) for both miniature and exponential lattices and taking the ratio, we obtain the relation:

$$C^*_{EX} = \frac{1 + S_{28}^{EX} \psi_{EX}(r^E, z^E)}{1 + S_{28}^{ML} \psi_{ML}(r,z)} \; \frac{1 + S_{25}^{ML} \psi_{ML}(r,z)}{1 + S_{25}^{EX} \psi_{EX}(r^E, z^E)} \; C^*_{ML}(r,z), \tag{3.79}$$

since the factor in front of Eq. (3.78) cancels when the ratio is taken.

3.5.4 The Fast Fission Ratio, δ_{28}

The parameter δ_{28} was defined as:

$$\delta_{28} = \frac{\text{fission rate in } U^{238}}{\text{total fission rate in } U^{235}} ,$$

or

$$\delta_{28} = \frac{\int_{E_f}^{\infty} \sigma_f^{28}(E)\, \phi(E)\, dE}{\int_0^{\infty} \sigma_f^{25}(E)\, \phi(E)\, dE} ,$$

where E_f is the threshold energy for the U^{238} fission cross section

(~1 Mev). In U^{235}, most of the fissions occur for neutrons in the thermal energy range. In fact, for all the lattices investigated, more than 90% of the fissions in U^{235} are caused by thermal neutrons; thus,

$$\delta_{28} \simeq \frac{\bar{\sigma}_f^{28} \phi_F}{\bar{\sigma}_f^{25} \phi_t}, \tag{3.80}$$

where $\bar{\sigma}_f^{28}$ is the average fission cross section of U^{238} and $\bar{\sigma}_f^{25}$ is the average fission cross section of U^{235}; ϕ_F is the average fast flux in the fuel and ϕ_t is the average thermal flux in the fuel. If the measurements are normalized to the same thermal flux, the required extrapolation correction is:

$$\delta_{28}^{EX} = \frac{\phi_F^{EX}}{\phi_F^{ML}} \delta_{28}^{ML} . \tag{3.81}$$

To understand the application of Eq. (3.81), the following considerations are necessary. The contributions to the fast flux inside a fuel element come from two sources: first, the neutrons born from fission in the same fuel element; second, the neutrons born in the surrounding rings of rods. The latter neutrons escape from their respective fuel rods and reach the fuel element under consideration without undergoing any collisions. The difference between ϕ_F^{EX} and ϕ_F^{ML} comes from the interaction effect. That is, the single rod portion of the total fast flux is the same independently of the type of assembly used. The interaction effect depends: first, on the number of rings of fuel rods contributing to the fast flux in the fuel rod under consideration; and second, on the number of fission neutrons produced in these fuel rods; i.e., the fission rate in U^{235} in the surrounding rods which is approximately proportional to the thermal flux. In the miniature lattice, the number of contributing rings of rods is smaller than in the other types of assemblies; moreover, the thermal neutron flux goes to zero more rapidly than in the larger assemblies since the boundaries are closer to the centermost rod. Thus, the correction factor in Eq. (3.81) is always greater than unity.

To calculate the ratio, $\phi_F^{EX} / \phi_F^{ML}$, the theory developed by Woodruff (W4) was used. The fast flux distribution in a cell was calculated by means of the computer program UNCOL. In Woodruff's work, the following assumptions are made:

1. Fast neutrons suffering one collision are slowed down below the U^{238} fission threshold energy.

2. The single collision kernel for cylinders of infinite length may be used for cylinders of finite length.

3. The homogeneous kernel may be used for heterogeneous configurations by making suitable adjustments in the cross sections.

4. The spatial distribution of the fission rate within a fuel rod may be expressed by the relation:

$$S(r') = C_o + C_1 r'^2,$$

where $C_o = 1$; C_1 is an arbitrary constant and r' is the distance of a point in the rod from the center of the rod.

The computation consists in integrating the single collision transport kernel for cylindrical shell sources. The integration is over the volume of each fuel rod in the assembly. The results are multiplied by the appropriate weighting factors (usually a J_o function) and then added to give the relative fast flux at points of interest.

In the case of the miniature lattice, Assumption 2 requires further discussion. It would seem, at first, that it is not valid in the miniature lattice. To show that this assumption is valid, even in miniature lattices, consider the single collision transport kernel for a point source. It is given by the expression:

$$K(\underline{r}, \underline{r}') = \frac{1}{4\pi} \frac{e^{-\Sigma|\underline{r}-\underline{r}'|}}{|\underline{r} - \underline{r}'|^2}, \tag{3.82}$$

where Σ is the removal cross section for neutrons with energy greater than E_f; $K(\underline{r}, \underline{r}')$ represents the uncollided flux at $\underline{r}$ due to a point source at $\underline{r}'$. In a cylindrical assembly, the configuration is that shown in Fig. 3.3. From the figure, we can see that:

$$R^2 = |\underline{r} - \underline{r}'|^2 = \ell^2 + (z-z')^2,$$

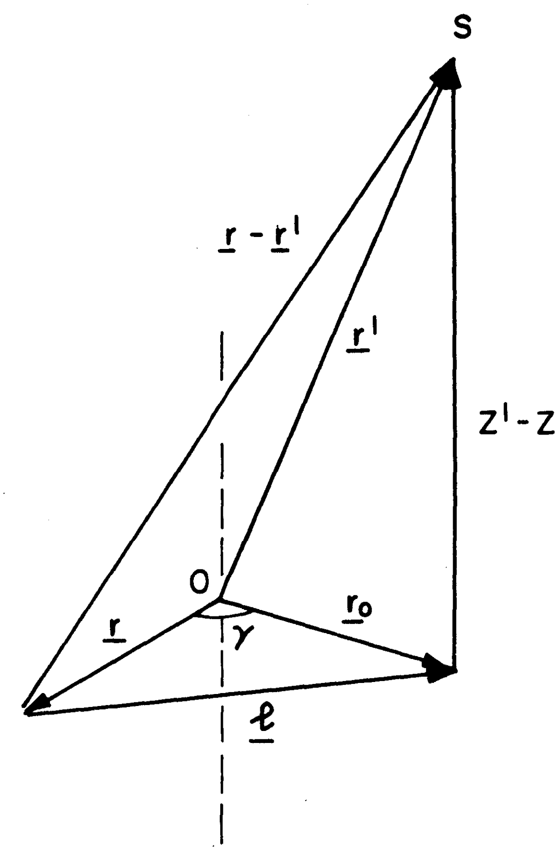

FIG. 3.3 COORDINATES OF INTEREST IN THE CALCULATION OF THE FAST FLUX DISTRIBUTION

where

$$\ell^2 = r^2 + r_o^2 - 2rr_o \cos\gamma .$$

The infinite length collision kernel is obtained by integrating Eq. (3.82) over γ and z'; thus,

$$\phi(r, r_o) = \frac{1}{4\pi}\frac{S}{2\pi}\int_0^{2\pi} d\gamma \int_{-\infty}^{\infty} dz' \frac{e^{-\Sigma R}}{R^2} .$$

Without loss of generality, z may be set equal to zero and $\phi(r, r_o)$ may be written as:

$$\phi(r, r_o) = \frac{S}{4\pi^2}\int_0^{2\pi} d\gamma \int_0^{\infty} dz' \frac{e^{-\Sigma(\ell^2+z'^2)^{1/2}}}{\ell^2 + z'^2} . \tag{3.83}$$

The question is, whether in the miniature lattice the same limits of integration can be used for z'. Consider the worst possible case, $\ell = 0$. If $\ell \neq 0$, the point kernel is smaller in magnitude. Figure 3.4 shows a plot of $K(z=0, z')$ as a function of z'. We see from the figure that the fast flux decreases very rapidly with increasing values of z' and, indeed, at $z' = 1$ cm, the contribution to the fast flux at $z = 0$ is already less than 1% of that at $z' = 0.1$ cm. It is, therefore, apparent that very little is added to the fast flux at $z = 0$, by extending the integration to infinity.

In the discussion of the second assumption, another question arises. In assuming an infinite length, it is, in effect, being assumed that the axial flux distribution is constant; yet we know that this is not the case in a finite lattice. Indeed, in subcritical assemblies, the thermal flux distribution is nearly an exponential function. From the previous argument, however, the contribution to the fast flux at $z = 0$ comes mainly from a region about one inch long about $z = 0$. In this small region, the flux may be expanded in a Taylor series about $z = 0$, and only the first two terms kept. It will be given by an expression of the form:

$$\phi(z') = a + bz' .$$

Hence, when $\phi(z')$ is multiplied by the point kernel $K(z=0, z')$ and integrated over the region of interest, the deviation from a constant will cancel since the point kernel is an even function of z'.

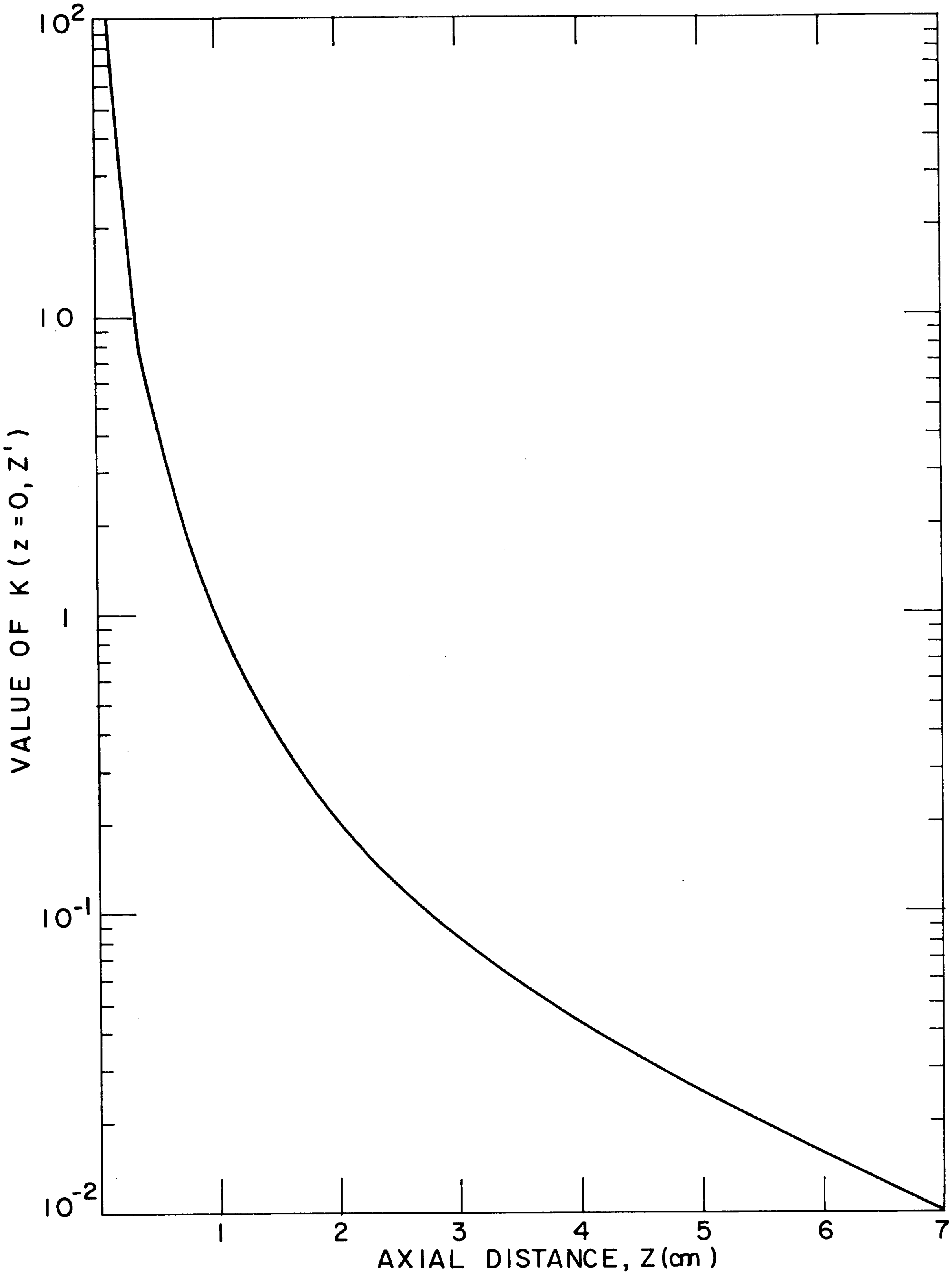

FIG. 3.4 SINGLE COLLISION POINT KERNEL K(z=0, Z')

These results and discussion show that the assumptions made in Ref. (W4) to develop the UNCOL program may be applied to the miniature lattice.

The procedure to correct the values of δ_{28} measured in the miniature lattice was the following: the UNCOL program was used to calculate the average fast flux in the miniature lattice, the exponential assembly at M.I.T. and an infinite assembly, respectively, and the necessary ratios substituted in Eq. (3.81).

3.5.5 Intracellular Subcadmium Activity Distribution of Gold

In the discussion of the thermal utilization in Section 3.1.1, it was noted that the values of the average fluxes in the different regions, which appear in Eq. (3.7), are those corresponding to an infinite assembly. This was implied in Eq. (3.7) by the superscript ∞ on the average fluxes.

To obtain extrapolation corrections for the intracellular distributions of the gold activity measured in the miniature lattice, consider an infinite array of fuel rods placed periodically in an assembly. The thermal neutron flux distribution in the assembly may be written as:

$$\phi(r) = \phi_M \phi_f(r) , \tag{3.84}$$

where ϕ_M denotes the macroscopic flux distribution, in this case, a constant; $\phi_f(r)$, the intracellular flux distribution, represents the perturbation produced by the rods. In determining f, the thermal utilization, the distribution of interest is $\phi_f(r)$.

When the measurement is made in a finite assembly, ϕ_M is no longer a constant. For a cylindrical lattice, it is given by:

$$\phi_M(r, z) = A' J_o(\alpha r) \, f(z) , \tag{3.85}$$

where A' is a constant; f(z) gives the axial variation of the flux ($\sin(\pi z/H)$ and $\sinh \gamma(H-z)$ in critical and subcritical assemblies, respectively). The subcadmium intracellular activity distribution of gold observed at a given height, $z = z_o$, is given by:

$$A(r) = C J_o(\alpha r) \, \phi_f(r) , \tag{3.86}$$

where

$$C = \epsilon A' f(z_o)\, \sigma_{Au} ;$$

ϵ is a factor incorporating the counter efficiency, corrections for activity decay and the number of atoms per cm^3 of the gold foil; σ_{Au} is the subcadmium activation cross section of gold. Since C is the same for all the foils in a microscopic traverse, it can be set equal to unity.

To obtain $\phi_f(r)$, the fine structure, the measured intracellular subcadmium activities must be corrected for the macroscopic flux distribution; thus,

$$\phi_f(r) = \frac{A(r)}{J_o(\alpha r)} , \tag{3.87}$$

where $\alpha = 2.405/R$. It will be shown in Section 4.3.1 that the macroscopic subcadmium flux distributions — at least, within the cell in which the measurements were made — has, indeed, a J_o-functional dependence.

For completeness, another effect must also be investigated, which arises from the fact that an appreciable portion of the measured activities comes from source neutrons. Since the source neutrons may have a different thermal energy spectrum than the neutrons born in the lattice, a possible perturbation on the intracellular distribution can be expected. The activation per unit atom that is measured, A(r), may be expressed as a combination of activities produced by source and lattice-born neutrons. At a given height, $z = z_o$, we have:

$$A(r) = \sigma_s \phi_s(r, z_o) + \sigma_\ell \phi_\ell(r, z_o) , \tag{3.88}$$

where σ_s and σ_ℓ are the thermal activation cross sections of gold for source and lattice-born neutrons, respectively; ϕ_s and ϕ_ℓ represent the corresponding thermal fluxes. The quantity of interest is:

$$A_\ell(r) = \sigma_\ell \phi_\ell(r, z_o) , \tag{3.89}$$

which can be factored out of Eq. (3.88); thus,

$$A_\ell(r) = \frac{A(r)}{1 + \dfrac{\sigma_s \phi_s(r, z_o)}{\sigma_\ell \phi_\ell(r, z_o)}} . \tag{3.90}$$

Within a cell, at a given value of z_o, ϕ_s/ϕ_ℓ is a constant. Hence, only if the ratio σ_s/σ_ℓ is considerably different across the cell, will this correction be significant.

In Section 4.3.2, it will be shown that the experimental evidence indicates that even in miniature lattices, the variation in the ratio σ_s/σ_ℓ is much smaller than the experimental uncertainties involved in the measurements. Hence, the factor in front of A(r) in Eq. (3.90) is constant across the cell and the correction need not be applied.

3.6 SUMMARY

The results obtained in this chapter are summarized in this section. In Table 3.1, the expressions for the thermal flux and slowing-down density in subcritical lattices are listed. The extrapolation corrections for ρ_{28}, δ_{25}, δ_{28} and C^* derived in Section 3.5 are summarized in Table 3.2.

Table 3.1

Summary of Results for Subcritical Assemblies

$$\phi_s(r,z) = \frac{2S}{R^2 D^s} \sum_{i=1}^{\infty} \frac{\bar{f}_i}{\beta_i} \frac{\sinh \beta_i (H-z)}{\cosh \beta_i H} \frac{J_o(\alpha_i r)}{[J_1(\alpha_i R)]^2} . \qquad (3.31)$$

$$\phi_\ell(r,z) = \frac{4S}{R^2 D^s} \frac{\Sigma_a^s}{\Sigma_a^\ell} \sum_{i=1}^{\infty} \sum_{n=1}^{\infty} \frac{\bar{f}_i}{\beta_i} \frac{k_{in}}{1-k_{in}} \frac{n\pi \tanh \beta_i H}{(n\pi)^2 + (\beta_i H)^2} \sin\left(\frac{n\pi z}{H}\right) \frac{J_o(\alpha_i r)}{[J_1(\alpha_i R)]^2} . \qquad (3.41)$$

$$pq(r,z,\tau) = \frac{4S}{R^2 D^s} k_\infty \Sigma_a^s \sum_{i=1}^{\infty} \sum_{n=1}^{\infty} \frac{\bar{f}_i}{\beta_i} \frac{1}{1-k_{in}} \frac{n\pi \tanh \beta_i H}{(n\pi)^2 + (\beta_i H)^2} e^{-B_{in}^2 \tau} \sin\left(\frac{n\pi z}{H}\right) \frac{J_o(\alpha_i r)}{[J_1(\alpha_i R)]^2} . \qquad (3.43)$$

$$\phi_t(r,z) = \phi_s(r,z) + \phi_\ell(r,z) . \qquad (3.44)$$

$$S(r) = Sf(r) = \frac{2S}{R^2} \sum_{i=1}^{\infty} \bar{f}_i \frac{J_o(\alpha_i r)}{[J_1(\alpha_i R)]^2} . \qquad (3.24)$$

$$\bar{f}_i = \int_0^R rf(r)\, J_o(\alpha_i r)\, dr . \qquad (3.25)$$

$$\beta_i^2 = \frac{\Sigma_a^s}{D^s} + \alpha_i^2 = \frac{1}{L_s^2} + \alpha_i^2 . \qquad (3.28)$$

$$B_{in}^2 = \alpha_i^2 + \left(\frac{n\pi}{H}\right)^2 . \qquad (3.35)$$

$$k_{in} = \frac{k_\infty e^{-B_{in}^2 \tau_t}}{1 + L_\ell^2 B_{in}^2} . \qquad (3.37)$$

Table 3.2

Summary of Correction Factors for ρ_{28}, δ_{25}, δ_{28} and C^*

Measured Quantity	Correction Factor to Extrapolate Value of Parameter Measured in Miniature Lattice to Assembly Below		
	Exponential Assembly	Critical Lattice	Infinite Assembly
$\rho_{28}^{ML}(r,z)$ (Sect. 3.5.1)	$\dfrac{S_{28}^{EX}}{S_{28}^{ML}} \dfrac{\psi_{EX}(r^E, z^E)}{\psi_{ML}(r,z)}$	$\dfrac{S_{28}^{C}}{S_{28}^{ML}} \dfrac{\psi_{C}}{\psi_{ML}(r,z)}$	$\dfrac{S_{28}^{\infty}}{S_{28}^{ML}} \dfrac{\psi_{\infty}}{\psi_{ML}(r,z)}$
$\delta_{25}^{ML}(r,z)$ (Sect. 3.5.2)	$\dfrac{S_{25}^{EX}}{S_{25}^{ML}} \dfrac{\psi_{EX}(r^E, z^E)}{\psi_{ML}(r,z)}$	$\dfrac{S_{25}^{C}}{S_{25}^{ML}} \dfrac{\psi_{C}}{\psi_{ML}(r,z)}$	$\dfrac{S_{25}^{\infty}}{S_{25}^{ML}} \dfrac{\psi_{\infty}}{\psi_{ML}(r,z)}$
$C_{ML}^*(r,z)^{(1)}$ (Sect. 3.5.3)	$\dfrac{1 + S_{28}^{EX}\psi_{EX}(r^E, z^E)}{1 + S_{28}^{ML}\psi_{ML}(r,z)} \dfrac{1 + S_{25}^{ML}\psi_{ML}(r,z)}{1 + S_{25}^{EX}\psi_{EX}(r^E, z^E)}$	$\dfrac{1 + S_{28}^{C}\psi_{C}}{1 + S_{28}^{ML}\psi_{ML}(r,z)} \dfrac{\psi + S_{25}^{ML}\psi_{ML}(r,z)}{1 + S_{25}^{C}\psi_{c}}$	$\dfrac{1 + S_{28}^{\infty}\psi_{\infty}}{1 + S_{28}^{ML}\psi_{ML}(r,z)} \dfrac{1 + S_{25}^{ML}\psi_{ML}(r,z)}{1 + S_{25}^{\infty}\psi_{\infty}}$
$C_{ML}^*(r,z)^{(2)}$ (Sect. 3.5.3)	$\dfrac{1 + \rho_{28}^{EX}}{1 + \rho_{28}^{ML}(r,z)} \dfrac{1 + \delta_{25}^{ML}(r,z)}{1 + \delta_{25}^{EX}}$	$\dfrac{1 + \rho_{28}^{C}}{1 + \rho_{28}^{ML}(r,z)} \dfrac{1 + \delta_{25}^{ML}(r,z)}{1 + \delta_{25}^{C}}$	$\dfrac{1 + \rho_{28}^{\infty}}{1 + \rho_{28}^{ML}(r,z)} \dfrac{1 + \delta_{25}^{ML}(r,z)}{1 + \delta_{25}^{\infty}}$
δ_{28}^{ML} (Sect. 3.5.4)	$\dfrac{\phi_F^{EX}}{\phi_F^{ML}}$		$\dfrac{\phi_F^{\infty}}{\phi_F^{ML}}$

(1) $C_{ML}^*(r,z) = C_M^* \dfrac{R_N^{ML}(r,z)}{R_F^{ML}(r,z)}$.

(2) $C_{ML}^*(r,z) = \dfrac{1 + \rho_{28}^{ML}(r,z)}{1 + \delta_{25}^{ML}(r,z)} \left(\dfrac{\Sigma_a^{28}}{\Sigma_f^{25}}\right)_{SC}$.

CHAPTER 4

DATA ANALYSIS AND RESULTS

4.1 INTRODUCTION

The techniques used to analyze the raw data will be described in this chapter. This discussion will be followed by a presentation of the experimental results obtained in the miniature lattice. The correction procedures described in Section 3.5 will also be applied to the experimental data, and the final results will be compared with the corresponding measurements in the exponential facility at M.I.T.

The results obtained and the parameters that enter in the theory and extrapolation corrections derived in Chapter 3 will be given in Chapter 5.

4.2 DATA ANALYSIS

The methods used have been developed by various workers on the Heavy Water Lattice Project (S1,D1).

4.2.1 Macroscopic Gold Traverses

To reduce the gold foil counting data, the ACT-5 computer program written by Simms (S1) and modified by Clikeman (C2) was used. The ACT-5 program was designed to process the raw data from either of the automatic counters described in Section 2.6 for activity decaying with a single half-life.

The program corrects for the following:

1. Decay of activity from the time the irradiation is ended to the time at which the counting of the foils begins.
2. Decay of activity during the time interval in which the foils are being counted.
3. Background.
4. Counter dead time.
5. Foil weight.

Corrections 2, 3 and 4 are applied to each counting pass; corrections 1 and 5 are applied to the average count rate over all the passes. The average is calculated by weighting the individual results with the number of preset counts for the pass. The ACT-5 program was used for the raw data from both bare and cadmium-covered foils. The cadmium ratio was then obtained from the activities of a bare foil and a cadmium-covered foil irradiated in equivalent positions inside the miniature lattice.

4.2.2 Intracellular Gold Traverses

The ACT-5 code was also used to reduce the raw data for the intracellular gold activity traverses.

The following procedure was used to obtain the subcadmium activity distribution within a cell.

1. To obtain the average activity at a position in the cell, the arithmetic mean was taken of the corrected activities of two foils, irradiated in equivalent positions along the rod-to-rod directions shown in Fig. 2.8. Similarly, within the fuel, the average was assumed to be the arithmetic mean of the corrected activity of the two foils in each position, one on each side of the fuel button foil holder.

2. The corrected activities of the cadmium-covered foils both in the fuel and the moderator were corrected to the height at which the bare foils were irradiated. This was accomplished with the aid of the axial gold activity distributions obtained with bare and cadmium-covered foils. The activity of each cadmium-covered foil was multiplied by the ratio of the measured epicadmium activity of gold at the height of the bare foils to the measured epicadmium activity at the height at which the foil holder with the cadmium-covered foils was located.

3. The average activity of the cadmium-covered foils in the moderator was subtracted from the activity of each bare foil in the moderator. In the fuel, the subtraction was done foil by foil, since bare and cadmium-covered foils were irradiated at equivalent positions.

4. The subcadmium and epicadmium activity distributions of gold were then corrected to those that would be observed in an infinite assembly. The method described in Section 3.5.5 was used.

In following the procedure described above, the question arises as to whether it is valid to apply steps 2 and 3 above before correcting the activities to an infinite assembly. The justification for the order followed in the procedure above comes from the experimental data. It will be shown in Section 4.3.2 that the activities measured inside the fuel are not significantly affected by their extrapolation to an infinite assembly. Furthermore, it will be shown in Section 4.3.1 that the macroscopic radial distribution of the cadmium ratio of gold measured in the moderator is constant over a region of the assembly which includes the cell in which the intracellular measurements were made. The order followed in the procedure described above is, therefore, immaterial.

4.2.3 ρ_{28}, δ_{25}, δ_{28} and C^*

The total number of counts in each counting pass of each of the detector foils in the packets described in Section 2.7.5 was corrected for each of the following items:

1. Room background.
2. Natural and residual activity.
3. Difference in times at which the activities of foils to be used to calculate a ratio are measured.
4. Decay of activity during counting.
5. Counter dead time and pulse pile-up.
6. Foil weight.
7. Axial and radial position in the miniature lattice tank.

These corrections were applied to the measured fission product activity of the uranium detector foils and to the Np^{239} activity of the depleted uranium detector foils.

The decay of the fission product activity of the uranium detector foils is given by a sum of exponentials. A special technique was developed to correct for the decay of the activity between counting passes. A polynomial was fitted by the method of least squares to the corrected foil activities as a function of the time at which the activities were determined. The computer program LSQ-4D, listed in Ref. (D1), was used to make the least square fitting. The input to the program consisted of the raw data and adequate information to correct the measured total number of counts. The output consisted of the polynomial coefficients, the corrected data, and values of the activity at times of interest, namely, common times for all the uranium foils within the packets. The LSQ-4D program was also used to process the Np^{239} raw counting data.

The polynomial coefficients obtained from LSQ-4D to describe the fission product activities and the Np^{239} corrected activities were then used to calculate ρ_{28}, δ_{25} and C^*. This was accomplished with the aid of the computer program EPIFAST, described in Appendix E. The EPIFAST program has provisions to correct the results for differences in axial and/or radial position of the foil packets involved in the calculation. Corrections may also be included for the reduction in activities of the detector foils within a packet because of the presence of cadmium and/or uranium of a U^{235} concentration different from that of the fuel in the lattice. A discussion of the perturbations produced in the measurements by these foreign materials is given in Ref. (D1).

The procedure followed in the EPIFAST program was to use the polynomial coefficients and their uncertainties, to calculate δ_{25} and R_F at common times in each counting pass as well as their standard deviation. The corrected Np^{239} activities of the depleted uranium foils and their standard deviation were used to determine ρ_{28} and R_N at common times in each pass. The average value for each quantity was then determined by weighting each result with its uncertainty; Eqs. (2.12) and (2.17) were then used to obtain weighted values of C^*. It was found that the final results and uncertainties were independent of how the weighting was done, since the uncertainty due to counting statistics was approximately the same for all detectors. Hence, the final value was taken as an unweighted average.

The data used to obtain δ_{28} were processed with the assistance of the computer program PEG, described in Ref. (W3).

The extrapolation methods derived in Sections 3.5.1 through 3.5.4 were then applied to the values of the parameters obtained in the miniature lattice to get the values of the parameters in exponential, critical and infinite assemblies.

4.3 RESULTS AND COMPARISON WITH DATA FROM EXPONENTIAL ASSEMBLIES

4.3.1 Axial and Radial Gold Activity Traverses

Axial and radial activity traverses of gold were made in all the lattices investigated. As discussed in Section 3.4, their purpose was twofold. The distribution of the cadmium ratio of gold permits the testing of the model derived in Section 3.2. The activity distributions obtained with bare and cadmium-covered foils assisted in the correlation of measurements in various positions within the miniature lattice.

The axial distribution of the cadmium ratio of gold in the six lattices investigated is shown in Figs. 4.1 through 4.6. The solid curves represent the values predicted by Eq. (3.65). The theoretical computations were made with the aid of the computer program MINIFLUX, described in Appendix A. The parameters required for the use of MINIFLUX are listed in Table 4.1. The analytical methods used to obtain these quantities are discussed in Chapter 5.

It is evident from Figs. 4.1 through 4.6 that in all the lattices the computed value of the cadmium ratio of gold agrees well with the measured value over the bottom half of the assembly. In the lattices with rod spacing of 1.25 inches, the agreement is good except near the source; the discrepancy between calculated and measured values increases with increasing lattice spacing.

There are two reasons for the discrepancy between calculated and measured values of the cadmium ratio near the source end. First, the diffusion approximation breaks down near the source. Second, the expansion in Fourier harmonics fails near the discontinuity at $z = 0$. This is the result of fitting a discontinuous function with a finite number of continuous functions. These effects will be discussed in more detail in Section 5.4. Since the effect of the source extends further into the lattice with increasing rod-to-rod separation (as implied by the increase in the value of L_s), the predicted value of the cadmium ratio of gold should agree better with the measured results as the lattice spacing decreases.

For the purpose of this work, the important point of these results is that the theory predicts the cadmium ratio of gold accurately in the region where ρ_{28}, δ_{25}, δ_{28} and C^* were measured. Hence, the theory

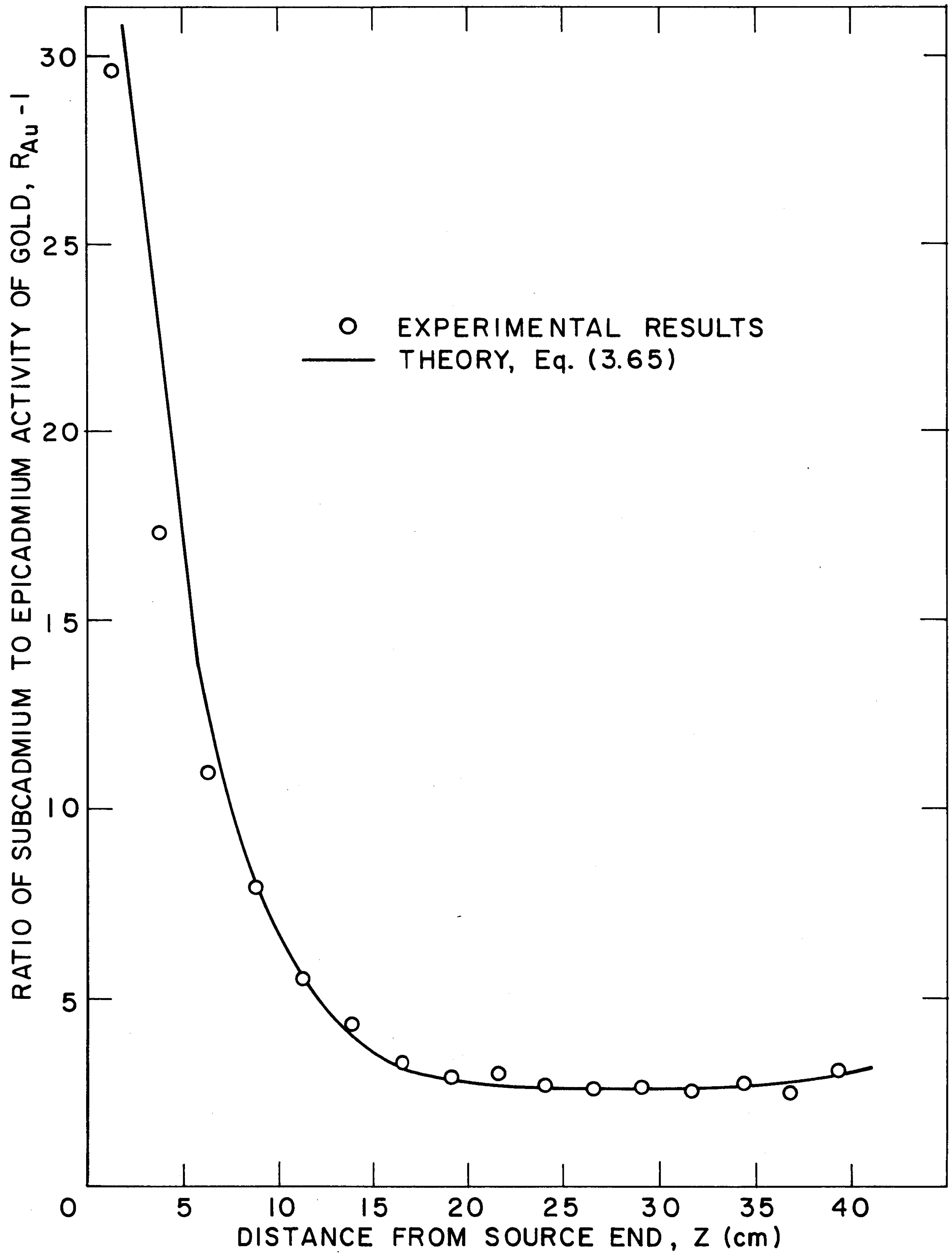

FIG. 4.1 AXIAL DISTRIBUTION FOR CADMIUM RATIO OF GOLD IN ML2
ML2: 1.143% ENRICHED FUEL, D_2O MODERATED,
1.25-INCH SPACING

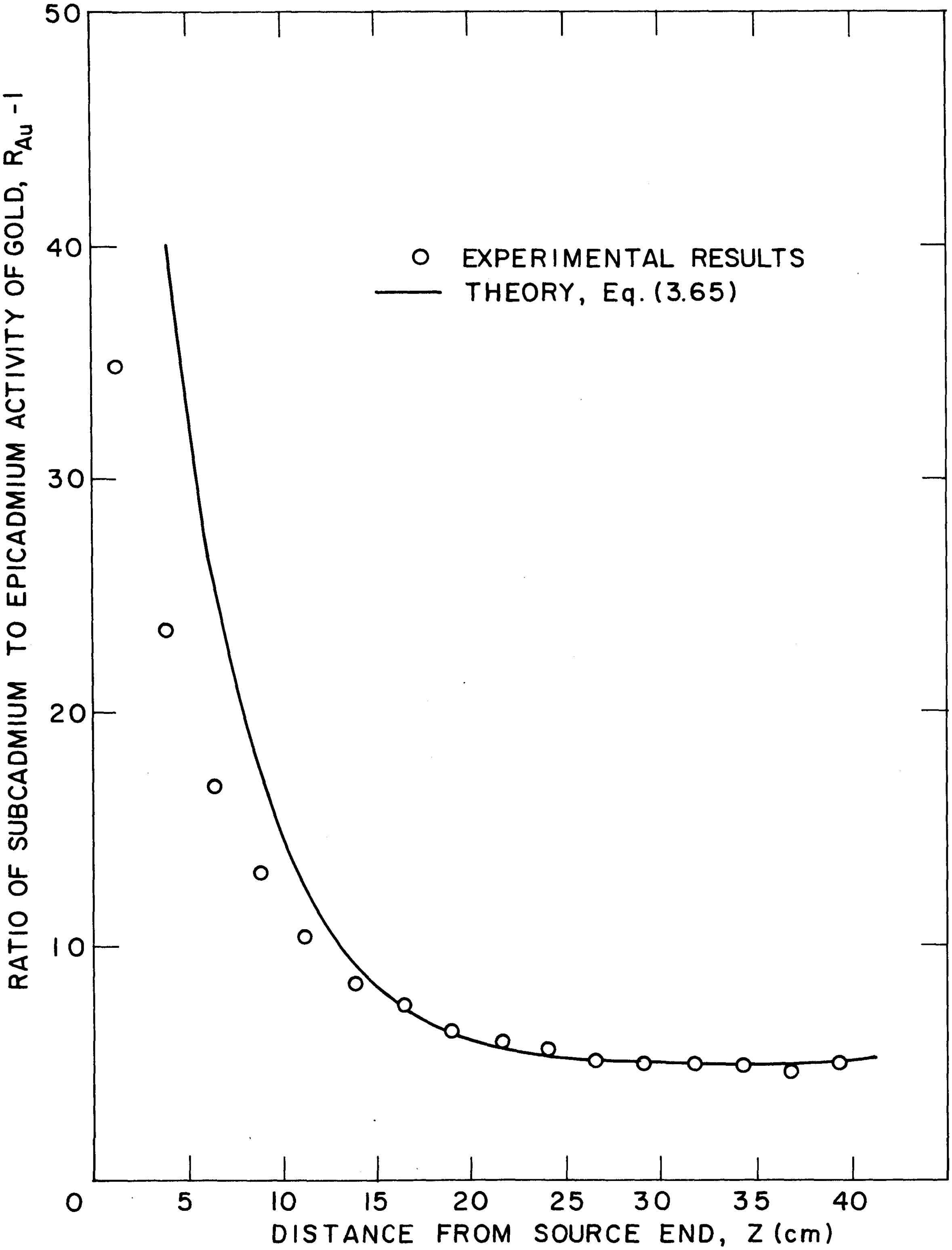

FIG. 4.2 AXIAL DISTRIBUTION OF CADMIUM RATIO OF GOLD IN ML7
ML7: 1.143 % ENRICHED FUEL, D_2O MODERATED
1.75 - INCH SPACING

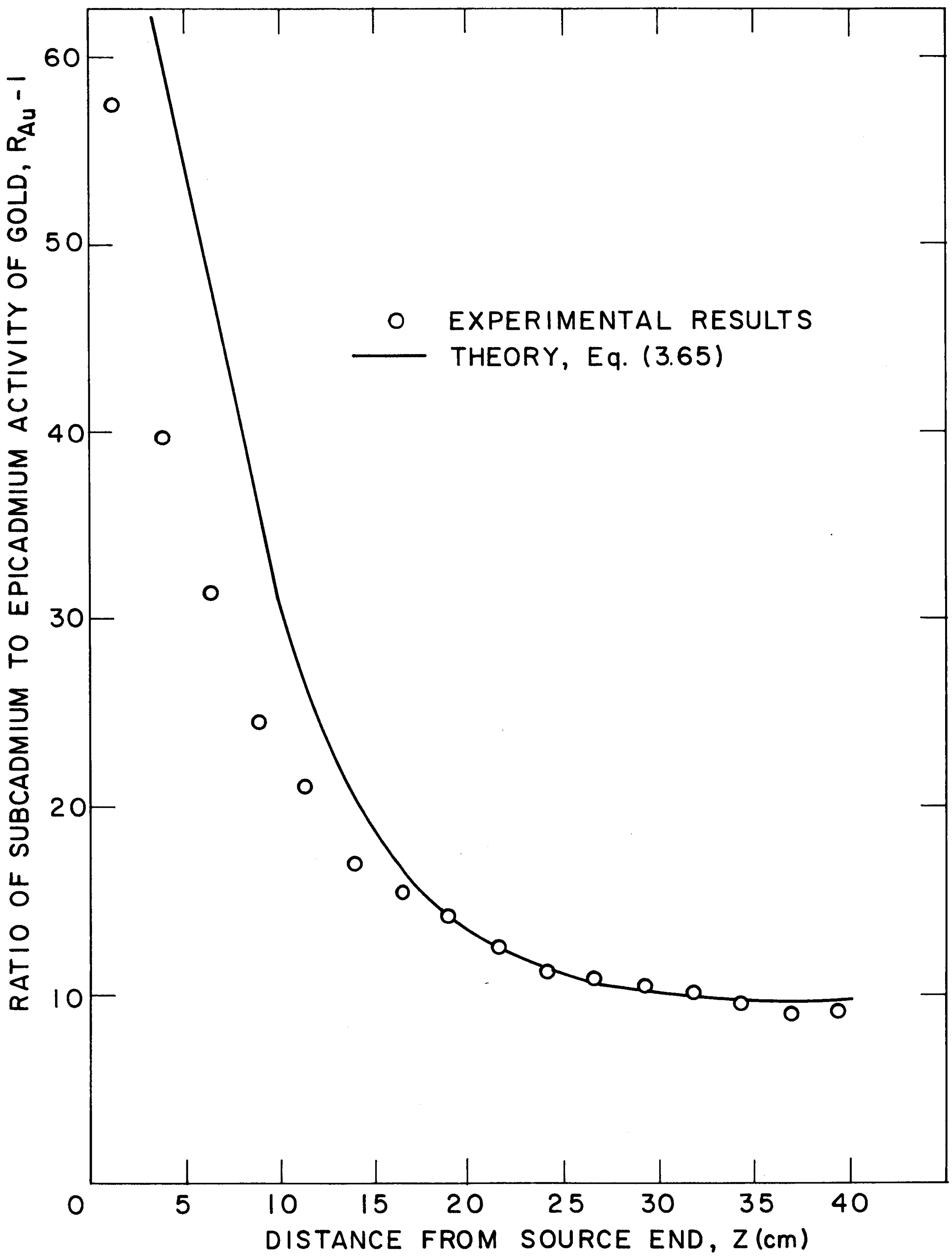

FIG. 4.3 AXIAL DISTRIBUTION OF CADMIUM RATIO OF GOLD IN ML3
ML3: 1.143% ENRICHED FUEL, D_2O MODERATED, 2.50 - INCH SPACING

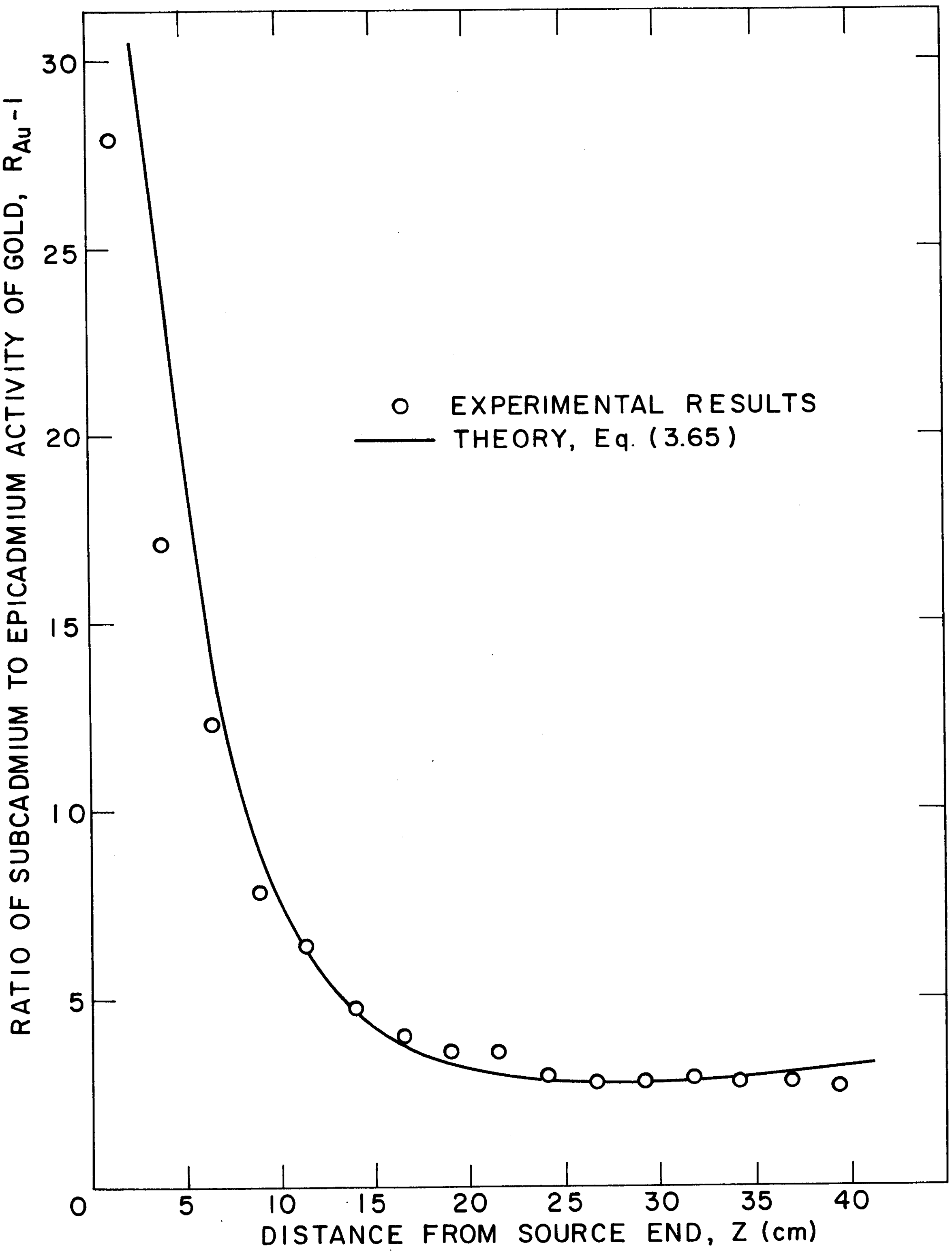

FIG. 4.4 AXIAL DISTRIBUTION OF CADMIUM RATIO OF GOLD IN ML4
ML4 : 1.027 % ENRICHED FUEL, D_2O MODERATED, 1.25 - INCH SPACING

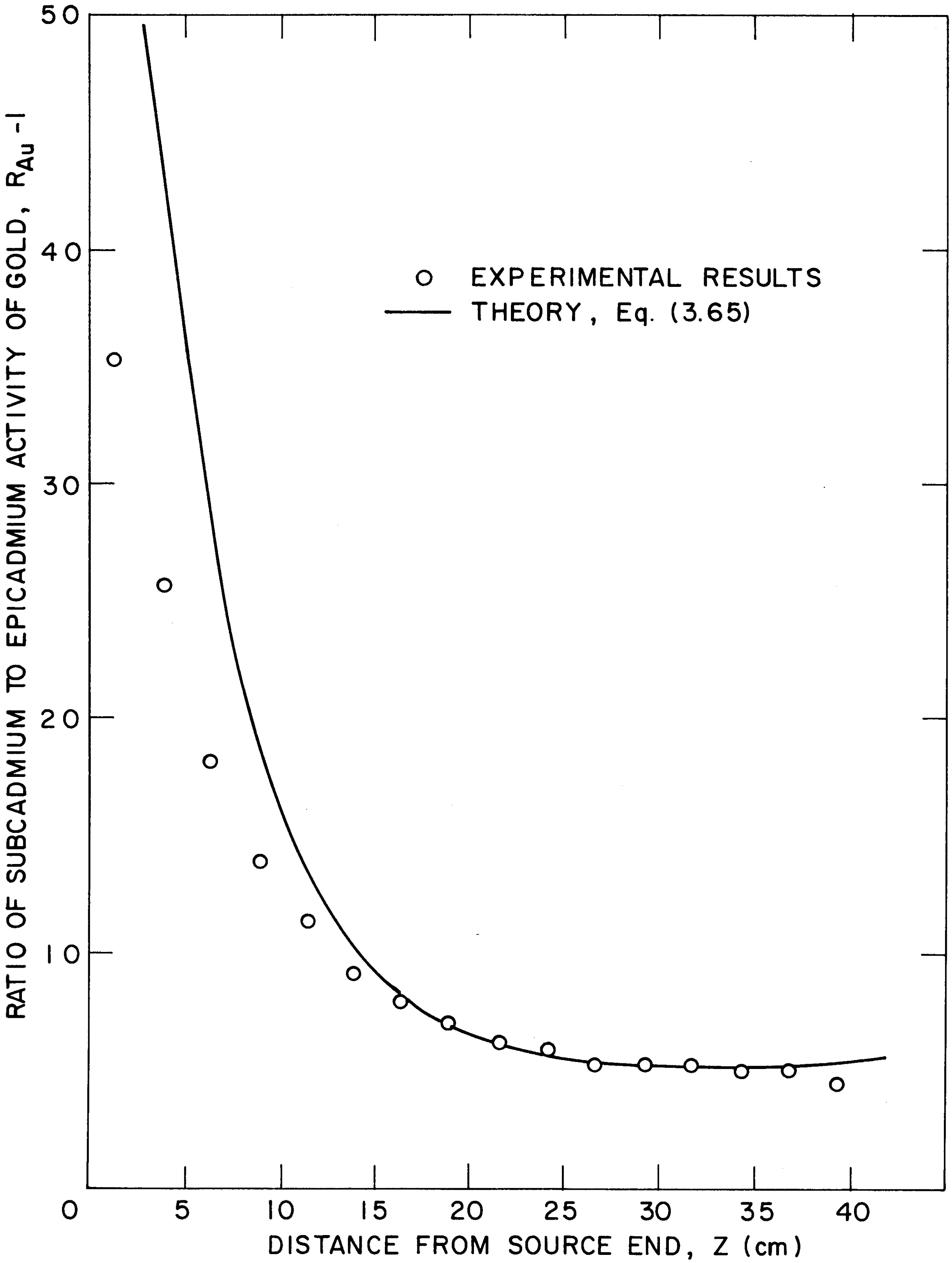

FIG. 4.5 AXIAL DISTRIBUTION OF CADMIUM RATIO OF GOLD IN ML6
ML6: 1.027% ENRICHED FUEL, D_2O MODERATED
1.75 - INCH SPACING

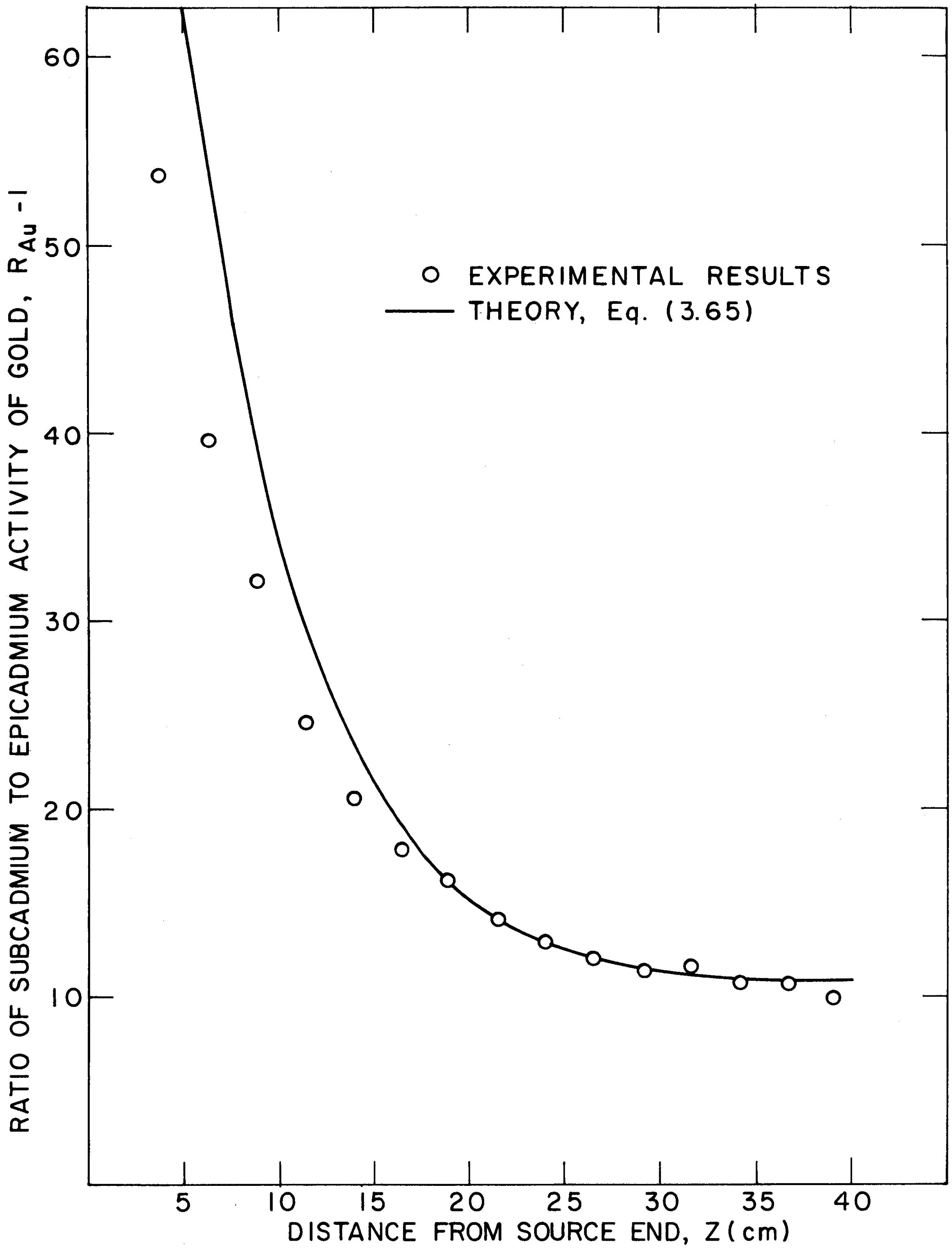

FIG. 4.6 AXIAL DISTRIBUTION OF CADMIUM RATIO OF GOLD IN ML5
ML5 : 1.027% ENRICHED FUEL, D_2O MODERATED,
2.50 - INCH SPACING.

Table 4.1

Parameters Used in MINIFLUX Calculations

Lattice[1]	Spacing (inches)	Enrichment %	V_M/V_F	Radius (cm)	Height (cm)	Σ_a^{ℓ}[4] (cm^{-1})	L_{ℓ}[4] (cm)
ML2	1.25	1.143	25.833	27.641	49.421	0.01191	8.493
ML7	1.75	1.143	52.164	27.576	47.366	0.00640	11.382
ML3	2.50	1.143	108.304	27.522	48.476	0.00326	15.705
ML4	1.25	1.027	25.833	27.617	49.421	0.01131	8.661
ML6	1.75	1.027	52.164	27.573	47.366	0.00608	11.668
ML5	2.50	1.027	108.304	27.528	48.476	0.00308	16.186

Lattice	Σ_a^{s}[4] (cm^{-1})	L_s[4] (cm)	k_∞	τ_{28}[5] (cm^2)	τ_t[4] (cm^2)	$\xi\Sigma_s$ (cm^{-1})	S_{Au}[5]
ML2	0.01072	8.952	1.328[2]	82.30	128.55	0.17455	2.851
ML7	0.00576	11.950	1.416[2]	81.34	124.90	0.17700	2.807
ML3	0.00326	15.705	1.419[2]	79.20	123.69	0.18206	2.787
ML4	0.00961	9.396	1.304[3]	82.30	128.55	0.17455	2.848
ML6	0.00547	12.310	1.375[3]	81.34	124.90	0.17700	2.806
ML5	0.00293	16.595	1.395[3]	79.20	123.69	0.18206	2.788

(1) All lattices have 0.25-inch-diameter rods clad in 0.318-inch-O.D. aluminum tubes in 99.75% D_2O.
(2) Ref. (H7).
(3) Ref. (D1); values corrected for epicadmium fission in U^{235}.
(4) Definitions in Section 3.2.2.
(5) Definitions in Section 3.4.1.

can be used to extrapolate the values of these parameters obtained in the miniature lattice to those that would be obtained in an exponential, a critical or an infinite assembly.

A typical example of the results obtained for the radial distribution of the cadmium ratio of gold is shown in Fig. 4.7. Since each data point in Fig. 4.7 corresponds to a position halfway between adjacent rings of rods, it follows that $R_{Au} - 1$ is constant over a portion of the lattice that includes at least half the total number of rings present. The drop in the value of $R_{Au} - 1$ near the boundary is a consequence of the cadmium layer surrounding the assembly. The density of neutrons with energies below the cadmium cutoff vanishes at the extrapolated radius, whereas the epicadmium neutrons are practically unaffected.

The effect of the cadmium layer is best illustrated in Fig. 4.8, where the subcadmium and epicadmium activities of gold are shown for the lattice ML7.

The results shown in Figs. 4.7 and 4.8, which are typical of the radial distributions observed in all the lattices studied, serve several purposes. First, they indicate that the area corresponding to about half the number of rings in each lattice can be used to measure ρ_{28}, δ_{25} and C^*. Second, they justify the procedure described in Section 4.2.2 to analyze the intracellular subcadmium activity distribution of gold. Third, since the radial distribution of the subcadmium activity of gold follows very closely a J_o-function, as indicated in Fig. 4.8, then to correct δ_{28} as described in Section 3.5.4, the interaction effect can be obtained by weighting the contribution of the surrounding rods with a J_o-function.

4.3.2 Intracellular Activity Distribution of Gold

Intracellular activity distributions of bare and cadmium-covered gold foils were measured in all the lattices investigated. The data were analyzed in accordance with the procedure described in Section 4.2.2.

The magnitude of the correction required to extrapolate the measured distribution of the subcadmium activity of gold to an infinite assembly is illustrated in Fig. 4.9 for the case of ML7. Since $J_o(\alpha r)$ decreases with increasing r, the correction is larger the farther the position of the foil is from the center of the rod. In the lattices with the

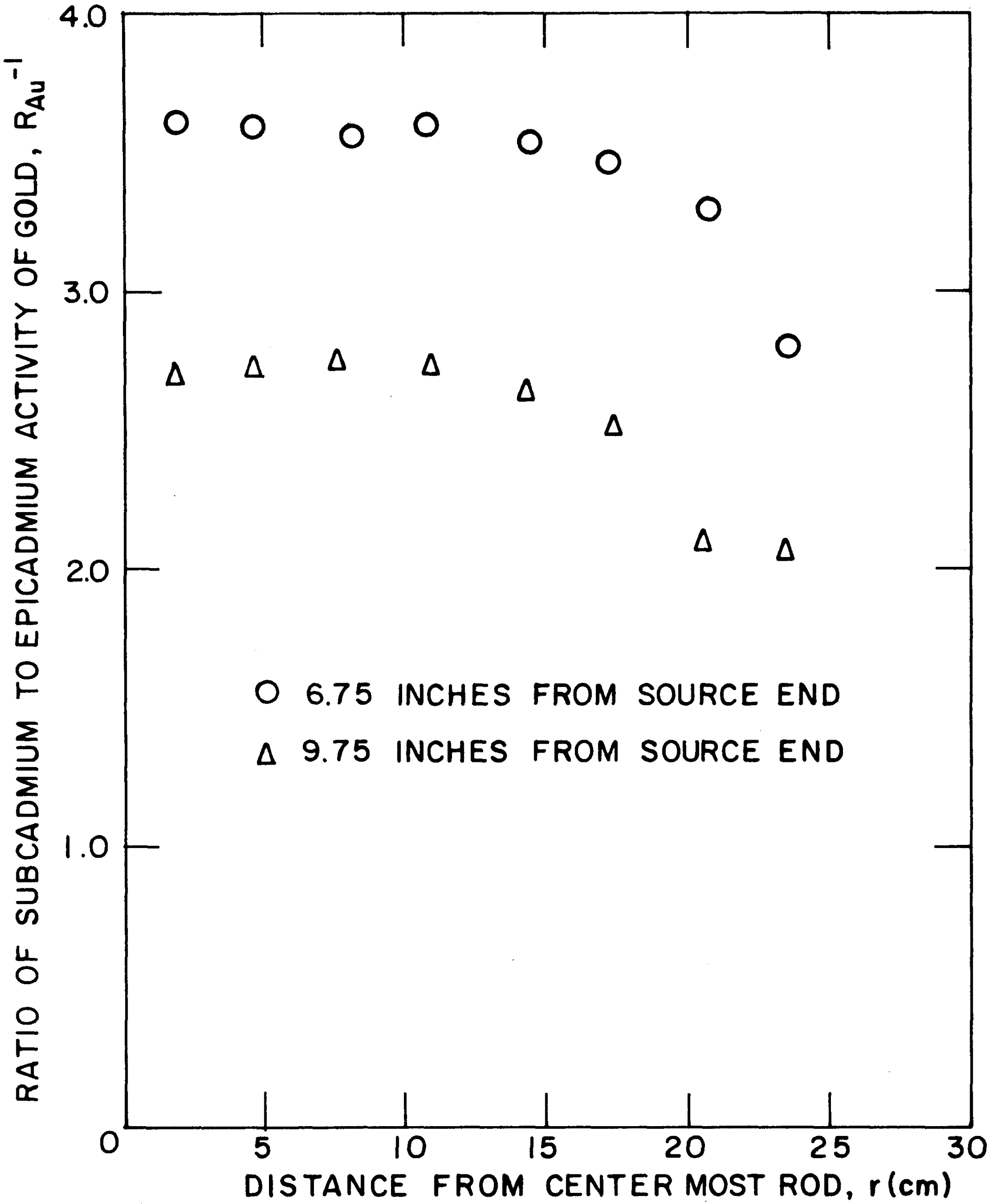

FIG. 4.7 RADIAL DISTRIBUTION OF CADMIUM RATIO OF GOLD IN ML2
ML2: 1.143% ENRICHED FUEL, D_2O MODERATED, 1.25 - INCH SPACING

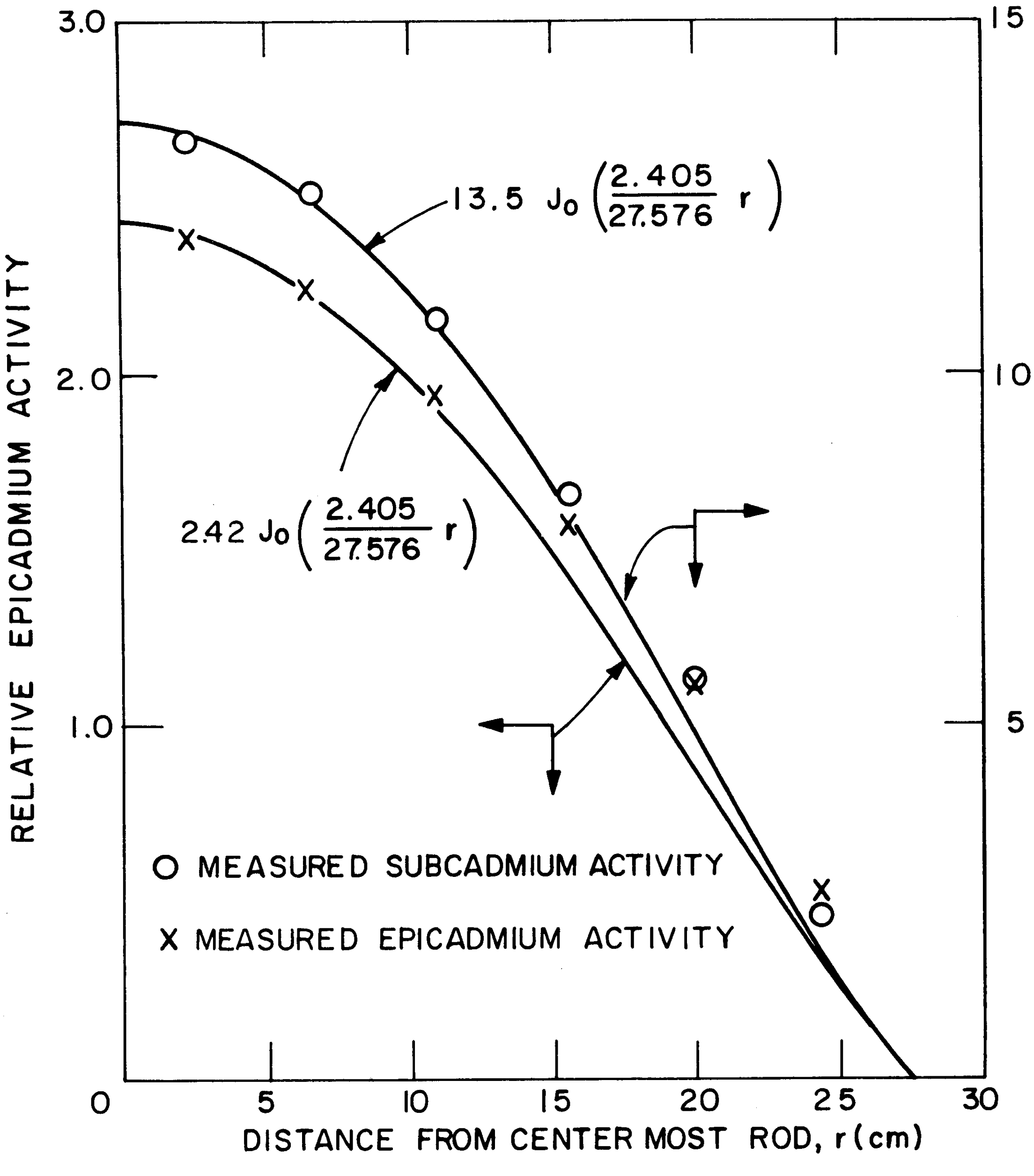

FIG. 4.8 RELATIVE RADIAL ACTIVITY DISTRIBUTION OF GOLD IN ML7, 9.75 INCHES FROM SOURCE END. ML7: 1.143 % ENRICHED FUEL, D_2O MODERATED 1.75 - INCH SPACING

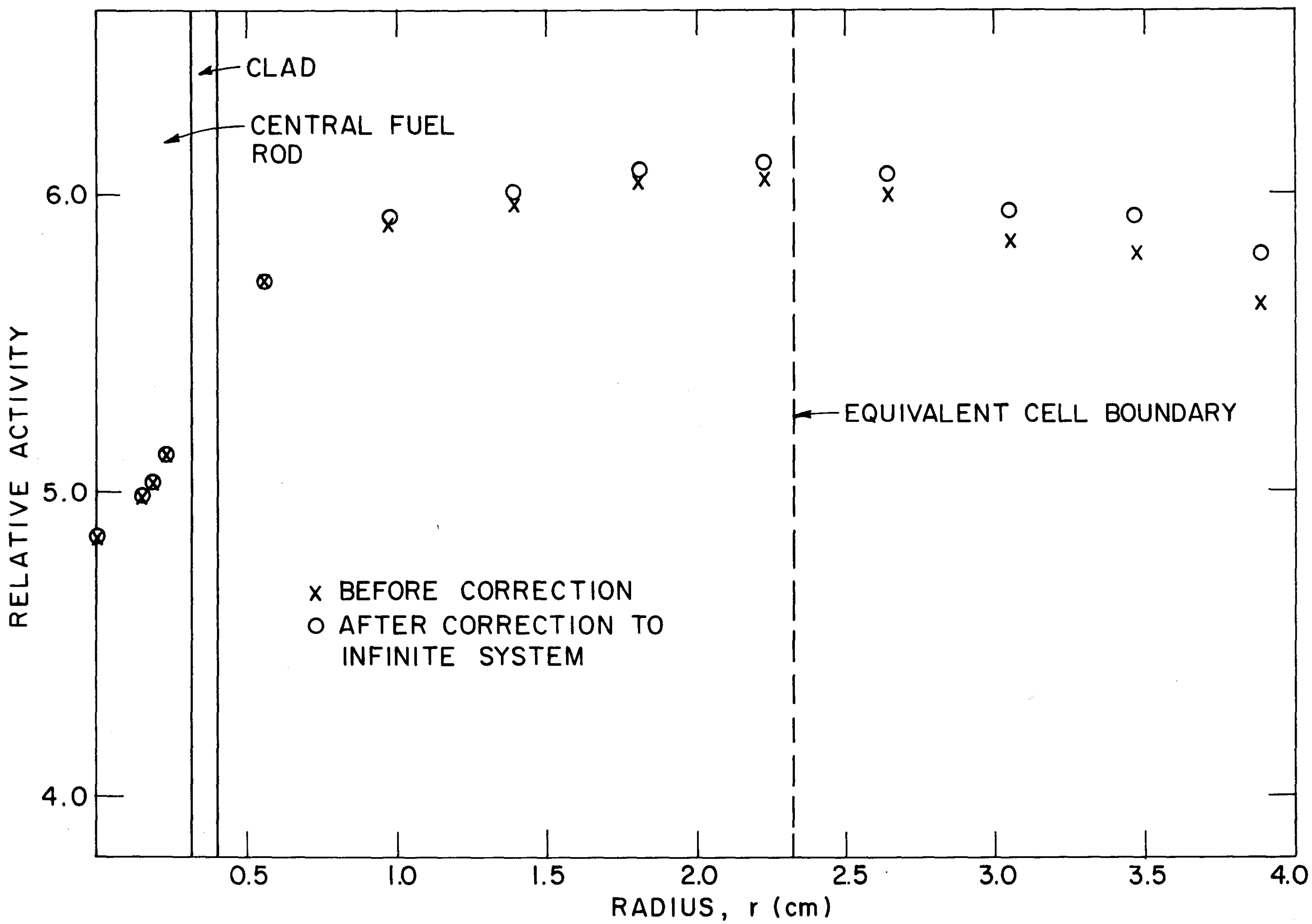

FIG. 4.9 SUBCADMIUM ACTIVITY DISTRIBUTION IN ML7 BEFORE AND AFTER CORRECTION TO INFINITE SYSTEM
ML7: 1.143% ENRICHED FUEL, D_2O MODERATED, 1.75-INCH SPACING

greatest rod separation, those with 2.50-inch spacing, the correction is close to 7% for the foil position farthest away from the center of the rod. If one considers only the foils placed between the center of the rod and the cell boundary, then the correction is at most 2.5% to 3%.

The intracellular epicadmium and subcadmium activity distributions of gold foils observed in ML2 are shown in Fig. 4.10. Two independent measurements were made; the results are shown in Fig. 4.10 and indicate the spread observed in the data. A detailed discussion of the uncertainties in intracellular measurements is given in Refs. (S1) and (B2). In Fig. 4.10, the results obtained in similar measurements in the exponential facility at M. I. T. are also shown. The results in the miniature lattice compare favorably with those made in the exponential assembly. The activation distribution of gold predicted by THERMOS is also shown. The distributions obtained in both the miniature and exponential lattices agree with those predicted by THERMOS.

Figures 4.11 and 4.12 show the intracellular gold activity distributions measured in ML4. The measurements were made at two different heights, 9 and 13 inches from the source end. In both cases, the agreement between the results in the miniature and exponential lattices is good, and both agree with the predictions of THERMOS. Calculations made with the MINIFLUX program indicate that for:

$$z = 9 \text{ inches}, \quad \phi_\ell/\phi_s \simeq 1 \;;$$

$$z = 13 \text{ inches}, \quad \phi_\ell/\phi_s \simeq 4 \;;$$

yet there is no essential difference in the intracellular distributions observed.

Physically, this effect can be explained as follows. The neutrons coming from the source which impinge on the fuel rods disappear very rapidly, since the thermal mean free path in the fuel is small. Thus, after a few centimeters, the only source neutrons that are in the lattice are those diffusing through the moderator. After a few mean free paths of the assembly, the spectrum of these neutrons approaches the energy distribution of the neutrons born in the lattice.

The results just discussed substantiate the statement made in Section 3.5.5, regarding Eq. (3.90). If the ratio $(\sigma_s/\sigma_\ell)_{Au}$ varied strongly across the cell, the effect of the difference between the spectra

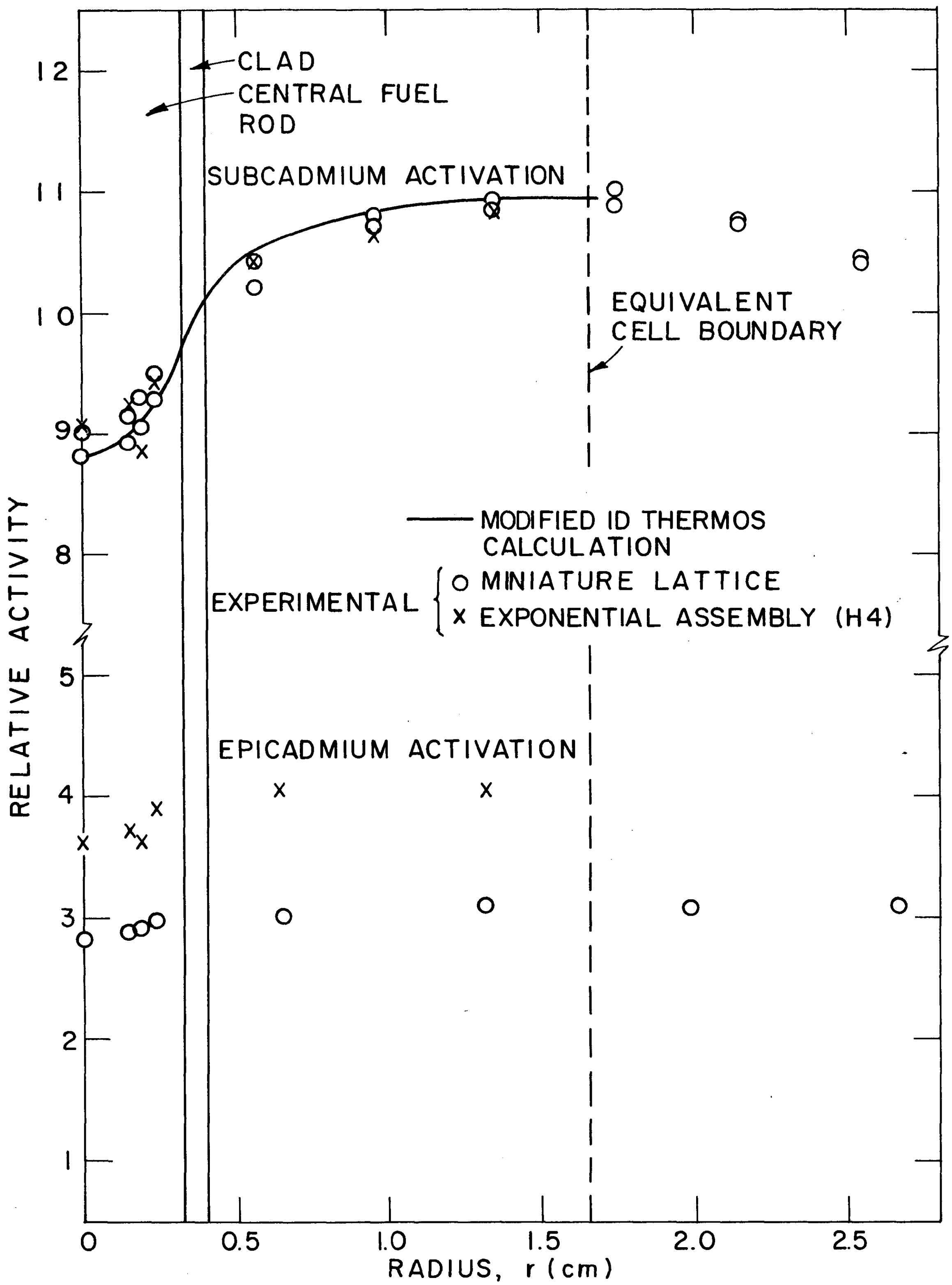

FIG. 4.10 INTRACELLULAR ACTIVITY DISTRIBUTION OF GOLD IN ML2
ML2: 1.143 % ENRICHED FUEL, D_2O MODERATED LATTICE ON A 1.25-INCH TRIANGULAR SPACING

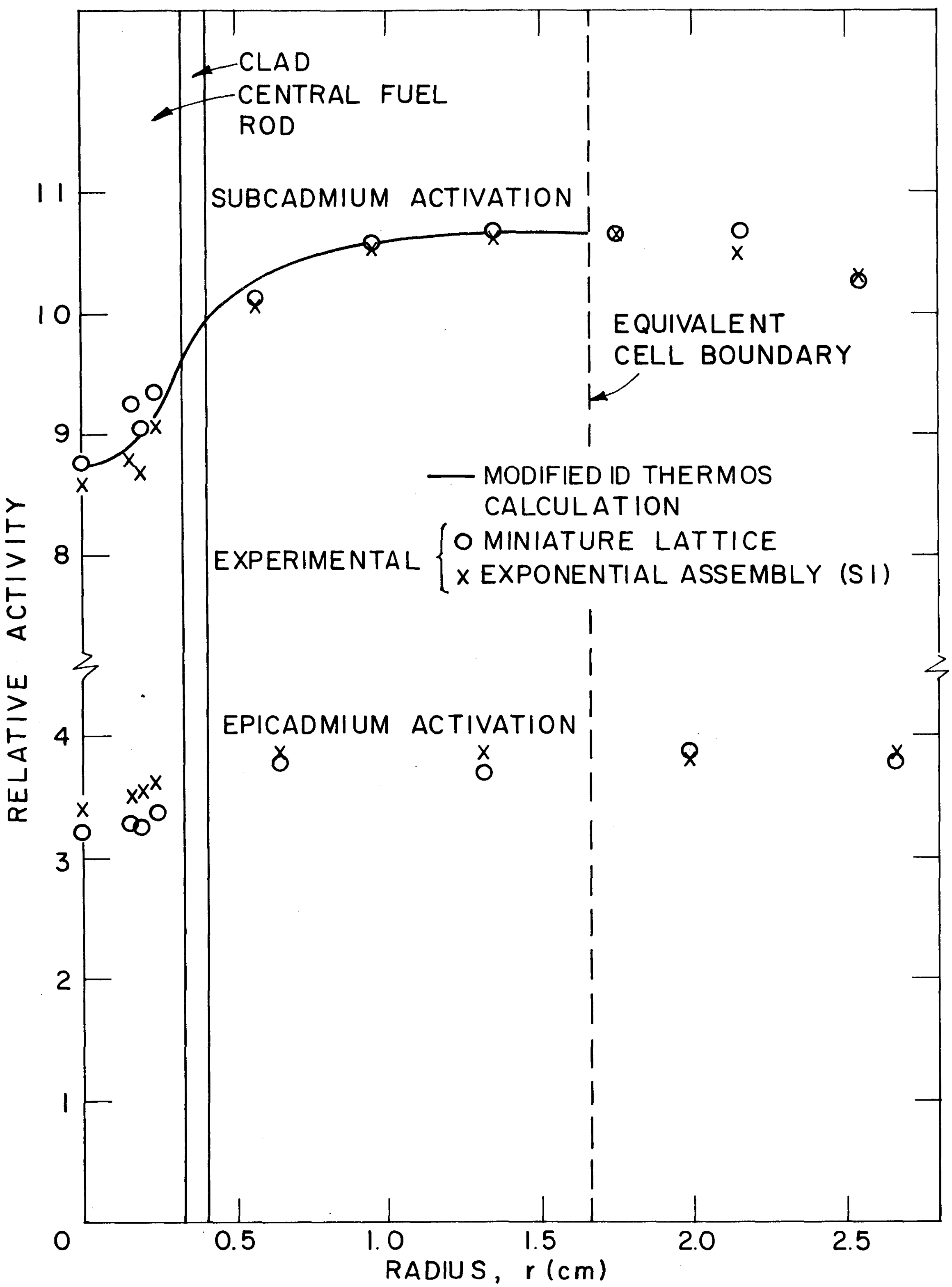

FIG. 4.11 INTRACELLULAR ACTIVITY DISTRIBUTION OF GOLD IN ML4; 9-INCHES FROM SOURCE END.
ML4: 1.027 % ENRICHED FUEL, D_2O MODERATED LATTICE ON 1.25-INCH TRIANGULAR SPACING

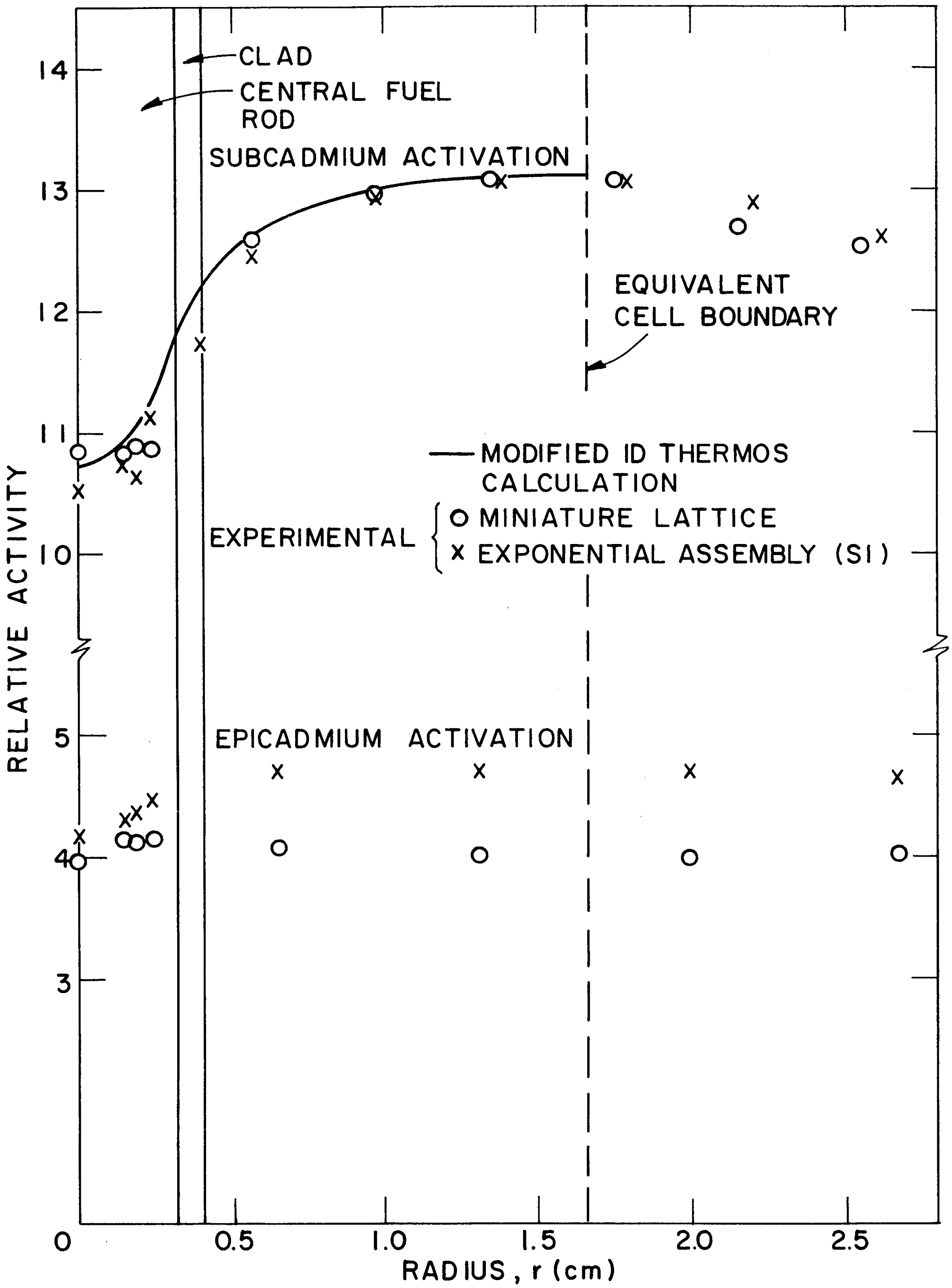

FIG. 4.12 INTRACELLULAR ACTIVITY DISTRIBUTION OF GOLD IN ML4; 13 INCHES FROM SOURCE END.
ML4: 1.027% ENRICHED FUEL, D_2O MODERATED LATTICE ON 1.25-INCH TRIANGULAR SPACING

of source and lattice-born neutrons would have been observed in the intracellular measurements made at two heights in ML4; the difference in the ratio ϕ_ℓ/ϕ_s at the two heights is large enough so that some perturbation in the intracellular distribution should become apparent. Since no significant difference was observed in the results obtained at the two heights, the ratio $(\sigma_s/\sigma_\ell)_{Au}$ must be constant across the cell, and no correction needs to be applied for the fact that an appreciable portion of the activity of the gold foils in an intracellular measurement comes from source neutrons.

Figures 4.13 through 4.16 show the subcadmium and epicadmium activity distributions observed in the rest of the lattices investigated. The results obtained in the miniature lattice agree well with those in exponential lattices for all the assemblies studied. The activity distributions predicted by THERMOS agree well with the distributions measured in both the miniature lattice and in the exponential facility at M. I. T.

To compare the intracellular measurements in miniature lattices and exponential assemblies, the activity distributions were normalized so that the mean value of the two data points nearest to the cell boundary in the subcadmium activity distribution agreed in the two assemblies. As a result of this normalization, the magnitude of the epicadmium activity is not necessarily the same in the miniature and exponential lattices, although the shape of the radial dependence is nearly the same. But, when the epicadmium gold activity is subtracted from the activities measured in the bare foils, the resulting distributions in the miniature and exponential lattices coincide. This result was expected because the measurements in the exponential facility at M. I. T. were made in the equilibrium region of the assembly (as indicated by the constant value of the cadmium ratio), while those in the miniature lattice were made in a region which was far from equilibrium.

As a result of the agreement between the measured subcadmium activity distributions of gold and those predicted by THERMOS, the values of the thermal energy region parameters and of the thermal utilization f computed by THERMOS will be assumed to be valid for the lattices under study. The use of THERMOS is discussed in Section 5.2.2.

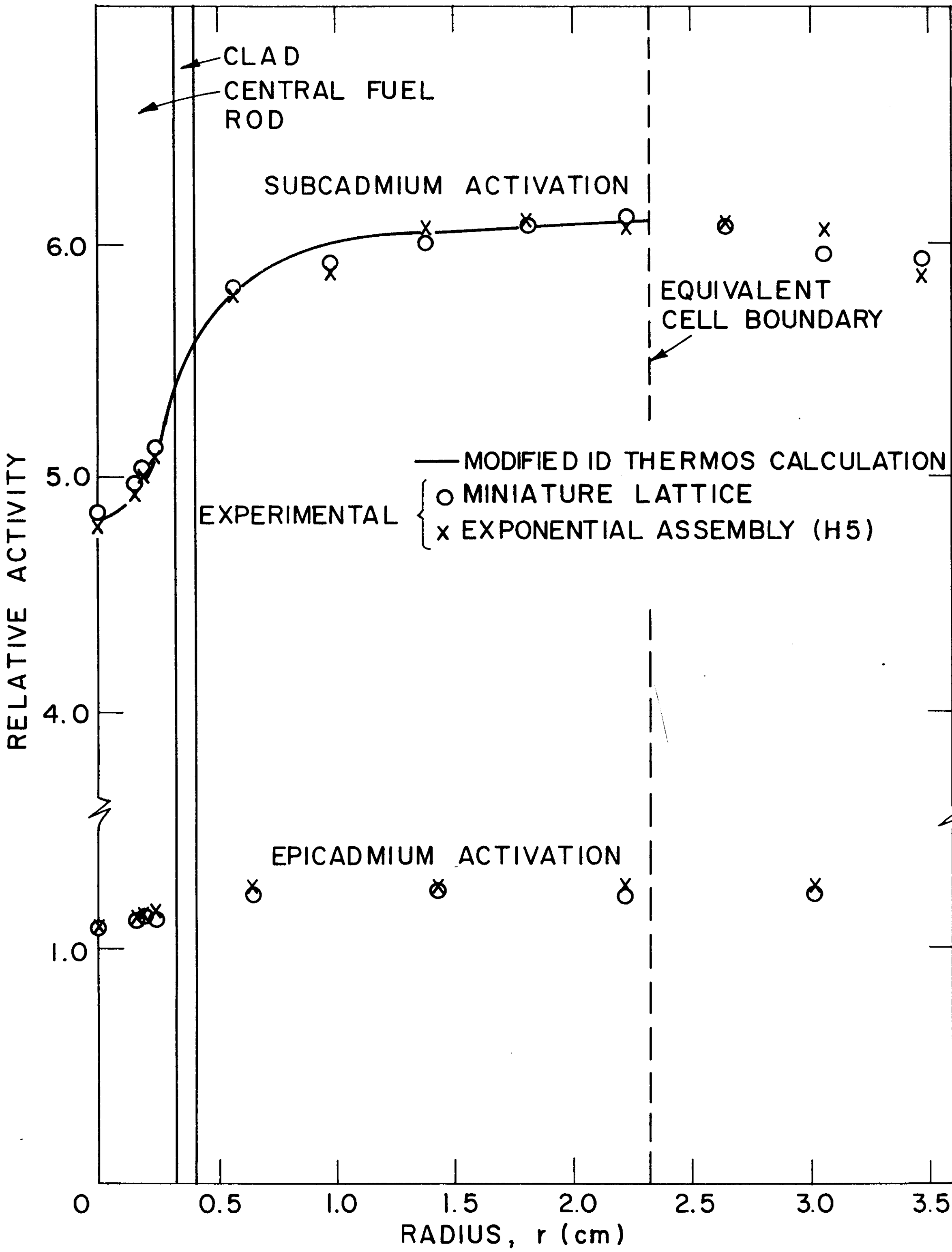

FIG. 4.13 INTRACELLULAR ACTIVITY DISTRIBUTION OF GOLD IN ML7
ML7: 1.143% ENRICHED FUEL, D_2O MODERATED LATTICE ON A 1.75-INCH TRIANGULAR SPACING

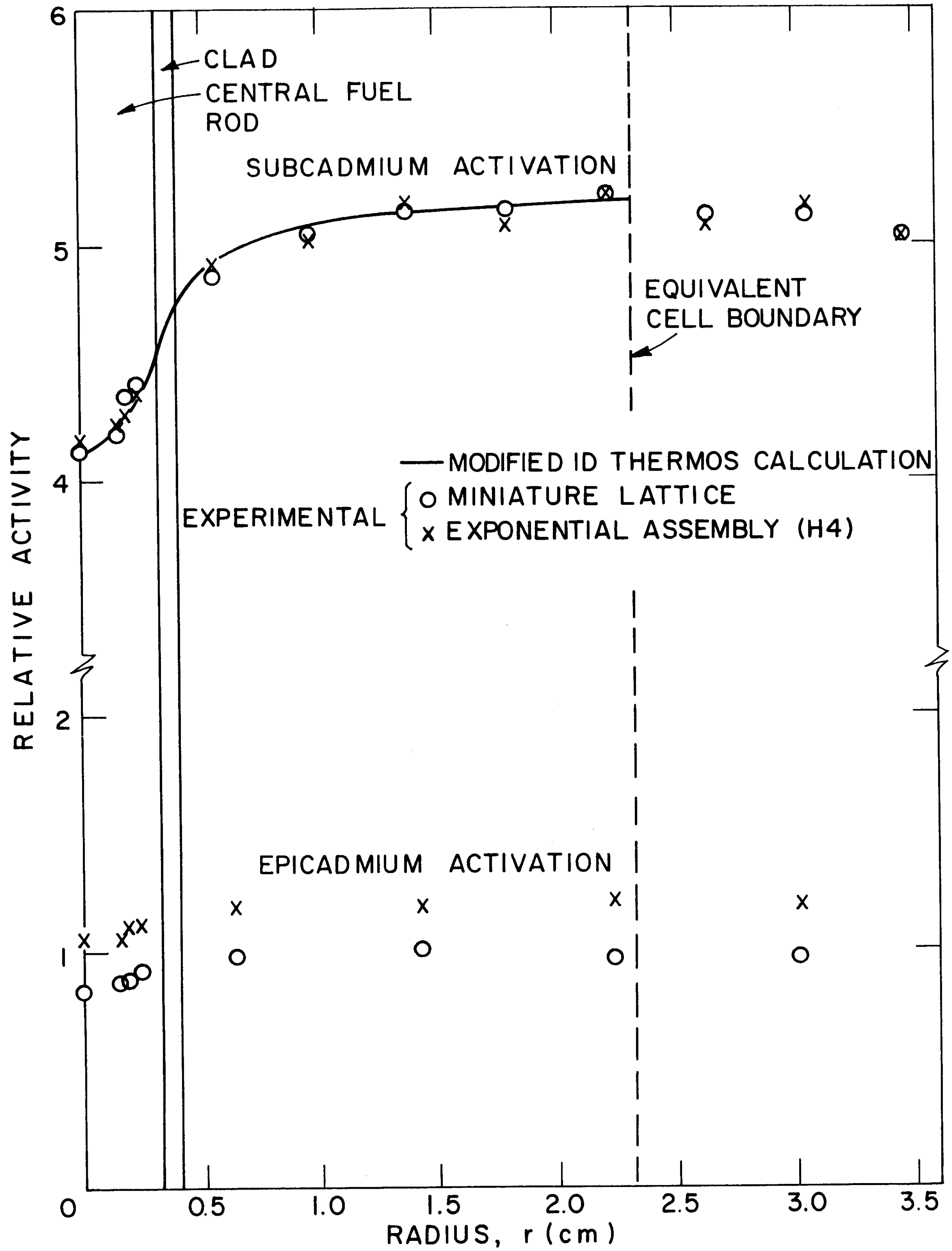

FIG. 4.14 INTRACELLULAR ACTIVITY DISTRIBUTION OF GOLD IN ML6
ML6 : 1.027% ENRICHED FUEL, D_2O MODERATED LATTICE
ON A 1.75-INCH TRIANGULAR SPACING

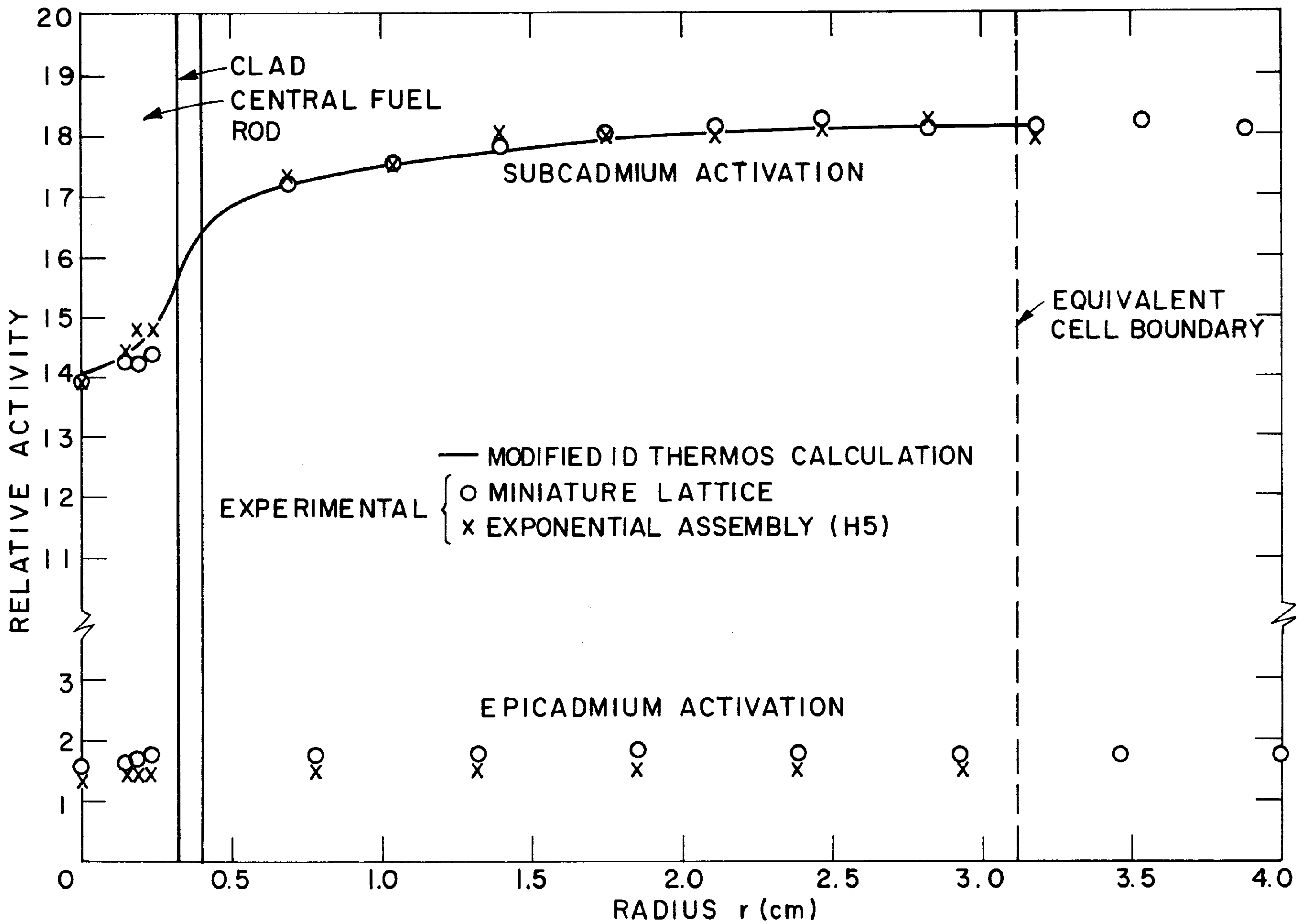

FIG. 4.15 INTRACELLULAR ACTIVITY DISTRIBUTION OF GOLD IN ML3
ML3: 1.143 % ENRICHED FUEL, D O MODERATED LATTICE ON A 2.50-INCH TRIANGULAR SPACING

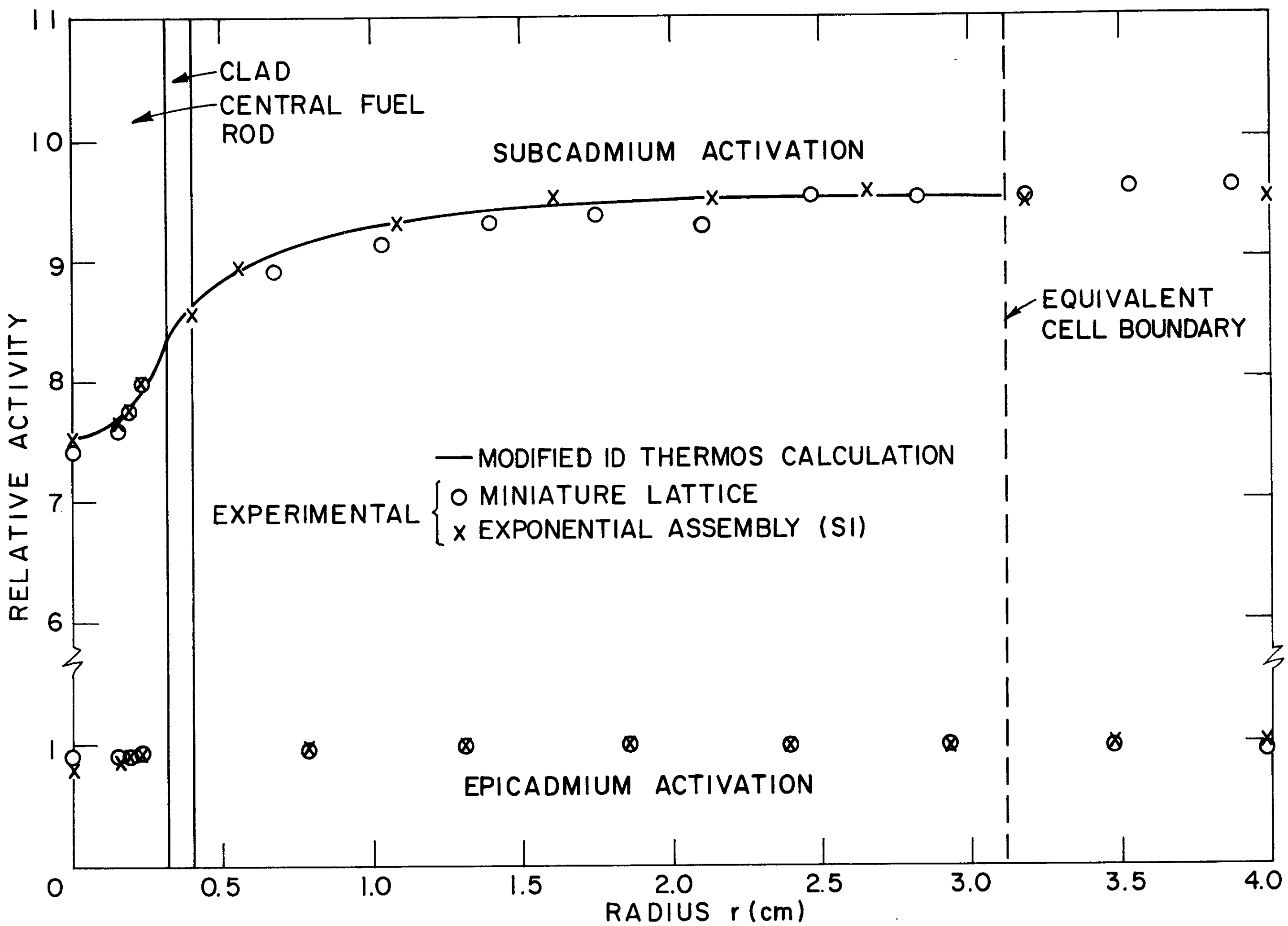

FIG. 4.16 INTRACELLULAR ACTIVITY DISTRIBUTION OF GOLD IN ML5
ML5: 1.027% ENRICHED FUEL, D_2O MODERATED LATTICE ON A 2.50-INCH TRIANGULAR SPACING

4.3.3 ρ_{28}, δ_{25}, δ_{28} and C^*

The parameters ρ_{28}, δ_{25}, δ_{28} and C^*, defined in Section 2.7, were measured in all the lattices investigated. The extrapolation techniques, developed in Sections 3.5.1 through 3.5.4, were applied to the results obtained for these parameters in miniature lattices. Extrapolations were made to exponential (EX), critical (C) and infinite (∞) assemblies, of similar composition and geometric configuration. The required extrapolation corrections were summarized in Table 3.2.

Except for the extrapolation factor for δ_{28}, all corrections involve the functions $\psi(r, z)$. This function, which was defined in Eq. (3.66), is a measure of the ratio of the epithermal flux to the thermal flux in a given assembly. This ratio will vary with the size of the assembly. The variation of $\psi(r, z)$ with z/H is illustrated in Figs. 4.17 and 4.18; the function is plotted for a miniature lattice and for an exponential assembly. Figure 4.17 shows $\psi(r, z)$ for ML2, the tightest lattice studied, and Fig. 4.18 shows $\psi(r, z)$ for ML5. The axial position in which the miniature lattice measurements were made is indicated in both cases. In the exponential assembly, the determinations were all made in the equilibrium region, i. e., the region in which $\psi(r, z)$ is constant. It is evident from Figs. 4.17 and 4.18 that in none of the miniature lattices studied is an equilibrium region obtained.

It may be inferred from these results that before measurements are made in an exponential assembly, it is necessary to determine where the equilibrium region is. According to Eq. (3.65), the cadmium ratio of gold measured in the moderator depends on $\psi(r, z)$, so that the cadmium ratio can be used to determine where the equilibrium region begins. This procedure is usually followed in reactor physics studies in exponential assemblies.

The values of ρ_{28}, δ_{25}, δ_{28} and C^* measured in the miniature lattices are shown in Tables 4.2 and 4.3. Table 4.2 shows the results in the lattices with 1.143% enriched fuel and Table 4.3, the data for the assemblies with 1.027% enriched fuel. The two tables also show the values of these parameters extrapolated to exponential, critical and infinite assemblies. The values to be compared are those measured in the exponential assembly (third row) and those extrapolated from measurements in miniature lattices (second row). The miniature

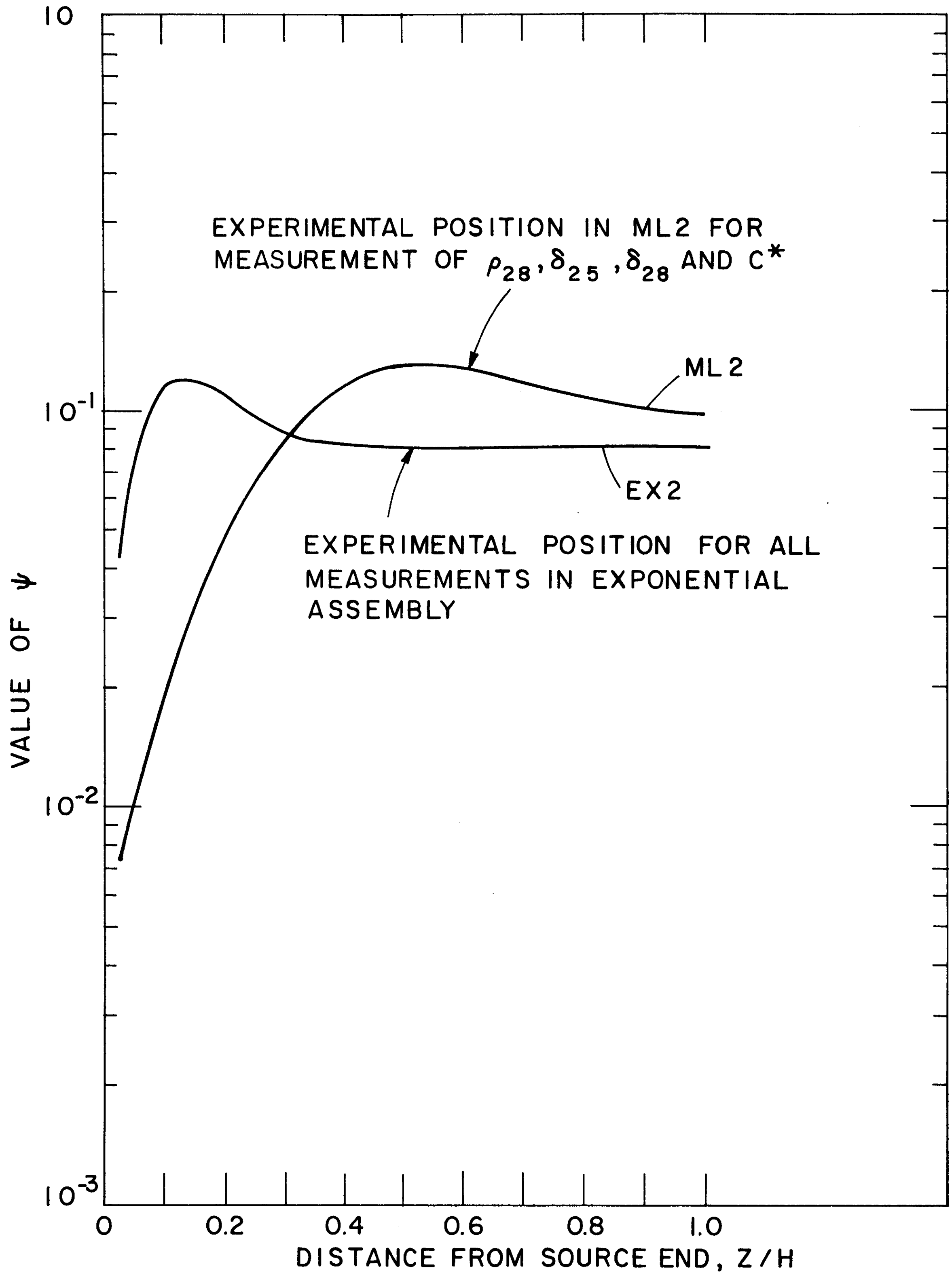

FIG. 4.17 VARIATION OF THE FUNCTION $\psi = pq/\zeta \Sigma_s \phi_t$ WITH Z, FOR ML2 AND THE CORRESPONDING EXPONENTIAL ASSEMBLY
ML2: 1.143% ENRICHED FUEL, D_2O MODERATED
1.25-INCH SPACING

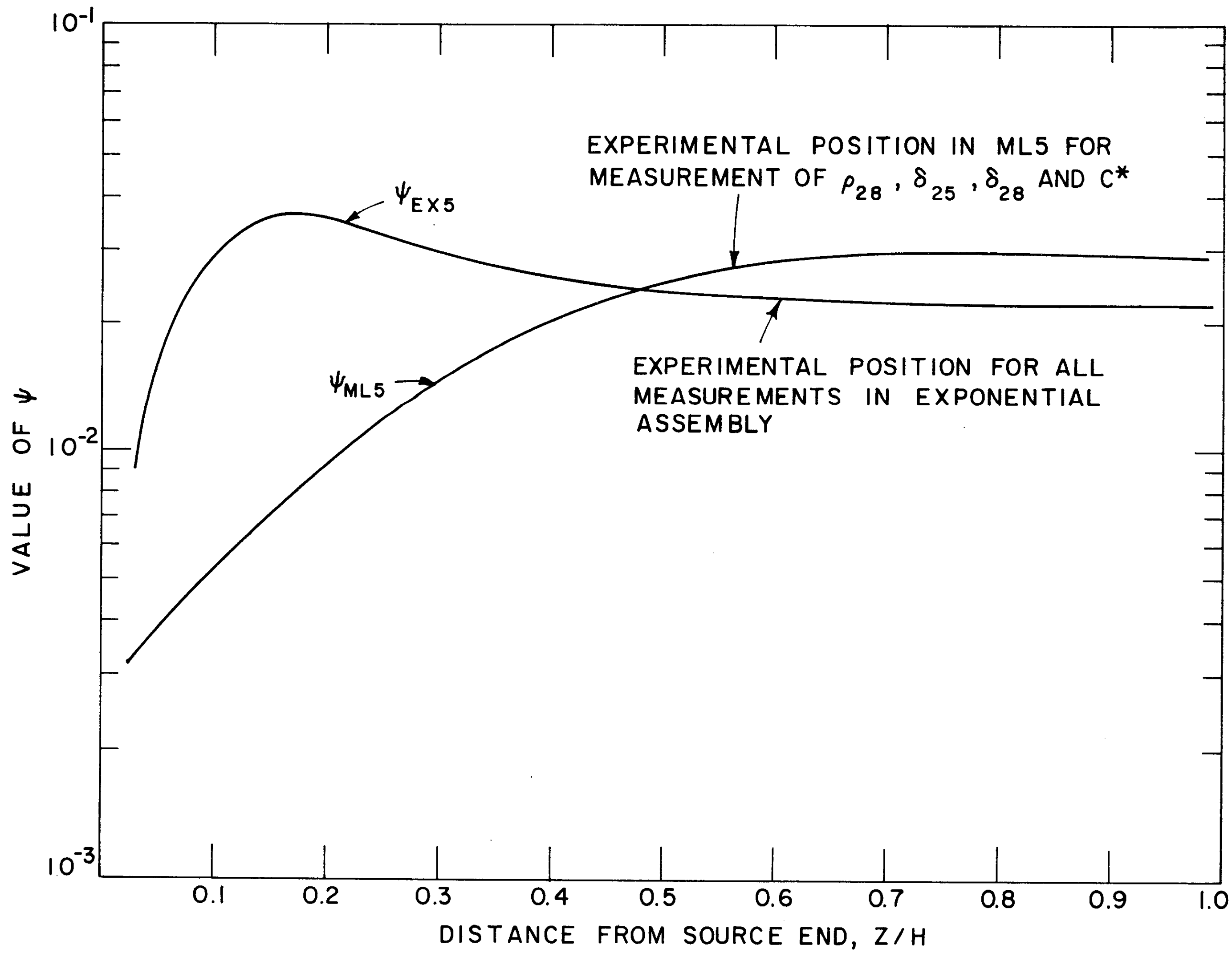

FIG. 4.18 VARIATION OF THE FUNCTION $\psi = pq/\xi \Sigma_s \phi_t$ WITH Z, FOR ML5 AND THE CORRESPONDING EXPONENTIAL ASSEMBLY.
ML5 : 1.027 % ENRICHED FUEL, D_2O MODERATED, 2.5-INCH SPACING

Table 4.2

Experimental Data and Extrapolated Results for Lattices with 1.143% Enriched Fuel. Similar Data in Exponential Assemblies (EX).

Assembly	δ_{28}	ρ_{28}	δ_{25}	C^*_{MAX} (1)	C^*_{SC} (2)	ψ (3)
ML2	0.0252 ±.0010	0.916 ±.017	0.0863 ±.0033	0.740 ±.009	0.739 ±.007	0.1280
ML2 to EX	0.0268 ±.0011	0.861 ±.016	0.0609 ±.0023	0.732 ±.009	0.734 ±.007	0.0805
EX (meas.)	0.0264 (4) ±.0040	0.813 (5) ±.067	0.0584 (5) ±.0044	0.799 (5) ±.084	0.717 (5) ±.026	0.0805
ML2 to C		0.927 ±.017	0.0624 ±.0024	0.748 ±.009	0.759 ±.007	0.0809
ML2 to ∞	0.0278 ±.0011	1.111 ±.021	0.0716 ±.0027	0.802 ±.010	0.824 ±.008	0.0908
ML7	0.0195 ±.0007	0.395 ±.007	0.0398 ±.0010	0.571 ±.025	0.556 ±.003	0.05625
ML7 to EX	0.0204 ±.0007	0.476 ±.009	0.0364 ±.0009	0.597 ±.026	0.591 ±.003	0.04562
EX (meas.)	0.0204 (4) ±.0030	0.471 (5) ±.017	0.0385 (5) ±.0099	0.630 (5) ±.051	0.589 (5) ±.010	0.04562
ML7 to C		0.514 ±.010	0.0374 ±.0009	0.606 ±.026	0.605 ±.003	0.04580
ML7 to ∞	0.0209 ±.0007	0.624 ±.012	0.0434 ±.0011	0.639 ±.028	0.644 ±.004	0.05230
ML3	0.0169 ±.0040	0.198 ±.002	0.0159 ±.0010	0.487 ±.017	0.488 ±.001	0.02780
ML3 to EX	0.0174 ±.0041	0.251 ±.003	0.0153 ±.0010	0.504 ±.018	0.509 ±.001	0.02380
EX (meas.)	0.0164 (4) ±.0010	0.222 (5) ±.026	0.0160 (5) ±.0056	0.492 (5) ±.050	0.498 (5) ±.011	0.02380
ML3 to C		0.272 ±.003	0.0156 ±.0010	0.511 ±.018	0.520 ±.001	0.02360
ML3 to ∞	0.0176 ±.0042	0.306 ±.004	0.0170 ±.0011	0.521 ±.018	0.531 ±.001	0.02540

(1) $C^*_{MAX} = C^*_M \dfrac{R_N}{R_F}$.

(2) $C^*_{SC} = \dfrac{1+\rho_{28}}{1+\delta_{25}} \left(\dfrac{\Sigma_a^{28}}{\Sigma_f^{25}}\right)_{SC}$.

(3) $\psi(r,z) = \dfrac{pq(r,z,\tau_{28})}{\xi\Sigma_s\phi_t(r,z)}$.

(4) Ref. (H5).

(5) Data from Ref. (R3) reanalyzed by present author.

Table 4.3

Experimental Data and Extrapolated Results for Lattices with 1.027% Enriched Fuel. Similar Data in Exponential Assemblies (EX).

Assembly	δ_{28}	ρ_{28}	δ_{25}	C^{*}_{MAX} (1)	C^{*}_{SC} (2)	ψ (3)
ML4	0.0259 ±.0012	0.876 ±.024	0.0826 ±.0021	0.829 ±.060	0.804 ±.010	0.1160
ML4 to EX	0.0274 ±.0013	0.856 ±.023	0.0609 ±.0015	0.831 ±.060	0.809 ±.010	0.0758
EX (meas.)	0.0274 (4) ±.0012	0.845 (5) ±.007	0.0525 (4) ±.0100	0.814 (5) ±.007	0.792 (5) ±.002	0.0758
ML4 to C		0.937 ±.026	0.0631 ±.0016	0.856 ±.062	0.842 ±.010	0.0766
ML4 to ∞	0.0285 ±.0013	1.087 ±.030	0.0705 ±.0018	0.900 ±.065	0.901 ±.011	0.0844
ML6	0.0200 ±.0008	0.345 ±.005	0.0336 ±.0007	0.631 ±.035	0.601 ±.002	0.0515
ML6 to EX	0.0209 ±.0008	0.425 ±.006	0.0318 ±.0007	0.655 ±.036	0.637 ±.003	0.0427
EX (meas.)	0.0217 (4) ±.0007	0.437 (5) ±.003	0.0310 (4) ±.0013	0.625 (5) ±.016	0.644 (5) ±.003	0.0427
ML6 to C		0.462 ±.007	0.0328 ±.0007	0.669 ±.037	0.652 ±.003	0.0429
ML6 to ∞	0.0215 ±.0009	0.534 ±.008	0.0367 ±.0008	0.692 ±.038	0.680 ±.004	0.0473
ML5	0.0159 ±.0015	0.156 ±.002	0.0148 ±.0005	0.552 ±.017	0.525 ±.011	0.0214
ML5 to EX	0.0163 ±.0015	0.242 ±.003	0.0174 ±.0006	0.574 ±.018	0.563 ±.012	0.0224
EX (meas.)	0.0183 (4) ±.0007	0.227 (5) ±.0014	0.0188 (4) ±.0023	0.551 (5) ±.002	0.547 (5) ±.003	0.0224
ML5 to C		0.260 ±.003	0.0175 ±.0006	0.580 ±.018	0.570 ±.012	0.0219
ML5 to ∞	0.0165 ±.0015	0.290 ±.004	0.0193 ±.0007	0.588 ±.018	0.583 ±.012	0.0236

(1) $C^{*}_{MAX} = C^{*}_{M} \dfrac{R_N}{R_F}$.

(2) $C^{*}_{SC} = \dfrac{1+\rho_{28}}{1+\delta_{25}} \left(\dfrac{\Sigma_a^{28}}{\Sigma_f^{25}}\right)_{SC}$.

(3) $\psi(r,z) = \dfrac{pq(r,z,\tau_{28})}{\xi\Sigma_s\phi_t(r,z)}$.

(4) Ref. (B1).

(5) Ref. (D1).

lattice data are the result of a single measurement and the quoted errors, in each case, represent only the uncertainty of that determination due to counting statistics. The data for the exponential assemblies are usually the result of six independent measurements; the errors quoted, therefore, represent more closely the actual experimental accuracy of a measurement.

It is evident from the results shown in Tables 4.2 and 4.3 that the values of the parameters extrapolated from miniature lattices compare favorably with the results of similar measurements in exponential assemblies. The extrapolated values generally lie within the range given by the experimental uncertainties of the value of the parameter obtained in the exponential lattices.

The comparison between the values of the parameters obtained by extrapolating the miniature lattice results and the measurements made in corresponding exponential assemblies is more readily made in Figs. 4.19 through 4.22. The error flags shown to the right of the points represent the statistical accuracy for the single measurement in a miniature lattice. The error flag to the left represents the quoted error for the results obtained in the exponential assembly. As mentioned above, the two results agree, in general, within the experimental errors.

In Tables 4.2 and 4.3, the values of ψ are also quoted for each condition. In all cases, the value of ψ in the equilibrium region of the exponential assembly is different from that in the corresponding critical assembly. This difference, which is about 1% for the case of ML5, indicates that the spectrum of neutrons in the equilibrium region of an exponential assembly is not quite that which would be observed in a critical assembly. If only the value of the function ψ entered into the extrapolation of the parameters ρ_{28}, δ_{25} and C^*, the difference between ψ_{EX} and ψ_C would have no significant effect on the extrapolation. This conclusion follows from the fact that the errors quoted for the measured values of these parameters in the exponential facility are, in most cases, larger than the differences between ψ_{EX} and ψ_C. The quantity S, which will be discussed in Section 5.2.5, does, however, affect the extrapolation factors significantly, and the results listed in Tables 4.2 and 4.3 indicate that there should be an appreciable difference between the values

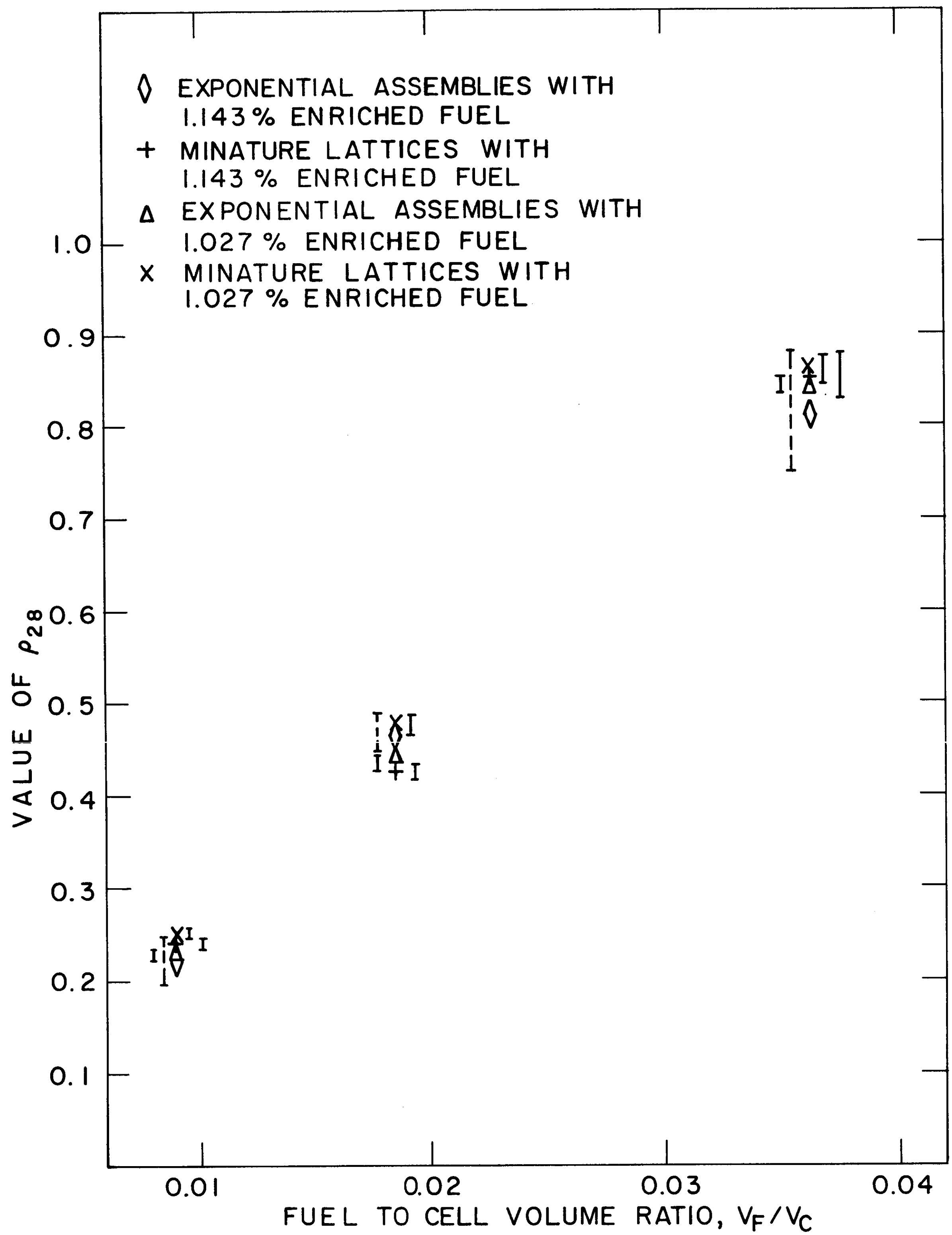

FIG. 4.19 COMPARISON BETWEEN VALUES OF ρ_{28} MEASURED IN EXPONENTIAL ASSEMBLY AND THOSE EXTRAPOLATED FROM MINIATURE LATTICE MEASUREMENTS

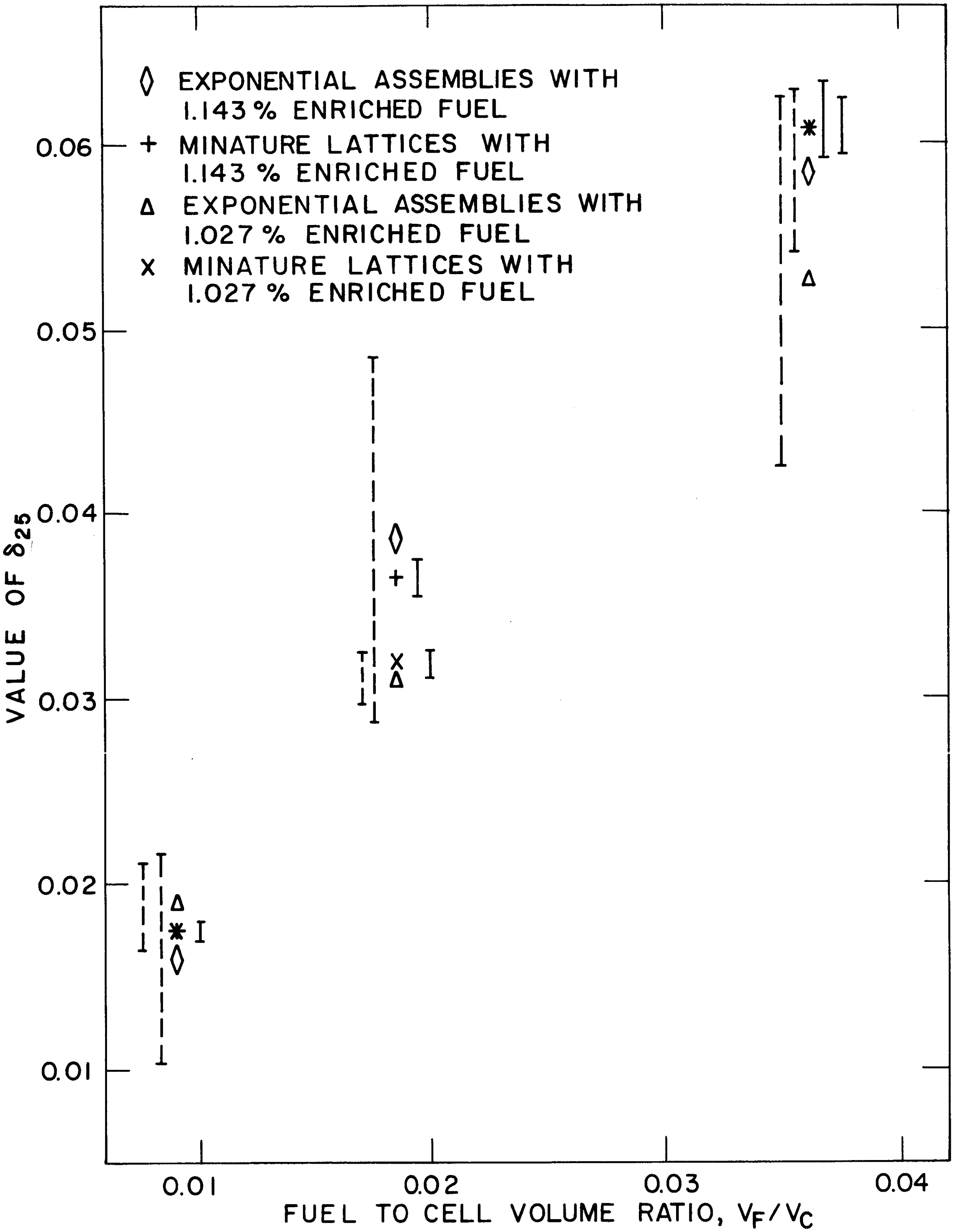

FIG. 4.20 COMPARISON BETWEEN VALUES OF δ_{25} MEASURED IN EXPONENTIAL ASSEMBLIES AND THOSE EXTRAPOLATED FROM MINIATURE LATTICE RESULTS

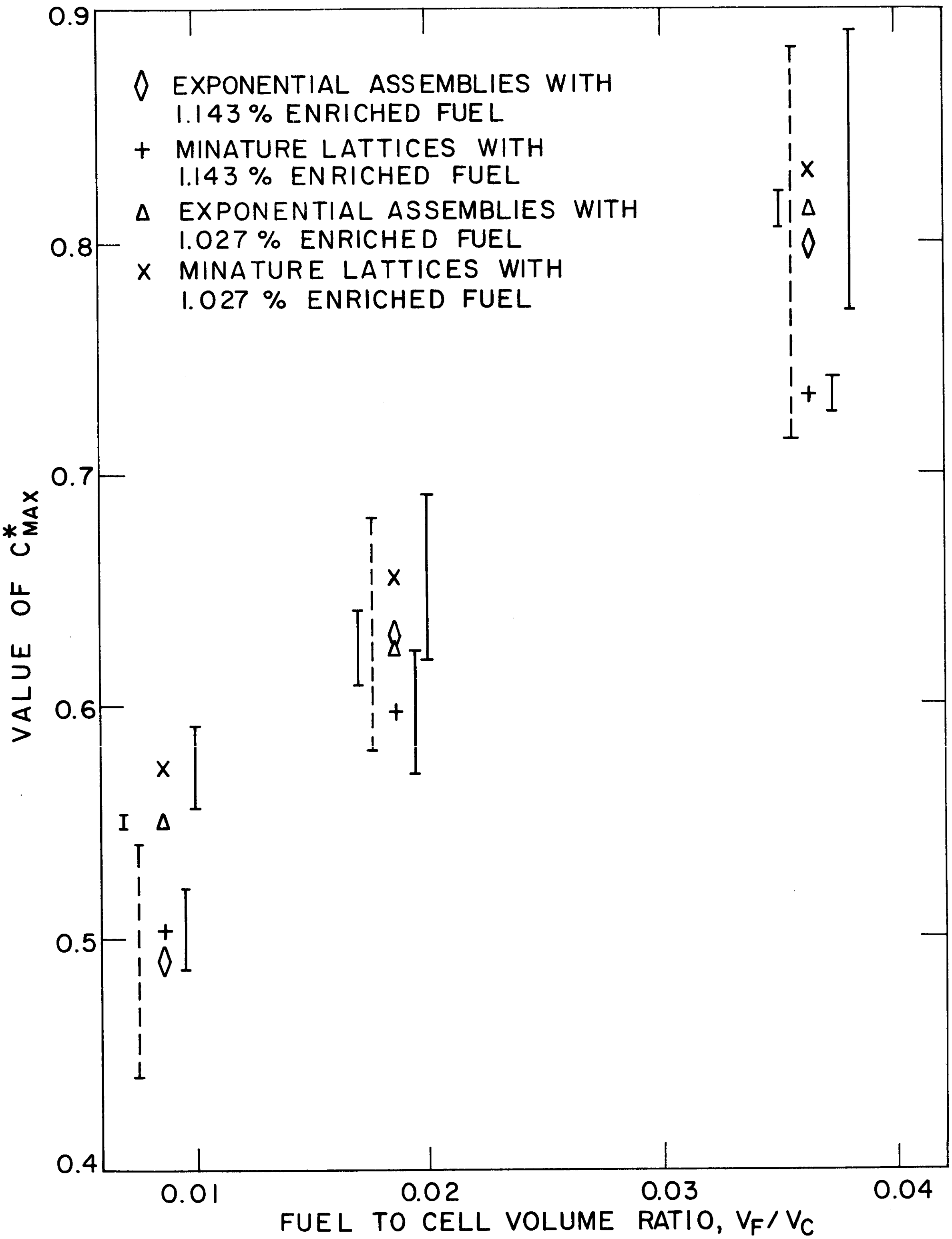

FIG. 4.21 COMPARISON BETWEEN VALUES OF $C^*_{MAX} = C^*_M R_N/R_F$ MEASURED IN EXPONENTIAL ASSEMBLIES AND THOSE EXTRAPOLATED FROM MINIATURE LATTICE RESULTS

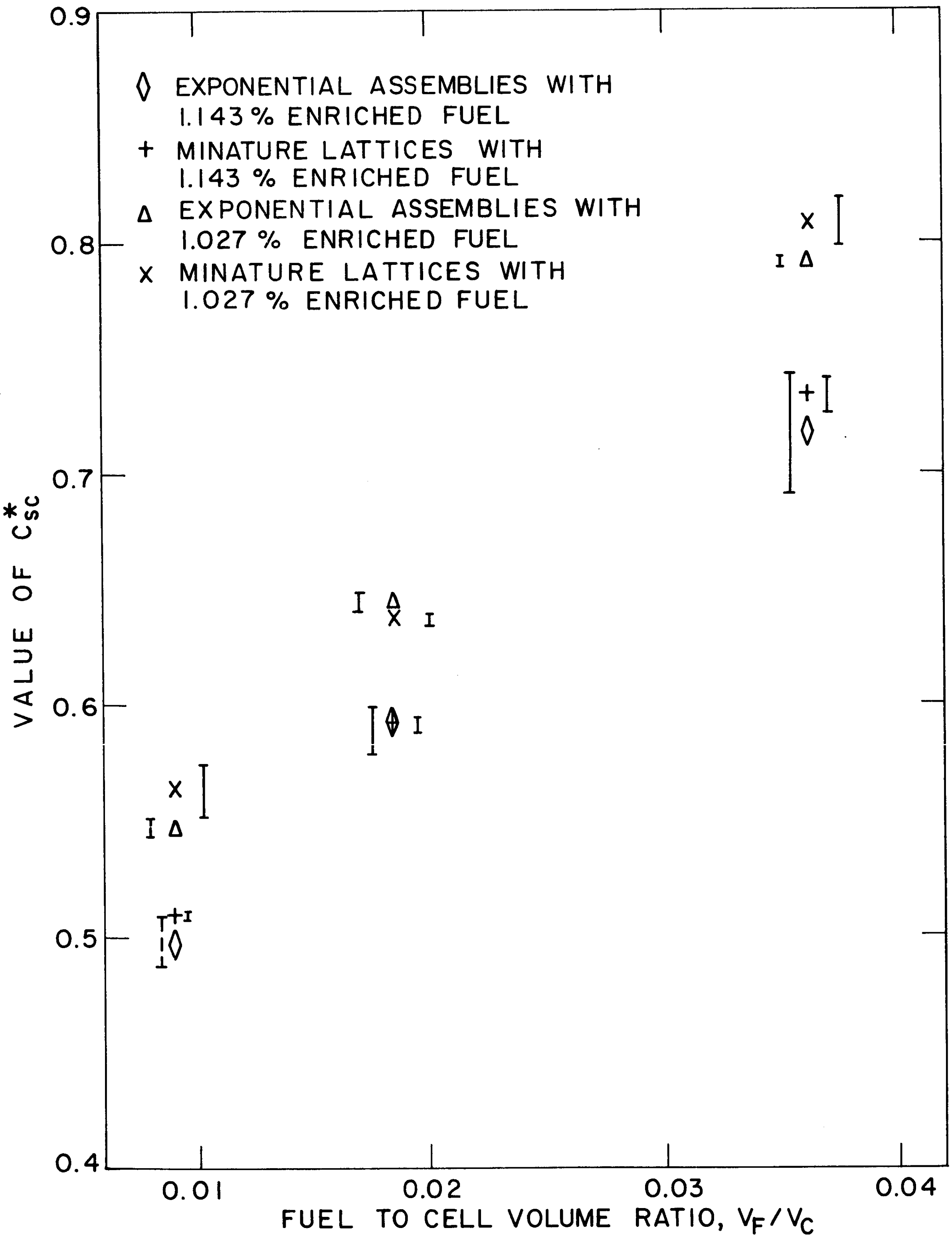

FIG. 4.22 COMPARISON BETWEEN VALUES OF $C^*_{sc} = \frac{1+\rho_{28}}{1+\delta_{25}}\left(\frac{\Sigma_a^{28}}{\Sigma_f^{25}}\right)_{sc}$ MEASURED IN EXPONENTIAL ASSEMBLIES AND THOSE EXTRAPOLATED FROM MINATURE LATTICE RESULTS

of the parameters obtained by extrapolating the data from the miniature lattice to the equilibrium region of an exponential assembly and to a critical lattice.

At the present time, this conclusion cannot be substantiated by experimental evidence. A large number of D_2O-moderated, exponential and critical assemblies with natural uranium fuel have been investigated at the Savannah River Laboratory (W7). This investigation concentrated, however, on the determination of the material buckling in these assemblies. Although systematic differences were encountered between the values of the material buckling obtained in the exponential and critical assemblies, there is still some question as to whether the differences are real or represent experimental uncertainties (H8). Measurements made in exponential and critical assemblies have been reviewed in Ref. (K1). It is unfortunate, however, that systematic studies like those made at Savannah River Laboratory for material bucklings do not seem to have been made for ρ_{28}, δ_{25} and C^*. Hence, for the present, the possible systematic difference between the values of these parameters in exponential and critical assemblies obtained from the extrapolation of miniature lattice results must wait for experimental tests, before any definite conclusion may be reached.

The results of Tables 4.2 and 4.3 show that the corrections are largest for ρ_{28} and δ_{25}. This result comes about from the fact that these parameters involve the ratio of a reaction rate in the epithermal energy region to the corresponding reaction rate in the subcadmium energy range. Since the greatest difference between assemblies of different sizes comes from the different leakage rates of neutrons during the slowing-down process, the relatively large corrections in ρ_{28} and δ_{25} are not surprising. This correction may be as large as 50% in some cases.

The values of δ_{28} and C^* are not affected nearly as much as those of ρ_{28} and δ_{25}, by the difference in leakage properties between assemblies. This result can be explained by the fact that δ_{28} and C^* represent ratios of quantities which vary nearly in the same manner, as is evident from their definitions in Section 2.7 and the discussion in Section 3.5.

To summarize, the extrapolation methods developed in Chapter 3 seem to be satisfactory for extrapolating data from miniature lattices to exponential assemblies.

CHAPTER 5

DISCUSSION OF THE ANALYTICAL TECHNIQUES AND THE EXPERIMENTAL RESULTS

5.1 INTRODUCTION

The nuclear and physical parameters required for the use of the theoretical model developed in Sections 3.2 and 3.3 will be discussed in this chapter together with the quantities needed to apply the correction factors derived in Section 3.5 and to test the theory as described in Section 3.4. The experiments made and the theoretical methods used, as well as the limitations inherent in the latter, will also be discussed.

5.2 NUCLEAR CONSTANTS WHICH APPEAR IN THE THEORY AND EXTRAPOLATION CORRECTIONS

5.2.1 Thermal Energy Parameters for the Lattice-Born Neutrons

The results shown in Section 4.3.2 indicate that the intracellular subcadmium gold activity distributions observed in the lattices studied were accurately predicted by the modified one-dimensional THERMOS program (S1). It was therefore assumed that the nuclear constants computed by THERMOS could be used in the analysis of the lattices investigated.

The details of the numerical procedures involved in THERMOS are described in Refs. (H9,H10). The application of THERMOS to the study of D_2O-moderated lattices has been studied in Ref. (S1); it is described briefly here.

The THERMOS program makes use of integral transport theory to solve for the intracellular neutron density distribution in both space and energy. The calculation is made for a cell in an infinite medium, with the assumption of a reflecting boundary condition at the edge of the cell. The cell is divided into concentric regions with a maximum of twenty regions because of computer requirements. Thirty thermal energy groups are considered. The source of thermal neutrons is usually assumed to be a spatially constant, 1/E distribution above 0.78 ev.

Scattering is assumed to be isotropic but the scattering kernel is arbitrary. It has been shown (S1) that the best results are obtained with the extension of the Nelkin kernel to D_2O made by Honeck (H11). This kernel was used throughout the present work. The solution of the integral transport equation involves an iterative procedure until the scalar flux converges.

The resulting flux $\phi(E, r)$ is then used to calculate energy averaged cross sections as functions of position, which are in turn employed to obtain reaction rates. The reaction rates are averaged over the different regions of the cell. Thus, one of the important results of the THERMOS calculation is the thermal utilization f, defined in Section 3.1.1.

The resulting average values of the quantities of interest were used to obtain Σ_a^{ℓ} and L_{ℓ}, the diffusion length of thermal lattice neutrons. The latter was defined as:

$$L_{\ell} = \frac{1}{\sqrt{3\Sigma_a^{\ell}\Sigma_{tr}^{\ell}}} , \tag{5.1}$$

where

$$\Sigma_a^{\ell} = \frac{\overline{\Sigma}_a^F V_F \overline{\phi}_F + \overline{\Sigma}_a^C V_C \overline{\phi}_C + \overline{\Sigma}_a^M V_M \overline{\phi}_M}{V_F \overline{\phi}_F + V_C \overline{\phi}_C + V_M \overline{\phi}_M} ; \tag{5.2}$$

here, the indices F, C and M stand for fuel, cladding and moderator, respectively. The macroscopic absorption cross section for the i^{th} region, $\overline{\Sigma}_a^i$, is obtained from THERMOS as:

$$\overline{\Sigma}_a^i V_i \overline{\phi}_i = \int_i d\underline{r} \int_0^{v^*} vN(r, v)\, \Sigma_a^i(v)\, dv, \tag{5.3}$$

where V_i and $\overline{\phi}_i$ are the volume and the average flux in the i^{th} region, respectively; the average flux is given by:

$$V_i \overline{\phi}_i = \int_i d\underline{r} \int_0^{v^*} vN(r, v)\, dv. \tag{5.4}$$

In Eqs. (5.3) and (5.4), N(r, v) denotes the neutron density as a function of position and velocity and v^* represents the upper limit of the velocity range under consideration. The integration is then carried out over the i^{th} volume.

The average transport cross section, Σ_{tr}^{ℓ}, is similarly defined by the relation:

$$\Sigma_{tr}^{\ell} = \frac{\overline{\Sigma}_{tr}^{F} V_F \overline{\phi}_F + \overline{\Sigma}_{tr}^{C} V_C \overline{\phi}_C + \overline{\Sigma}_{tr}^{M} V_M \overline{\phi}_M}{V_F \overline{\phi}_F + V_C \overline{\phi}_C + V_M \overline{\phi}_M} . \tag{5.5}$$

The transport cross section for the moderator is given directly by THERMOS. For the aluminum cladding, Σ_{tr} was assumed to be given by:

$$\overline{\Sigma}_{tr}^{C} = \overline{\Sigma}_{T}^{C} - \mu \overline{\Sigma}_{S}^{C} , \tag{5.6}$$

where $\overline{\Sigma}_T$ and $\overline{\Sigma}_S$ are the average total and scattering cross sections, respectively; $\mu = 2/3A$ is the average cosine of the scattering angle in the center of mass coordinate system, and A is the atomic mass of the aluminum. Although Eq. (5.6) is only approximate for uranium, this equation was also used for the uranium fuel. Since the volume fraction of the fuel in the lattices studied is small, the error introduced by this approximation is small.

The values of Σ_a^{ℓ} and L_{ℓ} used in the MINIFLUX calculations are listed in Table 4.1.

5.2.2 Nuclear Parameters for Source Neutrons

The parameters of interest for source neutrons are Σ_a^S and L_S. In obtaining their values, two difficulties are encountered. The first problem arises from the fact that the energy spectrum of the source neutrons is not really known. The second difficulty comes from the rapid variation of the energy spectrum of the source neutrons as these diffuse through the lattice. The spectrum of source neutrons changes considerably as these neutrons traverse the first five or six mean free paths in the lattice. This distance may amount to as much as one third of the height of the miniature lattice.

Because of these difficulties, it was decided to use, as a first approximation, the same absorption cross section and diffusion length as for lattice-born neutrons. The values of Σ_a^S and L_S were then varied about these values to obtain the best agreement between the measured distribution of the cadmium ratio of gold and that calculated by MINIFLUX.

Because of the small dimensions of the miniature lattice, the source has a strong effect on the cadmium ratio distribution. The cadmium ratio is, therefore, very sensitive to the values of Σ_a^s and L_s assumed. This effect is illustrated in Fig. 5.1. It is evident that, if one assumes $\Sigma_a^s = \Sigma_a^\ell$, the calculated curve lies below the experimental data. Similar results were obtained in all the lattices. The values of Σ_a^s and L_s that are necessary to bring the measured and calculated cadmium ratios into agreement are listed in Table 4.1. It is readily seen that in all cases, $\Sigma_a^s < \Sigma_a^\ell$ or $L_s > L_\ell$. The maximum difference between Σ_a^s and Σ_a^ℓ is about 12%, whereas the difference between L_s and L_ℓ is at most 3.5%. No quantitative explanation for this behavior can be offered because of the lack of information concerning the energy transient undergone by the source neutrons. The source constants were, however, the only parameters that were permitted to vary; all other quantities which appear either in the theoretical model or the correction factors are calculated.

In the exponential lattices, the values of the source parameters are immaterial because the contribution of the source neutrons to the flux in the equilibrium region is negligible.

5.2.3 Value of k_∞

The multiplication factor for an infinite assembly, k_∞, cannot be determined directly from measurements in the miniature lattice. This can readily be seen from the fact that the function $\psi(r, z)$, defined in Eq. (3.66), requires the knowledge of k_∞ for its computation.

In the six lattices investigated here, the value of k_∞ was known because these lattices had been investigated in the exponential facility at M.I.T. The values of k_∞ for the lattices with 1.027 percent enriched uranium fuel were obtained from the values of ρ_{28}, δ_{28}, and δ_{25} measured in the exponential facility at M.I.T. (D1, B1), and the equations in Section 3.1.1 which relate these parameters to k_∞. The thermal utilization, f, was obtained from THERMOS calculations. The values of k_∞ for the 1.143 percent enriched lattices were obtained by

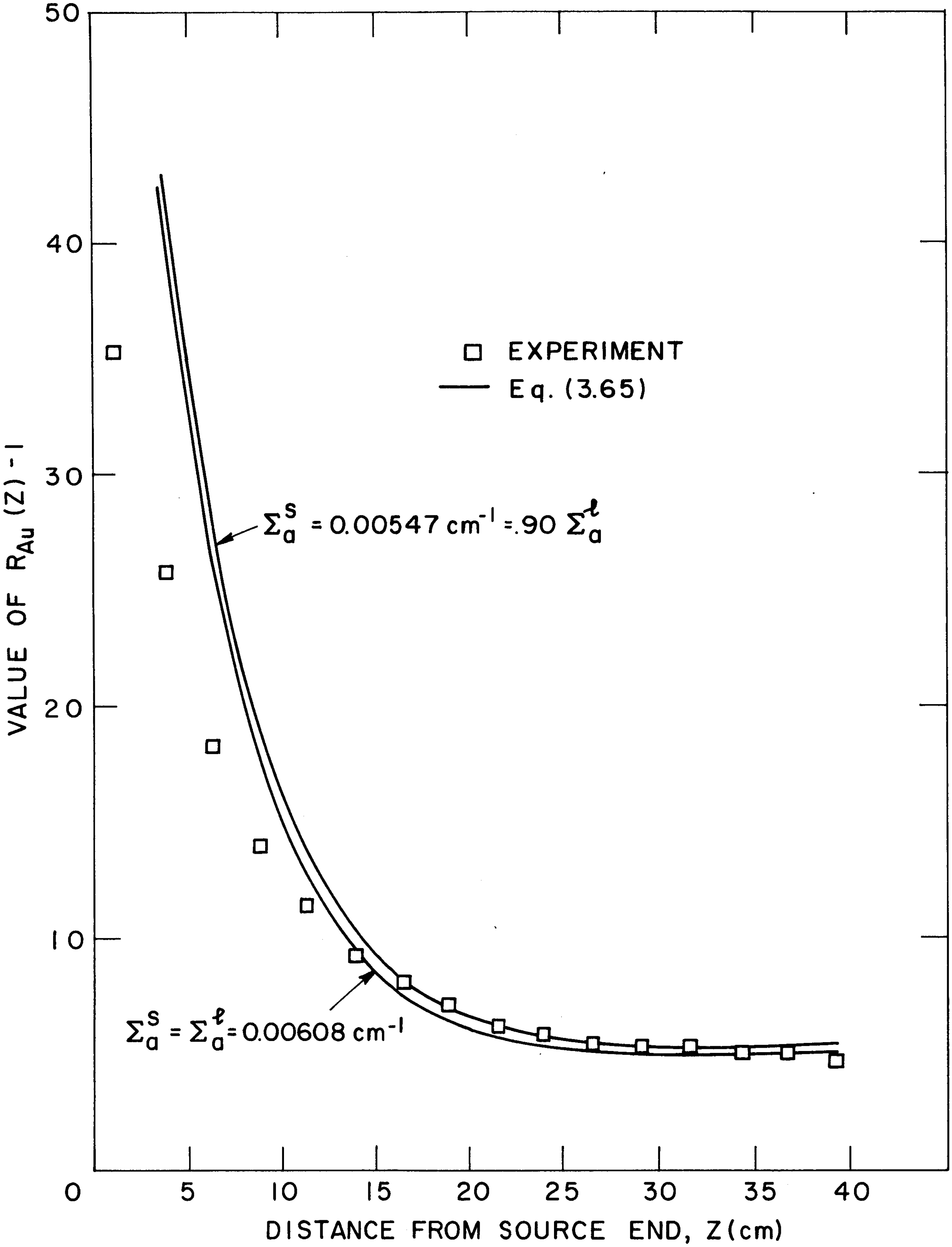

FIG. 5.1 VARIATION OF CALCULATED VALUE OF $R_{Au}(Z)-1$ WITH Σ_a^s IN ML6

ML6: 1.027 w/o ENRICHED FUEL, D_2O MODERATED, 1.75-INCH SPACING

J. Harrington (H7) by the use of neutron absorbers. The values of k_∞ used in the present work are listed in Table 4.1.

When lattices that have not been previously studied are investigated, an iterative technique must be employed to determine k_∞. This procedure involves the use of the measured parameters and the equations in Section 3.1.1 which relate these parameters to k_∞. A description of the iteration technique follows:

1. The intracellular subcadmium activity distribution of gold and δ_{28} can be extrapolated to the case of interest (∞) without knowledge of k_∞. Thus, f may be assumed to be given by THERMOS. Similarly, η_{SC}, Eq. (3.3), is also given by THERMOS. This is a good approximation as long as the rods in the lattices under study are not too closely spaced (S1). The fast fission factor, ϵ, given by Eq. (3.6), is calculated from the value of δ_{28} extrapolated to an infinite assembly.
2. A first value of k_∞ is obtained by neglecting ζ and calculating p by simple theory (see, for example, Ref. (G2)).
3. This value of k_∞ is then used with the theory in Sections 3.2 and 3.3. The correction factors shown in Table 3.2 can then be used to correct the measured values of ρ_{28} and δ_{25}.
4. The corrected values of ρ_{28} and δ_{25} are then used in Eqs. (3.4) and (3.8) and new values of ζ and p are obtained, leading to a new value of k_∞.
5. With this new value of k_∞, steps 3 and 4 are repeated to obtain a new value of k_∞.
6. The iterative procedure concludes when the results of the repeated use of steps 3, 4 and 5 converge.

This iterative process converges rapidly because ζ contributes only a few percent to k_∞ (at most, 5% in the lattices studied), while the calculated value of p in step 2 is usually only a few percent off from the final value. Hence, the initial value of k_∞ will be close to the final value. The progress of this iteration technique is illustrated for the six lattices investigated in Table 5.1. The results indicate that the process converges rapidly and that the final results are in agreement with the values of k_∞ determined in the exponential facility at M.I.T.

Table 5.1

Progress of Iteration Procedure to Obtain k_∞

Iteration Step	Value of k_∞					
	ML2	ML7	ML3	ML4	ML6	ML5
k_∞ calculated as in steps 1 and 2	1.254	1.363	1.413	1.205	1.313	1.362
1st iteration	1.307	1.390	1.405	1.245	1.341	1.379
2nd iteration	1.307	1.422	1.406	1.295	1.375	1.383
3rd iteration		1.422		1.295	1.375	1.383
MEASURED	1.330(1) ±.027	1.416(1) ±.011	1.419(1) ±.007	1.304(2) ±.020	1.375(2) ±.021	1.395(2) ±.021

(1) Ref. (H7).

(2) Ref. (D1); values corrected for epithermal fission in U^{235}.

5.2.4 Slowing-Down Power, $\xi\Sigma_s$

The average value of the slowing-down power for an assembly, $\xi\Sigma_s$, is given by (A1):

$$\xi\Sigma_s = \frac{(\xi\Sigma_s)^F V_F + (\xi\Sigma_s)^C V_C + (\xi\Sigma_s)^M V_M}{V_F + V_C + V_M}, \tag{5.7}$$

where

$$(\xi\Sigma_s)^M = (\xi\Sigma_s)^O + 2y(\xi\Sigma_s)^D + 2(1-y)(\xi\Sigma_s)^H, \tag{5.8}$$

in which the superscripts O, D and H stand for oxygen, deuterium and hydrogen, respectively, and y is the mole fraction of D_2O in the moderator. The concentration of D_2O in the moderator was 99.75 mole percent, as determined by a nuclear magnetic resonance method.

5.2.5 Values of S_{Au}, S_{28} and S_{25}

It is shown in Table 3.2 that the correction factors for δ_{25}, ρ_{28} and C^* involve either

$$S = \frac{ERI}{\sigma_o} + 0.5,$$

or the ratio of this quantity in an exponential, a critical or infinite assembly to its value in the miniature lattice. In the computation of the value of the cadmium ratio of gold, the value of S_{Au} in the miniature lattice is needed.

To obtain the value of S, one must consider the leakage of neutrons while slowing down. The leakage of neutrons is, obviously, larger in the miniature lattice than in any of the corresponding larger lattices. The epithermal cross sections in the miniature lattice must, therefore, be averaged over a harder spectrum than in a larger assembly.

The procedure used in this work to obtain S is semi-empirical in nature; a brief description follows.

Consider a nuclide x which could be either U^{238}, U^{235}, or gold. From the definition of S, one may write for an infinite system:

$$S_x^\infty = \frac{1}{\sigma^x} \int_{E_c}^{\infty} \sigma_x(E)\phi_\infty(E)\, dE, \tag{5.9}$$

where E_c is the cadmium cutoff energy (~ 0.4 ev); $\phi_\infty(E)$ is the neutron spectrum in an infinite system ($\sim 1/E$), and σ^x is the average thermal cross section for the process under consideration. In a finite assembly, the spectrum will deviate from $1/E$ because of the leakage during the slowing-down process. That is, one must weigh the higher energies more heavily than in an infinite assembly. The definition of the quantity S implies, however, that only the absorption rate in the epithermal energy range relative to the absorption rate in the thermal range is important. It follows, therefore, that only the leakage rate during the slowing-down process relative to the leakage rate to thermal energies is important. Under the assumption of age theory, one may, therefore, write:

$$\phi_{finite}(E) = \phi_\infty(E)\, e^{-B_g^2(\tau_t - \tau(E))} . \tag{5.10}$$

Hence, for a finite system, S_x will be given by:

$$S_x = \frac{1}{\sigma^x} \int_{E_c}^{\infty} \sigma_x(E)\phi_\infty(E)\, e^{-B_g^2(\tau_t - \tau(E))}\, dE. \tag{5.11}$$

Furthermore, the assumption is made that epithermal absorption or fission takes place at some effective energy. In the case of gold, this is a reasonable assumption because most of the absorption takes place at the 4.906-ev resonance. In U^{238} and U^{235}, the validity of this assumption is not obvious because of the large number of resonances in these nuclides; however, as will be discussed below, this assumption may again be made. Equation (5.11) can then be rewritten in the form:

$$S_x = S_x^\infty\, e^{-B_g^2(\tau_t - \tau_x)} ; \tag{5.12}$$

on letting

$$\Delta\tau_x = \tau_t - \tau_x , \tag{5.13}$$

we get:

$$S_x = S_x^\infty\, e^{-B_g^2 \Delta\tau_x} . \tag{5.14}$$

Applying Eq. (5.14) to U^{238}, for example, in both the miniature lattice (ML) and the exponential assembly (EX), one finds:

$$\frac{S_{28}^{EX}}{S_{28}^{ML}} = \exp\left\{\left({B_g^{ML}}^2 - {B_g^{EX}}^2\right)\right\} \cdot \Delta\tau_{28} \quad . \tag{5.15}$$

Table 5.2 lists the relations analogous to Eq. (5.15) for all the nuclides and cases of interest.

It is clear from the discussion above that the expression for ρ_{28}^{C} which is used to calculate p, Eq. (3.8), includes the leakage of neutrons from the effective resonance energy of U^{238} to thermal energies. This fact was mentioned in Section 3.4 in relation to the value of τ to be used in calculating the function $\psi(r, z)$.

The absolute value of S_{Au}^{ML} is required in Eq. (3.65) to calculate the cadmium ratio of gold. This quantity was obtained from the data of Brown (B2) and Simms (S1) who measured S_{Au}^{EX} as a function of foil thickness. The value of S_{Au}^{EX} for 0.005-inch-thick foils ($S_{Au}^{EX} = 3.720$) was used together with the corresponding expression in Table 5.2 to give the values of S_{Au}^{ML} listed in Table 4.1.

The correction factor, Eq. (3.79), for C^* requires the absolute value of S_{28} and S_{25}. The value of S_{28} was obtained by assuming the validity of the formula of Vernon (V1) for ERI_{28} and the value of σ_a^{28} given by THERMOS. The use of these results led to $S_{28}^{EX} = 7.14$ for all the lattices studied.

To obtain S_{25}, use was made of experimental evidence (P3) that, for the slightly enriched lattices being investigated, U^{235} inside a rod behaves as if it were infinite dilute with

$$\int_{E_c}^{\infty} \sigma_f(E)\, \frac{dE}{E} \simeq 270 \text{ b} .$$

This result and the value of σ_f^{25} given by THERMOS were used to get S_{25}. Table 5.3 lists values of S_{28} and S_{25} for the assemblies of interest.

Table 5.2

Relation Between the Values of S in Different Assemblies

Assembly (x)	Value of $\frac{S^x}{S^{ML}}$		
	$\frac{S_{28}^{x}}{S_{28}^{ML}}$	$\frac{S_{25}^{x}}{S_{25}^{ML}}$	$\frac{S_{Au}^{x}}{S_{Au}^{ML}}$
Exponential[1] Assembly (EX)	$\exp\left\{\left(B_g^{ML^2} - B_g^{EX^2}\right)\cdot\Delta\tau_{28}\right\}^{(3)}$	$\exp\left\{\left(B_g^{ML^2} - B_g^{EX^2}\right)\cdot\Delta\tau_{25}\right\}$	$\exp\left\{\left(B_g^{ML^2} - B_g^{EX^2}\right)\cdot\Delta\tau_{Au}\right\}$
Critical Assembly (C)[2]	$\exp\left\{\left(B_g^{ML^2} - B_m^2\right)\cdot\Delta\tau_{28}\right\}$	$\exp\left\{\left(B_g^{ML^2} - B_m^2\right)\cdot\Delta\tau_{25}\right\}$	$\exp\left\{\left(B_g^{ML^2} - B_m^2\right)\cdot\Delta\tau_{Au}\right\}$
Infinite Assembly(∞)	$\exp\left(B_g^{ML^2}\cdot\Delta\tau_{28}\right)$	$\exp\left(B_g^{ML^2}\cdot\Delta\tau_{25}\right)$	$\exp\left(B_g^{ML^2}\cdot\Delta\tau_{Au}\right)$

(1) B_g^2 = geometric buckling.

(2) B_m^2 = material buckling.

(3) $\Delta\tau_x = \tau_t - \tau_x$.

Table 5.3

Values of S_{25} and S_{28} for Different Size Assemblies

Lattice Spacing (inches)	Fuel Enrichment %	Value of S_{25}				Value of S_{28}			
		ML	EX	C	∞	ML	EX	C	∞
1.25	1.143	0.420	0.475	0.484	0.495	4.78	7.14	7.75	8.17
1.75	1.143	0.423	0.475	0.485	0.494	4.83	7.14	7.64	8.12
2.50	1.143	0.424	0.475	0.487	0.495	4.81	7.14	7.80	8.16
1.25	1.027	0.421	0.475	0.487	0.495	4.81	7.14	7.80	8.16
1.75	1.027	0.423	0.475	0.486	0.494	4.83	7.14	7.72	8.14
2.50	1.027	0.423	0.475	0.488	0.502	4.82	7.14	7.84	8.15

5.2.6 Age to Thermal Energies, τ_t

To obtain the age of fission neutrons to thermal energies in a lattice, two effects must be taken into account. First, since part of the volume is occupied by fuel and cladding, which are poor moderating materials as compared with heavy water, there will be an increase in the age over that in pure moderator. Second, part of this increase is compensated by the strong inelastic scattering in uranium.

The first effect can be taken into account as follows. The definition of τ_o is:

$$\tau_o = \int_{E_t}^{E_s} \frac{1}{3\xi\Sigma_s\Sigma_{tr}} \frac{dE}{E}\,, \tag{5.16}$$

where E_t and E_s denote thermal and source energies, respectively; $\xi\Sigma_s$ is the slowing-down power, and Σ_{tr} is the transport cross section. For a mixture, one may write:

$$\xi\Sigma_s = \sum_i \xi_i\Sigma_{si}u_i\,, \tag{5.17}$$

and

$$\Sigma_{tr} = \sum_i \Sigma_{tri}u_i\,, \tag{5.18}$$

where u_i is the volume fraction of the i^{th} material. Substitution of Eqs. (5.17) and (5.18) into Eq. (5.16) yields:

$$\tau_o = \frac{1}{\sum\limits_j \sum\limits_{k\geq j} u_j u_k} \int_{E_t}^{E_s} \frac{1}{3\xi_k\Sigma_{sk}\Sigma_{trj}} \frac{dE}{E}\,, \tag{5.19}$$

or

$$\frac{1}{\tau_o} = \sum_j \sum_{k\geq j} u_j u_k \frac{1}{\tau_{jk}}\,, \tag{5.20}$$

where

$$\tau_{jk} = \int_{E_t}^{E_s} \frac{1}{3\xi_k\Sigma_{sk}\Sigma_{trj}} \frac{dE}{E}\,. \tag{5.21}$$

The summation over k in Eqs. (5.19) and (5.20) is taken over all values of $k \geq j$, to avoid taking into account the same material twice. If we let

$$A_{jk} = \frac{1}{\tau_{jk}},$$

Eq. (5.20) may be rewritten as:

$$\frac{1}{\tau_o} = \sum_j \sum_{k \geq j} u_j u_k A_{jk} . \tag{5.22}$$

The parameters A_{jk} have been determined by Galanin (G1), and a table with their values for materials of interest is given in Ref. (A1).

To account for inelastic scattering in the fuel, Weinberg and Wigner (W1) give the formula:

$$\tau_t = \tau_o \left[1 - \left(1 - \frac{\tau_1}{\tau_o} \right) \frac{\sigma_i}{\sigma_e + \sigma_i} P \right], \tag{5.23}$$

where τ_o is the age given by Eq. (5.22); τ_1 is the age of neutrons that have undergone one collision; σ_i and σ_e are the inelastic and elastic scattering cross sections for virgin neutrons, respectively, and P is the probability that a virgin neutron will undergo its first collision in the fuel. The quantities to be used in Eq. (5.23) are listed in Ref. (W1).

The values of τ_t used in the MINIFLUX calculations are listed in Table 4.1.

5.2.7 Age to Gold Resonance Energy

The age to the resonance energy of gold, τ_{Au}, was obtained experimentally. The details of the measurement are given in Appendix D.

As the age cannot be measured directly inside a lattice, the following procedure was used. The age to the gold resonance energy was measured in heavy water as described in Appendix D, with the result:

$$\tau_{Au}^{M} = 95 \pm 3 \text{ cm}^2,$$

and the age to gold in the lattice was obtained by assuming the relation:

$$\left(\frac{\tau_{Au}}{\tau_t} \right)^{M} = \left(\frac{\tau_{Au}}{\tau_t} \right)^{LATT} . \tag{5.24}$$

Equation (5.24) is reasonable inasmuch as the lattices considered consist mostly of moderator. Consider the explicit expression of either side of Eq. (5.24):

$$\int_{E_{Au}}^{E_s} \frac{1}{3\xi\Sigma_s\Sigma_{tr}} \frac{dE}{E} \Bigg/ \int_{E_t}^{E_s} \frac{1}{3\xi\Sigma_s\Sigma_{tr}} \frac{dE}{E} ,$$

where E_{Au} is the resonance energy of gold. By equating the two sides of Eq. (5.24), it is implied that, in the energy interval between E_{Au} and E_t, the ratio indicated above is approximately the same in the moderator and in the lattice. In the range of energies of up to a few hundred ev, the cross sections are practically constant in heavy water (H12); thus, the ratio is essentially the ratio between the natural logarithms of the ratios of the energies indicated as limits of integration. Since the lattices investigated consist mainly of D_2O, the value of the ratio indicated above should be very closely that in pure moderator. If the values of τ_{Au} are used to determine τ_t by means of the relation (e.g., Ref. (W1)):

$$\tau_t = \tau_{Au} + \frac{D}{\xi\Sigma_s} \ln \frac{E_{Au}}{E_t} , \tag{5.25}$$

with E_t taken as 5 kT, the resulting values of τ_t are in close agreement with those obtained from Eqs. (5.22) and (5.23).

The values of τ_{Au} for the six miniature lattices investigated are listed in Table 5.4. In the previous discussion, the size of the assembly

Table 5.4

Age to the Resonance Energy of Gold

Lattice	Age to Gold Resonance, τ_{Au} (cm^2)
ML2	97.80
ML7	95.08
ML3	94.11
ML4	97.80
ML6	95.08
ML5	94.11

to be used did not appear in the argument. Hence, to a first approximation, it was assumed that the same values of τ_{Au} applied to exponential, critical and infinite assemblies.

5.2.8 Age to Effective Resonance Energy of U^{238}

The assumption that epicadmium capture in U^{238} occurs at an effective resonance energy, E_{28}, has been used successfully in the past by Critoph (C1) in Canada and by the French workers at Saclay (T1). A better justification for the use of this assumption has been obtained by Pilat (P3) for 1/4-inch uranium metal rods in D_2O. Pilat measured the age to an effective energy in U^{238} by irradiating cadmium-covered depleted uranium foils in the neighborhood of a single rod in heavy water. The foils were sandwiched between two fuel buttons to simulate the hardening of the 1/E flux within the fuel rod. The activity distribution observed could be well fitted by an expression of the form:

$$q(r,\tau) \sim e^{-r^2/4\tau} ,$$

which indicates that the assumption is reasonable. To obtain a more rigorous theoretical definition of τ_{28}, the experiment of Pilat will be analyzed in more detail.

The Np^{239} activity of a cadmium-covered, depleted uranium foil, at a distance r from a line source, is given by:

$$A^{39}(r) = \int_{E_c}^{\infty} \Sigma_a^{28}(E)\phi(E,r)\, dE, \tag{5.26}$$

where

$$\phi(E,r) = \frac{q(r,\tau)}{\xi\Sigma_s E} = \frac{1}{\xi\Sigma_s E}\, \frac{1}{4\pi\tau(E)}\, e^{-r^2/4\tau(E)} , \tag{5.27}$$

for a unit fission neutron source. Substitution of Eq. (5.27) into Eq. (5.26), under the assumption that $\xi\Sigma_s$ is constant, yields:

$$A^{39}(r) = \frac{1}{\xi\Sigma_s} \int_{E_c}^{\infty} \Sigma_a^{28}(E)\, \frac{e^{-r^2/4\tau(E)}}{4\pi\tau(E)}\, \frac{dE}{E} . \tag{5.28}$$

Let us assume now that the absorption cross section may be represented by widely spaced, narrow resonances; i.e.,

$$\Sigma_a^{28} = \sum_i \sigma_i \delta(E-E_i) \; . \tag{5.29}$$

Substituting Eq. (5.29) in Eq. (5.28) and doing the integration, we get:

$$A^{39}(r) = \frac{1}{\xi\Sigma_s} \sum_i \frac{\sigma_i}{E_i} \frac{e^{-r^2/4\tau_i}}{4\pi\tau_i} \; . \tag{5.30}$$

In Eq. (5.30),

$$\frac{\sigma_i}{E_i} = \text{capture due to resonance at } E_i,$$

and can be written as:

$$\frac{\sigma_i}{E_i} = f_i \, ERI_{28} , \tag{5.31}$$

where f_i is the fraction of the total effective resonance integral due to the i^{th} resonance, so that:

$$\sum_i f_i = 1 \; . \tag{5.32}$$

Hence, Eq. (5.30) may be rewritten as:

$$A^{39}(r) = \frac{1}{\xi\Sigma_s} ERI_{28} \sum_i f_i \frac{e^{-r^2/4\tau_i}}{4\pi\tau_i} \; . \tag{5.33}$$

The mean square distance $\overline{r^2_{28}}$, is defined by:

$$\overline{r^2_{28}} = \frac{2\pi \int_0^\infty A^{39}(r) \; r^2 r \, dr}{2\pi \int_0^\infty A^{39}(r) \, r \, dr} \; . \tag{5.34}$$

Using Eq. (5.33), we get:

$$\overline{r^2_{28}} = \frac{2\pi \sum_i f_i \int_0^\infty \frac{e^{-r^2/4\tau_i}}{4\pi\tau_i} r^3 \, dr}{2\pi \sum_i f_i \int_0^\infty \frac{e^{-r^2/4\tau_i}}{4\pi\tau_i} r \, dr} \; ; \tag{5.35}$$

but

$$2\pi \int_0^\infty \frac{e^{-r^2/4\tau_i}}{4\pi\tau_i} \, r \, dr = 1 ,$$

and on using Eq. (5.32), we find:

$$\overline{r_{28}^2} = \sum_i f_i \left(2\pi \int_0^\infty \frac{e^{-r^2/4\tau_i}}{4\pi\tau_i} \, r^3 \, dr \right) ,$$

or

$$\overline{r_{28}^2} = \sum_i f_i \overline{r_i^2} , \tag{5.36}$$

where $\overline{r_i^2}$ is the average square distance travelled by a neutron in slowing down from fission energies to the i^{th} resonance in U^{238}. The age τ_{28} will then be given by:

$$\tau_{28} = \frac{\overline{r_{28}^2}}{4} = \sum_i f_i \tau_i . \tag{5.37}$$

Wehmeyer (W8) has calculated the contribution of the different resonances to the total effective resonance integral of U^{238}, for 0.25-inch-diameter rods. The values of the f_i were obtained by assuming, for simplicity, that there are four resolved resonances: at 6.7 ev, 21 ev, 36.9 ev and 66.3 ev. The unresolved resonances are lumped into a single resonance assumed to be located at 200 ev. The computed values of the f_i are given in Table 5.5.

Table 5.5

Fractional Contribution of the i^{th} Resonance, f_i, to the Effective Resonance Integral of U^{238} in 0.25-Inch-Diameter Uranium Metal Rods

Energy (ev)	f_i
6.7	0.3970
21.0	0.1272
36.9	0.0799
66.3	0.0285
200.0 (unres.)	0.3674

To obtain the values of the τ_i, the following procedure was used. The age to the first resonance in U^{238} was obtained experimentally, as described in Appendix D. The value of τ_i for the other resonances was obtained from the relation (W1):

$$\tau_i = \tau_{6.7\ ev} - \frac{D}{\xi\Sigma_s} \ln \frac{E_i\,(ev)}{6.7} , \tag{5.38}$$

where $D/\xi\Sigma_s$ was assumed constant (which is a good approximation in the energy range under consideration). The various values of τ_i, together with the f_i in Table 5.5, were then used in Eq. (5.37), leading to a value of

$$\tau_{28}^{M} = 80.19\ cm^2,$$

which corresponds to an energy of

$$E_{28} = 34\ ev.$$

This value of E_{28} compares favorably with the value assumed by Critoph (C1) of $E_{28} = 25$ ev. The French group at Saclay (T1) used $E_{28} = 100$ ev, which gave the best agreement with their experimental results. The value found by Pilat corresponds to $E_{28} \simeq 60$ ev, which is reasonably close to the value obtained here or those quoted above. The differences probably come from the fact that the f_i depend on the diameter of the rod as indicated by the decrease in ERI_{28} with increasing rod diameter, and on the composition of the fuel. The rods used in the Canadian and French work were one-inch-diameter UO_2 rods; Pilat used 3/4-inch-diameter, metallic uranium rods. Determinations of E_{28} are scarce, and it would be premature to attempt, at the present time, any generalizations about the dependence of E_{28} with rod diameter and/or fuel composition. The fact that the values of E_{28} in all these cases fall in the energy region where the most prominent resonances in U^{238} are, is an indication of the consistency of the approach.

The value of τ_{28} in the lattice was obtained with the same method as τ_{Au}, with the aid of Eq. (5.24). The values of τ_{28} for the lattices investigated are given in Table 4.1.

5.2.9 Age to the Effective Resonance Energy of U^{235} Fission

The case of U^{235} is more complicated than that of U^{238} because the fission resonances are not widely spaced and overlap with neighboring resonances. Moreover, between resonances the cross section decays somewhat more rapidly than $1/v$. It has, therefore, not been possible, so far, to study resonance absorption in U^{235} inside a rod to the same extent as has been done in U^{238}.

In lattices of slightly enriched uranium rods, there are, however, several circumstances which mitigate the lack of knowledge of the epithermal behavior of U^{235} inside a rod. As mentioned in Section 5.2.5, there is experimental evidence (P3) that U^{235} inside a rod behaves as if it were infinitely dilute with

$$\int_{E_c}^{\infty} \sigma_f^{25}(E)\,\frac{dE}{E} \simeq 270\text{ b},$$

where E_c is the cadmium cutoff energy ($\sim$0.4 ev). It has also been shown by Kouts and Sher (K2) that if one writes:

$$\int_{E_c}^{\infty} \sigma_f^{25}(E)\,\frac{dE}{E} = \int_{E_c}^{\infty} \sigma_{res}^{25}(E)\,\frac{dE}{E} + \int_{E_c}^{\infty} \sigma_{f\,1/v}^{25}\,\frac{dE}{E},$$

$$= ERI_{25} + 0.5\,\sigma_{fo}^{25},$$

where σ_{fo}^{25} is the average thermal fission cross section of U^{235} and $E_c = 0.4$ ev, then the ERI_{25} term is very small compared with the $1/v$ term. In other words, it seems that the resonances that do occur tend to balance the "faster than $1/v$" behavior of the cross section. It may then be assumed without too much error, that all the epithermal fissions occur in a $1/v$ cross section. Because of the $1/v$ behavior of the cross section and the $1/E$ dependence of the epithermal flux, the fission rate will vary as $(1/E)^{3/2}$. The reaction rate will therefore decay very rapidly with increasing energy and most of the epithermal fissions will occur at low energies. Hence, it seems reasonable to assume that τ_{25} will correspond to an energy very close to the cadmium cutoff energy. Since 270 b is somewhat less than $0.5\,\sigma_{fo}^{25}$, it was assumed in this work that τ_{25} corresponds to $E_{25} = 0.5$ ev. The values of τ_{25} used in this work are listed in Table 5.6.

Table 5.6

Age to the Effective Resonance Energy of U^{235}, τ_{25}

Lattice Denomination	τ_{25} (cm^2)
ML2	114.6
ML7	112.0
ML3	110.6
ML4	114.6
ML6	112.0
ML5	110.6

The actual value of E_{25} has little effect on the final value of either k_∞ or C^*. The reason is that in k_∞, δ_{25} enters as $1 + \delta_{25}x$ (factor $\simeq 1/2$) and in C^* it appears as $1 + \delta_{25}$. In the lattices investigated, δ_{25} is at most 0.066 for the tightest lattice; thus, even if δ_{25} is obtained only to within 10%, the resulting uncertainty in k_∞ will be less than 1%. Furthermore, since the value of δ_{25} is small, its experimental determination is difficult and good statistical accuracy is hard to attain. As a consequence, the uncertainty in the value of τ_{25} affects the accuracy of k_∞ or C^* much less than the uncertainty in the experimental determination of δ_{25}.

The above discussion would not apply to lattices of highly enriched uranium rods because the assumption of infinite dilution would not be expected to hold.

5.3 DIMENSIONS OF ASSEMBLY

No particular difficulty was encountered in defining the dimensions of the miniature lattices. The physical radius of the assembly R' was obtained from the relation:

$$NA_c = \pi R'^2 \tag{5.39}$$

where A_c is the area of the unit cell and N is the number of cells in the lattice. The extrapolated radius R was obtained from the relation:

$$R = R' + d, \tag{5.40}$$

where d is the extrapolation length and is given by:

$$d = \frac{0.714}{\Sigma_{tr}} ; \tag{5.41}$$

Σ_{tr}, the macroscopic transport cross section of the assembly, was obtained from THERMOS calculations, as described in Section 5.2.1. Typical radial distributions of the subcadmium and epicadmium activities of gold measured in a miniature lattice were shown in Fig. 4.8. The subcadmium activity distribution was found to be described accurately by a J_o-function, with an extrapolated radius given by Eq. (5.40). The same radial dependence was found to describe the epicadmium activity distribution over the region of the assembly where the lattice parameters were measured. Thus, the experimental results substantiate the validity of Eqs. (5.40) and (5.41).

In obtaining the extrapolated height of the lattice, it was necessary to take into account the D_2O reflector which was always present under the bottom grid plate of the assembly. Since the thickness of the D_2O reflector was much smaller than the diffusion length of thermal neutrons, it was assumed that the extrapolated height, H, was obtained by adding to the physical height, H', the reflector saving δ. Thus:

$$H = H' + \delta, \tag{5.42}$$

with the reflector saving given by:

$$\delta = \frac{\Sigma_{tr}^{r}}{\Sigma_{tr}^{L}} T , \tag{5.43}$$

where the superscripts r and L refer to reflector and lattice, respectively, and T is the reflector thickness. The data shown in Figs. 4.1 through 4.6 indicate that the use of Eqs. (5.42) and (5.43) in the calculation of the axial distribution of the cadmium ratio of gold from Eq. (3.65) gives agreement with the measured distribution over the region of the assembly where the lattice parameters were measured.

The definition of the geometric buckling in subcritical assemblies presents several difficulties because of the presence of higher spatial harmonics and source effects. These effects are particularly important in the case of miniature lattices, where the geometric buckling is expected to be relatively large. An attempt to give a rigorous theoretical definition of the geometric buckling in a miniature lattice must take into account the fact that an accurate description of the thermal flux and slowing-down density in the miniature lattice requires the knowledge of transport effects near the source. As discussed in Section 5.4, this is not possible at the present time and further work in this direction is presently in progress. It was found, however, that the definition obtained by assuming the validity of asymptotic theory (W1) in subcritical assemblies led to results in agreement with experiment. Thus, it was assumed that the geometric buckling for miniature and exponential assemblies was defined by:

$$B_g^2 = \left(\frac{2.405}{R}\right)^2 + \left(\frac{\pi}{H}\right)^2 . \tag{5.44}$$

The values of R and H for the miniature lattices investigated are listed in Table 4.1. The values of R for the exponential assembly were obtained from the buckling measurements made at the M.I.T. exponential facility (H1, H2, H3, H4, H5). In a critical assembly, the geometric buckling, B_g^2, is, of course, equal to the material buckling, B_m^2. The values of B_m^2 were obtained from the measurements made in the exponential facility (H1, H2, H3, H4, H5). Table 5.7 lists the dimensions of the exponential assemblies and the values of the material buckling of the lattices studied here.

As shown in Table 5.7, the value of H was assumed to be the same for all the lattices. The reason is that, in measuring the material buckling, the extrapolated height is usually not determined since its precise value does not affect the value of the material buckling. The experimental results in the exponential assembly at M.I.T. indicate that, for all the lattices of interest in the present work, the variation in the material buckling is not significant for values of H that range from 127 cm to 129 cm; thus, the average value of H = 128 cm was assumed. An example of these results is given in Ref. (H3).

Table 5.7

Dimensions and Values of the Material Buckling in the Exponential Lattices

Lattice Spacing (inches)	Enrichment %	Radius (cm)	Height (cm)	Material Buckling (10^{-6} cm^{-2})
1.25	1.143	49.108	128	1444
1.75	1.143	49.092	128	1405
2.50	1.143	48.874	128	1007
1.25	1.027	49.474	128	1177
1.75	1.027	48.908	128	1200
2.50	1.027	48.813	128	891

5.4 MATERIAL BUCKLING B_m^2

To obtain the material buckling B_m^2, by steady-state measurements in a subcritical facility, the following procedure is generally used (P1,H6). The axial and radial subcadmium activity distributions are measured by means of an adequate neutron detector (e.g., gold). The resulting radial distribution is fitted to $J_o(\alpha r)$, and $\alpha = 2.405/R$ is determined. The axial distribution is fitted to a sinh $\gamma(H-z)$ and γ, the reciprocal of the axial relaxation length, is determined. The material buckling is then obtained by means of the relation (P1):

$$B_m^2 = \alpha^2 - \gamma^2 . \tag{5.45}$$

The validity of this procedure is based on the fact that over a large portion of a subcritical assembly, diffusion theory, or more accurately, asymptotic transport theory is valid (W1).

Near the source, however, asymptotic theory is not valid. To illustrate, consider a point source in an infinite nonmultiplying medium. Following Ref. (W1) and assuming one-velocity transport theory, we may write for the neutron flux at r:

$$\phi(r) = \phi_{As}(r) + \phi_{trans}(r), \tag{5.46}$$

where

$$\phi_{As}(r) = \frac{S\beta}{4\pi Dr} e^{-\kappa r} \tag{5.47}$$

is the asymptotic portion of the flux. In Eq. (5.47), κ, the reciprocal of the relaxation length, is given by:

$$\kappa = \frac{1}{L} = \sqrt{3\Sigma\Sigma_a(1-\mu)} \left(1 - \frac{2}{5}\frac{\Sigma_a}{\Sigma}\right),$$

and $\beta = 1 - \frac{4}{5}\frac{\Sigma_a}{\Sigma}$, while $D = \frac{\Sigma_a}{\kappa^2}$ is the diffusion coefficient. The extension of Eq. (5.47) to a multiplying finite cylindrical assembly leads to Eq. (5.45) for the material buckling.

The transient portion of the flux

$$\phi_{trans}(r) = \frac{S}{4\pi r^2} e^{-\Sigma' r}, \tag{5.48}$$

where $\Sigma' = \frac{4}{5}\Sigma$, gives a negligible contribution to the neutron flux in the equilibrium region of an exponential assembly. In the miniature lattice, however, ϕ_{trans} contributes appreciably to the neutron flux near the source. Figure 5.2 illustrates the experimental subcadmium and epicadmium axial gold activity distributions, and those predicted by MINIFLUX, which assumes diffusion theory, as discussed in Section 3.2.2. It is evident from the figure that, near the source, MINIFLUX seriously underestimates both the subcadmium and epicadmium activity distributions. To bring the calculated and measured activities into agreement, it would be necessary to add to the subcadmium activity distribution an expression similar to Eq. (5.48), but for a small, multiplying medium. The finite Fourier transform of this expression would have to be added to the epicadmium activity distribution. Since the Fourier transform of a function is proportional to the function itself, the function added to the epicadmium activity distribution will be proportional to that added to the subcadmium activity distribution; thus, the cadmium ratio is predicted much better than one would expect from looking at Fig. 5.2. As mentioned in Section 4.3.1, the cadmium ratio near the source is not accurately predicted because of the failure of

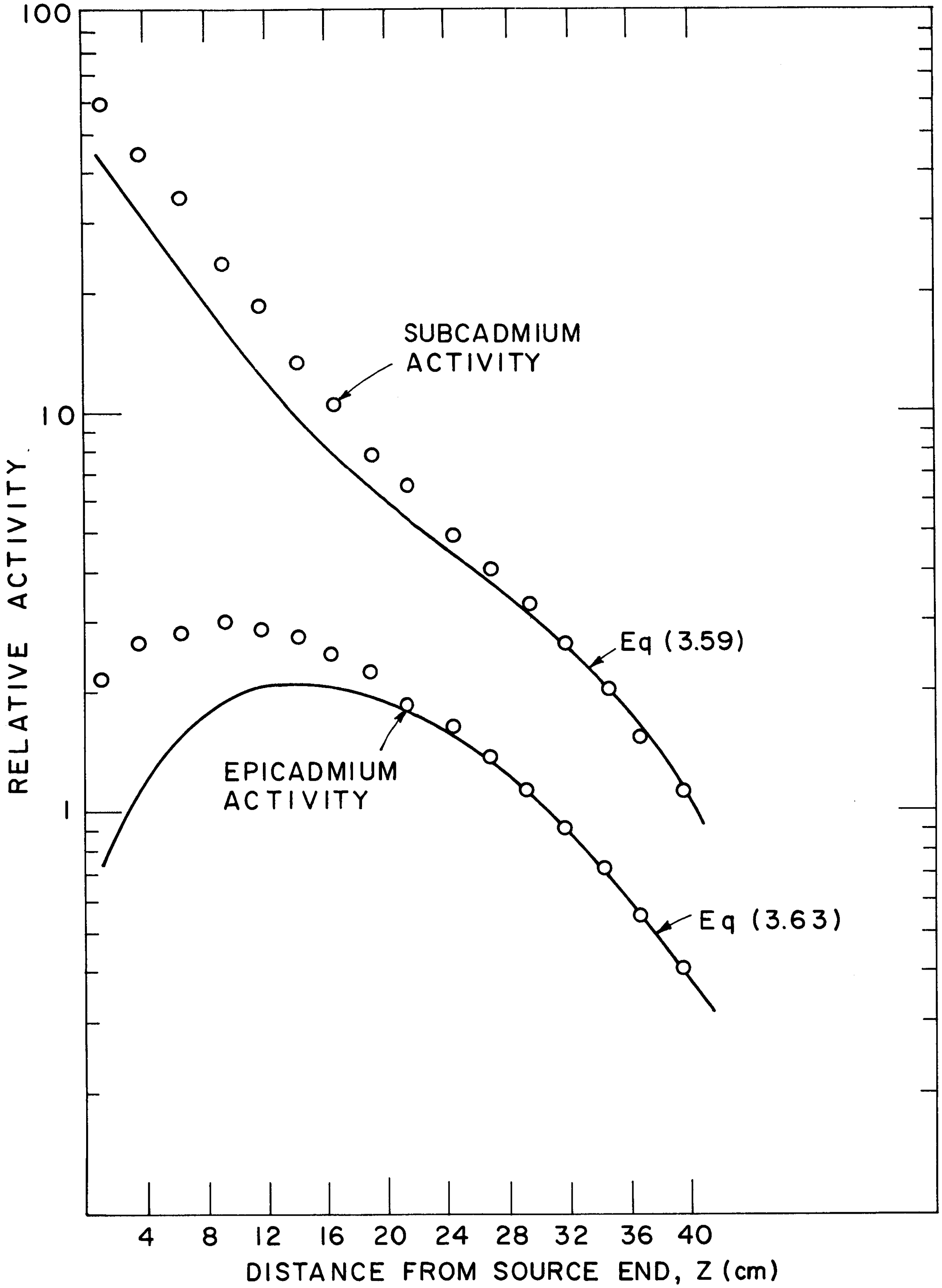

FIG. 5.2 AXIAL DISTRIBUTION OF THE EPICADMIUM AND SUBCADMIUM ACTIVIES OF GOLD IN ML4
ML4: 1.027 % ENRICHED FUEL, D_2O MODERATED
1.25 - INCH LATTICE SPACING

the Fourier expansion with a finite number of terms near the discontinuity at z = 0.

It may be inferred from this discussion that in order to obtain B_m^2 from the subcadmium activity distribution observed, with the aid of Eq. (5.45), the activity due to the transient portion of the flux must be subtracted from the observed activity. The fraction to be subtracted must be accurately determined since B_m^2 is given by the difference between two quantities which are (usually) not very different in magnitude.

Solutions to the neutron transport equation in a finite, small, multiplying medium are, however, hard to come by. Hence, at the present time, it appears that the material buckling cannot be determined accurately in miniature lattices. Further theoretical work is in progress.

5.5 DISCUSSION OF RESULTS

A discussion of the practical limitations inherent in miniature lattice measurements is in order. In particular, it is important to know how the fact that the measurements are made in a miniature lattice affects the accuracy of the results, in contrast to similar determinations in exponential assemblies.

The intracellular subcadmium and epicadmium activity distributions of gold are not appreciably affected by being measured in a miniature lattice. The spread of the data in the fuel is most probably due to the difficulty in positioning foils accurately in a 1/4-inch-diameter, fuel button foil holder. Small displacements in the foil position may lead to large errors because the flux gradient is large. This is particularly true for the foils closest to the surface of the fuel.

The corrections required to extrapolate the measured intracellular distribution to that observed in an infinite assembly may be as large as 7% for the lattices with the widest spacing between rods. This is a consequence of the small size of the assembly. Since the macroscopic flux gradients are large, the foil holders must, however, be positioned as accurately as possible.

The measurement of δ_{28} presents no particular difficulty. The extrapolation of the measured quantities to exponential assemblies involves small corrections (at most, 8%). The main difficulty affecting the accuracy of the measurement is independent of whether a miniature lattice is used or not. It is related to the fact that δ_{28} is generally a small number (0.01-0.03 for the lattices investigated). Hence, the observed U^{238} fission product activity that is measured is usually small and good statistical accuracy is difficult to attain. The experimental determination of δ_{25} involves the same difficulties as that of δ_{28}.

There are limitations on the measurements of ρ_{28}, δ_{25} and C^* which are inherent in the use of a miniature lattice. The most important limitation is related to the need to predict accurately the distribution of $R_{Au} - 1$, to be able to extrapolate the values of these parameters meaningfully.

As discussed in Section 4.3.3, the largest corrections are those applied to δ_{25} and ρ_{28}. It was mentioned that the reason was that they involved ratios of quantities measured in different portions of the neutron energy spectrum. Thus, the leakage of neutrons is considerably different, depending on the size of the assemblies considered. That the corrections are large is substantiated by the values of ψ shown in Tables 4.2 and 4.3 and the values of the quantities S listed in Table 5.3. It was shown, however, that the corrections for C^* were generally smaller because this parameter is defined as the ratio of two quantities which vary in similar ways.

The accuracy of the correction factor for δ_{25}, ρ_{28} and C^* depends strongly on the value of the function $\psi(r, z)$ at the experimental position. Examples of this function were shown in Figs. 4.17 and 4.18. It is evident from these figures that when the measurements are made in the equilibrium region of an exponential assembly, the actual experimental position has little, if any, influence, mainly because $\psi(r, z)$ is practically constant. It is evident from the same graphs that this is not the case in miniature lattices. In fact, in miniature lattices, it is frequently necessary, as in Fig. 4.18, to make the experiments in positions where the gradient of the function $\psi(r, z)$ is large. Thus, slight errors in positioning the foil packets might lead to relatively large errors in the value of $\psi(r, z)$, and great care must be exercised in carrying out the experiments.

CHAPTER 6

CONCLUSIONS AND RECOMMENDATIONS FOR FUTURE WORK

The present work has shown that significant measurements of lattice parameters can be made in miniature lattices of slightly enriched uranium rods in heavy water. Corrections derived from theory must be made to account for the effects of the external source and the boundaries. The theory developed by Peak (P2) has been improved and correction factors have been obtained which permit the extrapolation of miniature lattice data to exponential, critical and infinite assemblies. The values of the lattice parameters obtained by extrapolation of the results obtained in miniature lattices to exponential assemblies agree with the results of measurements made in exponential experiments at the M.I.T. Heavy Water Lattice Project.

The parameters studied were δ_{28}, ρ_{28}, δ_{25}, C^* and the intracellular distribution of the subcadmium activity of gold. These parameters and their relation to k_∞ and C, the initial conversion ratio, were discussed in Chapter 3. The conclusions reached are summarized in this chapter and suggestions for future work are also given.

6.1 SUMMARY

The present work has shown that the values of ρ_{28}, δ_{25} and C^* obtained from measurements made in the miniature lattice can be extrapolated meaningfully to exponential, critical and infinite assemblies, provided the spatial distribution of the cadmium ratio of gold can be predicted theoretically. This requirement is less stringent than that of Peak (P2), which required the separate prediction of the axial distribution of the subcadmium and epicadmium activations of gold. Thus, the validity of miniature lattice measurements has been extended to assemblies in which only the cadmium ratio of gold can be predicted. In fact, it was shown in Section 5.4 that the age-diffusion theoretical model used in this work failed to describe separately the axial distribution of the subcadmium and epicadmium activities of gold, although the cadmium ratio of gold is accurately represented over the region of the assembly where the lattice parameters were measured. As indicated in Section 5.4, the failure of the model to describe the separate axial distributions is due, first, to the presence of transport effects near the source, and second, to the failure of the Fourier harmonic expansion near the discontinuity at the source end.

The validity of the extrapolation methods was established by extrapolating the results obtained in the miniature lattice to exponential assemblies. These extrapolated results were then compared with the results of measurements made in the exponential assembly at M. I. T. Six lattices were investigated. Two U^{235} fuel concentrations were studied, 1.143 and 1.027 percent, and three rod-to-rod spacings, 1.25, 1.75 and 2.50 inches. The results are summarized in Tables 4.2 and 4.3 and in Figs. 4.19 through 4.22. The data indicated that the extrapolated and measured results agreed, in general, within the experimental error.

The values of ρ_{28}, δ_{25} and C^*, obtained by extrapolation of the miniature lattice results to critical assemblies, were consistently higher than those obtained by extrapolation to the equilibrium region of an exponential assembly. These theoretical results, which were discussed in Section 4.3.3, have not been tested experimentally. Although there are indications that there may be a difference between lattice parameters measured in exponential and critical assemblies (H8), these discrepancies are, however, still subject to debate. A general conclusion cannot be reached until more experimental determinations of ρ_{28}, δ_{25} and C^* in exponential and critical assemblies of similar composition are made.

The intracellular distributions of the subcadmium activity of gold, obtained by extrapolating the distributions measured in miniature lattices and in exponential assemblies to infinite lattices, were found to be in agreement, within the experimental error, with each other and with the intracellular activation distribution predicted by the THERMOS code (H10). Moreover, the accuracy of the intracellular distribution observed was found not to depend on the fact that the measurement is being made in a miniature lattice.

The extrapolation method, described in Section 3.5.4, to correct the values of δ_{28} measured in the miniature lattice, was shown to lead to results that were in agreement with the results of measurements in the exponential facility at M.I.T. The most important difficulty encountered in the determination of both δ_{28} and δ_{25} was that these parameters were usually small in magnitude, and good statistical accuracy was difficult to attain.

The function $\psi(r, z)$, which appears in the correction factors for ρ_{28}, δ_{25} and C^*, was shown to depend on the value of k_∞. Hence, k_∞ cannot be determined directly from measurements in the miniature lattice. But the iteration procedure to determine k_∞ that was described in Section 5.2.3 was found to converge rapidly and, for the lattices investigated, led to results that were in agreement with the values of k_∞ obtained from measurements in the exponential assembly at M.I.T.

The material buckling was discussed in Section 5.4. It is apparent from that discussion that the inclusion of transport effects may be necessary, first, to define a material buckling, and second, to calculate its value. Theoretical work on this problem is presently in progress.

The methods developed are also expected to be applicable to lattices with slightly enriched fuel moderated by either beryllium or graphite. In the case of lattices moderated by light water, the expressions for the extrapolation corrections, derived in Section 3.5, will remain the same. The calculation of the function $\psi(r, z)$ will, however, have to be made differently since age-diffusion theory is not applicable in light water.

As a consequence of the present investigation and that of Peak (P2), a flexible facility becomes available for lattice parameter measurements; a facility in which experiments can be made with relative ease and economy.

6.2 SUGGESTIONS FOR FUTURE WORK

6.2.1 Extension of This Work

The validity of measurements in miniature lattices has been established for lattices in which the fuel rods were 0.250-inch in diameter. The extrapolation methods are, however, expected to be valid, independently of the size of the rods used. Thus, if short fuel rods of other diameters become available, it would be desirable to test the applicability of these methods and, by so doing, extend their range of validity.

6.2.2 Values of the Age

The values of the quantity S, discussed in Section 5.2.5, which appear in the extrapolation factors for ρ_{28}, δ_{25} and C^* as listed in Table 3.2, were shown to depend on the value of the age of fission neutrons to energies other than thermal. Although numerous measurements have been made of the age of fission neutrons to the resonance energy of indium at 1.4 ev (e.g., (W6)), there appears to be a lack of experimental determinations of the age to other energies. Hence, it is strongly recommended that systematic measurements be made of the age of fission neutrons to energies higher than the resonance energy of indium. Resonance detectors and the method described in Appendix D could be used for this purpose. The range of energies of particular interest is that in which most of the resonance capture in U^{238} takes place, say, 5 to 1000 ev.

6.2.3 Theoretical Methods

From the discussion in Section 5.4, it appears that the introduction of transport effects is necessary, especially in the lattices with the widest rod-to-rod spacing. It is, therefore, suggested that transport effects be investigated.

For purposes of comparison, it would be of interest to investigate the treatment of the slowing-down process by means other than age theory, e.g., multigroup theory.

The expansion of the slowing-down density and the thermal flux of lattice-born neutrons in Fourier harmonics was shown to fail near the source end. Hence, an investigation of more sophisticated methods to treat the boundary conditions at the source end is recommended.

6.2.4 Improvement of Miniature Lattice Facility

From the experience acquired in the use of the miniature lattice, it is believed that several improvements in its design can be made. A discussion of the suggested changes follows.

The shielding used in the present work and shown schematically in Fig. 2.4 proved to be effective for the purposes of this work, but it was difficult to handle because of the large mass of paraffin involved. The positioning of the cylindrical annuli of paraffin around the miniature lattice usually required three men. It is believed that the situation can be improved by replacing the present shielding by an annular cylinder made of aluminum whose outside walls are lined with cadmium. This tank would be filled up with light water from the supply in the medical therapy room each time an experiment is made. Since it is difficult to handle an annular cylinder of aluminum of the size required, it is suggested that it be made up of three or four separate sectors which would be bolted together before they are filled up with water and placed around the miniature lattice.

In the course of this work, the medical therapy facility was frequently used by other experimenters. As a result, the following procedure had to be used in setting up an experiment. The lattice was thoroughly cleaned, the tank cover bolted tightly and the assembly filled with D_2O, in the Heavy Water Lattice Project area on the first floor of the M. I. T. reactor building. The assembly was then brought down to the reactor basement. The shielding was then positioned around the lattice and the irradiation made as described in Section 2.8. After the irradiation was completed, the same procedure was followed in reverse. As a result, the final drying of the assembly by nitrogen gas was usually carried out only for fifteen or twenty minutes. This was particularly important in the measurement of δ_{28}, ρ_{28}, δ_{25} and C^* because the fission product activities of the uranium foils decay rapidly. As a result, appreciable losses of heavy water by evaporation occurred during these experiments. The situation can be improved considerably if the whole process can be carried out in the medical area of the M. I. T. reactor. The draining and final drying of the assembly can be started as soon as the irradiation is completed. Moreover, the tank cover can then be altered to permit the removal of the experimental cluster without disassembling the miniature lattice. In this manner, the irradiation time may also be increased, if necessary, without increasing the dose rate to the experimenter.

An increase in the size of the assembly will, of course, yield smaller corrections. The axial dimension is, however, more important, since an increase in the height will lead to an increase in the size of the region over which the theory derived in Section 3.2.3 will predict accurately the cadmium ratio of gold. In the radial direction, it is only important that the cadmium ratio of gold be constant over a region which includes the ring of fuel rods where the lattice parameters are measured. In the lattices with 2.5-inch rod-to-rod spacing, however, only four rings of rods could be accommodated. If lattices with fuel rods of a diameter larger than the 0.25-inch-diameter rods used in this work are investigated, the rod-to-rod spacing will probably be larger than 2.5 inches. Hence, it is advisable to increase the diameter of the assembly, if only to accommodate a reasonable number of rings of rods.

APPENDIX A

COMPUTER PROGRAMS

A.1 MINIFLUX Computer Program

The MINIFLUX computer program calculates the thermal flux and the slowing-down density at any point in a subcritical assembly, in accordance with the assumptions and mathematical derivation of Section 3.2. The code was programmed in FORTRAN II language and run and compiled on the IBM 7094 computer at the M. I. T. Computation Center. The amount of computer time required depends on the number of space points for which the calculation is made, but is typically about 0.1 minute per case.

The MINIFLUX program calculates $\phi_{\ell}(r, z)$, $\phi_s(r, z)$, $\phi_t(r, z)$, $pq(r, z, \tau_{28})$, $\psi(r, z)$, the subcadmium activity distribution of gold, the epicadmium distribution of the activity of gold and $R_{Au}(r, z) - 1$.

The required input data are described in Section A.1.1. A listing of the FORTRAN source deck is given in Section A.1.2 and a sample problem is given in Section A.1.3.

A.1.1 Input Data for the MINIFLUX Program

The input instructions are given below in the order required. The names of the variables for each FORMAT statement are given, followed by the required FORMAT in parentheses, and then by a brief description of the variables.

ID(I), I = 1, 12 (12A6).

ID(I) is an arbitrary identification statement of 72 spaces or less, used to label each set of data.

N, M. ILMAX, IJMAX, R. H, EL, SIGAS, ELS (4I5, 5E10.5).

N is the number of radial harmonics to be used in the calculation. The maximum number of harmonics that may be used is fifteen. For miniature lattice calculations, N was set equal to 5.

M is the maximum number of axial harmonics allowed for in the computation (≤ 100). The program determines the number of axial harmonics required.

ILMAX is the number of axial points for which the program will calculate the quantities of interest (≤ 20).

IJMAX is the number of radial points for which the program will calculate the quantities of interest (≤ 20).

R is the extrapolated radius in cm.

H is the extrapolated height in cm.

EL is the thermal diffusion length calculated for the spectrum of the neutrons born in the lattice in cm.

SIGAS is the thermal absorption cross section of the assembly, calculated for the spectrum of the incident neutrons in cm^{-1}.

ELS is the thermal diffusion length of the assembly calculated for the spectrum of the incident neutrons in cm.

TAU, TAUT, CAIN, SIGA, CSIS, XIT, ERI (7E10.5).

TAU represents the age to the effective energy at which epithermal capture in U^{238} occurs.

TAUT is the age from fission energies to thermal energy, of the assembly.

CAIN denotes the value of k_∞.

SIGA represents the thermal absorption cross section of the assembly, calculated for the spectrum of neutrons born in the lattice.

CSIS is the slowing-down power of the assembly, $\xi\Sigma_s$.

XIT is the convergence criterion for the number of axial harmonics to be used in the computation. The number of harmonics used is fixed by the fact that the ratio of the i, n^{th} harmonic to the fundamental mode must be smaller or equal to XIT.

ERI represents the quantity S_{Au} defined in Eq. (3.64) by the relation:

$$S_{Au} = \frac{ERI_{Au}}{\sigma_o} + 0.5 \,. \tag{A.1}$$

RZ (E10.5).

RZ is the value of $R_{Au} - 1$ at $z = 0$. This quantity permits the introduction of an epithermal neutron source, if necessary. The epithermal source will be proportional to the thermal flux of source neutrons $\phi_s(r, z)$, and is given by:

$$\frac{pq_s(r, z)}{\xi \Sigma_s} = \frac{0.886\ \phi_s(r, z)}{(R_{Au}-1)_{z=0} S_{Au}} \ . \qquad (A.2)$$

in accordance with Eq. (3.65). If no epithermal source is required, it is sufficient to set RZ equal to a large number, say 500. For the lattices investigated, it was found that for any value of RZ larger than about 70, the contribution of $q_s(r, z)$ to the total slowing-down density was negligible.

X1(NX), NX = 1, ILMAX (7E10.5).

X1 denotes an axial position in units of the extrapolated height. In other words, the values of X1(NX) lie between zero and one. This card is repeated until ILMAX points have been included.

Y1(NY), NY = 1, IJMAX (7E10.5).

Y1 denotes a radial point in units of the extrapolated radius. This card is repeated until IJMAX positions have been included.

AMU(JI), JI = 1, N (7E10.5).

AMU(JI) represents the JIth root of the equation,

$$J_o(\mu_i) = 0, \quad i = 1, N.$$

G(JK), JK = 1, N (7E10.5).

This card is necessary only if N > 1, i. e., if the radial distribution of the source neutrons is not a J_o-function. G(JK) is the JKth radial component in the Bessel harmonic analysis of the neutron source. The determination of these quantities was described in Appendix C.

If it is desired to run another problem, one must go back to the first card. There is no limitation in the number of problems that can be run at the same time.

A.1.2 FORTRAN Listing and Summary of MINIFLUX

The MINIFLUX code consists of a MAIN program and four function subprograms. The function subprograms are called BJZERO, BJONE, SINH and COSH. A brief description of each part of the program is given below, followed by a FORTRAN listing of the entire program.

The subprogram BJZERO calculates the value of the function $J_o(x)$ for any value of x; BJONE calculates the value of $J_1(x)$ for any value of x. The subprogram SINH and COSH compute the value of sinh x and cosh x, respectively, for any value of the argument x. The MAIN program carries out the calculations described in Sections 3.2.2 and 3.4.

The output of the MINIFLUX program is self-explanatory. Aside from the input data, the output consists of the following quantities:

1. $y = r/R$.
2. $x = z/H$.
3. PHIS = $\phi_s(r, z)$.
4. PHIL = $\phi_\ell(r, z)$.
5. PHIT = $\phi_s(r, z) + \phi_\ell(r, z)$.
6. Q = $pq(r, z, \tau_{28})$.
7. CD = $\psi(r, z)$.
8. SUBC is the subcadmium activity of gold.
9. EPIC is the epicadmium activity of gold.
10. ARC = $R_{Au}(r, z) - 1$.

TABLE A.1

FORTRAN listing of the MINIFLUX program

```
*M2961-2465,FMS,DEBUG,1,1,500,250      E. SEFCHOVICH
*       LIST
*       LABEL
*       SYMBOL TABLE
        FUNCTION BJZERO(XX)
        U=XX/3.0
        IF(U-1.0) 1,1,2
      1 A=2.2499997*(U**2.0)
        B=1.2656208*(U**4.0)
        C=0.3163866*(U**6.0)
        D=0.0444479*(U**8.0)
        E=0.0039444*(U**10.0)
        G=0.0002100*(U**12.0)
        BJZERO= 1.0-A+B-C+D-E+G
        RETURN
      2 AA=0.79788456
        BB=0.00000077/U
        CC=0.00552740/(U**2.0)
        DD=0.00009512/(U**3.0)
        EE=0.00137237/(U**4.0)
        GG=0.00072805/(U**5.0)
        HH=0.00014476/(U**6.0)
        P=AA-BB-CC-DD+EE-GG+HH
        AAA=0.78539816
        BBB=0.04166397/U
        CCC=0.00003954/(U**2.0)
        DDD=0.00262573/(U**3.0)
        EEE=0.00054125/(U**4.0)
        GGG=0.00029333/(U**5.0)
        HHH=0.00013558/(U**6.0)
        TZERO= 3.0*U-AAA-BBB-CCC+DDD-EEE-GGG+HHH
        YY=1.0/SQRTF(3.0*U)
        BJZERO= YY*P*COSF(TZERO)
        RETURN
        END
*       LIST
*       LABEL
*       SYMBOL TABLE
        FUNCTION BJONE(UX)
        UY= UX/3.0
        IF(UY-1.0) 3,3,4
      3 AX= 0.5
        BX=0.56249985*(UY**2.0)
        VX=0.03954289*(UY**6.0)
        EX=0.00443319*(UY**8.0)
        GX=0.00031761*(UY**10.0)
        HX=0.00001109*(UY**12.0)
        PX=AX-BX+CX-VX+EX-GX+HX
        BJONE=3.0*UY*PX
        RETURN
      4 UUY=1.0/UY
```

```
      AAX=0.79788456
      BBX=0.00000156*UUY
      CCX=0.01659667*(UUY**2.0)
      DDX=0.00017105*(UUY**3.0)
      EEX=0.00249511*(UUY**4.0)
      GGX=0.00113653*(UUY**5.0)
      HHX=0.00020033*(UUY**6.0)
      PPX= AAX+BBX+CCX+DDX-EEX+GGX-HHX
      AXX=2.35619449
      BXX=0.12499612*UUY
      CXX=0.00005650*(UUY**2.0)
      DXX=0.00637879*(UUY**3.0)
      EXX=0.00074348*(UUY**4.0)
      GXX=0.00079824*(UUY**5.0)
      HXX=0.00029166*(UUY**6.0)
      TONE=3.0*UY-AXX+BXX+CXX-DXX+EXX+GXX-HXX
      PY=1.0/SQRTF(3.0*UY)
      BJONE=PY*PPX*COSF(TONE)
      RETURN
      END
      FUNCTION SINH(XXX)
      XY=EXPF(XXX)
      ZY=1.0/XY
      SINH=(XY-ZY)/2.0
      RETURN
      END
*     LABEL
      FUNCTION COSH(UUU)
      UV= EXPF(UUU)
      WV=1.0/UV
      COSH = (UV + WV)/2.0
      RETURN
      END
     0DIMENSION ALFA(15),G(15),B3(15),BETAR(15),BETAH(15),AL(15),RS(15),
     1AMU(15),PT(15,100),CA(15,100),CQ(15,100),RL(100),PQ(15,100),C5(15,
     2100),C7(15,100),X1(20),Y1(20),AS(15),RAL(15,100),PQQ(15,100),PHIS(
     320,20),PHIL(20,20),PHIT(20,20),Q(20,20),CD(20,20)
      DIMENSION SUBC(20,20),EPIC(20,20), ARC(20,20),SE(15)
      DIMENSION ID(12)
      DIMENSION XV(15),YV(15),ZR(15),QS(20,20),QL(20,20)
      PRINT 10
   10 FORMAT(1H1,20X,17H PROGRAM MINIFLUX//)
  100 READ 12,( ID(I), I=1,12)
   12 FORMAT(12A6)
C       12 IS A PROBLEM STATEMENT
      PRINT 12, (ID(I), I=1,12)
      READ 5, N,M,ILMAX,IJMAX,R,H,EL,SIGAS,ELS
      PRINT 12
C     ILMAX= NUMBER OF AXIAL POINTS LESS OR EQUAL THAN 20
C     IJMAX= NUMBER OF RADIAL POINTS LESS OR EQUAL THAN 20
C     SIGAS= ABS. CROSS SECTION FOR MAXWELLIAN
C     SAME THERMAL DIFFUSION LENGTH
    5 FORMAT(4I5,5E10.5)
      EL2= EL*EL
      AR=R/ELS
```

```
      AH= H/ELS
      READ 6, TAU,TAUT,CAIN,SIGA,CSIS,XIT,ERI
      READ 6, RZ
C     RZ=(RCD-1) AT SOURCE END
C     ERI-  EFFECTIVE RESONANCE INTEGRAL INCLUDING 1/V ABSORPTION
C     DIVIDED BY SIGMA-0
      READ 6, (X1(NX),NX=1,ILMAX)
      READ 6,  (Y1(NY), NY=1,IJMAX)
    6 FORMAT(7E10.5)
C     EL=THERMAL DIFFUSION LENGTH
C      R,H= EXTRAPOLATED RADIUS AND HEIGHT
C      N= NUMBER OF RADIAL HARMONICS, LESS THAN 15
C      M= NUMBER OF AXIAL HARMONICS, LESS THAN 100
C      TAU= AGE FORQ(TAU)
C      TAUT= AGE TO THERMAL
C      CAIN= K-INFINITY
C      SIGA= THERMAL ABSORPTION CROSS SECTION
C      CSIS= XI*SIGMA-S
C     XIT= ITERATION CRITERION
      W=TAU/EL2
      WT= TAUT/EL2
      XF=CSIS*0.886/(ERI*RZ)
      PI= 3.1415926535
      READ 6,(AMU(JI), JI=1,N)
      IF(N-1) 7,7,8
    7 ZIN = AMU(1)
      G(1)= (BJONE(ZIN)**2.0)/2.0
      GO TO 9
    8 READ 6, (G(JK), JK=1,N)
    9 CONTINUE
      DO 14 NR=1,N
      B3(NR)= AR**2.0 +AMU(NR)**2.0
      BETAR(NR) = SQRTF(B3(NR))
      BETAH(NR)= (AH/AR)*BETAR(NR)
      AL(NR)=  TANHF(BETAH(NR))
      RS(NR)= G(NR)/BETAR(NR)
      ALFA(NR)= AMU(NR)/R
      SE(NR)=XF*G(NR)
      UL=ALFA(NR)**2.0 + 1.0/TAU
      XV(NR)=H*SQRTF(UL)
      YV(NR)=R*SQRTF(UL)
      DO 15 MA=1,M
      AMA = MA
      RL(MA)=  (AMA*PI)/(AH*2.0)
      BUCK2=ALFA(NR)**2.0 +(AMA*PI/H)**2.0
      ROH2= EL2*BUCK2
      ST= ROH2*WT
       S= ROH2*W
      PA = EXPF(-S)
      PAT = EXPF(-ST)
      PT(NR,MA) = 1.0/(1.0+ROH2)
      CA(NR,MA) = CAIN*PAT*PT(NR,MA)
      CQ(NR,MA)= CA(NR,MA)/(1.0-CA(NR,MA))
      PQ(NR,MA) = PA/PAT
      C5(NR,MA)= RS(NR)*RL(MA)*AL(NR)*CQ(NR,MA)*PT(NR,MA)
```

```
      C7(NR,MA)= RS(NR)*RL(MA)*AL(NR)*CQ(NR,MA)*PQ(NR,MA)
   15 CONTINUE
   14 CONTINUE
      KI=1
   62 C6= ABSF(C5(1,KI)/C5(1,1))
      IF(C6-XIT) 60,61,61
   61 KI=KI+1
      GO TO 62
   60 KIL=KI
      KM=1
   65 C8= ABSF(C7(1,KM)/C7(1,1))
      IF(C8-XIT) 63,64,64
   64 KM=KM+1
      GO TO 65
   63 KMQ= KM
      CONTINUE
      DO 300 JL=1,IJMAX
      Y= Y1(JL)
      DO 301 JM=1,ILMAX
      X= X1(JM)
      SUMS = 0.0
      SUML= 0.0
      SUQS=0.0
      SUMQ= 0.0
      DO 26 KR=1,N
      ZIN = AMU(KR)
      TY = ZIN*Y
      B1= BJZERO(TY)
      B2= BJONE(ZIN)**2.0
      R1= B1/B2
      ZK = BETAH(KR)
      ZM = ZK*(1.0-X)
      SIR = SINH(ZM)/COSH(ZK)
      AS(KR)= RS(KR)*SIR*R1
      SUMS = SUMS+ AS(KR)
      RV= XV(KR)
      ZV = RV*(1.0-X)
      TR= SINH(ZV)/COSH(RV)
      ZR(KR) = (SE(KR)/YV(KR))*TR*R1
      SUQS = SUQS + ZR(KR)
      DO 27 KA=1,KIL
      AKA = KA
      ANG3= AKA*PI*X
      RAL(KR,KA)= C5(KR,KA)*R1*SINF(ANG3)
      SUML = SUML+ RAL(KR,KA)
   27 CONTINUE
      DO 28 KS=1,KMQ
      AKS = KS
      ANG4= AKS*PI*X
      PQQ(KR,KS)= C7(KR,KS)*R1*SINF(ANG4)
      SUMQ = SUMQ + PQQ(KR,KS)
   28 CONTINUE
   26 CONTINUE
      PHIS(JL,JM) = 2.0*SUMS
      PHIL(JL,JM)=4.0*SUML*SIGAS/SIGA
```

```
      PHIT(JL,JM)= PHIS(JL,JM) + PHIL(JL,JM)
      QS(JL,JM)= 2.0*SUQS
      QL(JL,JM)= 4.0*SIGAS*SUMQ
      Q(JL,JM)= QS(JL,JM) + QL(JL,JM)
      CD(JL,JM)= Q(JL,JM)/(PHIT(JL,JM)*CSIS)
      SUBC(JL,JM)=0.886*PHIT(JL,JM) +0.414*Q(JL,JM)/CSIS
      EPIC(JL,JM)=  ERI*Q(JL,JM)/CSIS
      ARC(JL,JM)= SUBC(JL,JM)/EPIC(JL,JM)
  301 CONTINUE
  300 CONTINUE
      PRINT 71
   71 FORMAT(55H       (RC-1)0  LS    SIGMA-S  (ERI+0.5SO)/SO     XIT    )
      PRINT 72, RZ,ELS,SIGAS,ERI,XIT
   72 FORMAT(6X,F7.3,F7.4,F10.7,F14.7,F11.5)
      IF(N-1) 13,13,30
   13 PRINT 150
  150 FORMAT(1H1,20X,14H J-ZERO SOURCE//)
      PRINT 16
   160FORMAT(120H          R       H       L       W       WT    K-INF   SIGMAT-
     1A  XI*SIGMA-S  KIL  KMQ                                            )
      PRINT 17, R,H,EL,W,WT,CAIN,SIGA,CSIS,KIL,KMQ
   17 FORMAT(5X,5F7.3,F7.4,F10.5,F10.5,2I5)
      GO TO 37
   30 PRINT 31
   31 FORMAT(20X,18H NON-J-ZERO SOURCE//)
      PRINT 32
   320FORMAT(120H       N     R       H       L       W       WT    K-INF   SIGM
     1AT-A  XI*SIGMA-S  KIL  KMQ                                         )
      PRINT 33,N,R,H,EL,W,WT,CAIN,SIGA,CSIS,KIL,KMQ
   33 FORMAT(5X,I3,5F7.3,F7.4,F10.5,F10.5,2I5)
   37 PRINT 18
   180FORMAT(120H      Y           X           PHIS          PHIL          PHI
     1T          Q           CD          SUBC          EPIC          ARC       )
     0PRINT 19,((Y1(J),X1(K),PHIS(J,K),PHIL(J,K),PHIT(J,K),Q(J,K),CD(J,K
     1),SUBC(J,K),EPIC(J,K),ARC(J,K),K=1,ILMAX),J=1,IJMAX)
   19 FORMAT(10E12.5)
      GO TO 100
      END
```

A.1.3 Sample Problems.

```
LL7    AXIAL    AU    DISTRIBUTION
   2  100    20     1     48.908       128.0      11.382   0.00576    11.950
    81.34      124.9       1.416    0.00640      0.177   0.00001     3.670
    500.0
     0.03       0.08        0.13       0.18       0.23      0.28       0.33
     0.38       0.43        0.48       0.53       0.58      0.63       0.68
     0.73       0.78        0.83       0.88       0.93      0.98
   0.0694
  2.40482    5.52007
   0.9413   0.000001
ML7    AXIAL    AU    DISTRIBUTION
   5  100    20     1     27.576      47.366      11.382   0.00576    11.950
    81.34      124.9       1.416    0.00640      0.177   0.00001     2.807
     70.0
     0.03       0.08        0.13       0.18       0.23      0.28       0.33
     0.38       0.43        0.48       0.53       0.58      0.63       0.68
     0.73       0.78        0.83       0.88       0.93      0.98
   0.1238
  2.40482    5.52007     8.65372   11.79153   14.93091
   0.9413   -0.01455     0.03055   -0.01395    0.01679
ML7   RADIAL    AU    DISTRIBUTION                Z/H=0.362
   5  100     1    20     27.576      47.366      11.382   0.00576    11.950
    81.34      124.9       1.416    0.00640      0.177   0.00001     2.807
     70.0
    0.362
     0.03       0.08        0.13       0.18       0.23      0.28       0.33
     0.38       0.43        0.48       0.53       0.58      0.63       0.68
     0.73       0.78        0.83       0.88       0.93      0.98
  2.40482    5.52007     8.65372   11.79153   14.93091
   0.9413   -0.01455     0.03055   -0.01395    0.01679
ML7   RADIAL    AU    DISTRIBUTION                 Z/H = 0.524
   5  100     1    20     27.576      47.366      11.382   0.00576    11.950
    81.34      124.9       1.416    0.00640      0.177   0.00001     2.807
     70.0
    0.524
     0.03       0.08        0.13       0.18       0.23      0.28       0.33
     0.38       0.43        0.48       0.53       0.58      0.63       0.68
     0.73       0.78        0.83       0.88       0.93      0.98
  2.40482    5.52007     8.65372   11.79153   14.93091
   0.9413   -0.01455     0.03055   -0.01395    0.01679
```

A.2 The RADIAL HARMONICS Code

The RADIAL HARMONICS program makes a Hankel harmonic analysis of the radial dependence of the neutrons coming from the source, as described in Appendix C. The input instructions are given below. The input consists of the measured radial activity distribution of the source, the radial positions of the foils, distance between foils and appropriate information to make the computation. The output consists of the Bessel coefficients $\bar{f}_i$ and the statistical uncertainties.

A.2.1 Input Instructions

N, NR, NS, RAD, DRAD, DR, ERY, ERA (3I5, 5E10.5).

N is the number of radial points at which the activity was measured.

NR is the maximum number of Bessel radial harmonics to be included in the calculation (≤ 20).

NS is the number of radial shifts. The extrapolated radius of the assembly will be shifted NS times by increasing and reducing the quantity RAD by NT*DRAD, where NT = 1, ..., NS/2. This artifice permits a check on the extrapolated radius. This approach indicates which value of the extrapolated radius gives the best fit.

RAD is the extrapolated radius in cm.

DRAD denotes the increment in RAD for the checking procedure described above in cm.

DR represents the separation between foils in cm.

ERY denotes the fractional uncertainty in the radial position of the foils.

ERA is the uncertainty in the activity of the foils.

A(L), L = 1,N (6E12.6).

A(L) is the activity of the foil at the L^{th} radial point (≤ 50).

R(L), L = 1, N (6E12.6).

R(L) is the radial location of the L^{th} foil.

AMU(M), M = 1, NR (6E12.6).

AMU(M) is the M^{th} positive root of the equation, $J_o(\mu_m) = 0$.

A.2.2 FORTRAN Listing of the RADIAL HARMONICS Code

The RADIAL HARMONICS code consists of the MAIN program and the BJZERO and BJONE function subprograms listed in Section A.1.3. The MAIN program computes the values of the coefficients $\bar{f}_i$ and their uncertainties as described in Appendix C. The two function subprograms were described in Section A.1.2. The FORTRAN II listing of the MAIN program is given in Table 3.2.

TABLE A.2

FORTRAN Listing of the RADIAL HARMONICS Code.

```
*M2961-2465,FMS,DEBUG,1,1,500,250      E. SEFCHOVICH
*      LIST
*      LABEL
      ODIMENSION A(50),R(50),AMU(20),Y(50),X(20,50),UT(20,50),W(20,50),Z(
      120,50),S(20),Q(20),SIG(20)
   50 READ 4, N,NR, NS, RAD, DRAD, DR, ERY, ERA
      PRINT 1
    1OFORMAT(1H1,20X62H PROGRAM TO CALCULATE RADIAL HARMONICS IN CYLINDR
      1ICAL GEOMETRY//)
C     N= NUMBER OF RADIAL POINTS
C     NR=  NUMBER OF RADIAL HARMONICS
C     NS= NUMBER OF RADIAL SHIFTS, EXAMPLE 1 RIGHT, 1 LEFT, NS=2
C     RAD= CLOSE GUESS AT RADIUS
C      DRAD= INCREMENT IN RADIUS FOR FURTHER  TRIALS
C     DR= SEPARATION BETWEEN FOILS
C     ERY= ERROR IN RADIAL POSITION
C     ERA= ERROR IN ACTIVITY
    4 FORMAT(3I5,5E10.5)
    5 FORMAT(6E12.6)
      READ 5, (A(L), L=1,N)
      READ 5, (R(L),L=1,N)
      READ 5,(AMU(M),M=1,NR)
      DO 12 NT=1,NS
      RAS = RAD
      LS = NS/2
      IF(NT-LS) 21,30,22
   21 ANT=NT
      RAS = RAS + ANT*DRAD
      GO TO 30
   22 ANT = NT-LS
      RAS = RAS - ANT*DRAD
      GO TO 30
   30 DY = DR/RAS
      SIGA =0.0
      DO 7  J=1,NR
      SUMR = 0.0
      SUMS = 0.0
      DO 6  I=1,N
      Y(I) = R(I)/RAS
      TY = AMU(J)*Y(I)
      X(J,I) = BJZERO(TY)
      UT(J,I) = Y(I)*A(I)*X(J,I)
      SUMS = SUMS + UT(J,I)
      W(J,I) = X(J,I) - TY*BJONE(TY)
      PR = (W(J,I)*A(I)*ERY)**2.0
      QR = (Y(I)*BJZERO(TY)*ERA)**2.0
      Z(J,I)  =  PR + QR
      SUMR = SUMR + Z(J,I)
    6 CONTINUE
      V = DY
      S(J) = SUMS*V
      Q(J) = (V**2.0)*SUMR
```

```
      P= ABSF(Q(J))
      SIG(J) = SQRTF(P)
      SIGA = SIGA + (SIG(J)**2.0)
    7 CONTINUE
      ER2 = SIGA
      PRINT 10, RAS
   10 FORMAT(//20H      THE RADIUS IS ,F10.5//)
      PRINT 9, ER2
    9 FORMAT(43H THE SUM OF THE SQUARES OF THE ERRORS IS   ,E12.5//)
      PRINT 11
   110FORMAT(120H  J    S    -   SIG      J    S         SIG         J
     1S        SIG      J    S         SIG      J    S          SIG        )
      PRINT 8, (J,S(J),SIG(J), J=1,NR)
    8 FORMAT(5(I3,2E10.4))
   12 CONTINUE
      GO TO 50
      END
*     DATA
```

A.3 The EPIFAST Program

The EPIFAST computer program is described in Appendix E. The program computes δ_{25}, ρ_{28} and C^*, using the input obtained from the LSQ-4D program (D1). The input instructions follow.

A.3.1 Input Data for the EPIFAST Program

ID(I), I = 1, 12 (12A6).

ID(I) is an arbitrary identification statement of 72 spaces or less; it is used to label each set of data.

N, M, L1, L2, L3, L4, L5, L6 (8I5).

N is the number of time points at which it is desired to calculate the fission product activity of each of the six uranium foils appearing in the calculation; N is usually equal to the number of counting passes made in measuring the fission product activity of these foils.

M is the number of counting passes made for the Np^{239} activity of the depleted uranium foils.

L1 is the degree of the polynomial fit for the fission product activity of the bare natural uranium foil.

L2 is the degree of the polynomial fit to the fission product activity of the bare depleted uranium foil.

L3 is similar to L1 but for the cadmium-covered foil.

L4 is similar to L2 but for the cadmium-covered foil.

L5 is similar to L1 but for the foil irradiated in a Maxwellian foil.

L6 is similar to L2 but for the foil irradiated in a Maxwellian flux.

EPSN, EPSD, STHER, SMAX (4E12.5).

EPSN is the U^{235} atom fraction in the natural uranium foils.

EPSD is the U^{235} atom fraction in the depleted uranium foils.

STHER is the ratio $\left(\Sigma_a^{28}/\Sigma_f^{25}\right)_{SC}$.

SMAX is the ratio $C_M^* = \left(\Sigma_a^{28}/\Sigma_f^{25}\right)_{MAX}$.

CORDEL, CORRHO, CORFL (3E12.5).

CORDEL is the correction factor ψ_δ for δ_{25} required by the presence of foreign materials in the foil packets.

CORRHO is the correction factor ψ_ρ for ρ_{28} for the presence of foreign materials in the foil packets.

CORFL is the ratio of the activity of the monitor foil placed below the foil packet with cadmium-covered foils to the activity of the monitor foil located below the other foil packet.

A1(I), I = 1, L1 + 1 (6E12.5).

A1(I) is the i^{th} coefficient in the polynomial fit to the fission product activity of the natural uranium bare foil.

P1(I), I = 1, L1 + 1. (6E12.5).

P1(I) is the uncertainty of A1(I).

A2(I), I = 1, L2 + 1 (6E12.5).

A2(I) is the i^{th} coefficient in the polynomial fitted to the fission product activity of the bare depleted uranium foil.

P2(I), I = 1, L2 + 1 (6E12.5).

P2(I) is the uncertainty in A2(I).

A3(I), I = 1, L3 + 1 (6E12.5).

A3(I) is the i^{th} coefficient of the polynomial fitted to the fission product activity of the cadmium-covered, natural uranium foil.

P3(I), I = 1, L3 + 1 (6E12.5).

P3(I) is the uncertainty in A3(I).

A4(I), I = 1, L4 + 1 (6E12.5).

A4(I) is the i^{th} coefficient of the polynomial fitted to the fission product activity of the cadmium-covered, depleted uranium foil.

P4(I), I = 1, L4 + 1 (6E12.5).

P4(I) is the uncertainty of A4(I).

A5(I), I = 1, L5 + 1 (6E12.5).

A5(I) is the i^{th} coefficient of the polynomial fitted to the fission product activity of the natural uranium foil irradiated in a Maxwellian flux.

P5(I), I = 1, L5 + 1 (6E12.5).

P5(I) is the uncertainty in A5(I).

A6(I), I = 1, L6 + 1 (6E12.5).

A6(I) is the i^{th} coefficient of the polynomial fitted to the fission product activity of the depleted uranium foil irradiated in a Maxwellian flux.

P6(I), I = 1, L6 + 1 (6E12.5).

P6(I) is the uncertainty in A6(I).

T(I), I = 1, N (6E12.5).

T(I) is the i^{th} time at which the fission product activities of all the foils are to be calculated.

DBN(J), J = 1, M (6E12.5).

DBN(J) is the Np^{239} corrected activity of the bare depleted uranium foil in the j^{th} counting pass.

DCN(J), J = 1, M (6E12.5).

DCN(J) is the corrected Np^{239} activity of the cadmium-covered uranium foil in the j^{th} counting pass.

DMN(J), J = 1, M (6E12.5).

DMN(J) is the corrected Np^{239} activity of the depleted uranium foil irradiated in a Maxwellian flux.

D1(J), J = 1, M (6E12.5).

D1(J) is the uncertainty in DBN(J).

D2(J), J = 1, M (6E12.5).

D2(J) is the uncertainty in DCN(J).

D3(J), J = 1, M (6E12.5).

D3(J) is the uncertainty in DMN(J).

A.3.2 FORTRAN II Listing and Summary of the EPIFAST Code

The EPIFAST program consists only of a MAIN program which uses the input information to carry out the computations discussed in Appendix E.

The output is self-explanatory from the discussion in Appendix E. Only the following headings in the output require identification.

1. BN is the fission product activity of the bare natural uranium foil.

2. BD is the fission product activity of the bare depleted uranium foil.

3. CN is the fission product activity of the cadmium-covered natural uranium foil.

4. CD is the fission product activity of the cadmium-covered depleted uranium foil.

5. FMN is the fission product activity of the natural uranium foil irradiated in a Maxwellian flux.

6. FMD is the fission product activity of the depleted uranium foil irradiated in a Maxwellian flux.

The FORTRAN II listing of the EPIFAST program is given in Table A.3.

TABLE A.3

FORTRAN Listing of the EPIFAST Program.

```
*M2961-2465,FMS,RESULT,1,1,500,250           E. SEFCHOVICH
*      LABEL
       DIMENSION SF1(50),SF2(50),SF3(50),SF4(50),SF5(50),SF6(50)
       DIMENSION A1(50),A2(50),A3(50),A4(50),A5(50),A6(50)
       DIMENSION P1(50),P2(50),P3(50),P4(50),P5(50),P6(50)
       DIMENSION BN(50),BD(50),CN(50),CD(50),FMN(50),FMD(50) ,T(50)
       DIMENSION DBN(50),DCN(50),DMN(50),D1(50),D2(50),D3(50)
       DIMENSION ID(12),DEL25(50),RHO28(50),RNP(50),RFP(50)
       DIMENSIONSD25(50),SD28(50),SDNP(50),SDFP(50)
       DIMENSION U(50),V(50),W(50),X(50),R(50),S(50),Q(50)
     1 FORMAT(1H1,//20X16H PROGRAM EPIFAST)
   100 READ 2,(ID(I), I=1,12)
     2 FORMAT(12A6)
       PRINT 1
       PRINT 2,(ID(I), I=1,12)
C      2 IS A PROBLEM STATEMENT
       READ 3,N,M,L1,L2,L3,L4,L5,L6
     3 FORMAT(8I5)
C      N= NUMBER OF T(I) AT WHICH DATA FROM LSQ FOR FP IS DESIRED
C      M= NO. OF DATA POINTS FOR NP COUNTED FOILS
C      L1= DEGREE OF FIT FOR BN
C      L2=  ''    ''    ''    ''   BD
C      L3=   ''    ''    ''    ''   CN
C      L4=   ''    ''    ''    ''    CD
C      L5=   ''    ''    ''    ''     FMN
C      L6=   ''    ''    ''    ''   FMD
       READ 4,EPSN,EPSD,STHER,SMAX
     4 FORMAT(4E12.5)
C      EPSN= U-235 ATOM FRACTION IN NAT-U FOIL
C      EPSD= U-235 ATOM FRACTION IN DEP-U FOIL
C      STHER=(SIG-A28/SIG-F25)THERMOS
C      SMAX= CM-STAR
       READ 5, CORDEL,CORRHO,CORFL
C      CORDEL= CORRECTION FACTOR FOR DELTA-25
C      CORRHO= CORRECTION FACTOR FOR RHO-28
C      CORFL= PHIT-B/PHIT-C
     5 FORMAT(3E12.5)
     6 FORMAT(6E12.5)
       N1=L1+I
       N2= L2+1
       N3=L3+1
       N4=L4+1
       N5=L5+1
       N6=L6+1
       READ 6,(A1(I), I=1,N1)
       READ 6,(P1(I), I=1,N1)
       READ 6, (A2(I), I=1,N2)
       READ 6,(P2(I), I=1,N2)
       READ 6, (A3(I), I=1,N3)
       READ 6, (P3(I), I=1,N3)
       READ 6,(A4(I), I=1,N4)
```

```
      READ 6,(P4(I), I=1,N4)
      READ 6,(A5(I), I=1,N5)
      READ 6,(P5(I), I=1,N5)
      READ 6,(A6(I), I=1,N6)
      READ 6,(P6(I), I=1,N6)
      READ 6, (T(I), I=1,N)
C     AJ(I)= I-TH COEFF OF FIT, LJ+1 COEFFS
C     J=1 NAT-BARE, J=2 DEP-BARE,J=3 NAT-COV,J=4 DEP COV
C     J=5 NAT HOLRAUM, J=6 DEP HOLRAUM
C     PJ(I)= ERROR CORRESPONDING TO AJ(I), LJ+1 OF THESE
C     T(I)= TIMES AT WHICH DATA ID DESIRED= N OF THESE
      READ 6, (DBN(J), J=1,M)
      READ 6, (DCN(J), J=1,M)
      READ 6, (DMN(J), J=1,M)
      READ 6, (D1(J), J=1,M)
      READ 6, (D2(J), J=1,M)
      READ 6,(D3(J), J=1,M)
C     DBN(J) = J-TH DEP-BARE NP CORRECTED COUNT, SD' D1(J)
C     DCN(J)' J-TH DEP-COV NP CORRECTED COUNT, SD= D2(J)
C     DMN(J)= J-TH DEP HOLRAUM NP CORRECTED COUNT, SD= D3(J)
      ENRC = (1.0-EPSN)/(1.0-EPSD)
      DO 15 KI=1,N
      Y= T(KI)
      SBN= 0.0
      SBD=0.0
      SCN=0.0
      SCD=0.0
      SMN=0.0
      SMD=0.0
      SSBN=0.0
      SSBD=0.0
      SSCN=0.0
      SSCD=0.0
      SSMN=0.0
      SSMD=0.0
      DO 7 KJ=1,N1
      SBN= SBN + A1(KJ)*(Y**(KJ-1))
      SSBN = SSBN +(P1(KJ)*(Y**(KJ-1)))**2.0
    7 CONTINUE
      BN(KI)=SBN
      SF1(KI)= SSBN
      DO 8 KK=1,N2
      SBD = SBD + A2(KK)*(Y**(KK-1))
      SSBD = SSBD +(P2(KK)*(Y**(KK-1)))**2.0
    8 CONTINUE
      BD(KI)= SBD
      SF2(KI) =SSBD
      DO 9 KL=1,N3
      SCN = SCN + A3(KL)*(Y**(KL-1))
            SSCN = SSCN +(P3(KL)*(Y**(KL-1)))**2.0
    9 CONTINUE
      CN(KI)= SCN
      SF3(KI)= SSCN
      DO 10 KM=1,N4
      SCD = SCD + A4(KM)*(Y**(KM-1))
```

```
      SSCD =SSCD +(P4(KM)*(Y**(KM-1)))**2.0
   10 CONTINUE
      CD(KI) = SCD
      SF4(KI) = SSCD
      DO 11 KN=1,N5
      SMN = SMN + A5(KN)*(Y**(KN-1))
      SSMN = SSMN + (P5(KN)*(Y**(KN-1)))**2.0
   11 CONTINUE
      FMN(KI)= SMN
      SF5(KI)= SSMN
      DO 12 JI=1,N6
      SMD = SMD + A6(JI)*(Y**(JI-1))
      SSMD = SSMD + (P6(JI)*(Y**(JI-1)))**2.0
   12 CONTINUE
      FMD(KI)= SMD
      SF6(KI) = SSMD
   15 CONTINUE
       SUMD = 0.0
      SUFP = 0.0
      SIGD = 0.0
      SIGFP = 0.0
      DO 20 K=1,N
      R(K)= BN(K)- ENRC*BD(K)
      S(K) = CN(K) -ENRC*CD(K)
      Q(K) = FMN(K) - ENRC*FMD(K)
      DEL25(K)= CORDEL*S(K)/(R(K)*CORFL-S(K))
      XR = SF1(K)+(ENRC**2.0)*SF2(K)
      XS = SF3(K) + (ENRC**2.0)*SF4(K)
      XQ = SF5(K) + (ENRC**2.0)*SF6(K)
      XDEL=(DEL25(K)**2.)*(XS/(S(K)**2.)+XRS/((CORFL*R(K)-S(K))**2.0))
      SD25(K)= SQRTF(XDEL)
      SUMD = SUMD + DEL25(K)/XDEL
      SIGD = SIGD + 1.0/XDEL
      RFP(K) = R(K)/Q(K)
      XFP=(RFP(K)**2.0)*(XR/(R(K)**2.0)+XQ/(Q(K)**2.0))
      SDFP(K) = SQRTF(XFP)
      SUFP = SUFP + RFP(K)/XFP
      SIGFP = SIGFP + 1.0 /XFP
   20 CONTINUE
      DELAV = SUMD/SIGD
      RFPAV = SUFP/SIGFP
      SIGDAV =0.0
      SIFPAV =0.0
      DO 21 L=1,N
      U(L) = ((DEL25(L)-DELAV)/SD25(L))**2.0
      SIGDAV = SIGDAV + U(L)
      X(L) = ((RFP(L)-RFPAV)/SDFP(L))**2.0
      SIFPAV = SIFPAV + X(L)
   21 CONTINUE
      UX = SIGDAV/(SIGD-1.0)
      SDEL = SQRTF(UX)
      UY= SIFPAV/(SIGD-1.0)
      SRFP = SQRTF(UY)
      SUNP =0.0
      SIGNP=0.0
```

```
      SUMRO =0.0
      SIGRO =0.0
      DO 22 LL=1,M
      RHO28(LL)= CORRHO*DCN(LL)/(DBN(LL)*CORFL-DCN(LL))
      XSB = (CORFL**2.0)*(D1(LL)**2.0)+ D2(LL)**2.0
      XRO=(RHO28(LL)**2.)*((D2(LL)/DCN(LL))**2.+XSB/((DBN(LL)*CORFL-DCN(
     1LL))**2.0))
      SD28(LL)= SQRTF(XRO)
      SIGRO = SIGRO + 1.0/XRO
      SUMRO = SUMRO + RHO28(LL)/XRO
      RNP(LL)= DBN(LL)/DMN(LL)
      XNP=(RNP(LL)**2.)*((D1(LL)/DBN(LL))**2. +(D3(LL)/DMN(LL))**2.0)
      SDNP(LL) = SQRTF(XNP)
      SUNP = SUNP + RNP(LL)/XNP
      SIGNP = SIGNP + 1.0/XNP
   22 CONTINUE
      RHOAV = SUMRO/SIGRO
      RNPAV = SUNP/SIGNP
      SRAV=0.0
      SINAV=0.0
      DO 23 LM=1,M
      V(LM)=((RHO28(LM)-RHOAV)/SD28(LM))**2.0
      SRAV = SRAV + V(LM)
      W(LM)= ((RNP(LM)-RNPAV)/SDNP(LM))**2.0
      SINAV = SINAV + W(LM)
   23 CONTINUE
      VX= SRAV/(SIGRO-1.0)
      SRHO= SQRTF(VX)
      VY= SINAV/(SIGNP-1.0)
      SRNP = SQRTF(VY)
      CTH= (1.0+RHOAV)*STHER/(1.0+DELAV)
      CMAX = SMAX*RNPAV/RFPAV
      TD= UX/((1.0+DELAV)**2.0)
      TR= VX/((1.0+RHOAV)**2.0)
      TX= (CTH**2.0)*(TD+TR)
      SDCTH= SQRTF(TX)
      ZFP = UY/(RFPAV**2.0)
      ZNP = VY/(RNPAV**2.0)
      ZY = (CMAX**2.0)*(ZFP+ZNP)
      SDCMAX = SQRTF(ZY)
   300FORMAT(120H     T             BN            BD            CN            CD            F
     1MN         FMD     DELTA-25   SD-DEL-25     RFP       SD-RFP              )
      PRINT 30
   31 FORMAT(11E10.4)
     0PRINT 31,(T(II),BN(II),BD(II),CN(II),CD(II),FMN(II),FMD(II),DEL25(
     1II),SD25(II),RFP(II),SDFP(II),II=1,N)
      PRINT 32, DELAV,SDEL,RFPAV,SRFP
   320FORMAT(//10X,12H DEL-25-AV= E12.5,15H SD OF DEL-25= E12.5,9H RFP-A
     1V= E12.5,12H SD OF RFP= E12.5)
      PRINT 33
   330FORMAT(120H     J     DCN         DBN         DMN         RHO-28   SD-RHO-28
     1    RNP       SD-RNP                                                    )
     0PRINT 34, (J,DCN(J),DBN(J),DMN(J),RHO28(J),SD28(J),RNP(J),SDNP(J),
     1 J=1,M)
   34 FORMAT(I5,7E10.4)
```

```
      PRINT 35, RHOAV,SRHO,RNPAV,SRNP
  350FORMAT(//10X,12H RHO-28-AV= E12.5,15H SD /F RHO-28= E12.5,9H RNP-A
     1V= E12.5,12H SD OF RNP= E12.5)
      PRINT 36, CTH, SDCTH, CMAX, SDCMAX
  360FORMAT(//10X,6H CTH= F12.5,8H SDCTH= E12.5,7H CMAX= E12.5,9H SDCMA
     1X= E12.5//)
      GO TO 100
      END
```

.A.3.3 Sample Problem.

```
RUN  ML7-4      1.143 PC  1.75''    PITCH  LATTICE
  6    9     3    4    3    3    4    3
   0.00714     0.000018       0.4145       0.4169
      0.95          1.1       1.0345
    244.54      -0.9067  -.29225E-06  0.39569E-05
       1.0
    6.8087    -.055514  0.53337E-03  -.29642E-05   .57045E-08
       1.0
    13.184   -0.046785  -.14239E-04    .25294E-06
       1.0
    3.6754   -0.019875  0.47594E-04  -.33819E-07
       1.0
    2075.7     -15.516      0.10480  -.45473E-03   .75605E-06
       1.0
    10.167   -0.044976  0.71207E-04  0.96590E-08
       1.0
      12.0        59.0        106.0        153.0        200.0        247.0
    117.41      115.66       117.21       120.49       120.77       120.87
    120.41      120.91       119.21
    31.595      31.683       31.240       33.020       32.623       33.444
    33.447      33.320       33.084
    677.90      673.82       670.74       701.00       698.88       699.46
    711.27      706.55       713.84
       1.0         1.0          1.0          1.0          1.0          1.0
       1.0         1.0          1.^
       1.0         1.0          1.0          1.0          1.0          1.0
       1.0         1.0          1.0
       1.0         1.0          1.0          1.0          1.0          1.0
       1.0         1.0          1.0
```

APPENDIX B

REFERENCES

A1 Argonne National Laboratory, "Reactor Physics Constants," ANL 5800 (July, 1963).

A2 Anderson, C. A., and T. J. Thompson, "Measurement of Neutron Energy Spectra with the Massachusetts Institute of Technology Fast Chopper," Trans. Am. Nucl. Soc., 5, No. 1, 39 (1962).

B1 Bliss, H. E., "Measurements of the Fast Effect in Heavy Water, Partially Enriched Uranium Lattices," M.S. Thesis, M.I.T. Nucl. Eng. Dept. (May, 1964).

B2 Brown, P. S., T. J. Thompson, I. Kaplan, and A. E. Profio, "Measurements of the Spatial and Energy Distribution of Thermal Neutrons in Uranium, Heavy Water Lattices," NYO-10205, MITNE-17 (August, 1962).

B3 Bratten, J., 22.42 course work M.I.T., unpublished (1959).

C1 Critoph, E., "Comparison of Theory and Experiment for: (a) Lattice Properties of D_2O-U Reactors; (b) Control Rod Experiments; (c) Foreign Rod Experiments," CRRP-655, AECL-No. 350 (1956).

C2 Clikeman, F. M., Private communication.

D1 D'Ardenne, W. H., T. J. Thompson, D. D. Lanning, and I. Kaplan, "Studies of Epithermal Neutrons in Uranium, Heavy Water Lattices," MIT-2344-2, MITNE-53 (August, 1964).

G1 Galanin, A. D., Thermal Reactor Theory (New York: Pergamon Press, 1960).

G2 Glasstone, S., and M. C. Edlund, The Elements of Nuclear Reactor Theory (Princeton, New Jersey: D. Van Nostrand Company, Inc., 1952).

H1 Thompson, T. J., I. Kaplan, and A. E. Profio, "Heavy Water Lattice Project Annual Report," NYO-9658 (September, 1961).

H2 Kaplan, I., A. E. Profio, and T. J. Thompson, "Heavy Water Lattice Project Annual Report," NYO-12208, MITNE-26 (September, 1962).

H3 Kaplan, I., D. D. Lanning, and T. J. Thompson, "Heavy Water Lattice Project Annual Report," NYO-10212, MITNE-46 (September, 1963).

H4 Lanning, D. D., I. Kaplan, and F. M. Clikeman, "Heavy Water Lattice Project Annual Report," MIT-2344-3, MITNE-60 (September, 1964).

H5 Thompson, T. J., I. Kaplan, F. M. Clikeman, and M. J. Driscoll, "Heavy Water Lattice Project Annual Report," MIT-2344-4, MITNE-65 (September, 1965).

H6 Harrington, J., "Measurement of the Material Buckling of a Lattice of Slightly Enriched Uranium Rods in Heavy Water," M.S. Thesis, M.I.T. Nucl. Eng. Dept. (July, 1963).

H7 Harrington, J., D. D. Lanning, I. Kaplan, and T. J. Thompson, "Use of Neutron Absorbers for the Experimental Determination of Lattice Parameters in Subcritical Assemblies," MIT-2344-6, MITNE-69 (February, 1966).

H8 Heavy Water Lattices: Second Panel Report, Report of a Panel Held in Vienna, 18-22 February, 1963, Technical Report Series No. 20 (Vienna: IAEA, September, 1963).

H9 Honeck, H. C., "The Distribution of Thermal Neutrons in Space and Energy in Reactor Lattices. Part I: Theory," Nuclear Sci. Eng., 8, 193 (1960).

Honeck, H. C., and I. Kaplan, "The Distribution of Thermal Neutrons in Space and Energy in Reactor Lattices. Part II: Comparison of Theory and Experiment," Nuclear Sci. Eng., 8, 203 (1960).

H10 Honeck, H. C., "THERMOS, A Thermalization Transport Theory Code for Reactor Lattice Calculations," BNL-5826 (September, 1961).

H11 Honeck, H. C., "An Incoherent Thermal Scattering Model for Heavy Water," Trans. Am. Nucl. Soc., 5, No. 1, 47 (1962).

H12 Hughes, D. J., and R. B. Schwartz, "Neutron Cross Sections," BNL-325 (Second Edition, July, 1958).

K1 Kaplan, I., "Measurements of Reactor Parameters in Subcritical and Critical Assemblies: A Review," NYO-10207, MITNE-25 (August, 1962).

Kaplan, I., "Measurements of Reactor Parameters in Subcritical and Critical Assemblies," Advances in Nuclear Science and Technology, edited by E. J. Henley and H. Kouts, Vol. II, p. 139 (New York: Academic Press, Inc., 1964).

K2 Kouts, H. and R. Sher, "Experimental Studies of Slightly Enriched Uranium, Water Moderated Lattices, Part I. 0.600-inch Diameter Rods," BNL-486 (September, 1957).

L1 Levine, M. M., K. E. Roach, D. B. Wehmeyer, and P. F. Zweifel, "The Slowing Down of Neutrons by Deuterium," Nuclear Sci. Eng., 7, 14 (1960).

P1 Palmedo, P. F., I. Kaplan, and T. J. Thompson, "Measurements of the Material Bucklings of Lattices of Natural Uranium Rods in D_2O," NYO-9660, MITNE-13 (January, 1962).

P2 Peak, J. C., I. Kaplan, and T. J. Thompson, "Theory and Use of Small Subcritical Assemblies for the Measurement of Reactor Parameters," NYO-10204, MITNE-16 (April, 1962).

P3 Pilat, E. E., Ph.D. Thesis, Nucl. Eng. Dept., M.I.T. (forthcoming).

R1 Reactor Handbook, edited by H. Soodak, Second Edition, Vol. 3, Part A: Physics, Table 3.8 (New York: Interscience Publishers, 1962).

R2 Rydin, R. A., N. C. Rasmussen, and G. L. Brownell, "Fast Neutron Spectroscopy and Dosimetry of the M.I.T. Reactor Medical Therapy Facility Beam," AFCRL-64-404, MITNE-47 (May, 1964).

R3 Robertson, C. G., "Measurements of Neutron Utilization for Lattices of Slightly Enriched Uranium Rods," M.S. Thesis, M.I.T. Nucl. Eng. Dept. (June, 1965).

S1 Simms, R., I. Kaplan, T. J. Thompson, and D. D. Lanning, "Analytical and Experimental Investigations of the Behavior of Thermal Neutrons in Lattices of Uranium Metal Rods in Heavy Water," NYO-10211, MITNE-33 (October, 1963).

S2 Sampson, J. B., and J. Chernick, "Resonance Escape Probability in Thermal Reactors," Progress in Nuclear Energy, edited by D. J. Hughes, J. E. Sanders, and J. Horowitz, Series I, Physics and Mathematics, Vol. 2 (New York: Pergamon Press, 1958).

S3 Sneddon, I. A., Fourier Transforms (New York: McGraw-Hill Book Co., 1951).

T1 Thie, J. A., Heavy Water Exponential Experiments Using ThO_2 and UO_2, p. 89 (New York: Pergamon Press, 1961).

T2 Topping, J., Errors of Observation and Their Treatment, The Institute of Physics, London; Monographs for Students (New York: Reinhold Publishing Corp., 1960).

V1 Vernon, A. R., "Calculation of the Effective Resonance Integral of U^{238}," Nuclear Sci. Eng., 7, 3, 252 (March, 1960).

W1 Weinberg, A. M., and E. P. Wigner, The Physical Theory of Neutron Chain Reactors, (Chicago: University of Chicago Press, 1958).

W2 Weitzberg, A., I. Kaplan, and T. J. Thompson, "Measurements of Neutron Capture in U^{238} in Lattices of Uranium Rods in Heavy Water," NYO-9659, MITNE-11 (January, 1962).

W3 Wolberg, J. R., T. J. Thompson, and I. Kaplan, "A Study of the Fast Fission Effect in Lattices of Uranium Rods in Heavy Water," NYO-9661, MITNE-15 (February, 1962).

W4 Woodruff, G. L., I. Kaplan, and T. J. Thompson, "A Study of the Spatial Distributions of Fast Neutrons in Lattices of Slightly Enriched Uranium Rods Moderated by Heavy Water," MIT-2344-5, MITNE-67 (November, 1965).

W5 Wikdahl, C. E., and F. Akerhielm, "Measurements of Disadvantage Factors in a Small Mockup," PICG, Vol. 12, 162 (1958).

W6 Wade, J. W., "Neutron Age in Mixtures of D_2O and H_2O," Nuclear Sci. Eng., 4, 12 (1958).

W7 Wingfield, E. C., and E. J. Hennelly, "Exponential Measurements of Natural Uranium Rods in Heavy Water and Comparisons with Critical Experiments," Nuclear Sci. Eng., 12, 348 (March, 1962).

W8 Wehmeyer, D., Private communication to J. C. Peak (December, 1961).

APPENDIX C

NEUTRON SOURCE

Because of the small dimensions of the assembly, the neutron source is of particular importance in the miniature lattice. In the interpretation of measurements made in such a lattice, it is desirable to reduce as much as possible the number of effects that must be taken into account.

For the purpose of these measurements, it is desirable that the neutron source be as well thermalized as possible. This is, indeed, the case for the neutron beam of the Medical Therapy Facility where the cadmium ratio for gold is at least 100 (R2). Furthermore, since the assembly is cylindrical, it is desirable that the radial dependence of the source be of the form $J_0(\mu_1 r/R)$, where $\mu_1 = 2.405$, and R is the extrapolated radius of the assembly. More important is the desirability of having a neutron source which is axially symmetric. An azimuthal dependence of the neutron source complicates the problem without adding anything to the understanding of the basic physical behavior of the lattice under consideration.

In the medical facility at the M.I.T. Reactor, the center of the beam is 4 inches off the centerline of the reactor core. It was, therefore, expected that the neutron source have a maximum somewhat away from the center of the beam in the direction of the centerline of the reactor core.

Steps were taken to investigate the neutron source. The purpose was to find whether or not this asymmetry existed, and if so, what could be done to correct it. Measurements were made on top of the empty lattice tank. Bare gold foils were used to map the radial and azimuthal dependence of the neutron source. The circular foil holder was made of 1/8-inch-thick aluminum; recesses for the foils were made along eight radial directions 45° apart. The foils were positioned on a spiral. Each foil was 45° and 0.25 inch from the adjacent foil. Thus, each eight radial consecutive points complete a cycle in the spiral. The positioning of the foils in the holder is shown in Fig. C.1. Figure C.2 shows the results that were obtained. A definite peaking is observed at 2, 4, 6, 8 and 10 inches, which corresponds to the fourth quadrant in Fig. C.1. This result was expected as it is in the direction of the reactor core centerline.

To flatten the source distribution, a series of aluminum plates and a piece of lucite were arranged above the LiF collimator, as shown in Fig. C.3. The source distribution observed with the collimator in place is shown in Fig. C.4. The improvement in the neutron source is evident, since the azimuthal asymmetry has nearly disappeared.

The distribution of interest is that which would be observed directly on top of the miniature lattice grid plate that is located about 5 inches below the top of the lattice tank. The angle subtended by the beam is somewhat smaller at this location. Thus, the source distribution above the grid plate should be slightly different from that shown in Fig. C.4. It was, therefore, necessary to measure the neutron source distribution above the lattice grid plate with a lattice in the tank. The result is shown in Fig. C.5.

It is evident from these results that the source is axially symmetric and it can be assumed to be only a function of r. Furthermore, it can be expanded in a series of J_o functions as follows (S3):

$$S(r) = \frac{2}{R^2} \sum_{i=1}^{\infty} \bar{f}(\mu_i) \frac{J_o(\mu_i r/R)}{[J_1(\mu_i)]^2}, \tag{C.1}$$

where the μ_i's are the zeros of the transcendental equation

$$J_o(\mu_i) = 0; \tag{C.2}$$

$\bar{f}(\mu_i)$ is given by:

$$\bar{f}(\mu_i) = \int_0^R rS(r)\, J_o(\mu_i r/R)\, dr, \tag{C.3}$$

and R is the extrapolated radius.

The integration of Eq. (C.3) was done numerically. For this purpose, let

$$y = r/R. \tag{C.4}$$

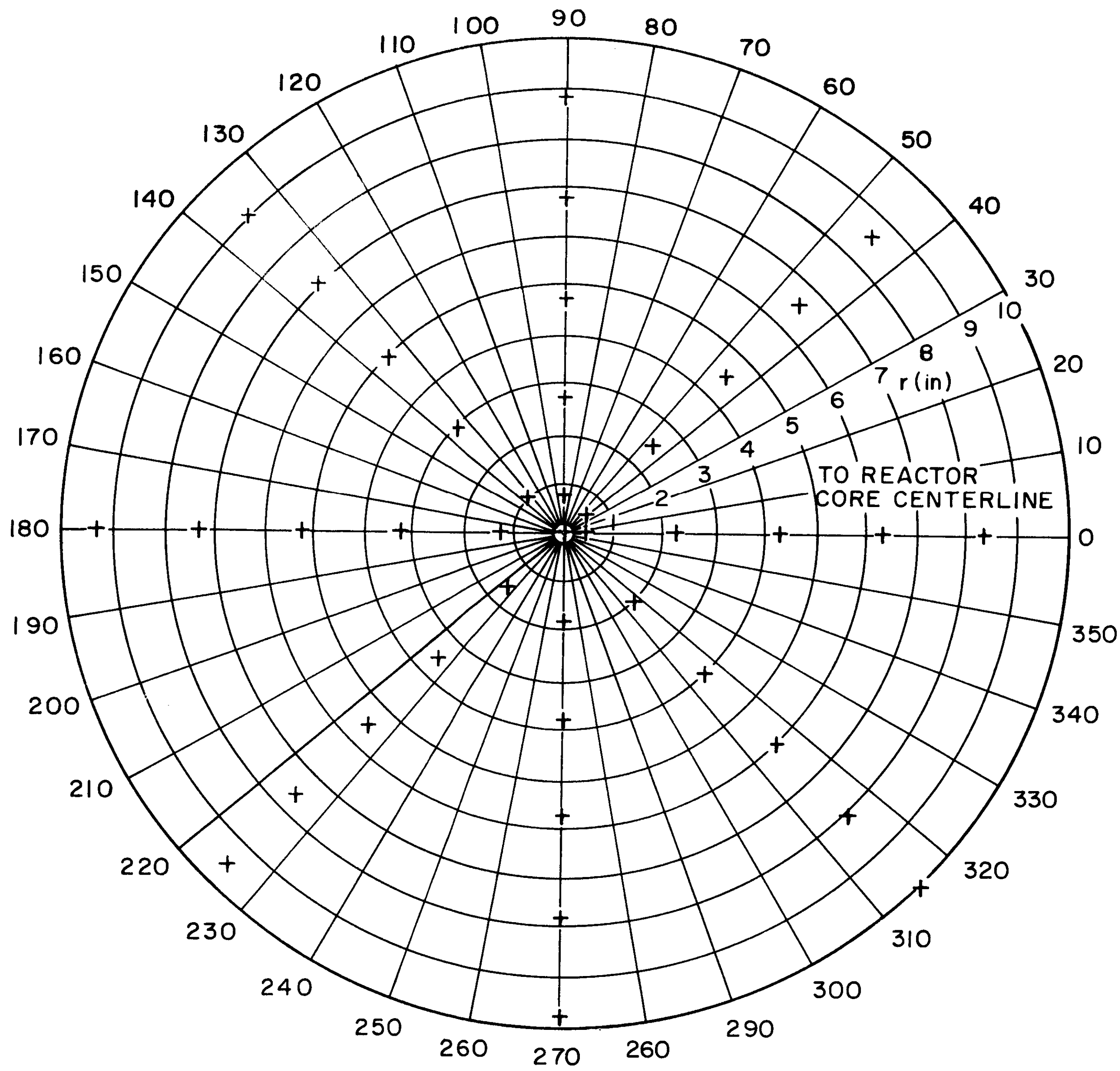

FIG.C.1 FOIL HOLDER FOR SOURCE INVESTIGATION

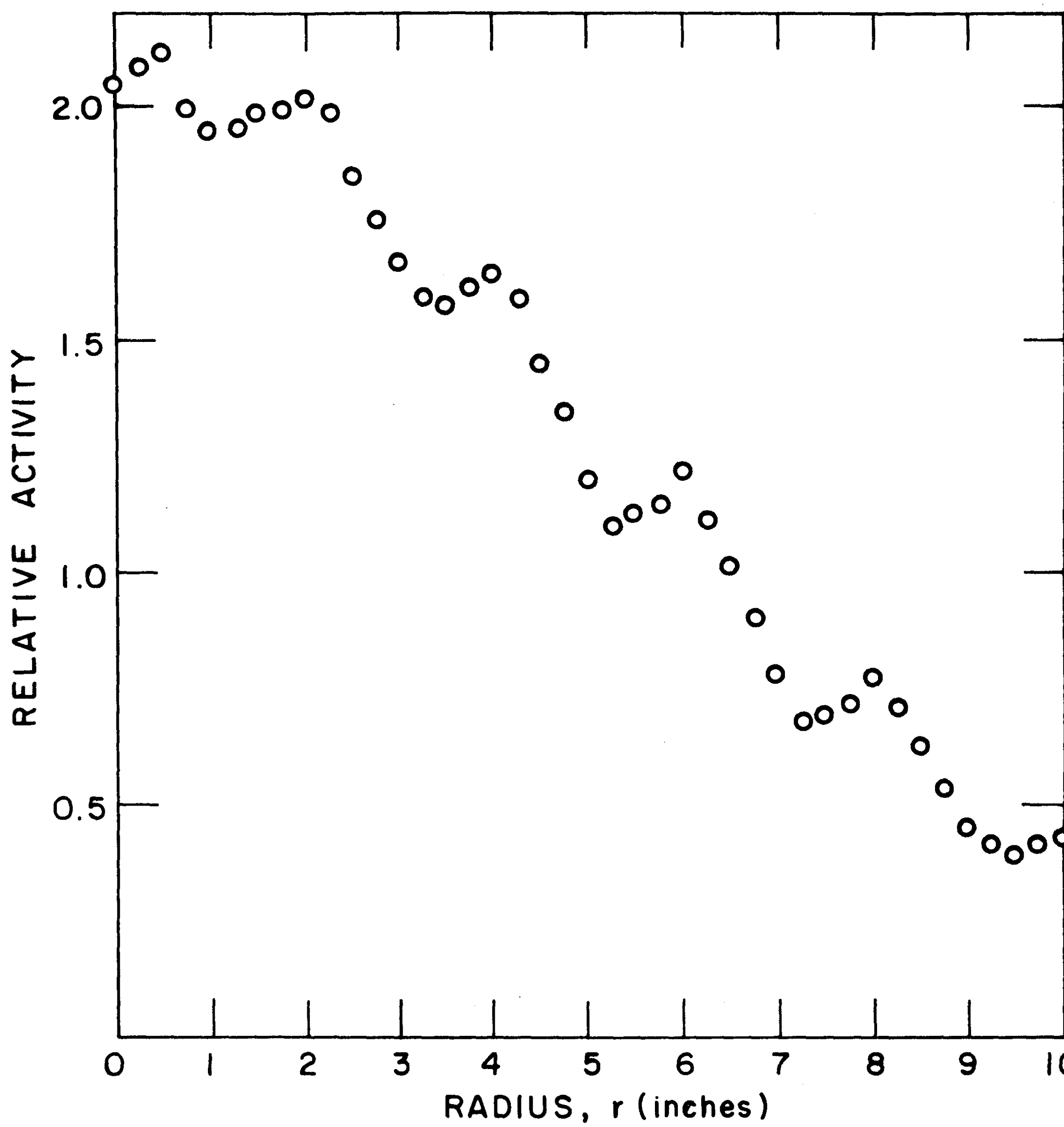

FIG. C.2 ORIGINAL RADIAL AND AZIMUTHAL DISTRIBUTION OF SOURCE NEUTRONS ON TOP OF LATTICE TANK

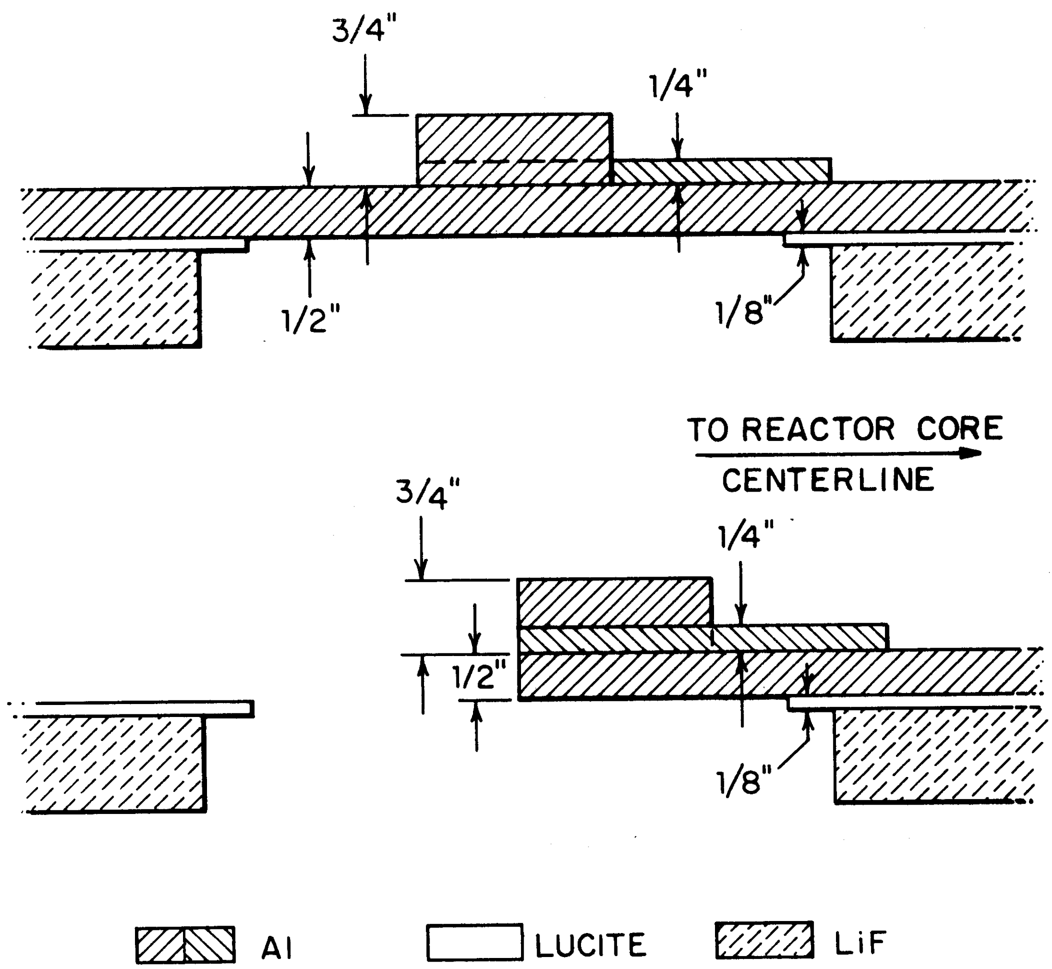

FIG. C.3 SCHEMATIC DIAGRAM OF COLLIMATOR USED TO MODIFY THE RADIAL AND AZIMUTHAL DEPENDENCE OF SOURCE NEUTRONS.

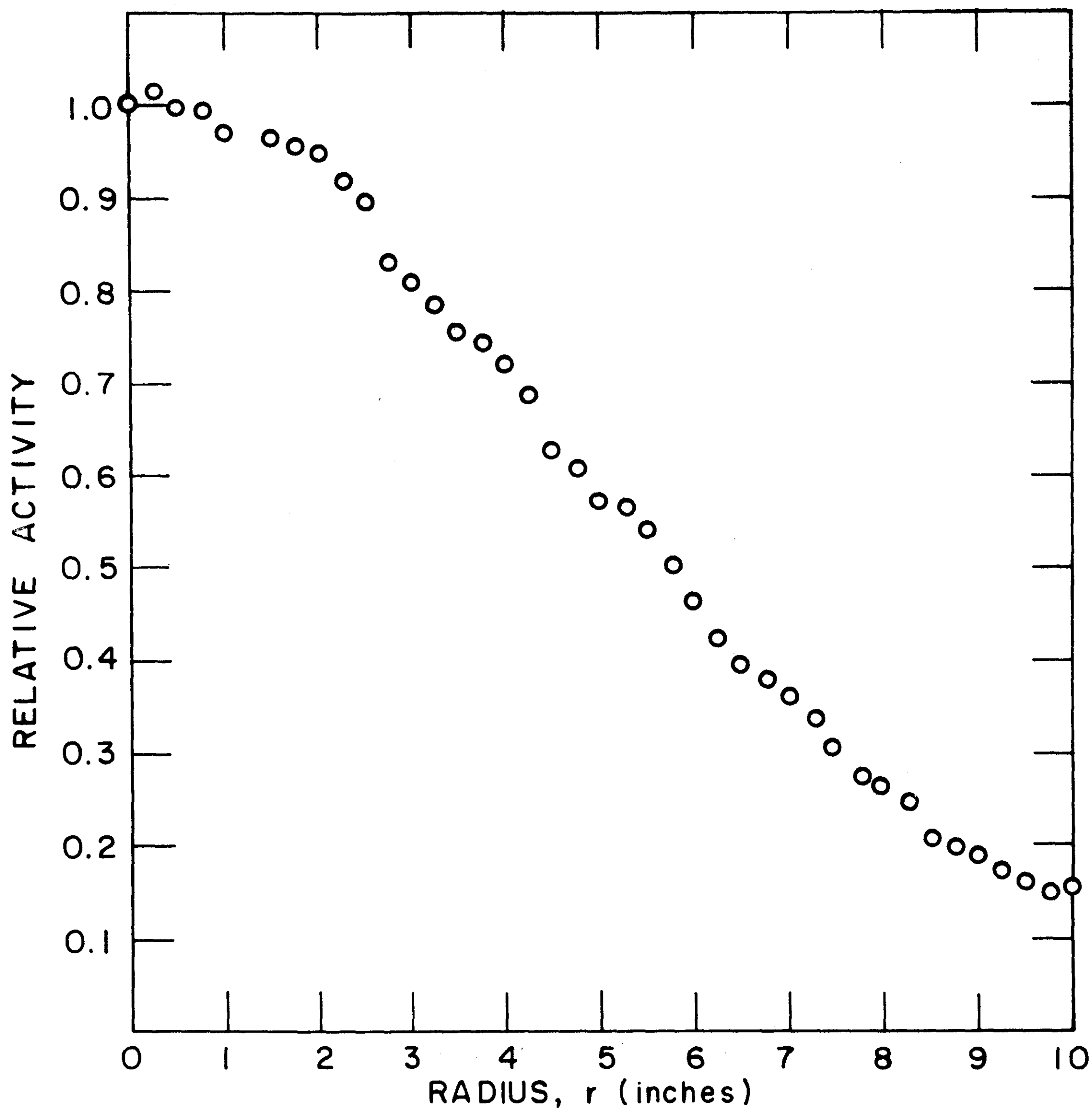

FIG. C.4 RADIAL AND AZIMUTHAL DISTRIBUTION OF SOURCE NEUTRONS ON TOP OF THE MINIATURE LATTICE TANK WITH COLLIMATOR IN PLACE

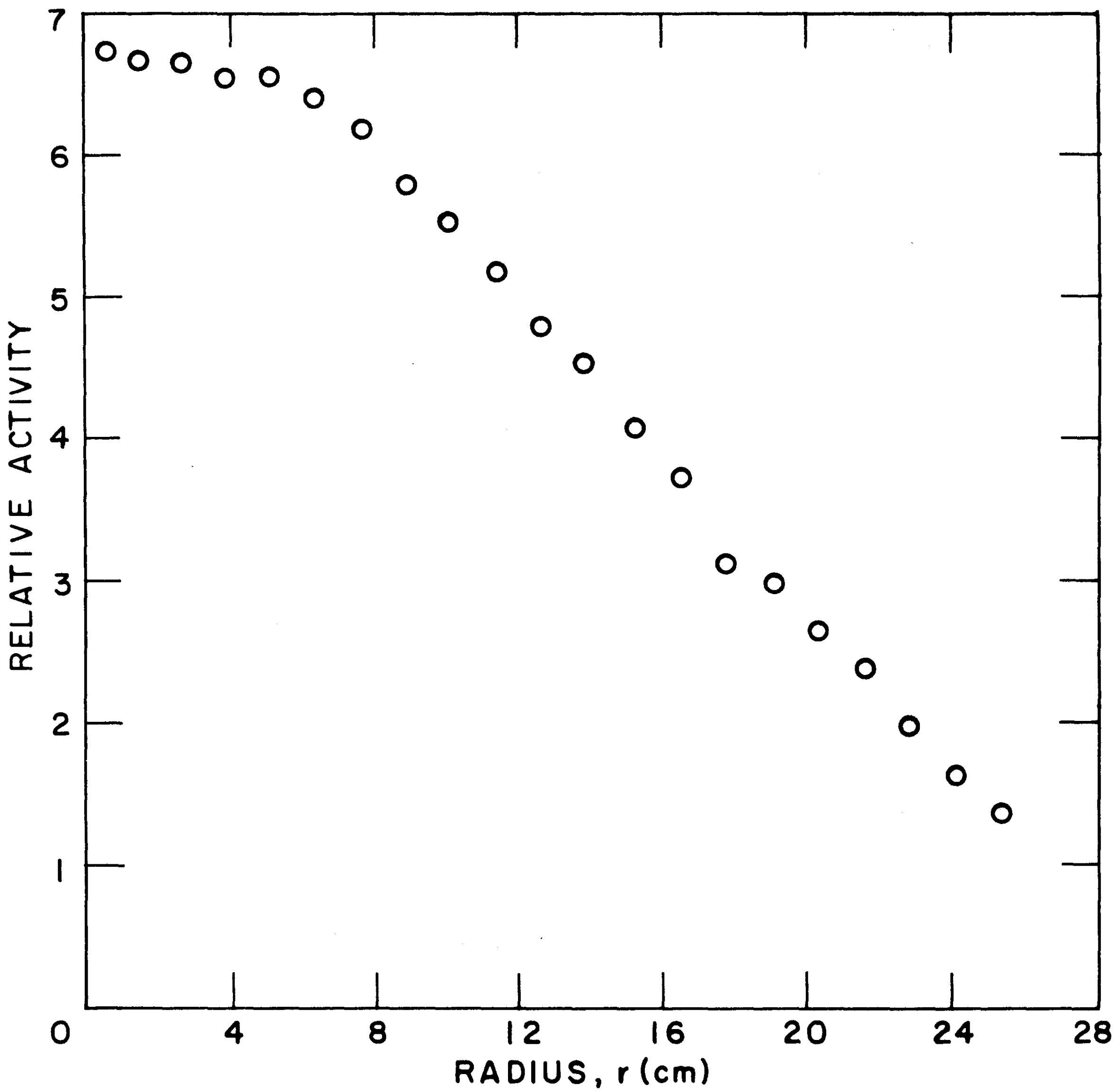

FIG. C.5 RADIAL DISTRIBUTION OF SOURCE NEUTRONS ENTERING THE MINIATURE LATTICE

Equation (C.3) may then be written as:

$$\bar{f}(\mu_i) = R^2 \int_0^1 yS(y)\, J_o(\mu_i y)\, dy, \tag{C.5}$$

and Eq. (C.1) can be written as:

$$S(y) = 2 \sum_{i=1}^{\infty} \bar{f}_i \, \frac{J_o(\mu_i y)}{[J_1(\mu_i)]^2}, \tag{C.6}$$

with

$$\bar{f}_i = \int_0^1 yS(y)\, J_o(\mu_i y)\, dy. \tag{C.7}$$

To integrate Eq. (C.7) numerically, let N equal the number of equal intervals Δy between 0 and 1. Let A_ℓ be the measured gold activity at y_ℓ; then

$$\bar{f}_i = \Delta y \sum_{\ell=1}^{N} y_\ell A_\ell J_o(\mu_i y_\ell). \tag{C.8}$$

To estimate the standard deviation σ_i of $\bar{f}_i$, let

σ_{A_ℓ} = standard deviation of A_ℓ,

σ_{y_ℓ} = standard deviation of y_ℓ.

The variance σ_i^2 of $\bar{f}_i$ is then given by (T2):

$$\sigma_i^2 = \sum_{\ell=1}^{N} \left\{ \left(\frac{\partial \bar{f}_i}{\partial A_\ell}\right)^2 \sigma_{A_\ell}^2 + \left(\frac{\partial \bar{f}_i}{\partial y_\ell}\right)^2 \sigma_{y_\ell}^2 \right\}, \tag{C.9}$$

or

$$\sigma_i^2 = (\Delta y)^2 \sum_{\ell=1}^{N} \left\{ \left(y_\ell J_o(\mu_i y_\ell)\sigma_{A_\ell}\right)^2 + \right.$$

$$\left. + \left[J_o(\mu_i y_\ell) - \mu_i y_\ell J_1(\mu_i y_\ell)\right]^2 A_\ell^2 \sigma_{y_\ell}^2 \right\}. \tag{C.10}$$

The results were obtained by using the IBM-7094 digital computer at the M.I.T. Computation Center. The RADIAL HARMONICS code is described in Appendix A. The results were normalized so that

$$\sum_i \bar{f}_i = 1 ; \tag{C.11}$$

thus, each $\bar{f}_i$ is a measure of the contribution of the i^{th} harmonic to the neutron source. The results are tabulated below:

i	$\bar{f}_i$
1	0.9413
2	-0.01455
3	0.03055
4	-0.01395
5	0.01679
6	-0.00316
7	0.008375
8	0.001843
9	0.008554
etc.	

It follows, therefore, that the source distribution has very nearly a $J_o(\mu_1 r/R)$ radial dependence, although the other harmonics have a measurable contribution. In the theory developed in Section 3.2.3, it has been assumed that five terms will suffice to describe the source. The basis for this assumption is that the contributions from higher harmonics damp out rapidly as neutrons diffuse through the lattice. Moreover, since only 20 points were used for the harmonic analysis, the accuracy of the values of $\bar{f}_i$ for values of i that are larger than about five is questionable. Their contribution to the total thermal flux is negligible.

APPENDIX D

AGE MEASUREMENTS IN PURE MODERATOR

The expressions for the quantity S for gold, U^{238} and U^{235} for an exponential, a critical and an infinite assembly, in terms of its value for the miniature lattice, were listed in Table 5.1. They were shown to depend on the age of fission neutrons to other than thermal energies. The procedures followed to determine the values of these ages were described in Sections (5.2.7) through (5.2.9). Lack of experimental information with respect to these quantities made necessary the measurement of the age of fission neutrons to the resonance energy of gold at 4.906 ev, and to the U^{238} resonance at 6.7 ev. The intent of these measurements was to check the values used for τ_{Au} and $\tau_{6.7}$ in Section 5.2.5.

The experimental method used to determine τ_{Au} and $\tau_{6.7}$ was to measure the radial activity distribution of cadmium-covered foils of the material under consideration. The irradiation was made about a 0.25-inch-diameter, 1.143% enriched uranium rod. The assumption was made that the fission neutrons were produced by a line source. The measured activity distribution was then fitted to a function of the form:

$$A(r) \propto e^{-r^2/4\tau}, \tag{D.1}$$

or

$$\ln A(r) \propto -r^2/4\tau . \tag{D.2}$$

The curve-fitting process was done by means of the computer program LSQ-4D (D1). The age was obtained from the slope of the straight line which results from plotting ln A(r) against r^2.

The line source assumption and the measurements performed are discussed below.

D.1 LINE SOURCE HYPOTHESIS

To investigate the effect of the source volume on the observed radial activity distribution, consider the slowing-down kernel for a cylindrical shell source, $K(r, r', \tau)$. For fission neutrons born with an age equal to zero (R1):

$$K(r, r', \tau) = \frac{1}{4\pi\tau} e^{-\frac{r^2+r'^2}{4\tau}} I_o\left(\frac{rr'}{2\tau}\right) \tag{D.3}$$

Equation (D.3) represents the slowing-down density at age τ and a distance r due to a unit source located in a cylindrical shell source at a distance r' from the origin, and born with an age equal to zero. The slowing-down density at age τ and distance $r, q(r, \tau)$ due to a cylindrical source is obtained by multiplying Eq. (D.3) by the source $S(r')$ per unit area and the surface element $2\pi r' dr'$ and integrating over the area of the source. Thus,

$$q(r, \tau) = \frac{1}{2\tau} \int_0^{r_o} r' dr' S(r') e^{-\frac{r^2+r'^2}{4\tau}} I_o\left(\frac{rr'}{2\tau}\right), \tag{D.4}$$

where r_o is the radius of the cylinder. If a flat source is assumed:

$$S(r') = \frac{Q}{\pi r_o^2}, \tag{D.5}$$

and

$$q(r, \tau) = \frac{Q}{2\pi\tau r_o^2} e^{-r^2/4\tau} \int_0^{r_o} r' dr' e^{-r'^2/4\tau} I_o\left(\frac{rr'}{2\tau}\right). \tag{D.6}$$

For the fuel rod utilized in these measurements and the dimensions of the miniature lattice tank:

$$0 \leq r' \leq 0.317 \text{ cm},$$

$$0.317 \leq r \leq 25 \text{ cm}$$

and

$$\tau \simeq 100 \text{ cm}^2.$$

It follows then, that $\frac{rr'}{2\tau} \leq 0.04$ and, therefore, $I_o\left(\frac{rr'}{2\tau}\right) \simeq 1$. Under these conditions, Eq. (D.6) becomes,

$$q(r, \tau) = \frac{Q}{2\pi\tau r_o^2} e^{-r^2/4\tau} \int_0^{r_o} r' \, dr' \, e^{-r'^2/4\tau}, \tag{D.7}$$

which can be readily integrated to yield:

$$q(r, \tau) = \frac{Q}{2\pi\tau r_o^2} e^{-r^2/4\tau} \, 2\tau\left[1 - e^{-r_o^2/4\tau}\right]. \tag{D.8}$$

In Eq. (D.8), $r_o^2 \simeq .1 \text{ cm}^2$ and $4\tau \simeq 400 \text{ cm}^2$; the exponential in parentheses can then be expanded in a Taylor series; thus,

$$q(r, \tau) = \frac{Q}{2\pi\tau r_o^2} e^{-r^2/4\tau} \, 2\tau\left(\frac{r_o^2}{4\tau}\right), \tag{D.9}$$

or

$$q(r, \tau) = \frac{Q}{4\pi\tau} e^{-r^2/4\tau}. \tag{D.10}$$

Hence, for the conditions of the experiments performed, the line source hypothesis is valid.

D.2 AGE TO THE RESONANCE ENERGY OF GOLD

To measure the age of fission neutrons to the resonance energy of gold at 4.906 ev, cadmium-covered gold foils, 1/4 inch in diameter and 0.005 inch thick, were irradiated for twelve hours about a single uranium rod placed in the center of the miniature lattice facility. The foils were placed alternately, 1/2 inch apart in recesses made on an aluminum bar 3/16 inch thick and 1/2 inch wide. The irradiation was made at a distance of ten inches from the source end. At this distance, which is about twice the slowing-down length in D_2O, it was estimated that the effect on the radial activity distribution of the small fraction ($\simeq 0.01$) of epithermal neutrons coming from the source is negligible. Hence, all the epithermal neutrons detected by the foils were assumed to come from the single rod. The gold foils were counted according to the method described in Section 2.6. The raw counting rates were reduced following the procedure described in Section 4.2.1.

The radial distribution of the corrected gold activity is plotted against r^2 in Fig. D.1. The fitted curve was obtained with the aid of the LSQ-4D code (D1). The slope of the curve in Fig. D.1 led to

$$\tau_{Au}^{M} = 95 \pm 3 \text{ cm}^2,$$

which, in conjunction with Eq. (5.24), led to the values of τ_{Au} for the different lattices investigated that are listed in Table 5.3.

D.3 AGE TO THE U^{238} RESONANCE AT 6.7 EV

The irradiation procedure used to measure the age to the U^{238} resonance at 6.7 ev was similar to that used to determine τ_{Au}^{M}. The detectors used were 1/4-inch-diameter, 0.005-inch-thick, depleted uranium foils. The cadmium-covered foils were placed alternately, 1.5 inch apart in the recesses made on the same aluminum bar used for the measurement of τ_{Au}^{M}. The Np^{239} activity of the depleted uranium foils was counted by means of the procedure described in Section 2.7.6. The gross count rates of each depleted uranium foil were reduced in the manner described in Section 4.2.3.

The radial distribution of the corrected Np^{239} activity is plotted against r^2 in Fig. D.2. As in the determination of τ_{Au}^{M}, the LSQ-4D (D1) code was used to obtain the fitted curve. The slope of the curve yields:

$$\tau_{6.7}^{M} = 92 \pm 3 \text{ cm}^2.$$

Consider Eq. (5.38),

$$\tau_{6.7} = \tau_i - \frac{D}{\xi \Sigma_s} \ln (6.7/E_i). \tag{5.38}$$

If, in this equation, one substitutes τ_{Au}^{M} and 4.906 ev for τ_i and E_i, respectively, the value of $\tau_{6.7}^{M}$ obtained is in close agreement with the value given above. This result indicates that the age measured in this manner is the age to the U^{238} resonance at 6.7 ev. Physically, this result can be understood from the fact that in the experimental arrangement used for the determination of $\tau_{6.7}$, the depleted uranium foils are, in effect, placed in an infinite medium of heavy water. Hence, the captures in U^{238} take place as if it were infinitely dilute; thus, the majority of neutron captures take place at the lowest lying resonance

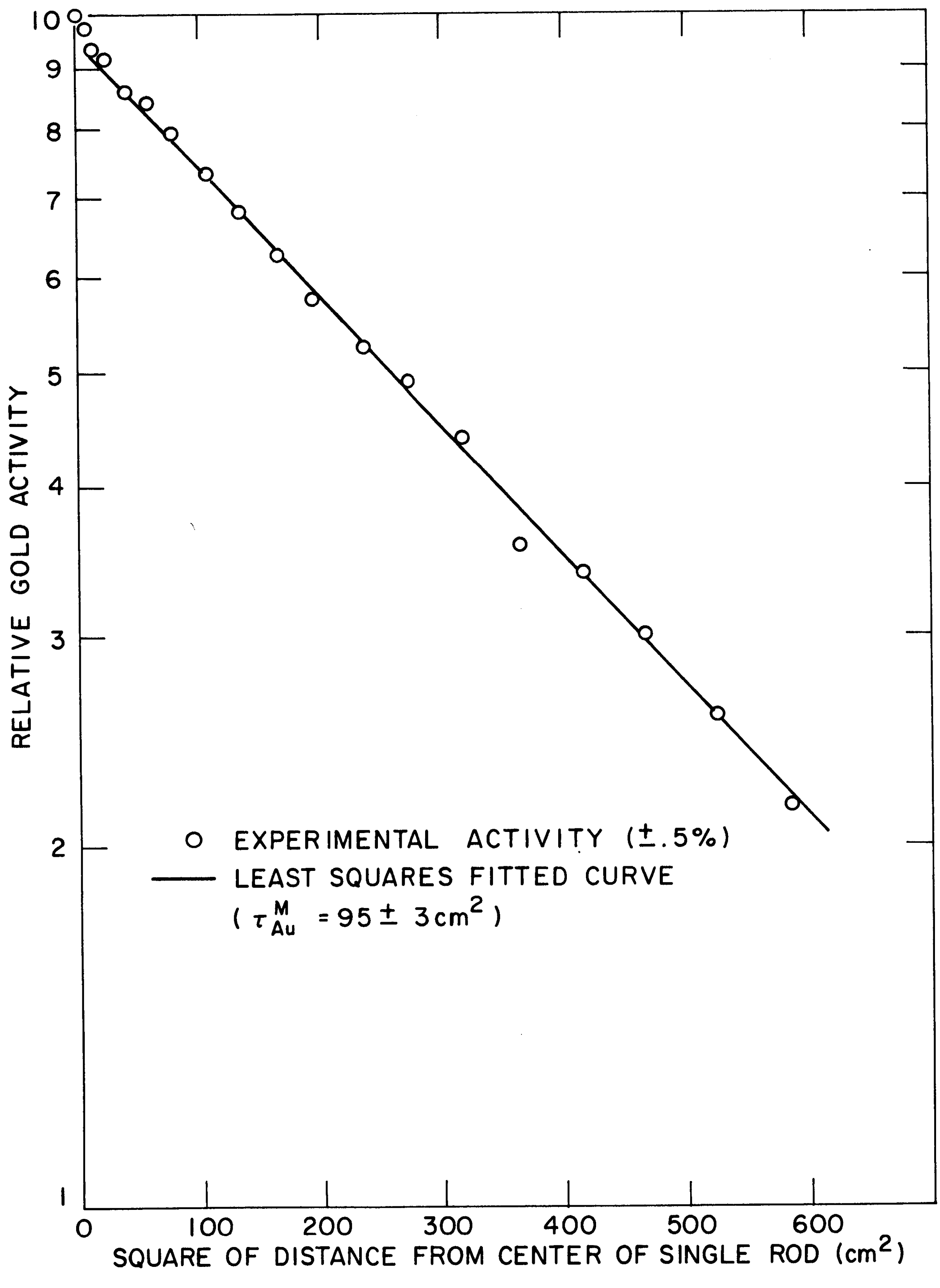

FIG. D.1 RADIAL ACTIVITY DISTRIBUTION OF CADMIUM COVERED GOLD FOILS ABOUT A SINGLE ROD IN HEAVY WATER

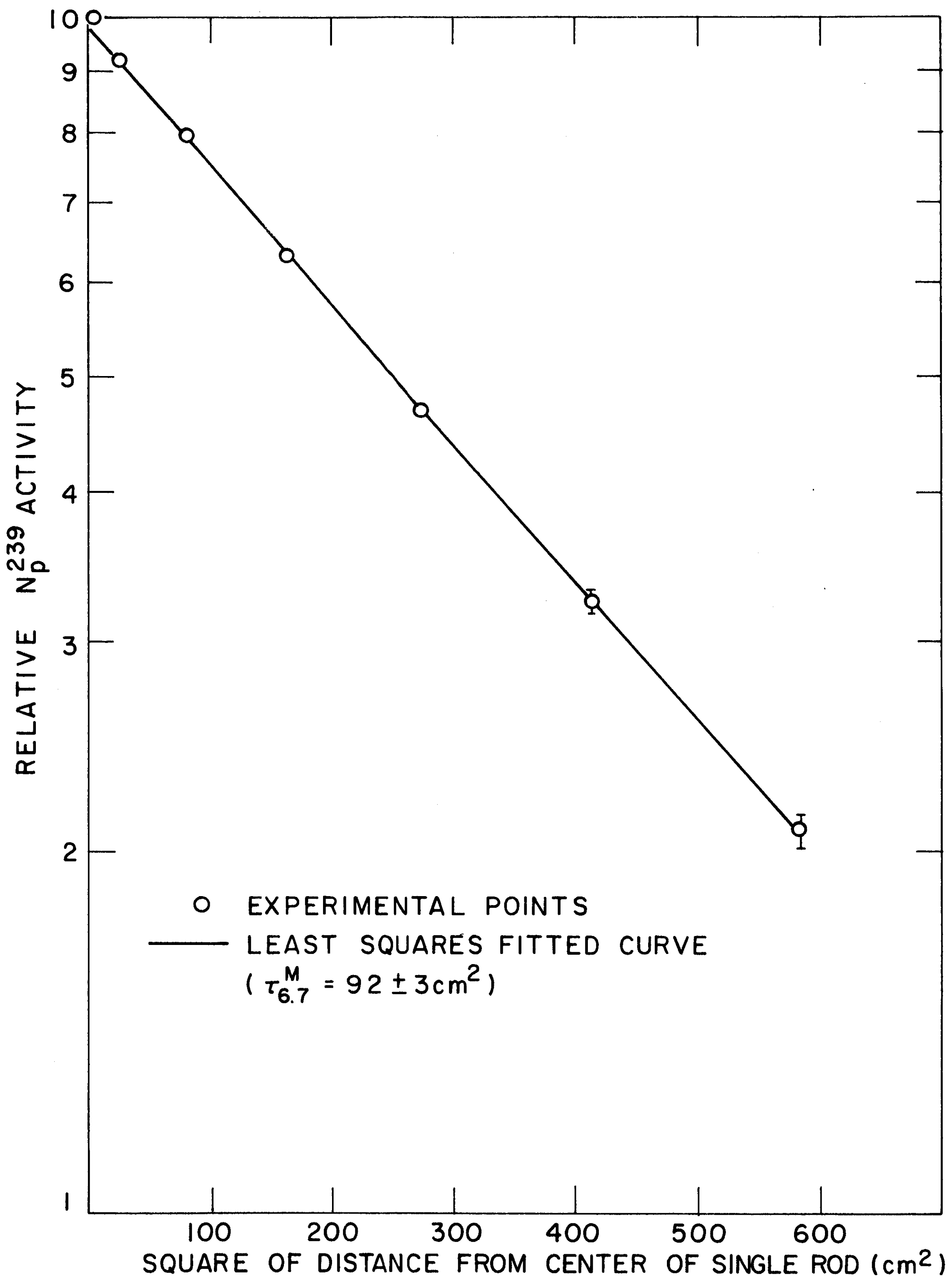

FIG. D.2 RADIAL N_p^{239} ACTIVITY DISTRIBUTION OF CADMIUM COVERED DEPLETED URANIUM FOILS ABOUT A SINGLE ROD IN HEAVY WATER

(S2) at 6.7 ev. Thus, the result of this measurement is expected.

The procedure followed to compute τ_{28}, the age to the effective resonance energy for U^{238}, from the measured value of $\tau_{6.7}$ is described in Section 5.2.8. The values of τ_{28} for the lattices investigated are listed in Table 4.1.

APPENDIX E

DETERMINATION OF δ_{25}, ρ_{28} AND C^*

The EPIFAST computer program used to reduce the fission product and Np^{239} activity is discussed in this appendix.

The purpose of the EPIFAST program is to reduce the data obtained from the LSQ-4D program, as described in Section 4.2.3, to obtain the average values of ρ_{28}, δ_{25} and C^*, and the corresponding standard deviations.

The EPIFAST computer program makes use of the coefficients obtained by the LSQ-4D code for the least squares polynomial fitted to the time dependence of the fission product activity of both natural and depleted uranium foils. The coefficients are used to calculate the fission product activity at common times, T_j, for each foil involved in the calculation of either δ_{25} or C^*. These activities are used in Eqs. (2.10) and (2.17) to obtain δ_{25} and R_F, respectively, at the times T_j. The corrected Np^{239} activities of the depleted uranium foils are used in Eqs. (2.1) and (2.16) to obtain ρ_{28} and R_N, respectively, for each of the counting passes made for the depleted uranium foils in an experiment. The average values of R_N and R_F are then substituted in Eq. (2.12) to obtain the average value of C^*. An independent value of C^* is also obtained when the average values of δ^{25} and ρ_{28} are substituted in Eq. (2.18). The standard deviations of the various parameters are obtained from the uncertainties of the polynomial coefficients obtained by means of the LSQ-4D code and the statistical errors in the corrected Np^{239} activities of the depleted uranium foils. The details of the calculation are given below.

E.1 NOTATION

The different foils that enter in the calculation are denoted by the subscript k as follows:

$k = 1$, bare natural uranium foil;

$k = 2$, bare depleted uranium foil;

k = 3, cadmium-covered natural uranium foil;

k = 4, cadmium-covered depleted uranium foil;

k = 5, natural uranium foil irradiated in a Maxwellian flux;

k = 6, depleted uranium foil irradiated in a Maxwellian flux.

A_{ki} is the i^{th} coefficient of the polynomial fitted to the activity of the k^{th} foil. There are L_k+1 coefficients, where L_k is the degree of the polynomial. P_{ki} is the uncertainty in the value of A_{ki}.

C_{kj} denotes the fission product activity of the k^{th} foil at a time T_j; S_{kj} is the variance of the calculated activity for the k^{th} foil at T_j.

N_{km} denotes the corrected Np^{239} activity of the k^{th} foil in the m^{th} counting pass, where k=2, 4 and 6; D_{km} is the standard deviation of N_{km}.

The quantity ψ_δ denotes the correction factor to be applied to δ_{25} for the presence of "foreign" materials in the foil packets used in the measurement; ψ_ρ is the corresponding correction factor for ρ_{28}. A discussion of the effect of foreign materials in the measurement of δ_{25} and ρ_{28} is given in Ref. (D1).

The quantity ψ_A denotes the ratio of the activity of the monitor gold foil irradiated below the packet with cadmium-covered foils, to the activity of the monitor gold foils irradiated below the packet with the bare foils. The quantity ψ_A permits the correction of δ_{25} and ρ_{25} for differences in the flux at the location of the detector foils, if necessary.

The quantity EC is given by:

$$EC = \frac{1 - \epsilon_N}{1 - \epsilon_D},$$

where ϵ_N and ϵ_D denote the U^{235} atom fraction in natural and a depleted uranium foil, respectively.

E.2 COMPUTATION PROCEDURE

The fission product activity of the k^{th} foil at time T_j is obtained from the coefficients of the polynomial fitted by the LSQ-4D program. It is given by:

$$C_{kj} = \sum_{i=1}^{L_k+1} A_{ki} T_j^{i-1} \,. \tag{E.1}$$

The corresponding variance is obtained from the formula for the propagation of error (T2); thus, if y is a function of n parameters,

$$y = f(x_1, \ldots, x_n),$$

then the variance of the function y is given by:

$$\sigma_y^2 = \sum_{\ell=1}^{n} \left(\frac{\partial f}{\partial x_\ell}\right)^2 \sigma_{x_\ell}^2 \,, \tag{E.2}$$

where σ_{x_ℓ} denotes the standard deviation of x_ℓ. Accordingly, the variance of C_{kj} is:

$$S_{kj} = \sum_{i=1}^{L_k+1} \left(P_{ki} T_j^{i-1}\right)^2 . \tag{E.3}$$

The fission product activity due to fissions in U^{235} only at time T_j, for the bare uranium foils, the cadmium-covered uranium foils and those irradiated in a Maxwellian flux is given, respectively, by:

$$R_j = C_{1j} - (EC) \cdot C_{2j} \,, \tag{E.4}$$

$$S_j = C_{3j} - (EC) \cdot C_{4j} \tag{E.5}$$

and

$$Q_j = C_{5j} - (EC) \cdot C_{6j} \,. \tag{E.6}$$

The corresponding variances are obtained with the aid of Eq. (E.2). Thus,

$$\sigma^2(R_j) = S_{1j} + (EC)^2 \cdot S_{2j} \,, \tag{E.7}$$

$$\sigma^2(S_j) = S_{3j} + (EC)^2 \cdot S_{4j} \tag{E.8}$$

and

$$\sigma^2(Q_j) = S_{5j} + (EC)^2 \cdot S_{6j} \,. \tag{E.9}$$

The value of δ_{25} at time T_j, δ_{25_j}, is obtained from Eqs. (E.4) and (E.5) and the correction factors ψ_δ^j and ψ_A; thus,

$$\delta_{25_j} = \psi_\delta \left[\frac{S_j}{R_j \psi_A - S_j} \right] . \tag{E.10}$$

The corresponding variance is:

$$\sigma^2_{25_j} = \delta^2_{25_j} \left[\frac{\sigma^2(S_j)}{S_j^2} + \frac{\psi_A^2 \sigma^2(R_j) + \sigma^2(S_j)}{[R_j \psi_A - S_j]^2} \right] . \tag{E.11}$$

The ratio R_F at T_j is obtained from Eqs. (E.4) and (E.6); thus,

$$R_{F_j} = \frac{R_j}{Q_j} , \tag{E.12}$$

and its variance is given by:

$$\sigma^2_{F_j} = R^2_{F_j} \left[\frac{\sigma^2(R_j)}{R_j^2} + \frac{\sigma^2(Q_j)}{Q_j^2} \right] . \tag{E.13}$$

The values of ρ_{28} and R_N for the m^{th} Np^{239} activity counting pass are obtained as follows:

$$\rho_{28m} = \psi_\rho \left[\frac{N_{4m}}{N_{2m} \psi_A - N_{4m}} \right] \tag{E.14}$$

and

$$R_{Nm} = \frac{N_{2m}}{N_{6m}} . \tag{E.15}$$

The corresponding variances are obtained with the aid of Eq. (E.2); thus,

$$\sigma^2_{28m} = \rho^2_{28m} \left[\frac{(D_{2m})^2}{(N_{2m})^2} + \frac{\psi_A^2 (D_{2m})^2 + (D_{4m})^2}{(N_{2m} \psi_A - N_{4m})^2} \right] \tag{E.16}$$

and

$$\sigma^2_{Nm} = R^2_{Nm} \left[\frac{(D_{2m})^2}{(N_{2m})^2} + \frac{(D_{6m})^2}{(N_{6m})^2} \right] . \tag{E.17}$$

The values of δ_{25} and R_F calculated at the various times T_j are averaged by weighting with respect to the reciprocal of the corresponding variance. Hence,

$$\bar{\delta}_{25} = \frac{\sum_{j=1}^{N} \left(\delta_{25j} / \sigma^2_{25j} \right)}{\sum_{j=1}^{N} \left(1/\sigma^2_{25j} \right)} \tag{E.18}$$

and

$$\bar{R}_F = \frac{\sum_{j=1}^{N} \left(R_{Fj} / \sigma^2_{Fj} \right)}{\sum_{j=1}^{N} \left(1/\sigma^2_{Fj} \right)} , \tag{E.19}$$

where N is the number of times at which the activities were calculated (normally N equals the number of counting passes for each of the uranium foils). The average values of ρ_{28} and R_N are obtained in a similar manner; thus,

$$\bar{\rho}_{28} = \frac{\sum_{m=1}^{M} \left(\rho_{28m} / \sigma^2_{28m} \right)}{\sum_{m=1}^{M} \left(1/\sigma^2_{28m} \right)} \tag{E.20}$$

and

$$\bar{R}_N = \frac{\sum_{m=1}^{M} \left(R_{Nm} / \sigma^2_{Nm} \right)}{\sum_{m=1}^{M} \left(1/\sigma^2_{Nm} \right)} , \tag{E.21}$$

where M is the number of passes made for Np^{239} activity counting of the depleted uranium foils. The corresponding variances are given by (T2):

$$\sigma^2(\bar{\delta}_{25}) = \frac{\sum_{j=1}^{N} \left[(\delta_{25j} - \bar{\delta}_{25}) / \sigma_{25j} \right]^2}{\sum_{j=1}^{N} \left(1/\sigma_{25j} \right)^2 - 1} , \tag{E.22}$$

$$\sigma^2(\bar{R}_F) = \frac{\sum_{j=1}^{N} [(R_{Fj} - \bar{R}_F)/\sigma_{Fj}]^2}{\sum_{j=1}^{N} (1/\sigma_{Fj})^2 - 1} , \tag{E.23}$$

$$\sigma^2(\bar{\rho}_{28}) = \frac{\sum_{m=1}^{M} [(\rho_{28m}-\bar{\rho}_{28})/\sigma_{28j}]^2}{\sum_{m=1}^{M} (1/\sigma_{28m})^2 - 1} \tag{E.24}$$

and

$$\sigma^2(\bar{R}_N) = \frac{\sum_{m=1}^{M} [(R_{Nm}-\bar{R}_N)/\sigma_{Nm}]^2}{\sum_{m=1}^{M} (1/\sigma_{Nm})^2 - 1} . \tag{E.25}$$

In Eqs. (E.22) through (E.25), account has been taken of the fact that one degree of freedom has been used to obtain the averages.

Equations (E.18) through (E.25) are used to obtain the average value of C^* by the two independent methods, Eqs. (2.12) and (2.18). The corresponding variances are obtained with the aid of Eq. (E.2). Thus,

$$C^*_{SC} = \frac{1 + \bar{\rho}_{28}}{1 + \bar{\delta}_{25}} \left(\frac{\Sigma_a^{28}}{\Sigma_f^{25}} \right)_{SC} \tag{E.26}$$

and

$$C^*_{MAX} = C^*_M \, \bar{R}_N/\bar{R}_F . \tag{E.27}$$

The corresponding variances are, respectively,

$$\sigma^2_{SC} = C^{*2}_{SC} \left[\frac{\sigma^2(\bar{\rho}_{28})}{(1+\bar{\rho}_{28})^2} + \frac{\sigma^2(\bar{\delta}_{25})}{(1+\bar{\delta}_{25})} \right] \tag{E.28}$$

and

$$\sigma^2_{MAX} = C^*_{MAX} \left[\frac{\sigma^2(\bar{R}_N)}{\bar{R}_N^2} + \frac{\sigma^2(\bar{R}_F)}{\bar{R}_F^2} \right] . \tag{E.29}$$

The standard deviations of all the quantities of interest are obtained as the square root of the corresponding variance.

The input instructions and Fortran listing for the EPIFAST program are given in Appendix A.